

Hyperspectral Coastal Image Analysis Toolbox (HyCIAT) Enhancement: Subsurface linear
unmixing and object detection by means of regularization

By:

Emmanuel Carpena-Colón

A project submitted in partial fulfillment of the requirements for the degree of

MASTER OF ENGINEERING
in
ELECTRICAL ENGINEERING

UNIVERSITY OF PUERTO RICO
MAYAGÜEZ CAMPUS
2017

Approved by:

Luis O. Jiménez, Ph.D.
President, Graduate Committee

Date

Emmanuel Arzuaga, Ph.D.
Member, Graduate Committee

Date

Shawn Hunt, Ph.D.
Member, Graduate Committee

Date

Dorial Castellano Rodriguez, Ph. D.
Representative of Graduate Studies

Date

José Colom Ustariz, Ph.D.
Chairperson of the Department

Date

ABSTRACT

This work presents an enhancement to the Hyperspectral Coastal Image Analysis Toolbox (HyCIAT). HyCIAT is a graphic interface developed in MATLAB, for the estimation of water optical properties, bathymetry and bottom composition using a hyperspectral image of a shallow underwater environment [1]. The implemented algorithms for the estimation of the submerged bottom are based on the inversion model developed by Z. P. Lee combined with unmixing techniques developed by J. A. Goodman and A. Castrodad [2]–[5]. The graphic interface ceased to work on MATLAB versions over 2008b due to some compatibility issues. With this work, HyCIAT was enabled to be used on MATLAB 2013a. New functionalities are implemented to allow additional configurations of the unmixing algorithms. HyCIAT was further enhanced with the integration of a new subsurface classification algorithm by means of regularization techniques developed by L. O. Jiménez-Rodríguez and E. Rodríguez-Díaz [6], [7]. Algorithms were tested using a hyperspectral data set obtained from an indoor controlled environment that simulates an object submerged on fresh and turbid water. A new method was presented for the empirically retrieval of the optical properties of water using Z. P. Lee inversion model and the obtained hyperspectral data set. Results shows that the new functionalities have a positive impact on unmixing results by increasing the overall accuracy on objects submerged in fresh and turbid waters. At the other hand, the classification accuracy of objects submerged in fresh and turbid water was also increased with the use of the regularization algorithms. Finally, additional tools were included in the toolbox that extends HyCIAT capabilities for a more complete and robust interface.

RESUMEN

Este trabajo presenta una mejora realizada a un programa desarrollado en MATLAB llamado HyCIAT. HyCIAT es una interface gráfica que integra algoritmos para la estimación de propiedades ópticas del agua, batimetría y composición del fondo marino utilizando imágenes hiperespectrales de poca profundidad [1]. Los algoritmos integrados para la estimación de la composición del fondo marino son basados en el modelo establecido por Z. P. Lee y combinados con técnicas de descomposición lineal para la estimación de abundancias desarrollados por J. A. Goodman y A. Castrodad [2]–[5]. La interface gráfica dejó de funcionar en las versiones de MATLAB sobre la 2008b debido a problemas de compatibilidad. Con este trabajo la funcionalidad de HyCIAT se re-estableció en la versión de MATLAB 2013a. Nuevas funcionalidades fueron implementadas para lograr un grado mayor de libertad al momento de configurar los algoritmos de estimación de abundancia. HyCIAT se extendió aún más con la integración de un nuevo algoritmo de clasificación submarina basado en técnicas de regularización desarrollado por L. O. Jiménez-Rodríguez y E. Rodríguez-Díaz [6], [7]. Los algoritmos fueron probados utilizando un conjunto de datos hiperespectrales obtenidos de un ambiente controlado en el interior que simula un objeto sumergido tanto en agua limpia como en agua turbia. Un nuevo método fue desarrollado y presentado para estimación empírica de las propiedades ópticas del agua utilizando el modelo de Z. P. Lee y el conjunto de datos hiperespectrales obtenido. Los resultados demuestran que las funcionalidades propuestas tienen un impacto positivo en los algoritmos de estimación de abundancia aumentando la precisión general aumento en objetos sumergidos en agua limpia y turbia. Por otro lado la clasificación de objetos sumergidos tanto en agua limpia como en agua turbia también aumento con el uso del algoritmo de regularización. Finalmente, herramientas adicionales fueron incluidas en la interface para extender sus capacidades hacia un a más completa y robusta.

Table of Content

Title Page	I
ABSTRACT.....	II
RESUMEN	III
Table of Content	IV
List of Figures	IX
List of Tables	XIV
1 Introduction	1
1.1 Justification.....	1
1.1.1 HyCIAT Enhancement.....	1
1.1.2 Regularization Algorithm	2
1.2 Objectives	2
1.3 Contributions of this Work	2
1.4 Thesis Outline.....	3
2 Theoretical Background and Previous Publications	4
2.1 Spectral Unmixing.....	7
2.2 Lee's Bio-optical Semi-analytical model	9
2.3 Lee's Inversion with Goodman's Unmixing (LIGU)	11
2.4 Combined Inversion with Linear Unmixing at the Surface (CIUS)	11
2.5 Combined Inversion with Linear Unmixing at the Bottom (CIUB).....	12
2.6 Regularization Algorithm	14
2.6.1 Selecting the Optimum Bottom and the Optimum Regularization Parameter	16
2.6.2 Pseudo Code.....	18
2.7 TiO ₂ – Titanium Dioxide	18
2.8 HyCIAT 2007	19
3 Materials and Methods	23

3.1	Dataset Acquisition for Validation Data.....	23
3.1.1	Materials.....	24
3.1.2	Experimental Setup.....	24
3.1.3	Experimental Procedure.....	25
3.1.4	Images Names and Descriptions.....	26
3.2	Image Pre-Processing	27
3.2.1	Image Masking.....	27
3.2.2	Calibration.....	29
3.2.3	Image Registration	30
3.2.4	Final Images: After pre-processing.....	33
3.3	Regions of Interest.....	35
3.3.1	Endmembers.....	35
3.4	Optical Properties Retrieval thorough an Empirical Procedure.....	37
3.4.1	Empirical derivation of a and b values.....	37
3.4.2	Masks	38
3.4.3	Dividing Sub-Regions.....	39
3.4.4	Absorption and Backscattering Empirical Calculations	40
3.5	Calculating Maximum Curvature	42
3.5.1	Numerical Approximation	43
3.5.2	Derived Equations.....	43
3.5.3	Single Regularization Parameter.....	44
3.6	Classification Algorithms	45
4	Software Development and Implementation	47
4.1	Updating and Enhancement of HyCIAT Underwater Unmixing Functions.....	47
4.1.1	<code>lsqnonlin</code> Optimization Functions Default Parameters.....	47
4.1.2	HyCIAT Spectral Region for Unmixing	51

4.1.3	HyCIAT Default Bottom Spectral Signature	52
4.1.4	Other Functionalities.....	53
4.2	Regularization Algorithm Development.....	54
4.2.1	General Functional Specifications	56
4.2.2	Integration into HyCIAT.....	62
4.2.3	Regularization Result Analysis GUI.....	67
4.3	Additional tool: Region of Interest Tools.....	72
5	Results	73
5.1	Underwater Linear Unmixing with AVIRIS Data.....	73
5.1.1	Obtained Similarity of AVIRIS – Image A using LIGU algorithm:.....	76
5.1.2	Obtained Similarity of AVIRIS – Image B using LIGU.....	76
5.1.3	Obtained Similarity of AVIRIS – Image A using CIUB algorithm.....	77
5.1.4	Obtained Similarity of AVIRIS – Image B using CIUB algorithm	77
5.2	Underwater Linear Unmixing applied to Real Controlled Data.....	77
5.2.1	LIGU Results from the 12.0 in without TiO ₂ Image and 5 Colors Endmembers	78
5.2.2	LIGU Results from the 12.0 in without TiO ₂ Image and 4 Colors Endmembers	79
5.2.3	CIUB Results from the 12.0 in without TiO ₂ Image and 5 Colors Endmembers	80
5.2.4	CIUB Results from the 12.0 in without TiO ₂ Image and 4 Colors Endmembers	80
5.2.5	LIGU Results from the 12.0 in with 0.5 g TiO ₂ Image and 4 Colors Endmembers.....	81
5.2.6	CIUB Results from the 12.0 in with 0.5 g of TiO ₂ Image and 4 Colors Endmembers ..	81
5.3	Regularization Algorithm	82
5.3.1	Regularization Baseline Results.....	83
5.3.2	Numerical Approximation Classification Results after Regularization.....	84
5.3.3	Derived Equations Classification Results after Regularization	85
5.3.4	Example with Reduced Bands using SVD Algorithm – Derived Equations	87
6	Discussion of Results.....	89

6.1	Underwater Linear Unmixing with AVIRIS Data.....	89
6.2	Underwater Linear Unmixing with Real Controlled Data.....	91
6.3	Regularization Algorithm	98
7	Conclusions & Future Work.....	110
7.1	Conclusion	110
7.2	Future Studies	112
8	References	114
9	Appendix	116
9.1	Additional Results – Image A LIGU Unmixing Result.....	116
9.1.1	Without Bathymetry: without parameter modification	116
9.1.2	With Bathymetry: without parameter modifications.....	117
9.1.3	Without Bathymetry: with parameter modification	119
9.1.4	With Bathymetry: with parameter modifications.....	120
9.2	Extended Results – Underwater Linear Unmixing Results with Previous Data.....	122
9.2.1	LIGU Results Improvements: Image A without Bathymetry	122
9.2.2	LIGU Results Improvements: Image B without Bathymetry	123
9.2.3	LIGU Results Improvements: Image A with Bathymetry	124
9.2.4	LIGU Results Improvements: Image B with Bathymetry.....	125
9.2.5	CIUB Results Improvements: Image A without Bathymetry:	126
9.2.6	CIUB Results Improvements: Image B without Bathymetry	127
9.2.7	CIUB Results Improvements: Image A with Bathymetry	128
9.2.8	CIUB Results Improvements: Image B with Bathymetry.....	129
9.3	Extended Results – Underwater Linear Unmixing with Real Controlled Data.....	130
9.3.1	LIGU 12.0 in Image with 5 Colors Endmembers	130
9.3.2	LIGU 12.0 in Image with 4 Colors Endmembers	134
9.3.3	CIUB 12.0 in Image with 5 Colors Endmembers	137

9.3.4	CIUB 12.0 in Image with 4 Colors Endmembers	139
9.3.5	LIGU 12.0 in 0.5 g TiO ₂ Image with 4 Colors Endmembers	141
9.3.6	CIUB 12.0 in 0.5 g TiO ₂ Image with 4 Colors Endmembers	143
9.4	Extended Results – Regularization Algorithm	145
9.4.1	Baseline Results	145
9.4.2	Numerical Approximation Classifications Results after Regularization	147
9.4.3	Derived Equations Classification Results after Regularization	154
9.4.4	Example with Reduced Bands using SVD Algorithm – Derived Equations	160
9.5	Performance Matrices of the Regularization Results	163
9.5.1	Baseline Results 12.0 in image:	163
9.5.2	Baseline Results 12.0 in 0.5 g TiO ₂ image:	164
9.5.3	Numerical Approximations: 12.0 in.....	165
9.5.4	Numerical Approximation: 12.0 in 0.5 <i>g</i> TiO ₂	169
9.5.5	Derived Equations: 12.0 in.....	173
9.5.6	Derived Equations: 12.0 in 0.5 <i>g</i> TiO ₂	177
9.5.7	Derived Equations: Reduced Bands using SVD Algorithm	181
9.6	User Manual	185

List of Figures

Figure 1: Comparison between three ways of sampling the spectrum.....	4
Figure 2: Typical remote sensed benthic environment	5
Figure 3: LIGU Block Diagram.....	11
Figure 4: CIUS Block Diagram	12
Figure 5: CIUB Block Diagram.....	14
Figure 6: Example of choosing γ that produce the smallest $\gamma_{optk,i}$	17
Figure 7: Example of choosing γ that produce the smallest error per pixel	17
Figure 8: Measured Reflectance of TiO ₂	19
Figure 9: Main Interface	20
Figure 10: Block diagram of the implementation of the unmixing algorithms into HyCIAT[1]	20
Figure 11: Initial Parameters Interface (HyCIAT 2007).....	21
Figure 12: Results interface	22
Figure 13: Known bottom with the white standard over it	24
Figure 14: Image of the setup	25
Figure 15: Example of some of the images taken with no processing.....	27
Figure 16: 12.0 in image with saturated pixels	28
Figure 17: Spectral Response of A) Saturated Pixels vs. B) White Standard.....	28
Figure 18: 12.0 in image with saturated pixels being masked (un-calibrated)	29
Figure 19: Difference between A) Radiance image and B) Reflectance image	29
Figure 20: Optical offset created by 12.0 in of water	30
Figure 21: MATLAB cpselect function GUI.....	31
Figure 22: Selecting point on cpselect interface	32
Figure 23: Resulting image after registration procedure	32
Figure 24: Region of Interest Selected: Training (solid line) and Testing (dashed line).....	35
Figure 25: Endmembers from 0'' hyperspectral image.....	36
Figure 26: Endmembers extracted from 1.8'' hyperspectral image.....	36
Figure 27: Masking operation	38
Figure 28: Divided sub-regions	40
Figure 29: Blue masked resulting image showing discarded sub- regions.....	40
Figure 30: Modeled Reflectance vs. Measured Reflectance.....	41
Figure 31: Empirically Derived Total Absorption (a).....	41

Figure 32: Empirically Derived Backscattering (<i>b</i>)	42
Figure 33: Typical Curvature Graph of the Regularization Algorithm.....	44
Figure 34: Result of the same parameters between two MATLAB versions.	48
Figure 35: Difference of the two images show in figure 34	48
Figure 36: Same result as figure 34 but with modified parameters	49
Figure 37: Difference of the two images showed in figure 36.....	50
Figure 38: Modification for default Parameter PrecondBandWidth.....	50
Figure 39: Independent interface to change the PrecondBandWidth parameter.....	50
Figure 40: Functionality to selects a region to perform the unmixing.....	51
Figure 41: Configuring a custom unmixing range in a single section of the spectrum	51
Figure 42: Configuring a custom unmixing range in multiple section of the spectrum	52
Figure 43: Added functionality: Custom bottom	53
Figure 44: Interface to assist the user to analyze and modify its own custom bottom	53
Figure 45: Interface modification on the Optimization Parameters section	54
Figure 46: Load and save configuration menu.....	54
Figure 47: Regularization Menu Sequence Diagram.....	57
Figure 48: Regularization Algorithm Block Diagram 1	58
Figure 49: Regularization Algorithm Block Diagram 2	59
Figure 50: Regularization Block Diagram 3.....	59
Figure 51: Regularization Function General Operation Flowchart.....	61
Figure 52: Opening Regularization Menu from HyCIAT GUI	62
Figure 53: Regularization Main Menu.....	62
Figure 54: Processing Settings Panel from the Regularization Menu	63
Figure 55: Maximum Curvature Algorithm Selection.....	63
Figure 56: Subset of bands for processing example.	64
Figure 57: Classification Settings Panel from the Regularization Menu.....	65
Figure 58: Selecting a subset of bands for classification example	65
Figure 59: Optical Properties, Opt. Gamma Selection Criteria and Extra Functions Panels.....	66
Figure 60: Other Properties and Save Results Panels from the Regularization Menu.....	66
Figure 61: Regularization Result GUI	67
Figure 62: Regularized Images Panel Form Regularization Result GUI.....	68
Figure 63: Original Images Panel from the Regularization Result GUI.....	68

Figure 64: Classification Maps Panel Form Regularization Result GUI.....	69
Figure 65: Performance Matrices GUI.....	69
Figure 66: Update Color Map Interface.....	70
Figure 67: Regularization Result GUI with a Reflectance plot of a certain pixel	70
Figure 68: Regularization Result GUI with multiple endmembers plotted	71
Figure 69: Information panel from the Regularization Result GUI.....	71
Figure 70: Region of Interest Tool GUI.....	72
Figure 71: AVIRIS Images: A and B selected from [1] to be processed.....	74
Figure 72: Improvement by modifying parameters – Image A LIGU without Bathymetry	76
Figure 73: Improvement by modifying parameters – Image B LIGU without Bathymetry	76
Figure 74: Improvement by modifying parameters – Image A CIUB without Bathymetry	77
Figure 75: Improvement by modifying parameters – Image B CIUB without Bathymetry	77
Figure 76: Endmember used for the 5 colors underwater unmixing processing.....	79
Figure 77: Endmembers used for 4 colors underwater unmixing processing.....	80
Figure 78: Baseline Classification Accuracy	83
Figure 79: Classification Accuracy of the 12.0 in without TiO ₂ Image using NA & 0.1 Gamma Res	84
Figure 80: Classification Accuracy of the 12.0 in without TiO ₂ using: NA & 0.01 Gamma Res	84
Figure 81: Classification Accuracy of the 12 in 0.5 g of TiO ₂ Image using: NA & 0.1 Gamma Res ..	85
Figure 82: Classification Accuracy of the 12 in 0.5 g TiO ₂ Image using NA & 0.01 Gamma Res	85
Figure 83: Classification Accuracy of the 12 in without TiO ₂ Image using DE & 0.1 Gamma Res...	86
Figure 84: Classification Accuracy of the 12 in without TiO ₂ Image using DE & 0.01 Gamma Res.	86
Figure 85: Classification Accuracy of the 12 in 0.5 g of TiO ₂ Image using DE & 0.1 Gamma Res...	87
Figure 86: Classification Accuracy of the 12 in 0.5 g of TiO ₂ Image using DE & 0.01 Gamma Res.	87
Figure 87: Example with Reduce Bands Obtained Accuracy after Regularization	88
Figure 88: Overall similarity improvement by Modifying Parameters.....	90
Figure 89: Similarity Improvement: Image A CIUB without Bathymetry	91
Figure 90: Similarity Improvement: Image B CIUB without Bathymetry	91
Figure 91: LIGU overall accuracy using the 12 in without TiO ₂ Image and 5 color endmembers.	92
Figure 92: LIGU overall accuracy using the 12 in without TiO ₂ Image and 4 color endmembers.	93
Figure 93: 12.0 in CIUB 5 Colors Blue Individual Accuracy	94
Figure 94: 12.0 in CIUB 4 Colors – Blue Individual accuracy.....	95
Figure 95: 12.0 in LIGU 5 Colors – Blue Individual accuracy.....	95
Figure 96: 12.0 in LIGU 4 Colors – Blue Individual accuracy.....	96

Figure 97: 12.0 in LIGU 5 Colors – Green Individual accuracy	96
Figure 98: 12.0 in LIGU 4 Colors – Green Individual accuracy	96
Figure 99: Blue and Green Endmember Spectral Signature and unmixing results.....	97
Figure 100: 12.0 in 0.5 g TiO ₂ LIGU 4 Colors –Individual accuracy	98
Figure 101: 12.0 in 0.5 g TiO ₂ LIGU 4 Colors –Individual accuracy	98
Figure 102: Comparative graph of baseline result with multiple TiO ₂ concentrations.....	99
Figure 103: 12.0 in Image Numerical Approximation Results Comparison with Baseline Results..	100
Figure 104: 12.0 in Image Derived Equations Results Comparison with Baseline Results	100
Figure 105: Multiple measure HSI images and Reconstructed ones with Regularization.....	102
Figure 106: Obtained spectral signature from the training regions showed on figure 106.....	102
Figure 107: 12.0 in 0.5 g TiO ₂ Image Numerical Approximations Results Comparison	103
Figure 108: 12.0 in 0.5 g TiO ₂ Image Derived Equations Results Comparison	103
Figure 109: 12.0 in Improvement by Regularization – Derived Equations	104
Figure 110: 12.0 in Improvement by Regularization – Numerical Approximations	104
Figure 111: 12.0 in 0.5 g TiO ₂ Improvement by Regularization – Derived Equations	105
Figure 112: 12.0 in 0.5 g TiO ₂ Improvement by Regularization – Numerical Approximations	105
Figure 113: Circular light pattern created by the lamp over the water with TiO ₂	106
Figure 114: Example of the Circular Patterns obtained on the Classification Maps	107
Figure 115: Dry Image to observed the light intensity variation over the white standard.....	107
Figure 116: A Linearly Obtained Regions; B Spectral Signatures of those regions.....	108
Figure 117: Reduced bands images result comparison – Minimum Gamma	108
Figure 118: Reduced bands images result comparison – Gamma of Minimum Error.....	109
Figure 119: Improvement by modifying parameters – Image A LIGU without Bathymetry	122
Figure 120: Improvement by modifying parameters – Image B LIGU without Bathymetry	123
Figure 121: Improvement by modifying parameters – Image A LIGU with Bathymetry	124
Figure 122: Improvement by modifying parameters – Image B LIGU with Bathymetry	125
Figure 123: Improvement by modifying parameters – Image A CIUB without Bathymetry	126
Figure 124: Improvement by modifying parameters – Image B CIUB without Bathymetry	127
Figure 125: Improvement by modifying parameters – Image A CIUB with Bathymetry	128
Figure 126: Improvement by modifying parameters – Image B CIUB with Bathymetry	129
Figure 127: Endmember Used for the 5 Colors processing	130
Figure 128: Enhanced color scale for reference.....	131
Figure 129: 12.0 in LIGU 5 Colors Overall accuracy graph	133

Figure 130: Endmembers used for 4 Colors processing	134
Figure 131: 12.0 in LIGU 4 Colors Overall accuracy graph	136
Figure 132: 12.0 in CIUB 5 Colors Overall accuracy graph	137
Figure 133: 12.0 in CIUB 4 Colors Overall accuracy graph	139
Figure 134: 12.0 in 0.5 TiO ₂ LIGU 4 Colors Individual Accuracy	141
Figure 135: 12.0 in 0.5 TiO ₂ CIUB 4 Colors Individual Accuracy	143
Figure 136: Baseline Result - Obtained Accuracy before Regularization	147
Figure 137: 12.0 in Classification Accuracy after Regularization: NA, Gamma Res: 0.1	148
Figure 138: 12.0 in Classification Accuracy after Regularization: NA, Gamma Res: 0.01	148
Figure 139: 12.0 in TiO ₂ Classification Accuracy after Regularization: NA, Gamma Res: 0.1.....	151
Figure 140: 12.0 in TiO ₂ Classification Accuracy after Regularization: NA, Gamma Res: 0.01.....	151
Figure 141: 12.0 in Classification Accuracy after Regularization: DE, Gamma Res: 0.1.....	154
Figure 142: 12.0 in Classification Accuracy after Regularization: DE, Gamma Res: 0.01.....	154
Figure 143: 12.0 in TiO ₂ Classification Accuracy after Regularization: DE, Gamma Res: 0.1	157
Figure 144: 12.0 in TiO ₂ Classification Accuracy after Regularization: DE, Gamma Res: 0.01	157
Figure 145: Example with Reduce Bands Obtained Accuracy after Regularization	161

List of Tables

Table 1: Material List.....	24
Table 2: Images names with their respective water levels and TiO ₂ amount	26
Table 3: Images Preprocessed – With different water levels.....	33
Table 4: Images Preprocessed – 12.0’’ with different TiO ₂ concentrations	34
Table 5: Masks created for each Region of Interest.....	39
Table 6: lsqnonlin parameters default value between MATLAB versions 2007 and 2013a.....	49
Table 7: Inputs Parameter of the Regularization Algorithm.....	55
Table 8: Optional Input Parameters for the Regularization Algorithm.....	56
Table 9: Result File Variables Descriptions	60
Table 10: Result’s SSE Differences LIGU of Image A without Bathymetry	75
Table 11: Configuration Descriptions.....	78
Table 12: LIGU results from the 12.0 in image without TiO ₂ and 5 color endmembers.....	79
Table 13: LIGU results from the 12.0 in without TiO ₂ image and 4 color endmembers.....	79
Table 14: CIUB results from the 12.0 in without TiO ₂ image and 5 color endmembers.....	80
Table 15 CIUB results from the 12.0 in without TiO ₂ image and 4 Color Endmembers	81
Table 16: LIGU results from the 12.0 in with 0.5 g TiO ₂ image and 4 colors endmembers	81
Table 17: CIUB results from the 12.0 in with 0.5 g of TiO ₂ Image and 4 Colors Endmembers	82
Table 18: Configuration Descriptions.....	92
Table 19: Euclidean Distance Classification after Regularization of the 12.0 in image.....	101
Table 20: Result LIGU w/o bathymetry and w/o Parameter Modifications	116
Table 21: Result LIGU with bathymetry and w/o Parameter Modifications	117
Table 22: Result LIGU w/o bathymetry and with Parameter Modifications: Water Properties.....	119
Table 23: Result LIGU with bathymetry and with Parameter Modifications: Water Properties.....	120
Table 24: Result’s SSE Differences LIGU of Image A without Bathymetry	122
Table 25: Result’s SSE Differences LIGU of Image B without Bathymetry	123
Table 26: Result’s SSE Differences LIGU of Image A with Bathymetry	124
Table 27: Result’s SSE Differences LIGU of Image B with Bathymetry	125
Table 28: Result’s SSE Differences CIUB of Image A without Bathymetry	126
Table 29: Result’s SSE Differences CIUB of Image B without Bathymetry	127
Table 30: Result’s SSE Differences CIUB of Image A with Bathymetry	128
Table 31: Result’s SSE Differences CIUB of Image B with Bathymetry	129

Table 32: LIGU 5 Color Endmembers Results.....	132
Table 33: 12.0 in 5 Color Endmember LIGU Results	133
Table 34: LIGU 4 Color Endmembers Results.....	135
Table 35: 12.0 in 4 Color Endmember LIGU Results	136
Table 36: 12.0 in 5 Color Endmember CIUB Results	137
Table 37: CIUB 5 Color Endmembers Results.....	138
Table 38: 12.0 in 4 Color Endmember CIUB Results	139
Table 39: CIUB 5 Color Endmembers Results.....	140
Table 40: 12.0 in 0.5 TiO ₂ 4 Colors Endmembers LIGU Results	141
Table 41: LIGU 12.0 in 0.5 g TiO ₂ Image with 4 Colors Endmembers.....	142
Table 42: 12.0 in 0.5 TiO ₂ 4 Colors Endmembers CIUB Results.....	143
Table 43: CIUB 12.0 in 0.5 g TiO ₂ Image with 4 Colors Endmembers.....	144
Table 44: Regularization Baseline Results Classification Maps	146
Table 45: 12.0 in Classification Maps after Regularization: NA, Gamma Res: 0.1	149
Table 46: 12.0 in Classification Maps after Regularization: NA, Gamma Res: 0.01	150
Table 47: 12.0 in TiO ₂ Classification Map after Regularization: NA, Gamma Res: 0.1	152
Table 48: 12.0 in TiO ₂ Classification Maps after Regularization: NA, Gamma Res: 0.01	153
Table 49: 12.0 in Classification Maps after Regularization: DE, Gamma Res: 0.1	155
Table 50: 12.0 in Classification Maps after Regularization: DE, Gamma Res: 0.01	156
Table 51: 12.0 in TiO ₂ Classification Maps after Regularization: DE, Gamma Res: 0.1	158
Table 52: 12.0 in TiO ₂ Classification Maps after Regularization: DE, Gamma Res: 0.01	159
Table 53: Baseline Results from the 12.0 in without TiO ₂ SVD40	160
Table 54: 12.0 in SVD40 Classification Maps after Regularization: DE, Gamma Res: 0.01	162

1 Introduction

1.1 Justification

This project is based on a toolbox named Hyperspectral Coastal Image Analysis Toolbox (HyCIAT) developed by Maria Torres Madroñero on the Laboratory for Applied Remote Sensing and Image Processing (LARSIP) and previous work by Luis O. Jiménez and Eladio Rodriguez which proposed a subsurface classification algorithm by means of regularization techniques. The justification of the toolbox and the regularization algorithm will be discussed on section 1.1.1 and 1.1.2 respectively.

1.1.1 HyCIAT Enhancement

In the Laboratory for Applied Remote Sensing and Image Processing (LARSIP) at the University of Puerto Rico – Mayaguez Campus researchers have developed different applications for the analysis of remote sensed hyperspectral images. Particularly a toolbox named Hyperspectral Coastal Image Analysis Toolbox (HyCIAT) was designed to perform analysis of hyperspectral images of shallow waters [1]. The interface, coded in MATLAB, implements three different algorithms based on the semi-analytical model proposed by Lee *et al.* [2], [3] which derive the inherent optical properties of the water column and bathymetry assuming that the whole bottom is sand. This algorithm was modified by Goodman [4] and Castrodad [5] to determine individual contributions to the measured signal of given spectra of materials that are known to be present on the ocean or sea floor. Individual contribution to the measured spectra are called “abundance”, and they are retrieved using unmixing algorithms. The objective of HyCIAT is to study the sea bottom using hyperspectral images. Its application includes: spatial and temporal monitoring of coral reef, subsurface object detection and classification, water quality monitoring, entertainment, coastal engineering, coastal science, etc. [8]

Due to the constant update of MATLAB’s native functions this toolbox ceases to work on MATLAB version over 2008b. The reason is that several default parameters of functions have been changed in different MATLAB versions and are no longer compatible to each other. Therefore, an update is proposed to make this toolbox work on MATLAB 2013a. Since there are some compatibility issues, this update will be accompanied by a comparative analysis between the results published on [1] and the ones obtained from the new version. Controlled experiments will be performed by simulating a benthic environment to test the Lee’s model combined with unmixing algorithms.

1.1.2 Regularization Algorithm

Previous studies in LARSIP by Professor Luis O. Jiménez and former graduate student Eladio Rodríguez-Díaz, have presented a subsurface classification algorithm by means of regularization techniques. This approach was applied for mapping coastal water floor based on the spectra of objects that are known to be present on the bottom. Preliminary results were promising on a laboratory controlled environment and on real hyperspectral images of benthic environments. Therefore, a more thorough evaluation of this algorithm as well as its implementation in MATLAB are proposed. This algorithm will be integrated to HyCIAT as another tool for the analysis, classification and mapping of the coastal water floor using remotely sensed hyperspectral images. This contribution will extend HyCIAT capabilities into concrete classification of the bottom reflectance based on *a priori* spectras¹.

1.2 Objectives

The objectives of this project are:

- Update HyCIAT to MATLAB 2013a.
 - Validate the results.
- Recode the regularization algorithms in MATLAB.
- Experimentation and validation of regularization algorithm.
- Integrate the regularization algorithm into HyCIAT.

1.3 Contributions of this Work

The contribution of this work can be defined by, but not limited to, these descriptions:

- Enable the use of the Hyperspectral Coastal Image Analysis Toolbox in a recent MATLAB version.
- Enhance HyCIAT usability by providing new tools and functionalities.
- Extends HyCIAT functionalities into concrete classification of underwater objects by means of regularization Techniques.

¹ Spectra or spectral signature can be defined as a unique representation of the amount light reflected on several wavelengths from an object.

- Establish an experimental procedure that can be used as baseline for future indoor/outdoor hyperspectral imaging experiment with a simulated benthic environment.
- Establish a mathematical procedure that can be used as a baseline for future studies on the empirically retrieval of optical properties: absorption and backscattering, coefficients of water, using Lee's equations and a HSI of a real or simulated benthic environment.
- Establish an algorithm for the future geometrical registration of HSI using a common tool among hyperspectral images researchers (MATLAB).
- Establish a baseline for future studies using HyCIAT. Especially on the regularization algorithm.

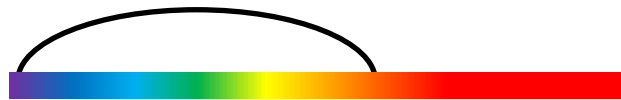
1.4 Thesis Outline

The rest of the thesis will be organized in the following manner: section 2 presents the theoretical background needed to understand the functionalities of this toolbox. It is not limited to just hyperspectral images, it also includes specific information about Spectral Unmixing, Lee Bio-optical Semi-Analytical model and underwater unmixing algorithms LIGU, CIUS and CIUB developed by Goodman and Castrodad. Also, on section 2, a detailed explanation of the regularization algorithm is presented. Section 3 will cover materials and methods including information of how the data was acquired and processed to obtain final results. Section 4 presents how HyCIAT was updated to MATLAB 2013a and enhanced by including the regularization algorithm and additional tools included for data processing. In sections 5 and 6 the results are presented and discussed. Conclusion and future work are presented on section 7. Section 9 is the appendix that include additional information.

2 Theoretical Background and Previous Publications

The study of benthic habitats by means of remotely sensed hyperspectral images has been in continuous development during the last four decades [9]–[15]. This is because hyperspectral images provide sufficient information for effective studies of these complicated environments [4], [12], [16]. Airborne or satellite hyperspectral sensors offer the ability to obtain spatial and temporal information over large areas, reducing the cost of conventional fields methods, thus making this technology essential for the studies of shallow water environments [17]. Hyperspectral imaging sensors measure reflected visible and non-visible light from objects by sampling the electromagnetic spectrum over hundreds of bands. Remotely sensed imageries are captured by digital spectrometers, which are instruments used to measure properties of light. The number of bands over which the imaging sensor samples the spectrum and their width determines what is called spectral resolution. There are three different types of spectral resolution in remote sensing imaging sensors as shown in figure bellow.

Panchromatic: One very big band



Multispectral: Several to tens of Bands



Hyperspectral: Hundreds of narrow continuous bands

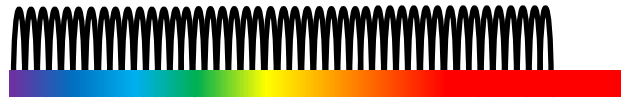


Figure 1: Comparison between three ways of sampling the spectrum

An example of a sensor with low spectral resolution is a **panchromatic** sensor, which is a sensor that measures the electromagnetic spectrum in a very wide band. Applications for panchromatic images are geological and topological mapping. Medium spectral resolution is commonly named **multispectral** resolution. Multispectral imagery is obtained from sensors that measure several to tens of bands of the electromagnetic spectrum. High resolution spectrometers are called **hyperspectral** sensors, which sample the electromagnetic spectrum in hundreds of narrow bands. Spectrometers resolution also varies in spatial or ground coverage per pixel. Spatial resolution can vary from less than a meter squared per pixel (QuickBird Panchromatic Sensor) up to 1000 of meter square per pixel (MODIS Multispectral Sensor). Airborne remote sensing of the earth surfaces adds

another resolution type to the data: temporal resolution. This attribute is very useful in the studies of temporal changes, i.e. change detection of specific habitats, mapping or measuring anthropogenic impact on nature and other applications that use past data to survey and compare changes of visible objects over time. [18]

The use of airborne hyperspectral sensor to study littoral underwater environment implies a very challenging task, due to diffusive and murky mediums like the atmosphere and the column of shallow coastal waters. A common shallow water remote sensed environment is showed in figure 2.

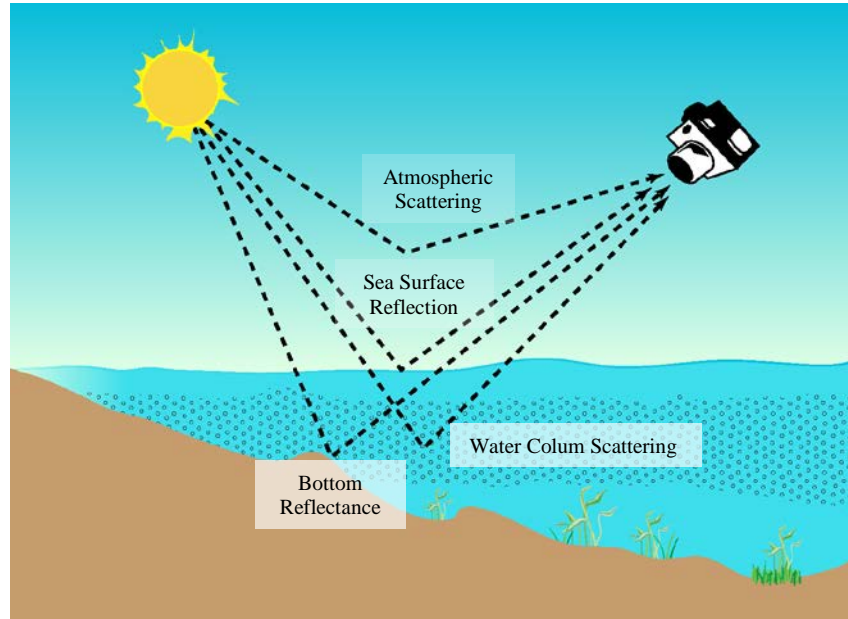


Figure 2: Typical remote sensed benthic environment

At the sensor, the measured reflectance usually includes scattered light from the atmosphere path radiance, specular reflection of the sun glint (sea surface reflection), water column scattering (due to dissolved matter particles and phytoplankton absorption) and the bottom reflectance. Scattered sunlight from the atmosphere and the water column typically contributes close to 90% of the at-sensor measured remote sensing reflectance ($R_{rs}^{at-sensor}$) [19].

For an effective study of shallow water environments using hyperspectral remotely sensed images, atmospheric correction algorithms must be applied to subtract the contribution of the atmosphere to the measured signal $R_{rs}^{at-sensor}$. With this correction, the measured signal is converted to remote sensed reflectance just above the water surface R_{rs} . R_{rs} includes contributions from the water column and the bottom reflectance. To study the bottom composition and classify it, the optical properties of the water column must be known or derived [20].

One the most commonly used algorithms for retrieval of the optical water properties and bathymetry is the one based on semi-analytical model developed by Lee *et al.* [2], [3] (referred here as the Lee's model). This algorithm is an inversion² model that uses optimization schemes to derive the optical properties of the water column and bathymetry based on the remote sensing reflectance just above the water and a sand input spectra normalized at 550nm. The optimization algorithm is a predictor-corrector, model-inversion scheme. One of its convenience is the fact that it doesn't require field measurements. The output is a solution vector γ that includes the following variables: the phytoplankton coefficient, absorption coefficient of gelbstoff and detritus, backscattering, the bottom albedo and the bottom depth. The optimization procedure does not solve for actual reflectance. Instead, it provides an approximation of the reflectance based on the input spectra at the 550 band. More details will be explained on section 2.2.

James A. Goodman integrated an additional layer of processing to the Lee's model to add a linear unmixing model³ to extract bottom composition. The bottom was modeled as a linear combination of different materials spectra. In Goodman's work three spectras were used: sand, coral and algae. The mentioned spectras were empirically measured, using underwater spectrometers, and were given to the algorithm. First, the optical properties of water were derived using Lee's method. The second step is to transform each input spectra to remote sensing reflectance just above the water surface by using Lee's forward model. As a final step, the transformed input spectras are used to unmix the original measured remote sensed reflectance at the water surface [4]. This method is called Lee's Inversion with Goodman's Unmixing (LIGU). LIGU algorithm will be explained in section 2.3.

Following Goodman's work, and also based on Lee's model, Castrodad proposed two algorithms. The Combined Inversion with Linear Unmixing at the Surface (CIUS) and the Combined Inversion with Linear Unmixing at the Bottom (CIUB) [5]. Both vary from LIGU by simulating the remote sensing reflectance as a linear mixture of the individual bottom types which were also sand, coral and algae. Castrodad models the remote sensing reflectance by multiplying each input spectra by the individual contribution of each one of them calculated from the unmixing algorithm. Then this approximation is used to calculate the error for the optimization scheme by subtracting it from the measured R_{rs} . Now, the main difference between CIUS and CIUB is where the unmixing is

² Inversion can be defined as a general methodology used to convert observed measurements into specific information of a physical object. For example, in this work, an inversion model is implemented to derive the optical properties of the water column from the remotely sensed measured spectra.

³ For an explanation of what is unmixing refer to section 2.1

performed. On CIUS the unmixing is performed at the water surface. Therefore, the water column contribution is added to the input spectra (coral, sand and algae). On CIUB the unmixing is performed at the bottom. Therefore, the water column contribution is subtracted from the measured remote sensing reflectance. CIUS will be explained on section 2.4 and CIUB will be explained on section 2.5.

These algorithms were integrated into a MATLAB toolbox called Hyperspectral Coastal Images Analysis Toolbox by Maria C. Torres-Madroño, with a focus on data fusion. Torres-Madroño integrates the toolbox into the mentioned platform and conducts studies focusing on the impact that bathymetry⁴ data collected using LIDAR had to results. It was observed that by adding this type of information their results improve significantly by eliminating one of the unknowns [1] from Lee's equation.

2.1 Spectral Unmixing

As explained in the work by Samuel Rosario-Torres, Spectral Unmixing is the process of decomposing the measured spectra into a collection of endmembers and a set of corresponding abundances [16]. Methods presented on [1], [4], [5] use linear unmixing schemes to determine the fractional abundances of each endmember to the measured or estimated spectra. Abundance can be explained as the fractional area that the endmembers occupies in the measured pixel [1].

The linear mixing model is given by:

$$b = \sum_{i=1}^n x_i a_i + w = Ax + w \quad (1)$$

where:

- b is a spectral signature based on a linear combination of endmembers.
- a_i is the spectral signature of the i^{th} endmember.
- x_i is the corresponding fractional abundance.
- w is the measurement noise.
- $A \in \mathbb{R}^{m \times n}$ where m is the number of spectral bands and n is the number of endmembers.

⁴ Bathymetry can be defined as the studies of the depth of water bodies.

In order for the fractional abundances to have physical meaning, the unmixing problem must satisfy the non-negative constrain: $x_i \geq 0$ for all i . Rosario-Torres on [16] adds two other constraints

1) Sum to one:

$$\sum_{i=1}^n x_i = 1 \quad (2)$$

2) And, in order to allowed a dark pixel [5], sum less or equal to one:

$$\sum_{i=1}^n x_i \leq 1 \quad (3)$$

The constraint described in equation 2 was developed in an algorithm called Non-Negative Sum To One (**NNSTO**) and the constraint described in equation 3 was developed in an algorithm called Non-Negative Sum Less or equal to One (**NNSLO**).

NNSTO algorithm solve the following problem:

$$\tilde{x} = \arg \min \|Ax - b\| \text{ subject to } x \geq 0 \text{ and } \mathbf{1}^T x = 1 \quad (4)$$

NNSLO algorithm solve the following problem:

$$\tilde{x} = \arg \min \|Ax - b\| \text{ subject to } x \geq 0 \text{ and } \mathbf{1}^T x \leq 1 \quad (5)$$

where $\mathbf{1}$ is a vector of ones of dimension N . It is important to say that matrix A is recalculated on every pixel to include the effect of the optical properties of water. The method to retrieve these properties is described on section 2.2.

Through the rest of this document the unmixing algorithms are going to be abbreviated as:

$$\tilde{x} = \text{Unmix}(A, r_{rs}) \quad (6)$$

Where:

- $A \in \Re^{m \times n}$, m is the number of spectral bands and n is the number of endmembers.
- r_{rs} is the measured spectral signature.
- \tilde{x} is the estimated fractional abundances of given endmembers to the measured signal.

2.2 Lee's Bio-optical Semi-analytical model

The Lee's model proposes an invertible equation for estimating the hyperspectral remote sensing reflectance of shallow waters just above the water surface [2], [3]. The model relates R_{rs} as follow:

$$R_{rs} = f[a, b_b, \rho, H, \theta_w, \theta, \varphi] \quad (7)$$

Where:

- a is the absorption coefficient.
- b_b is the backscattering.
- ρ bottom albedo.
- H is the bottom depth.
- θ_w is the subsurface solar zenith angle.
- θ is the subsurface viewing angle from nadir.
- φ is the azimuth angle.

R_{rs} is defined as the ratio of water leaving radiance to surface reflected irradiance.

$$R_{rs} = \frac{0.5r_{rs}}{1 - 1.5r_{rs}} \quad (8)$$

where r_{rs} is the subsurface remote sensing reflectance or the ratio of the upwelling radiance to the down-welling irradiance just below the water surface. r_{rs} is defined as the sum of the scattered light from the water column and the reflected light from the bottom.

$$r_{rs} = r_{rs}^C + r_{rs}^B \quad (9)$$

$$\hat{r}_{rs} = r_{rs}^{dp} \left(1 - \exp \left\{ - \left[1 + \frac{D_u^C}{\cos(\theta_w)} \right] kH \right\} \right) + \frac{1}{\pi} B\rho \exp \left\{ - \left[1 + \frac{D_u^B}{\cos(\theta_w)} \right] kH \right\} \quad (10)$$

where: r_{rs}^{dp} is the remote sensing reflectance for optically deep water defined as:

$$r_{rs}^{dp} \approx (0.084 + 0.170u)u \quad (11)$$

D_u^C and D_u^B are the path of elongation factor for scattered photons from the water column and bottom respectively defined as:

$$D_u^C \approx 1.03(1 + 2.4u)^{0.5} \text{ and } D_u^B \approx 1.04(1 + 5.4u)^{0.5} \quad (12)$$

with

$$u = b_b / (a + b_b) \text{ and } k = a + b_b \quad (13)$$

and

$$b_b = b_{bw} + b_{bp} \quad (14)$$

$$a = a_w + a_\phi + a_g \quad (15)$$

Where a_g is the absorption coefficient of gelbstoff ⁵ and a_ϕ is the absorption coefficient of phytoplankton pigments defined as:

$$a_g = G \exp\{0.014(\lambda - 440)\} \quad (16)$$

$$a_\phi = [a_0(\lambda) + a_1(\lambda) \ln(P)]P \quad (17)$$

And b_{bp} is the backscattering coefficient of suspended particles and b_{bw} is the backscattering coefficient of seawater both are defined as:

$$b_{bp} = BP \left(\frac{400}{\lambda} \right)^Y \quad (18)$$

$$b_{bw} = 0.0038 \left(\frac{400}{\lambda} \right)^{4.3} \quad (19)$$

Y is the spectral shape parameter estimated by the following relationship (Y is kept within the 0 to 2.5 range) [3]:

$$Y \approx 3.44(1 - 3.17 \exp[-2.01R_{rs}(440)/R_{rs}(490)]) \quad (20)$$

All the equation above, leaves the Lee's model as a function parameterized by the following five unknowns: P, G, BP, B, H .

Where:

- P is the phytoplankton coefficient.
- G is the absorption coefficient of gelbstoff and detritus.
- BP is the backscattering.
- B is the bottom albedo.
- H is the bottom depth.

It is important to mention that, in the original Lee's method, ρ is a 550 normalized sand spectrum. This is because the original model was not intended to estimate bottom reflectance. Instead, it was developed to study the inherent optical properties of the water column. The model assumed that the whole bottom was sand.

To solve for all the unknown, the following nonlinear least squares optimization problem must be solved:

⁵ Gelbstoff are colored dissolved organic matter.

$$\hat{\gamma} = \min \frac{\|R_{rs} - \hat{R}_{rs}(\gamma, \rho_{sand})\|_2^2}{\|R_{rs}\|_2^2} \quad (21)$$

Where γ is the solution vector and the optimization is performed using bands from 400nm to 675nm and from 750nm to 830nm.

2.3 Lee's Inversion with Goodman's Unmixing (LIGU)

Goodman took advantage of the spectral separability of different components of hyperspectral imagery to add a linear mixing model to Lee's Model to extract bottom composition. The first step is to obtain the solution vector γ with Lee's Model, then use it to add the water column contribution to each endmember (input spectra) and perform the unmixing with the original measured reflectance. The algorithm block diagram is shown on figure 3.

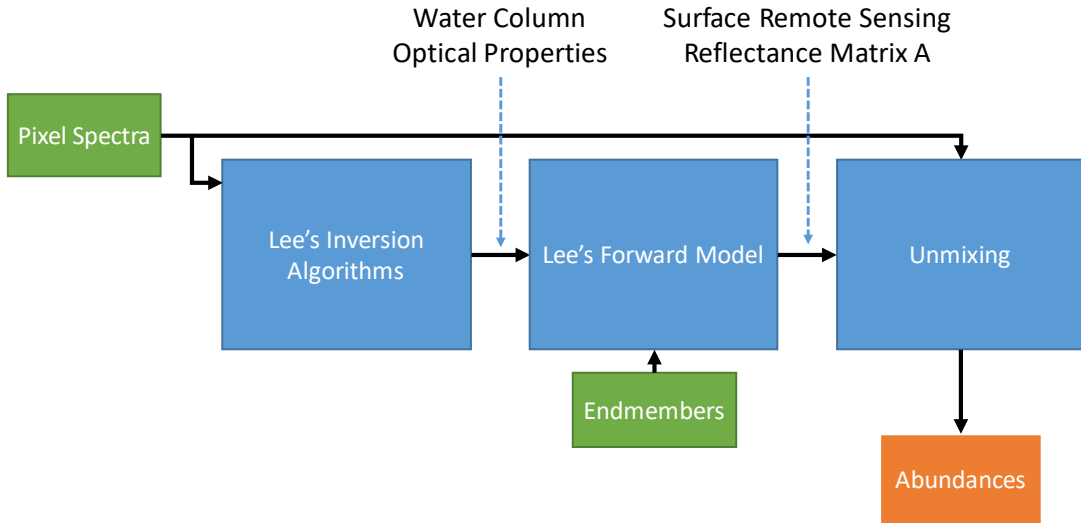


Figure 3: LIGU Block Diagram

2.4 Combined Inversion with Linear Unmixing at the Surface (CIUS)

Unlike LIGU, CIUS estimates the water optical properties, bathymetry and abundances together by modeling the remote sensing reflectance just above the water surface as:

$$\hat{R}_{rs} = A\hat{x} = \sum_{i=1}^3 x_i \bar{R}_{rs}(\rho_i, \gamma) \quad (22)$$

where A is a transformed endmembers matrix. Each column of A corresponds to a transformed endmember spectral signature to surface remote sensing reflectance. This transformation is performed by adding the water column contribution to each endmember. An endmember is the reflected light from the pure surface of a specific material measured by a spectrometer. \hat{x} is the

abundances vector obtained by unmixing endmember matrix A with R_{rs} and ρ_i is the i^{th} endmember. The Abundance vector contains the weight that represents the individual contribution of each endmember to the measured R_{rs} . \hat{R}_{rs} is the modeled remote sensing reflectance just above the water surface.

The error for the optimization scheme is:

$$error = R_{rs} - \hat{R}_{rs} \quad (23)$$

The optimization problem is the following:

$$(x, \gamma) = \min_{\gamma, x} \frac{\frac{1}{2} \|R_{rs} - \hat{R}_{rs}\|_2^2}{\|R_{rs}\|_2^2} \quad (24)$$

For each iteration, the algorithm uses the solution vector γ to add the water column to each endmember. Then, these transformed endmembers are unmixed with the measured R_{rs} to obtain abundance vector x . After that the remote sensing reflectance \hat{R}_{rs} is modeled as in (22) and the error is calculated as in (23). See the following figure for the block diagram of this algorithm:

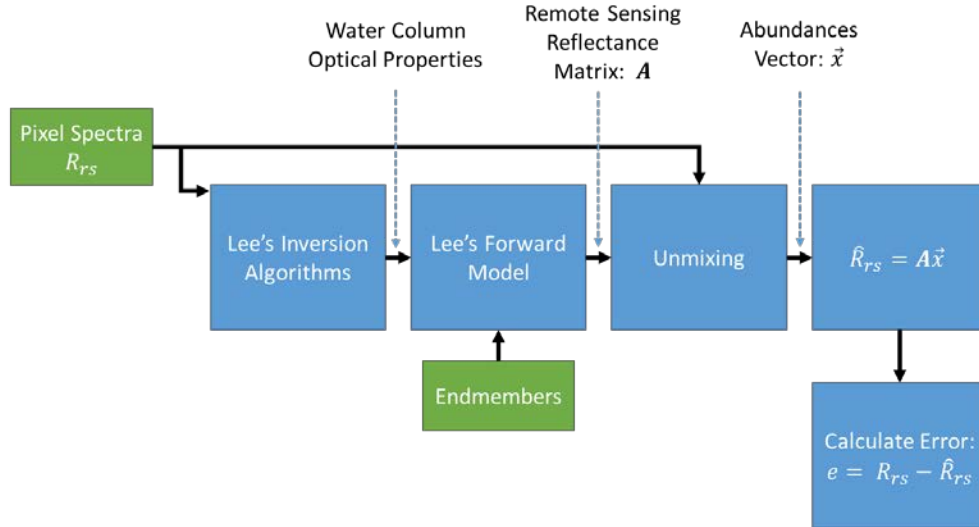


Figure 4: CIUS Block Diagram

2.5 Combined Inversion with Linear Unmixing at the Bottom (CIUB)

Unlike CIUS, CIUB tries to fit the subsurface remote sensing reflectance r_{rs} . CIUB uses the Lee's model to approximate the water column optical properties. The model is based on the optimization (i.e., minimization) of the following error.

$$error = r_{rs} - \hat{r}_{rs} \quad (25)$$

where

$$r_{rs} = \frac{R_{rs}}{0.5 + 1.5R_{rs}} \quad (26)$$

Following Lee's Model, subsurface remote sensing reflectance can be model as:

$$\hat{r}_{rs} = r_{rs}^{dp} \left(1 - \exp \left\{ - \left[1 + \frac{D_u^C}{\cos(\theta_w)} \right] kH \right\} \right) + \frac{1}{\pi} B\rho \exp \left\{ - \left[1 + \frac{D_u^B}{\cos(\theta_w)} \right] kH \right\} \quad (27)$$

and can be modified by reconstructing the bottom in the following way: $\rho = A\vec{x}$. For each iteration, the water column contribution is subtracted from the measured r_{rs} as follows:

$$\hat{r}_{rs} - r_{rs}^{dp} \left(1 - \exp \left\{ - \left[1 + \frac{D_u^C}{\cos(\theta_w)} \right] kH \right\} \right) = \frac{a_i^T}{\pi} \exp \left\{ - \left[1 + \frac{D_u^B}{\cos(\theta_w)} \right] kH \right\} \quad (28)$$

where a_i^T is the i^{th} row of endmember matrix A . Taking the left-hand side of the last equation as b , and the right-hand side is the i^{th} row of A :

$$b = r_{rs} - r_{rs}^{dp} \left(1 - \exp \left\{ - \left[1 + \frac{D_u^C}{\cos(\theta_w)} \right] kH \right\} \right) \quad (29)$$

$$\hat{a}_i = \frac{a_i}{\pi} \exp \left\{ - \left[1 + \frac{D_u^B}{\cos(\theta_w)} \right] kH \right\} \quad (30)$$

Then, the linear mixing model can be applied in the following way:

$$\hat{x} = \text{unmix}(A, b) \quad (31)$$

The optimization problem is the following:

$$(\hat{x}, \hat{\gamma}) = \min_{\gamma, x} \frac{\frac{1}{2} \|r_{rs} - \hat{r}_{rs}(\gamma, \rho)\|_2^2}{\|r_{rs}\|_2^2} \quad (32)$$

Figure 5 below shows a block diagram that explains the operation of the CIUB algorithm:

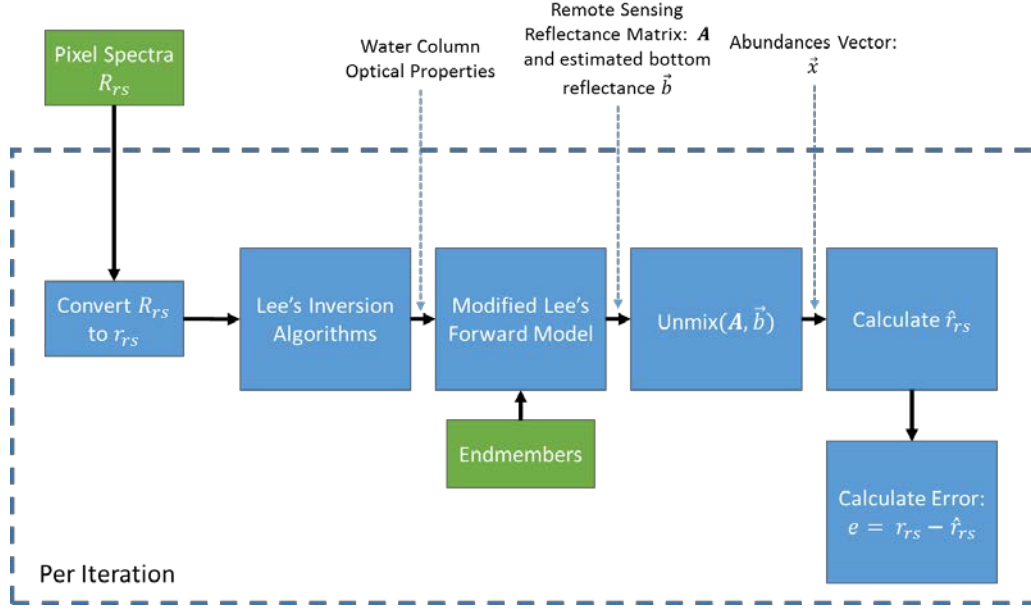


Figure 5: CIUB Block Diagram

2.6 Regularization Algorithm

Luis O. Jiménez and Eladio Rodríguez-Díaz proposed a subsurface classification algorithm by means of regularization techniques. It was developed into a thesis by Rodríguez-Díaz in [6]. Regularization is a method commonly used to solve ill posed or rank deficient problems. An ill posed problem is one where small perturbations in the data cause large perturbations in the solution. Moreover, rank deficiency is caused by linearly dependent rows and columns in the data. This work is also based on the Lee's Model described on section 2.2 of this document.

Recalling the surface remote sensing reflectance is expressed in the following way:

$$R_{rs} = f[a, b, \rho, H, \theta_w] \quad (33)$$

Where: also, as proposed by Lee's Model, the surface remote sensing reflectance is defined as:

$$R_{rs} = \frac{0.5\hat{r}_{rs}}{1 - 1.5\hat{r}_{rs}} \quad (34)$$

where \hat{r}_{rs} is the estimated subsurface remote sensing reflectance defined as:

$$\hat{r}_{rs} = r_{rs}^{dp} \left(1 - \exp \left\{ - \left[1 + \frac{D_u^C}{\cos(\theta_w)} \right] kH \right\} \right) + \frac{1}{\pi} \rho \exp \left\{ - \left[1 + \frac{D_u^B}{\cos(\theta_w)} \right] kH \right\} \quad (35)$$

with

$$r_{rs}^{dp} \approx (0.084 + 0.170u)u \quad (36)$$

$$D_u^C \approx 1.03(1 + 2.4u)^{0.5} \text{ and } D_u^C \approx 1.04(1 + 5.4u)^{0.5} \quad (37)$$

and

$$u = \frac{b}{a+b} \text{ and } k = a + b \quad (38)$$

Note: ρ , a and b are wavelength dependent.

Now, Lee's Model can be reformulated in a matrix form as follows:

$$b = AP = \begin{bmatrix} b(\lambda_1) \\ b(\lambda_2) \\ \vdots \\ b(\lambda_d) \end{bmatrix} = \begin{bmatrix} r_{rs}(\lambda_1) - S_{col}(\lambda_1) \\ r_{rs}(\lambda_2) - S_{col}(\lambda_2) \\ \vdots \\ r_{rs}(\lambda_d) - S_{col}(\lambda_d) \end{bmatrix} = \begin{bmatrix} a_{11} & 0 & \cdots & 0 \\ 0 & a_{22} & \cdots & 0 \\ \vdots & \vdots & \cdots & \vdots \\ \vdots & \vdots & \cdots & \vdots \\ 0 & 0 & \cdots & a_{dd} \end{bmatrix} \begin{bmatrix} \rho(\lambda_1) \\ \rho(\lambda_2) \\ \vdots \\ \rho(\lambda_d) \end{bmatrix} \quad (39)$$

where a_{ii} is defined as:

$$a_{ii} = \frac{1}{\pi} \exp \left\{ - \left[1 + \frac{D_u^B}{\cos(\theta_w)} \right] kH \right\} \quad (40)$$

and

$$S_{col} = r_{rs}^{dp} \left(1 - \exp \left\{ - \left[\frac{1}{\cos(\theta_w)} + D_u^C \right] kH \right\} \right) \quad (41)$$

is the water column contribution at λ_i wavelength. The inverse solution can be found using Tikhonov Regularization[6], [7]. Then, the problem is expressed in the following way:

$$P_{reg} = \arg \min \{ \|AP - b\|_2^2 + \eta^2 \|P - P_0\|_2^2 \} \quad (42)$$

and its solution is:

$$P_{reg} = (A^T A + \eta^2 I)^{-1} (A^T b + \eta^2 P_0) \quad (43)$$

The mathematical expression for each component of P_{reg} is:

$$\rho_{reg}(\lambda) = \frac{a_i^2(\lambda)}{a_i^2(\lambda) + \eta^2} \frac{r_{rs}(\lambda_1) - S_{col}(\lambda_i)}{a_i(\lambda)} + \frac{\eta^2}{a_i^2(\lambda) + \eta^2} \rho_0 \quad (44)$$

where ρ_0 is the spectral signature of individual objects of interest and η^2 is expressed as:

$$\eta^2 = \frac{\gamma}{1 - \gamma} \text{ with } \gamma \in [0,1). \quad (45)$$

where γ is the regularization parameter and is selected one per endmember per pixel. The bigger the regularization parameter the more similar P_{reg} will be to P_0 . Equations from 33 to 45 enable the

estimation of $\rho(\lambda)$ considering uncertainties present in the observation. $\rho(\lambda)$ will be used to detect our object of interest [6]. a and b are optical properties of the water column and, in this project, were retrieved using a special method described on section 3.4.

The spectral signature of the bottom ρ_0 and the regularization parameter γ needs special considerations for several reasons:

- These two parameters affect significantly the result of the algorithm.
- There can be multiple bottoms since it is common, in classification problems, to have more than two objects of interest.
- There is not a specific method to select the regularization parameter γ since it depends on the problem and usually is determined by *ad hoc* methods, particularly designed just for the current problem.

For these reasons, the algorithm proposed by Rodriguez [6] includes an automatic method that select the optimum bottom (ρ_0) from the given endmembers and the optimum regularization parameter (γ), based on the point of maximum curvature of the error function between the obtained P_{reg} and the given endmembers. The point of maximum curvature is selected because is the point that produce a small enough (γ) that also produce a small error as by Rodriguez in [6]. This methodology is going to be described in the next section.

2.6.1 Selecting the Optimum Bottom and the Optimum Regularization Parameter

While inverting the k^{th} pixel in the hyperspectral image using the i^{th} spectral signature from the objects of interest, the optimum γ will be selected based on **the point of maximum curvature** of the following error function:

$$E_{k,i}(\gamma) = \|P_{reg(k)} - P_{o(i)}\|_2^2 \quad (46)$$

that is calculated in the following way:

$$\gamma_{opt_{k,i}} = \arg \max_i \left\{ \frac{E(\gamma)''}{(1 + (E(\gamma)')^2)^{3/2}} \right\} \quad (47)$$

Where γ is a value from 0 to 1 and

$$\frac{E(\gamma)''}{(1 + (E(\gamma)')^2)^{3/2}} \quad (48)$$

is defined as the curvature for the current γ . The mathematical procedure to obtain $\gamma_{opt_{k,i}}$ will be explained on section 3.5. Once all the $\gamma_{opt_{k,i}}$ has been calculated for each endmember, the image is then inverted using one of the following possibilities:

1. The class and γ that produce the smallest $\gamma_{opt_{k,i}}$

$$\gamma = \min(\gamma_i), \text{ where } i = 1, 2, \dots, n \quad (49)$$

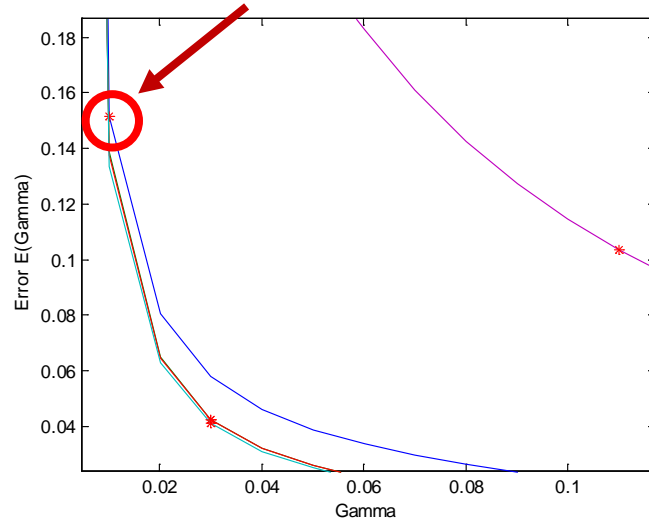


Figure 6: Example of choosing γ that produce the smallest $\gamma_{opt_{k,i}}$

2. By choosing the class and γ that produce the smallest error E_k .

$$\gamma = \arg \min_{\gamma_i} (E_k(\gamma_i)), \text{ where } i = 1, 2, \dots, n \quad (50)$$

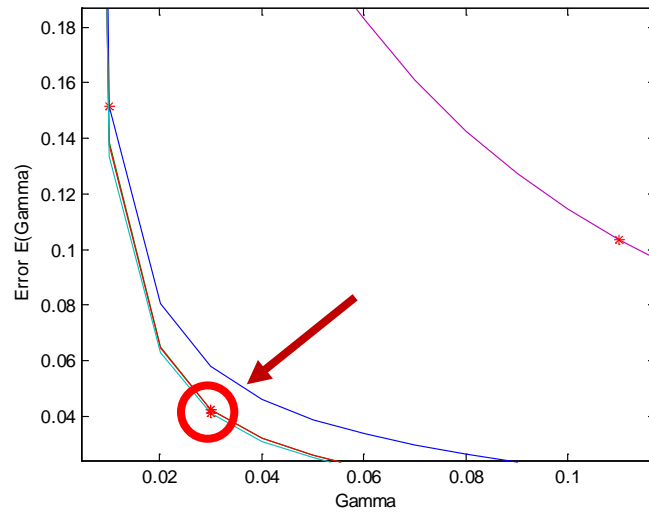


Figure 7: Example of choosing γ that produce the smallest error per pixel

After selecting the class and γ the image is re-inverted and can be classify using any classification method. The selected classification algorithms for this project are explained on section 3.6.

2.6.2 Pseudo Code

The regularization algorithm operates in the following way:

- **For each pixel**
 - Convert R_{rs} to r_{rs}
 - **For each endmember**
 - **For each regularization parameter**
 - **For each wavelength (λ)**
 - Invert pixel using endmember and current γ .
 - Calculate error between P_{reg} and current endmember P_0
 - Calculate point of maximum curvature of the error curve
 - Select γ and optimum bottom either based on the point of maximum curvature or the point of the minimum error.
 - Invert using γ and Optimum Bottom
 - Classify

2.7 TiO₂ – Titanium Dioxide

Titanium dioxide (TiO₂) is an odorless, insoluble, inflammable, chemically inert, non-toxic white solid chemical compound with interesting optical properties. TiO₂ has one of the highest refractive index among materials known to man. It's a Lambertian reflector [21] and its reflectance is almost perfect on the visible region (See figure 8). Around 1930 was discovered its photolytic activity and, since then, the number of studies has been increasing significantly. Its wide list of applications includes sunscreen lotions, paints, environmental decontamination, self-cleaning surfaces, water purification, solar cells, photocatalists, biocides, food, and many more. [22]–[28]

TiO₂ is being used in this project as light scattering agent. Since the compound is insoluble the particles will be suspended on the water column and will scatter the light in all direction making it difficult for the hyperspectral camera to measure the reflected light from the bottom of a water tank.

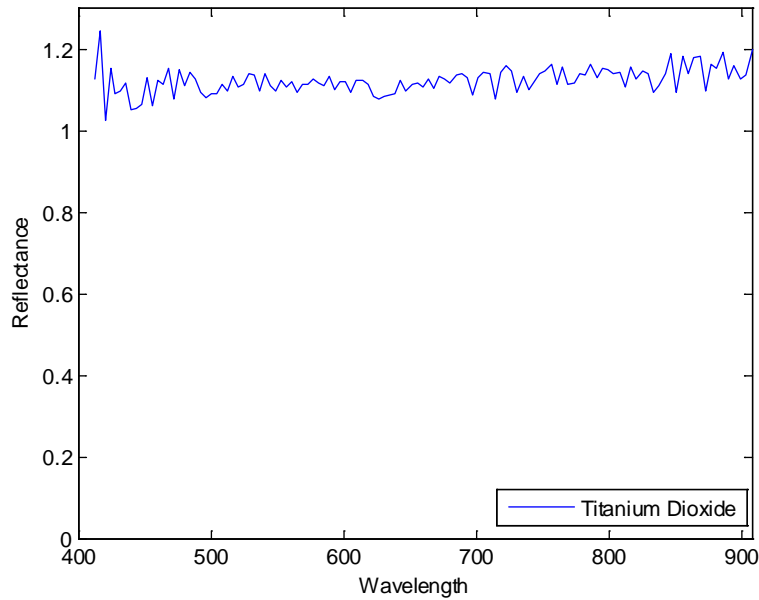


Figure 8: Measured Reflectance of TiO₂

2.8 HyCIAT 2007

HyCIAT 2007 is a toolbox developed using MATLAB 2007a for the estimation of the water optical properties, bathymetry and fractional abundances of the bottom using a hyperspectral image of shallow waters. After MATLAB 2008b this algorithm seized to work due to changes in defaults parameters of some MATLAB's native functions across MATLAB versions. One of the main objectives of this project was to update and enhance this legacy toolbox to use it on a more recent MATLAB platforms. This section will name and described the important interfaces as they will be named through the rest of the document.

HyCIAT's main interface is showed in figure 9. It contains a toolbar on the top with all the included functionalities, processing algorithms and tools. For example, it has a scroll bar to browse through the image. Also, it has some tools to visualize the image either by creating an RGB composite or by automatically calculating a true color image of it.

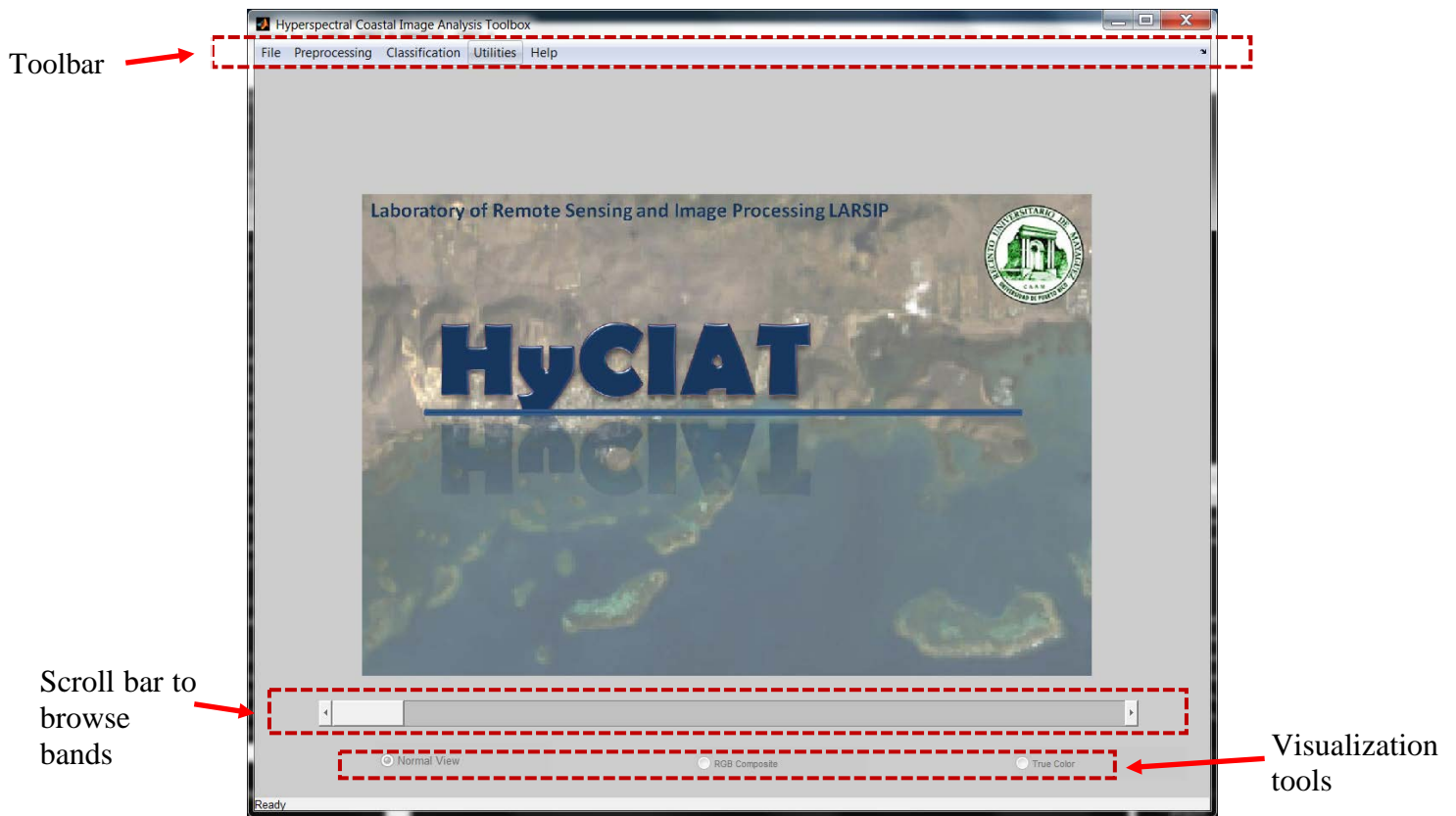


Figure 9: Main Interface

The integration of Lee based algorithms: LIGU, CIUS and CIUB algorithms into the toolbox was performed in the following way:

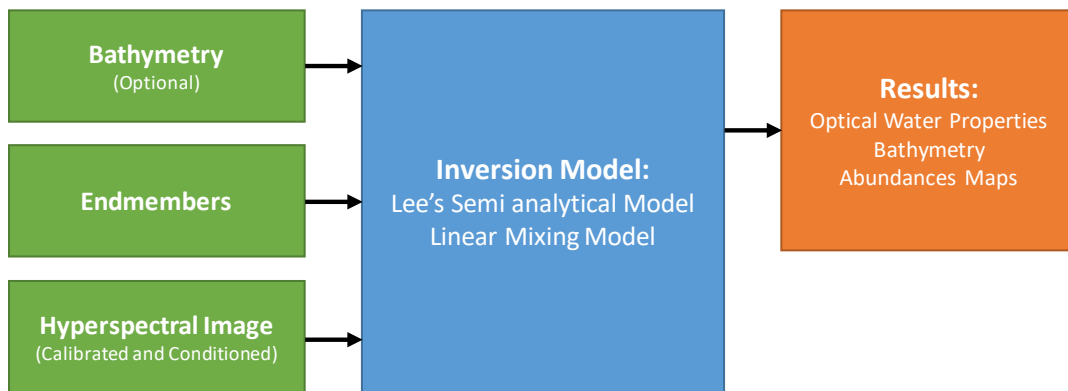


Figure 10: Block diagram of the implementation of the unmixing algorithms into HyCIAT[1]

The HSI before being process needs to be converted into reflectance and corrected. Remotely sensed hyperspectral images of shallow environments usually are corrected in two ways: atmospherically and the sun glint must be removed. The field spectra and the spectral endmembers are inputs to the inversion model implemented that retrieve the water column properties and

calculated the fractional abundances of each endmember to the measured spectra. The toolbox was developed and tested using three endmembers: sand, coral and algae by Torres-Madroño on [1]. Also, on the same work, it was demonstrated that results can be improved by integrating LIDAR derived bathymetry by eliminating one unknown from the inversion algorithm.

The inversion model needs another set of parameters to work, they are adjusted before the algorithm start in an interface called “Initial Parameters” showed on figure 11. As can be observed in the mentioned figure, the interface consists of initial values, optimization parameters, tools to select the abundances algorithms, tools to select the optimization algorithm and finally tools to include bathymetry data (data fusion). This interface was modified on this project to increase functionality and to include new features (see section 4.1).

At the end of every process, the interface showed in figure 12 shows the result in a graphical format. The Results interface includes tools to browse through the results where they can be visualized with the use of color pallets and color bars. The interface has two types of results: 1) the optical properties and 2) the fractional abundances of each endmember to the measured signal. Abundances can be visualized also by creating RGB composite by assigning an endmember to a certain RGB band.

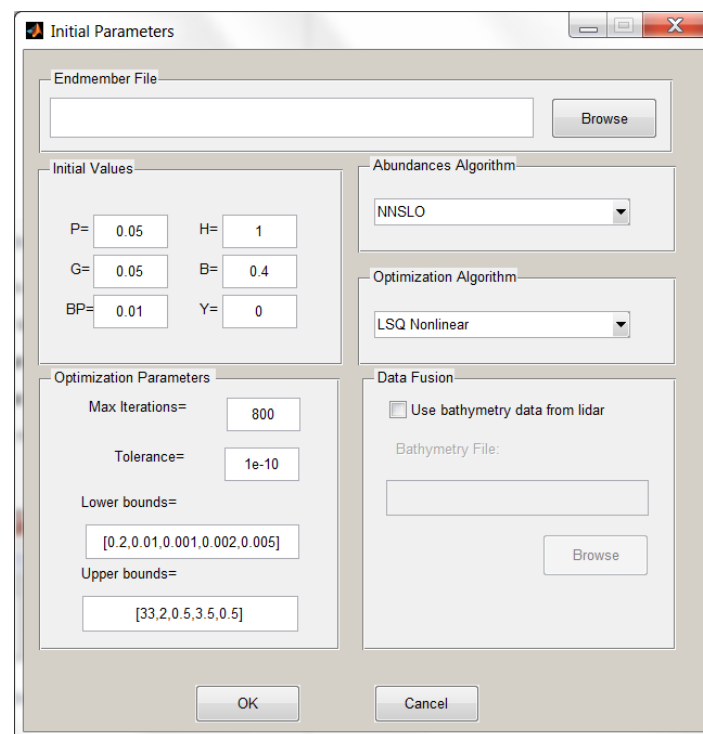


Figure 11: Initial Parameters Interface (HyCIAT 2007)

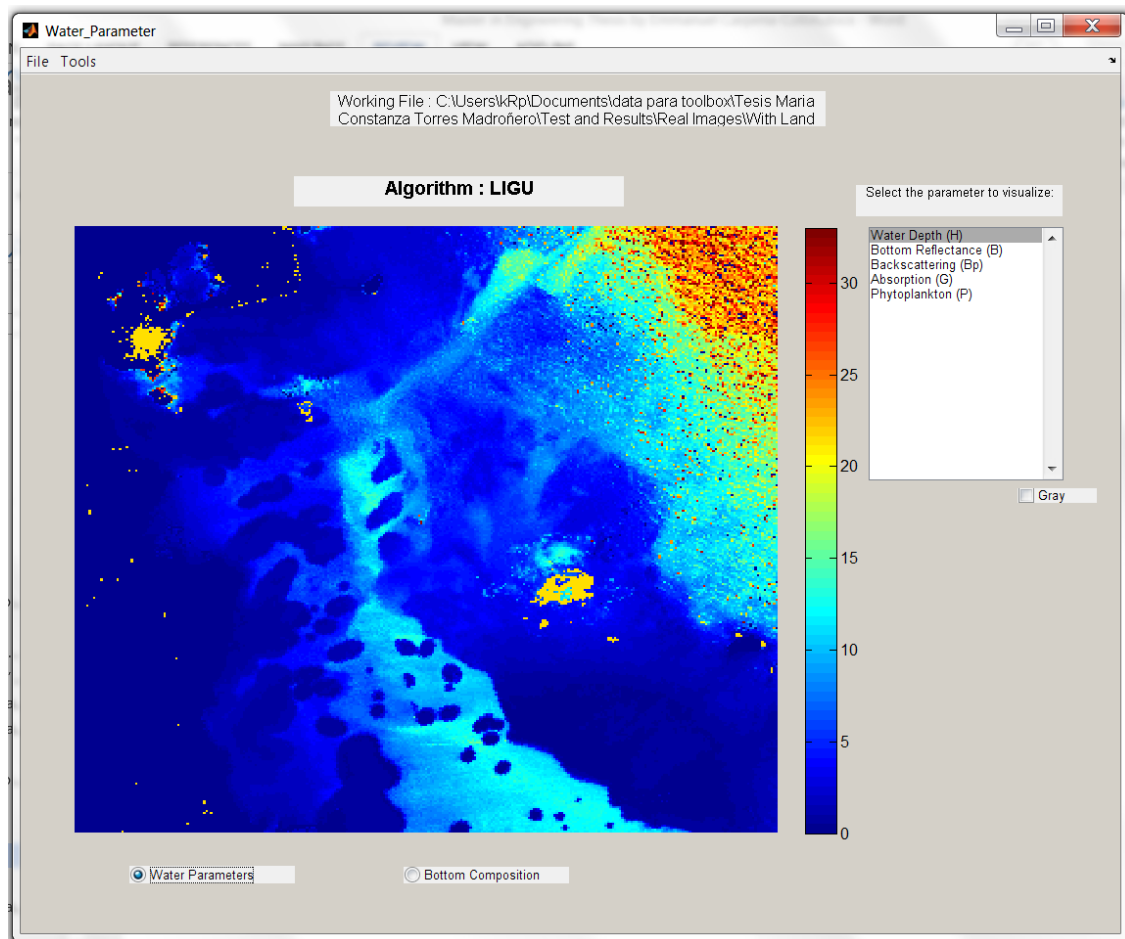


Figure 12: Results interface

3 Materials and Methods

This project consisted of two main software development aspects. The first one is the enhancement of a legacy toolbox named HyCIAT. The enhancement includes updating several functions that already were implemented on [1] but ceased to work after MATLAB 2008b. Other changes ensures better usability and result compatibility between the ones published in [1] and the ones obtained in this new version of the toolbox. Moreover, the second software development aspect includes the integration of a new algorithm of classification based on regularization techniques. The methodology and background, of this new algorithm, were developed by Luis O. Jiménez and its former graduate student Eladio Rodriguez [6]. Furthermore, additional tools and functions to manage HSI, create and save endmember files, manipulate regions of interest and extract its data for later processing were also integrated into the updated version of the toolbox.

An experiment was performed, to have a dataset to validate the new algorithms and tools, using a water tank with a fixed bottom and multiple layers of water. Also, this dataset consists of a controlled environment in a tank. A light scattering agent was added to the water to resemble a more realistic environment of coastal shallow waters (See section 2.7 for details on the chemical compound used).

The next section (section 3.1) will explain and describe the experiment performed to obtain the new dataset, including the experimental setup and how it was conducted. The succeeding section (section 3.2) will explain the needed pre-processing of the image for the validation of the algorithms. The specific procedure to retrieve empirically a and b , which are needed parameters of Lee's algorithm discussed on section 2.3, will be described on section 3.4. How the Regions of Interest⁶ (**ROI**) were selected will be explain in section 3.3 including the ROIs that were selected and used to validate the algorithm. The two different methods used to calculate the Maximum Curvature will be discussed on section 3.5. On section 3.6 the different classification methods used to validate the regularization algorithm are explained.

3.1 Dataset Acquisition for Validation Data

An experiment was performed in a laboratory controlled environment to obtain a unique dataset for the validation of the algorithms. The experiment consists of a water tank with a fixed bottom and multiple layers of water. TiO_2 was added to the water as a scattering agent in order resemble a more realistic environment. With this data set the optical properties " a " and " b " are going to be

⁶ ROI are specific regions of the HSI that are being studied usually represent a single object.

empirical derived (see section 3.4). Also, this data set is used to test the accuracy obtained from the classification algorithms. On the following section materials, setup and the experimental procedure will be discussed.

3.1.1 Materials

The following materials were used to perform the experimental procedure that will be discussed in the following section:

Table 1: Material List

Material Name	Material Name
1. Plastic Tank	8. White Standard (99.9%)
2. Dark Spray Paint	9. Lamp
3. Laminated Bottom	10. Tungsten Light Bulb
4. Water	11. Titanium Dioxide
5. 1 Gallon Water Bottle	12. Transparent Tape
6. Ruler	13. Computer
7. Hyperspectral Camera SOC 700 with Tripod	14. Data Acquisition Equipment

3.1.2 Experimental Setup

The experiment was performed in a closed room sealed from sunlight. A bottom sample was prepared to have a known object in the bottom of tank. The bottom sample consists of four color regions (red, yellow, green and blue) printed on a standard sheet (8 in by 11 in). The object was laminated and taped to the bottom of the tank and the white standard ⁷ was placed in the center of it, see figure 13. The white standard was then used for calibration purposes and retrieving empirically the absorption and backscattering vectors: " a " and " b ".

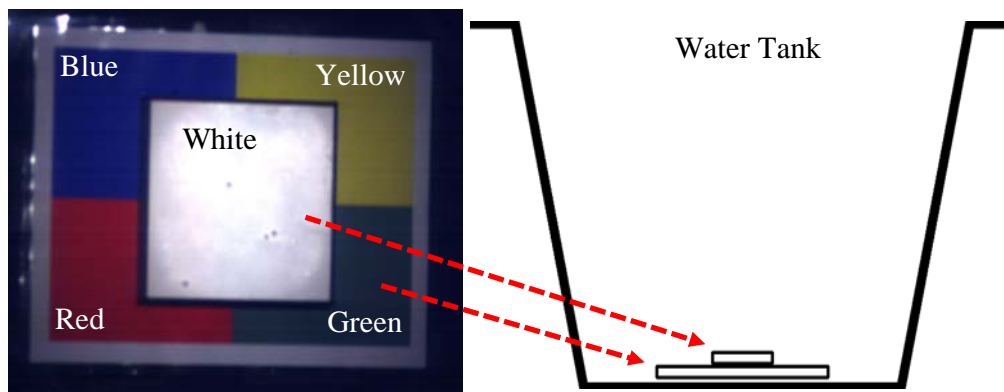


Figure 13: Known bottom with the white standard over it

⁷ White standard, also known as calibration standard, is an object used to measure the amount of light that is reaching the surface of the object being imaged. The calibration standard used on this work reflects 99.9% of the incident light over it. The measured light over this region on the image without the effect of water is then used to calibrate all the images (see section 3.2).

The Hyperspectral Camera, the water tank and the lamp were carefully placed to avoid glint over the region of interest. The tank was painted with non-gloss black paint spray. See figure 14 for the image of the setup. The setup was marked and never moved during the experiment.



Figure 14: Image of the setup

3.1.3 Experimental Procedure

The purpose of the experiment was to obtain a data set from a controlled environment to be used to validate the algorithms and to study the effect of water and TiO_2 on the measured reflectance from the bottom. The setup was fixed and never moved during the whole experiment. The experimental setup were configured to avoid glint over the colored regions of the sample. The room air conditioner's air stream was blocked to avoid vibration on the camera, also walking and talking activities were stopped during the image acquisition. Any vibration cause stripping noise in the captured HSI.

The experimental procedure established was as follows:

1. Take an HSI of the setup without water.

2. Pour gallons of water and measure the water depth.
3. Leave the water to rest so that is not moving and take an HSI.
4. Continue step 2 and 3 until the water depth reach 12.0 in.
5. Weight steps of 0.5 g of TiO_2 and add it to the water.
6. Stir the water until the TiO_2 is visually uniformly distributed.
7. Leave the water to rest so that is not moving and take an HSI.
8. Repeat steps 5 through 7 until 2.0 g of TiO_2 were successfully imaged.

Using this procedure several images were obtained and they will be explained on the next section.

3.1.4 Images Names and Descriptions

The following table has the names and description from which each image is going to be referenced during the rest of the document. On figure 15 there are some examples of the images taken without any pre-processing.

Table 2: Images names with their respective water levels and TiO_2 amount

Image Name	Type of Water	# Gallons	Depth	Volume (cm^3)
0.0 in without TiO_2	Clean	0	0 in	0
0.6 in without TiO_2	Clean	1	0.6 in	3785
1.2 in without TiO_2	Clean	2	1.2 in	7570
1.8 in without TiO_2	Clean	3	1.8 in	11356
3.0 in without TiO_2	Clean	5	3.0 in	18927
4.7 in without TiO_2	Clean	8	4.7 in	30283
6.0 in without TiO_2	Clean	10	6.0 in	37854
8.3 in without TiO_2	Clean	15	8.3 in	56781
10.8 in without TiO_2	Clean	20	10.8 in	75708
12.0 in without TiO_2	Clean	22	12.0 in	83279
12.0 in with 0.5 g of TiO_2	Turbid	22	12.0 in	83279
12.0 in with 1.0 g of TiO_2	Turbid	22	12.0 in	83279
12.0 in with 1.5 g of TiO_2	Turbid	22	12.0 in	83279
12.0 in with 2.0 g of TiO_2	Turbid	22	12.0 in	83279

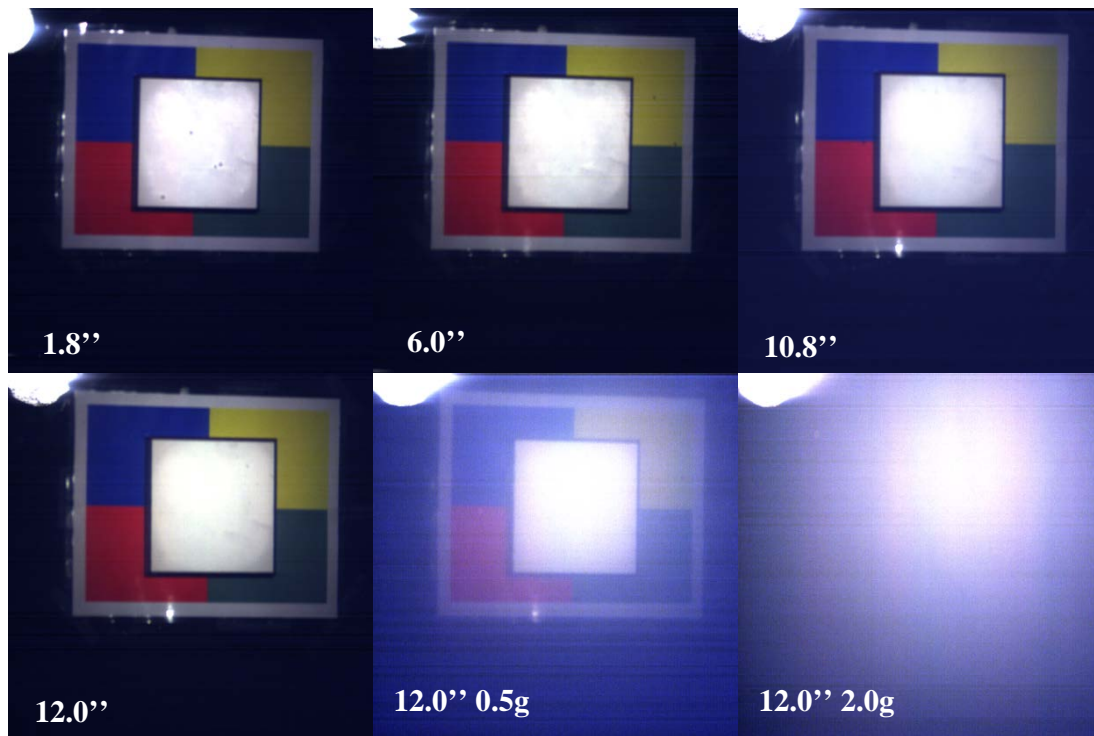


Figure 15: Example of some of the images taken with no processing

3.2 Image Pre-Processing

Images were masked, calibrated, registered and cropped before being processed by the algorithms. In the following section, each one of these steps are going to be explained in detail.

3.2.1 Image Masking

Images were masked to eliminate saturated pixels. In this experiment, saturated pixels are encountered due to the glint of the lamp on the water surface and/or on wrinkles that occur on the surface of the laminated bottoms (See figure 16). Experimental setup was carefully placed to avoid saturated pixels over the Region of Interest. See figure 17 to see the difference between a saturated pixel and the spectral response of the white standard.

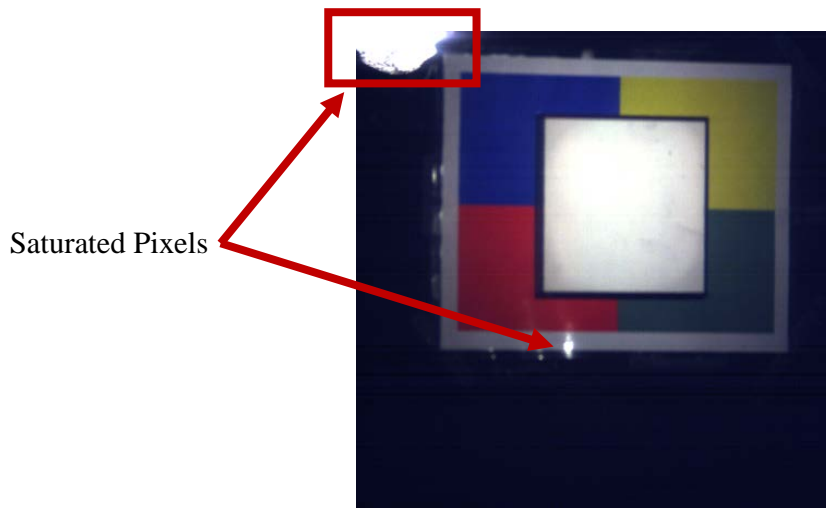


Figure 16: 12.0 in image with saturated pixels⁸

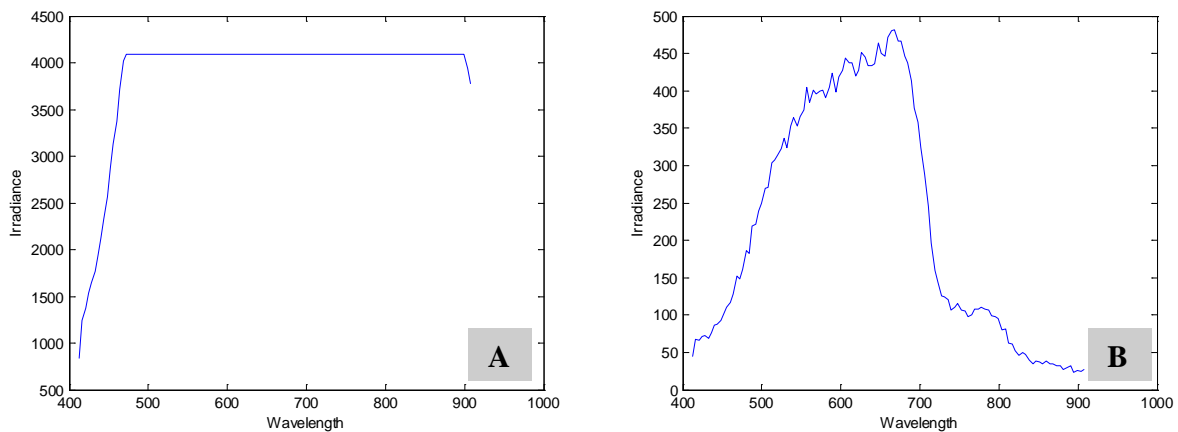


Figure 17: Spectral Response of A) Saturated Pixels vs. B) White Standard

To automatically mask bad pixels a special interface was developed to assist the researcher in accomplishing this task. Since the experiment was designed to have the white standard on every image, this region is conveniently used by the algorithm to mask saturated pixels.

To masked saturated pixels, the user first selects a region over the white standard, then the algorithm will calculate the average this region and divide each pixel in the image by the obtained value. The algorithm will zero every pixel that contains a spectral response bigger than y on any of its bands (y is configurable). Figure 18 shows the image from figure 16 with no calibration and with saturated pixel being masked.

⁸ Image was calibrated and conditioned for representation purposes.

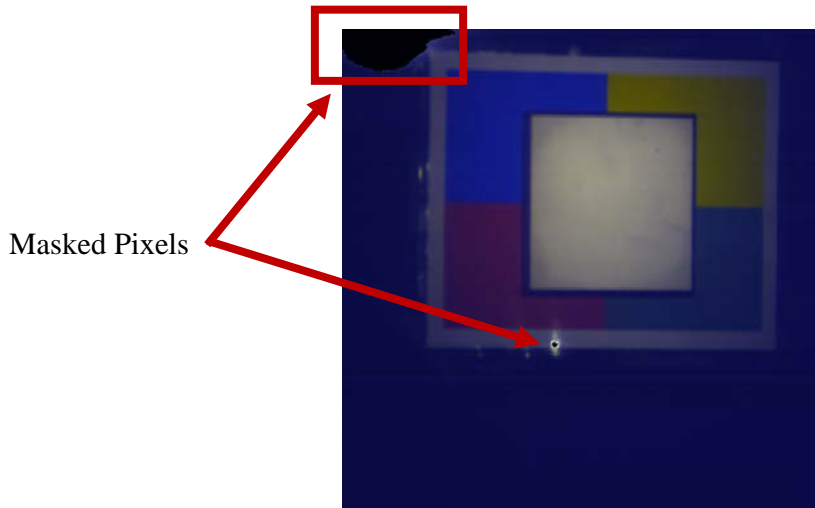


Figure 18: 12.0 in image with saturated pixels being masked (un-calibrated)

3.2.2 Calibration

The experiment was design to have a White Standard as part of the known bottom. In this project calibration means converting the image into reflectance. Two steps were required to achive this. The first step is to obtain a calibration vector. This vector is obtained by averaging the pixels enclose in a region selected over the white standard without the effect of water (Dry). The second step, for calibrating the image, is to divide every pixel by the obtained calibration vector. The calibration vector $c \in \mathbb{R}^{m \times 1}$ where m is the number of bands. See figure 19 for the visual differences between the obtained normal radiance image and reflectance image (Calibrated image).

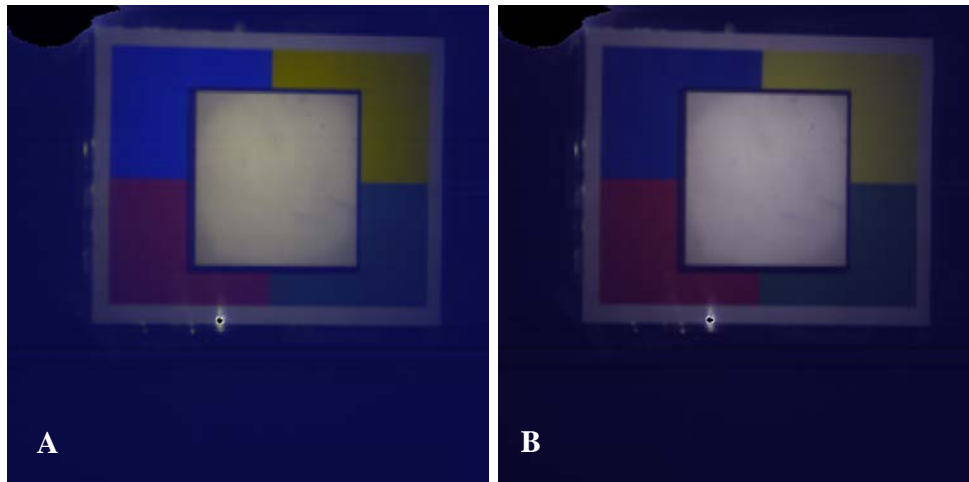


Figure 19: Difference between A) Radiance image and B) Reflectance image

3.2.3 Image Registration

The increasing water levels make the region of interest shift due to the optics of the water. Figure 20 is a RGB image crated by assigning a band from the 0 in image to the red channel and assigning the same band of the 12 in image to the blue channel. It can be observed that shapes don't fall within each other.

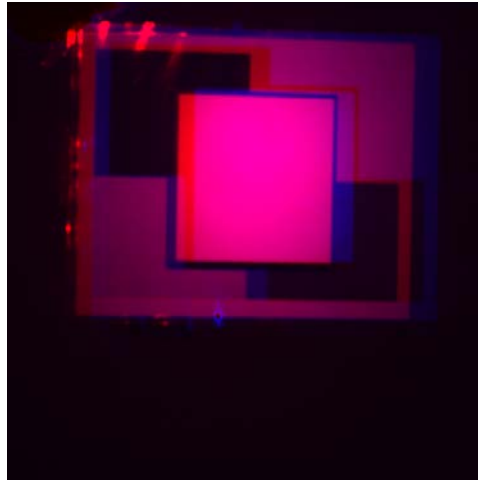


Figure 20: Optical offset created by 12.0 in of water

Due to the nature of this experiment, images need to be registered so that the region of interest overlaps within each other. Registered images are going to be used for the empirical retrieval of the optical properties vector a and b (The procedure will be explained in section 3.4). An algorithm was developed around MATLAB Image Processing Toolbox's functions: `cpselect`, `cp2tform` and `imtransform` for registering the images. As explained by The MathWorks Inc.

- `cpselect` – “Control point selection tool”
- `cp2tform` – “Infer spatial transformation from control point pairs”
- `imtransform` – “Apply 2-D spatial transformation to image”

The function `cpselect` provides an interface to select corresponding point pairs on the reference image and the image to be registered. This function generates two variables which contains the control point pairs selected by the user. These generated variables are then given to the `cp2tform` function that will generate the variables that include all the necessary information so that `imtransform` function can transform the image. `imtransform` was selected because it has a functionality very convenient to HSI images. If the image to be registered has more than two dimensions the same spatial transformation is applied to every plane along the higher dimensions [29].

`cp2tform` can infer 7 different spatial transformations: non-reflective similarity, similarity, affine, projective, polynomial, piecewise linear and `lwm`⁹. The selected transform was projective. As explained by The MATLAB Works, Inc. Projective transformation must be used “when the scene appears tilted. Straight lines remain straight, but parallel lines converge toward vanishing points that might or might not fall within the image” [29]. The algorithm will be explained on the next section.

3.2.3.1 Registration Procedure

The algorithm starts by opening the reference image and the image to be registered. Then they are passed to the `cpselect` function and the following interface that shows the given images side by side, will appear:

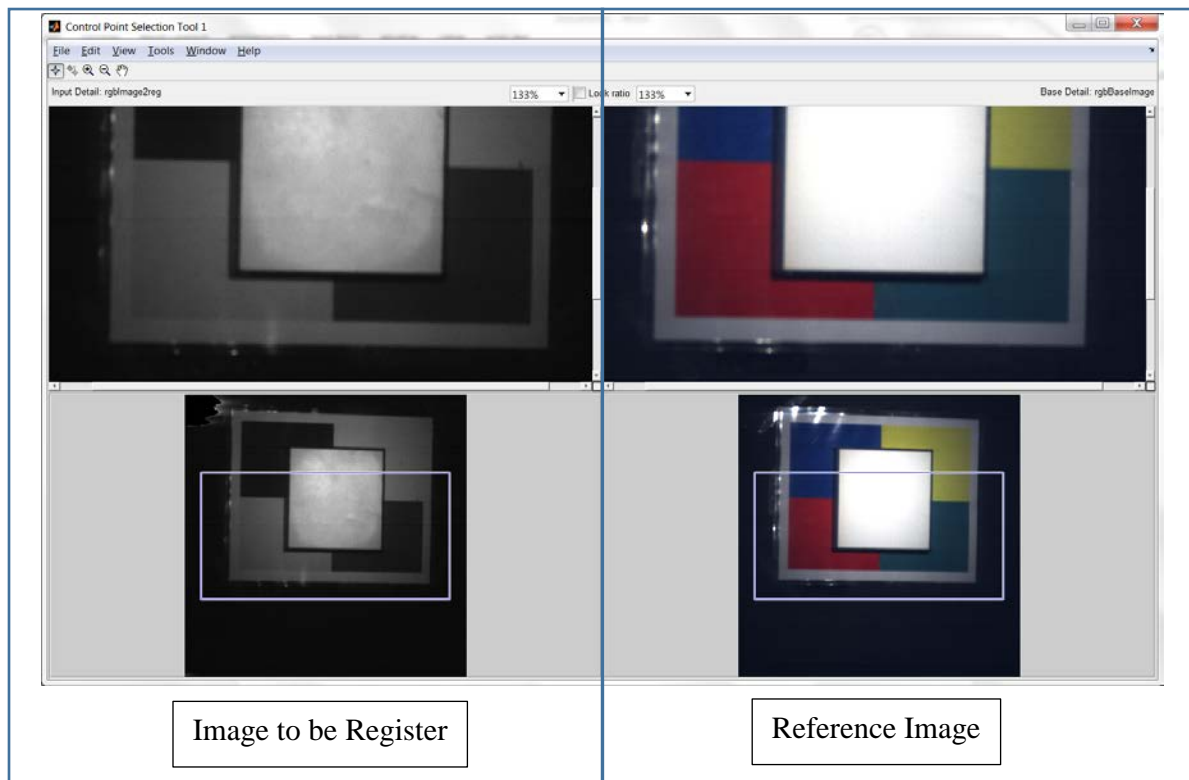


Figure 21: MATLAB `cpselect` function GUI

The interface will show the image to be registered on the left and the selected reference image on the right. Then, the user proceeds to select corresponding point pairs. Each point must be matched on both sides. See figure 22. Depending on the algorithm there are a minimum of points

⁹ For more information on each one of them visit MATLAB Online Documentation. Search for `cp2tform` MATLAB 2013a.

needed so that the transform can be performed. A total of 12 points were selected between each HSI to be registered and the reference one.

After all the points are selected the algorithm give the option to save the selected points, these points can be used to register other images. The algorithm proceeds by giving these points to `cp2tform` that infer the transformation for a single spatial plane, in this case projective algorithm was selected. After the transformation variables are computed by `cp2tform` they will be given to the `imtransform` function that will apply it to every spatial plane of the image. Figure 23 shows: A) unregistered and B) the same image registered using this procedure.

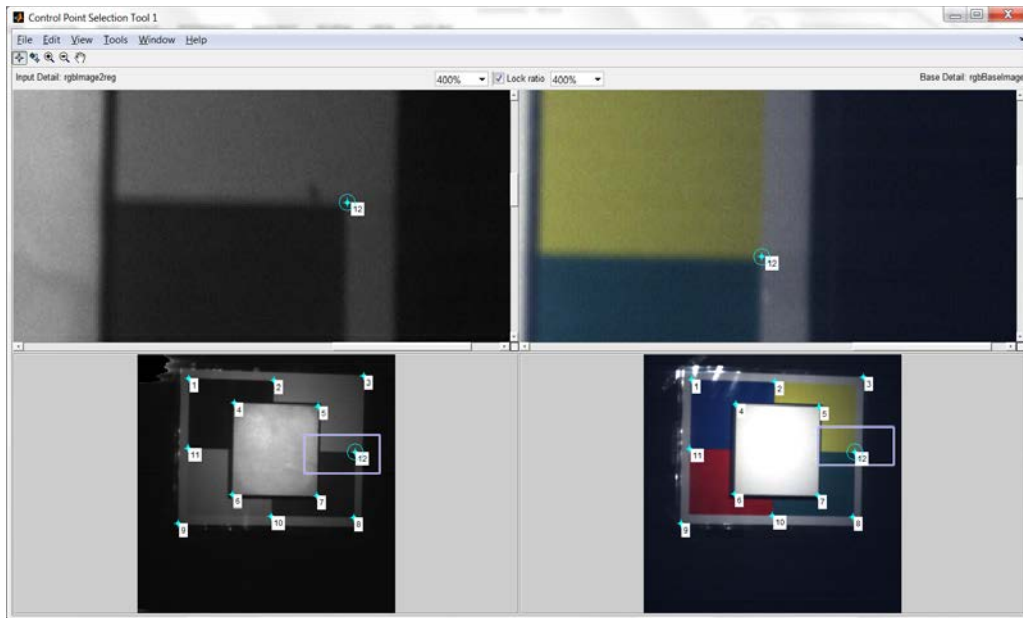


Figure 22: Selecting point on cpselect interface

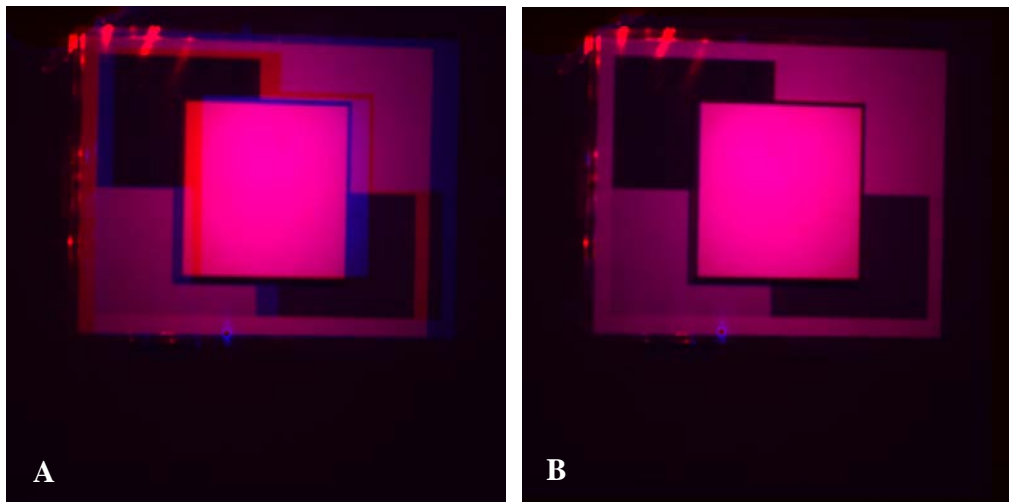


Figure 23: Resulting image after registration procedure

3.2.4 Final Images: After pre-processing

After all pre-processing steps, each image were cropped into a $433 \times 546 \times 120$ spectral cube where 433×546 is the spacial dimensions and 120 are the number of spectral bands between 412 nm and 908 nm . For showing the RGB images bellow, the bands selected for the corresponding channels were the following: Red – band 49, wavelength 605.9 nm ; Green – band 32, wavelength 536.4 nm ; Blue – band 18, wavelength 480.0 nm .

3.2.4.1 Images with Different Water Levels

This section shows the final images that were used to validate the algorithm, after all pre-processing steps. (On the next table the word “without” was abbreviated as “w/o”)

Table 3: Images Preprocessed – With different water levels


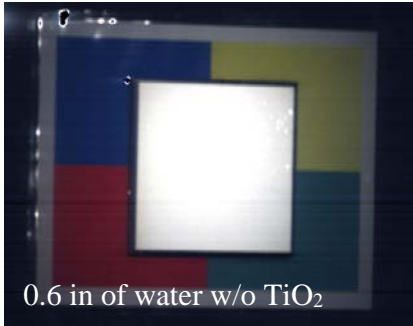
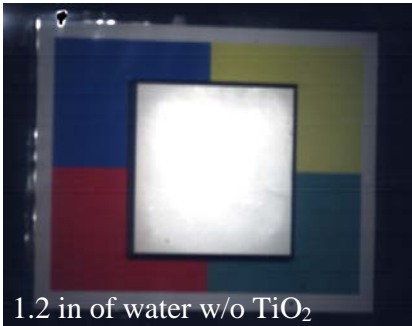
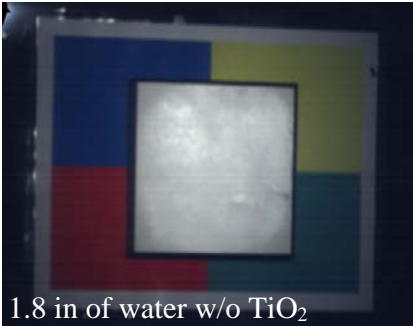
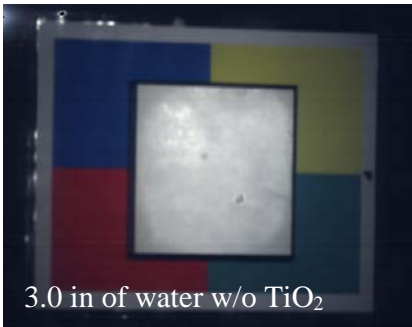
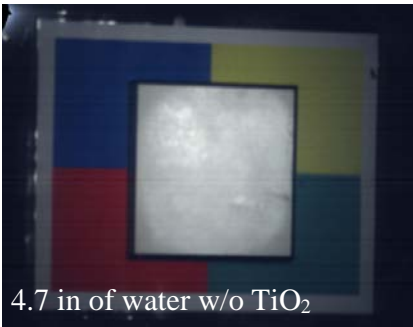
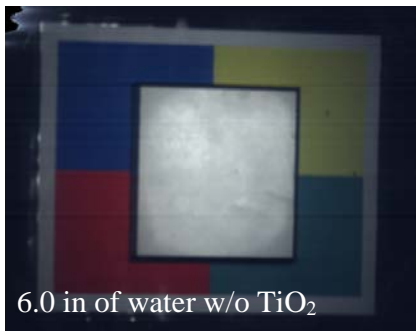
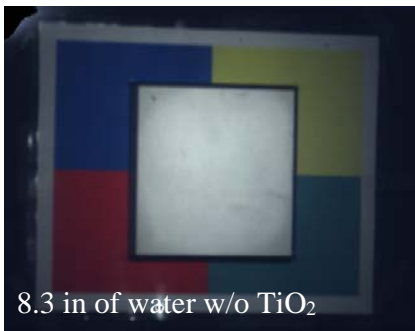
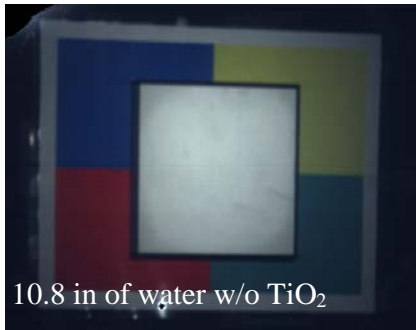
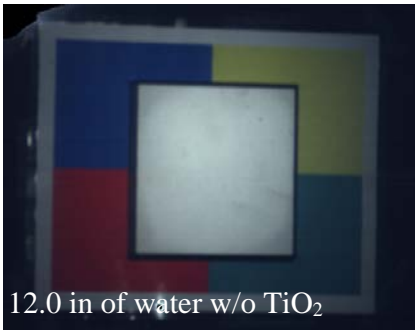
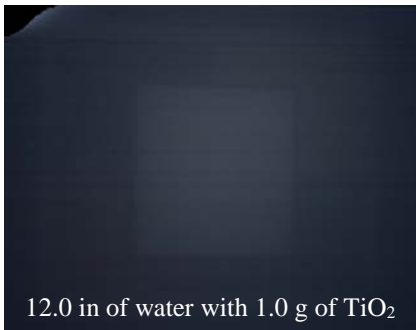
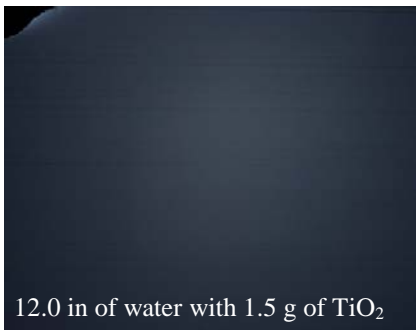
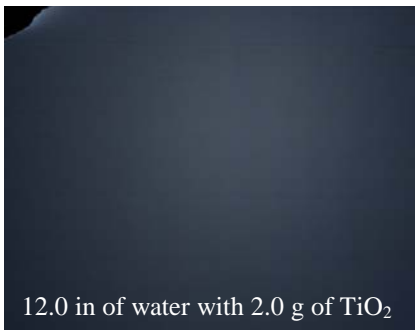
 <p>0.0 in of water w/o TiO_2</p>	 <p>0.6 in of water w/o TiO_2</p>
 <p>1.2 in of water w/o TiO_2</p>	 <p>1.8 in of water w/o TiO_2</p>
 <p>3.0 in of water w/o TiO_2</p>	 <p>4.7 in of water w/o TiO_2</p>

Table 3: Images Preprocessed – With different water levels

 <p>6.0 in of water w/o TiO_2</p>	 <p>8.3 in of water w/o TiO_2</p>
 <p>10.8 in of water w/o TiO_2</p>	 <p>12.0 in of water w/o TiO_2</p>

3.2.4.2 12.0'' Images with Different TiO_2 Concentrations

Table 4: Images Preprocessed – 12.0'' with different TiO_2 concentrations

 <p>12.0 in of water with 0.5 g of TiO_2</p>	 <p>12.0 in of water with 1.0 g of TiO_2</p>
 <p>12.0 in of water with 1.5 g of TiO_2</p>	 <p>12.0 in of water with 2.0 g of TiO_2</p>

3.3 Regions of Interest

The known bottom is composed of four different colors (Blue, Yellow, Green, Red). The White Standard was included as part of the bottom too, making five different regions of interest. A special interface was programmed to perform the task of selecting regions, extracting their information and saving them in a known format for later use. The coordinates of these regions are saved so that they can be used to create the same endmembers in similar or registered images.

Two different regions per ROI were selected: one for training another for testing. Training regions were used to extract the endmembers on different images and testing regions were used to test how the classification performed. Figure 24 shows training regions (solid lines) and the testing regions (dashed line) selected for this project.

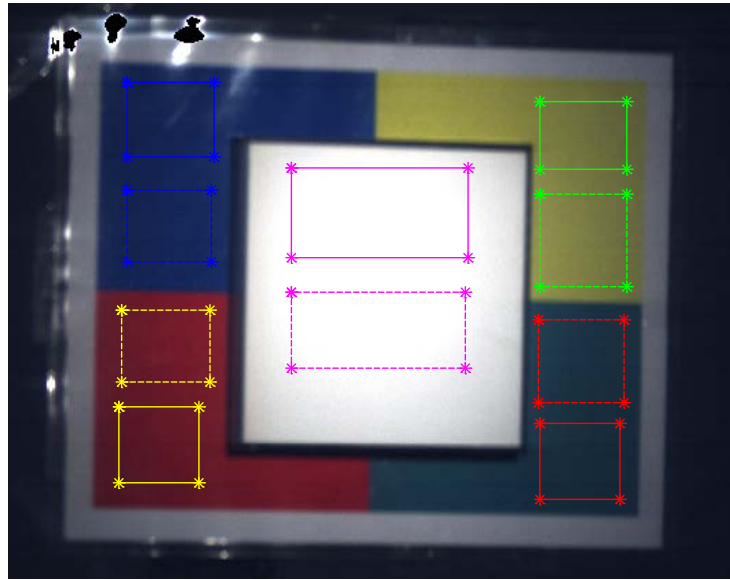


Figure 24: Region of Interest Selected: Training (solid line) and Testing (dashed line)

3.3.1 Endmembers

Endmembers were extracted by averaging every pixel on the training regions resulting in a $m \times n$ matrix where m is the number of bands and n is the number of endmembers. Two images were used to extract endmembers 0.0 in and 1.8 in. Dry image (0.0 in) was used because on the work presented by Rodríguez-Díaz on [6] the endmembers used to process the image were the representative ones of objects of interest without the effect of the water. 1.8 in was used as well in order to have the effect of a small layer of water this is the closest case to a realistic measure of the spectral signature of the objects of interest measured underwater.

Figure 25 shows the endmembers extracted from the 0 in image which does not contain any effect of water layers. Figure 26 shows the Normal Reflectance of endmembers extracted from the image 1.8 in which has the effect of a small layer of water.

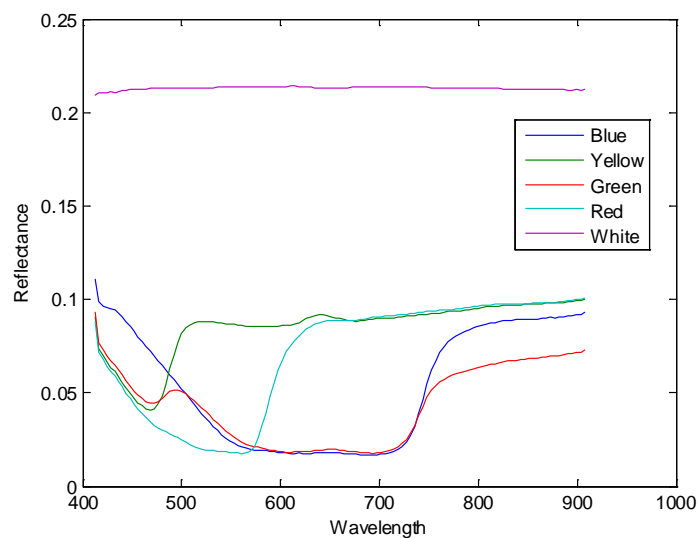


Figure 25: Endmembers from 0'' hyperspectral image

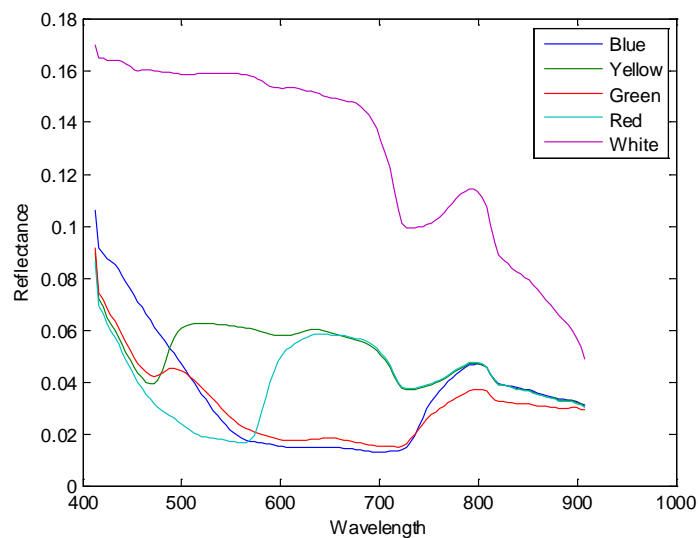


Figure 26: Endmembers extracted from 1.8'' hyperspectral image

3.4 Optical Properties Retrieval thorough an Empirical Procedure

The main algorithms used in this work are based on the Lee's function presented on section 2.2. Particularly, the regularization algorithm the function for the remote sensing reflectance is the following:

$$R_{rs} = f[a, b, \rho, H, \theta] \quad (51)$$

Where:

- R_{rs} is the remote sensing reflectance.
- a is the absorption coefficient.
- b is the backscattering.
- ρ bottom albedo (spectral signature of the object without the effect of the medium).
- H is the bottom depth.
- θ is the subsurface solar zenith angle.

In the original work by Lee *et. al.* in [2], [3] the optical properties vectors a and b are estimated in the optimization routine (see section 2.2). In the regularization algorithm, these parameters need to be given so that the algorithm can work. It is important to understand that the regularization algorithm was designed to consider high uncertainties of these optical properties. These algorithms don't need a high precision when it comes to a and b .

Many forms of a and b vectors can be used. For example, a constants value for each wave length (e.g. 1 or 0.5), or the values obtained using a new methodology that can empirically retrieve a and b vectors from the same images that were obtained during experiments. This methodology will be described in the next section.

3.4.1 Empirical derivation of a and b values

This methodology starts by masking and dividing every region into multiple sub-regions. Since all the images are registered every region of interest between two images will coincide within each other. For this method, only one region of interest at a time is selected. The selected region is then divided into a given amount of sub-region which then they are averaged. The average of each sub-region is taken as a solution to equation 51. For example, if the region is divided into 9 sub-regions then there will be 9 different solutions. Solutions must be more than the number of unknowns in the equations to retrieve the best solution in a least square sense.

The algorithm developed to retrieve the optical properties needs two images. One of them is the base image which, in this project, is the one without the effect of water and the second image is the one with the submerged bottoms. The mathematical description of the empirically retrieval of the optical properties vector a and b is described next.

Based on the Lee model determine a and b that best fit the least square error:

$$(a_{\lambda_i}, b_{\lambda_i}) = \min_{a,b} \left| \sum_R \left(r_{rs}(\lambda_i) - \hat{r}_{rs-lee}(\lambda_i, H, a, b, \theta_z, \rho_{\lambda_i}) \right)^2 \right| \quad (52)$$

Where:

- r_{rs} is the measured reflectance
- \hat{r}_{rs-lee} is the modeled reflectance using Lee's equations
- R is the value that signifies all the regions (See section 3.4.2)

The calculations are performed band by band. Each r_{rs} and \hat{r}_{rs} are solutions vectors that contains the same amounts of elements as of non-zero regions on the image. The algorithm only needs three regions to retrieve empirically a and b . The following sections will describe in details the steps performed to prepare the image and to obtain the solution of the optical properties vectors.

3.4.2 Masks











A mask is simply a binary matrix with the same spatial dimension of the main image. The mask contains a value 1 on the pixels that correspond to the region that is wanted to be isolated from the rest of the image and 0 elsewhere. The last operation is performed by multiplying the original image by the mask (See figure 27).



Figure 27: Masking operation

The masks created for this project were carefully selected to avoid shadows. Five different mask were created, one per region of interest. Table 5 shows all the created masks.

Table 5: Masks created for each Region of Interest

Name	Mask	Resulting Image
Blue		
Yellow		
Green		
Red		
White		

3.4.3 Dividing Sub-Regions

After masking the image, the algorithm will divide each region into sub-regions of equal size like a square matrix of " $y \times y$ " elements where y is configurable. See next figure for an example of dividing the white region with $y = 3$ into a 3×3 matrix.

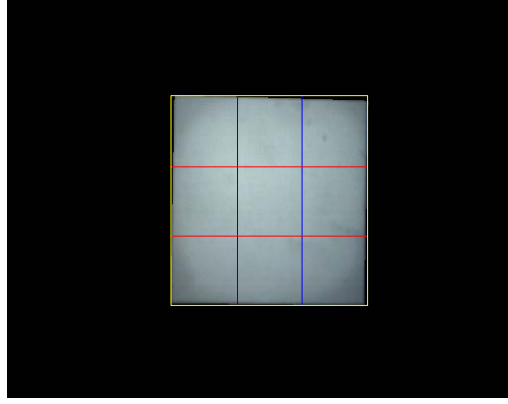


Figure 28: Divided sub-regions

As explained before, each region is averaged and taken as a solution to equation 51. The result is a matrix $R_{rs} \in \mathbb{R}^{m \times p}$ where m is the number of bands and p is the number of non-zero regions. Since the regions are divided evenly as a square region there are some cases when all the pixels on the sub-regions are zero. In these cases, the sub-region is discarded. See figure 29 for an example when this occur.

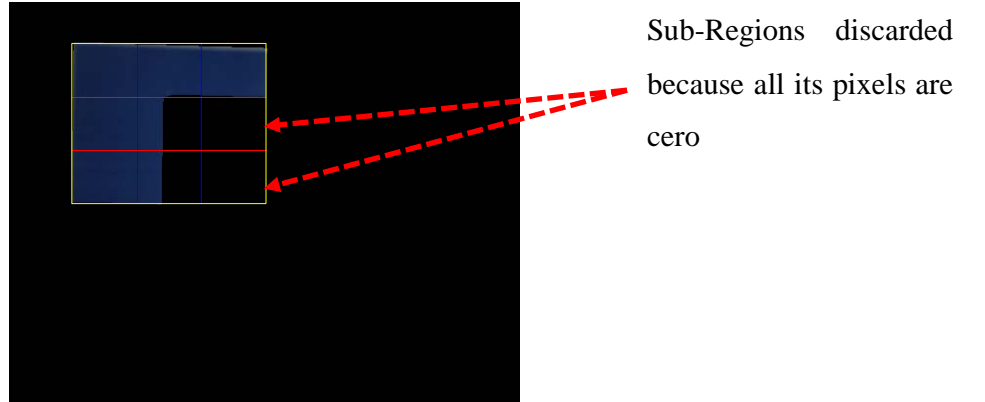


Figure 29: Blue masked resulting image showing discarded sub- regions

3.4.4 Absorption and Backscattering Empirical Calculations

Calculations are preformed band by band solving equation 52. For this the MATLAB function `lsqnonlin` was used. This function is very convenient because allows for bounded problems. The function needs more equations than unknowns and initial values to perform bounded calculations. For retrieving a and b only lower bounds were used leaving the upper bound open, $[0, \infty)$. Initial values were selected to be 0.2 for a and 0.1 for b . With the same configuration a and b vectors were retrieved using two image: one without the effect of water and another with 12.0 in of water. Figure 30 shows the modeled vs measured scatter plot. It can be observed in that

figure that the model could fit the measured reflectance successfully. Figures 31 and 32 shows an example of the empirically derived total absorption (*a*) and backscattering (*b*) vectors.

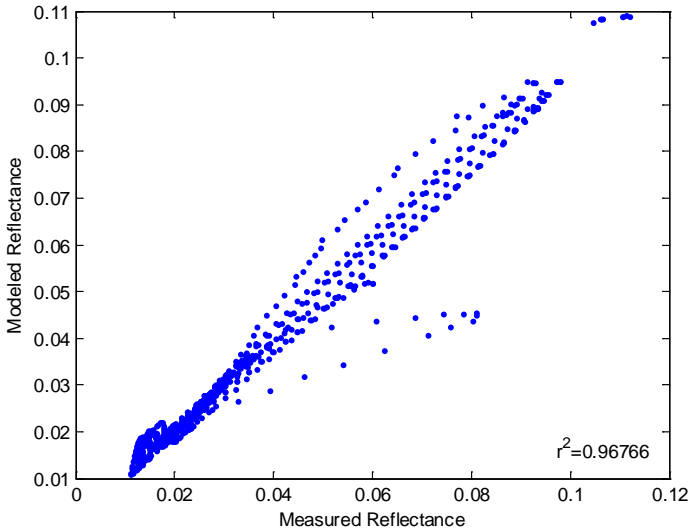


Figure 30: Modeled Reflectance vs. Measured Reflectance

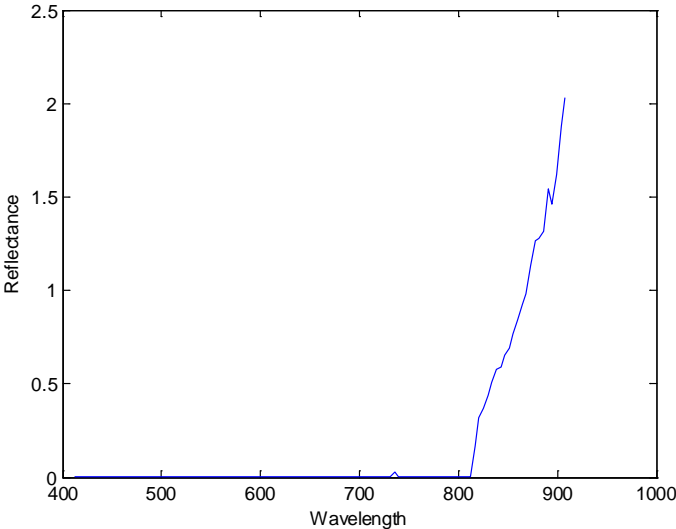


Figure 31: Empirically Derived Total Absorption (*a*)

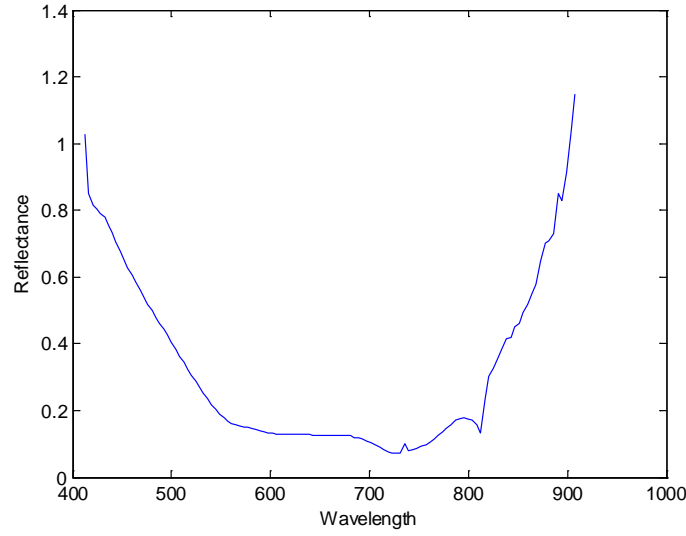


Figure 32: Empirically Derived Backscattering (b)

3.5 Calculating Maximum Curvature

As explained on section 2.6, and repeated here for simplicity, the mathematical expression for each component of P_{reg} of the regularization algorithm is the following:

$$\rho_{reg}(\lambda) = \frac{a_i^2(\lambda)}{a_i^2(\lambda) + \eta^2} \frac{r_{rs}(\lambda_1) - S_{col}(\lambda_i)}{a_i(\lambda)} + \frac{\eta^2}{a_i^2(\lambda) + \eta^2} \rho_0 \quad (53)$$

where ρ_0 is the spectral signature of individual objects of interest and η^2 is expressed as follows:

$$\eta^2 = \frac{\gamma}{1 - \gamma} \text{ with } \gamma \in [0,1). \quad (54)$$

where γ is the **regularization parameter** and is selected by using the point of **maximum curvature** which is calculated with the following formula:

$$\gamma = \arg \max_i \left\{ \frac{E(\gamma)''}{(1 + (E(\gamma)')^2)^{3/2}} \right\} \quad (55)$$

where:

$$E(\gamma) = \sum_{i=1}^N \left(P_{reg}(\lambda_i) - P_0(\lambda_i) \right)^2 \quad (56)$$

and $E(\gamma)'$ and $E(\gamma)''$ is the first and second derivative of equation 56. Two methods were used to calculate the first and second derivative of the established error function. 1) **Numerical Approximation** described in section 3.5.1 and 2) **Derived Equations** described in section 3.5.2.

3.5.1 Numerical Approximation

γ is a vector from 0 to 1 in $d\gamma$ steps and can be used to calculate the derivative numerically by using Forward Difference. The first derivative is formulated as:

$$E'(\gamma) = \frac{dE(\gamma)}{d\gamma} = [E(\gamma + 1) - E(\gamma)]/d\gamma \quad (57)$$

And the second derivative is formulated as:

$$E''(\gamma) = \frac{d^2E(\gamma)}{d\gamma^2} = [E'(\gamma + 1) - E'(\gamma)]/d\gamma \quad (58)$$

3.5.2 Derived Equations

Another method for calculating the derivative of the error function is by deriving the equations starting from:

$$E(\gamma) = \sum_{i=1}^N \left(P_{reg}(\lambda_i) - P_0(\lambda_i) \right)^2 \quad (59)$$

The first derivative is:

$$\frac{dE(\gamma)}{d\eta^2} = 2 \sum_{i=1}^N \left(\rho_{reg}(\lambda_i) - \rho_0(\lambda_i) \right) \frac{d\rho_{reg}(\lambda_i)}{d\eta^2} \quad (60)$$

and the second derivative is:

$$\frac{d^2E(\gamma)}{(d\eta^2)^2} = 2 \sum_{i=1}^N \left[\left(\frac{d\rho_{reg}(\lambda_i)}{d\eta^2} \right)^2 + \frac{d^2\rho_{reg}(\lambda_i)}{(d\eta^2)^2} \left(\rho_{reg}(\lambda_i) - \rho_0(\lambda_i) \right) \right] \quad (61)$$

Now, the partial derivatives $\frac{d\rho_{reg}(\lambda_i)}{d\eta^2}$ and $\frac{d^2\rho_{reg}(\lambda_i)}{(d\eta^2)^2}$ are needed. Expressing $\rho_{reg}(\lambda_i)$ as:

$$\rho_{reg}(\lambda) = \frac{a_i^2(\lambda)}{a_i^2(\lambda) + \eta^2} \frac{r_{rs}(\lambda_1) - S_{col}(\lambda_i)}{a_i(\lambda)} + \frac{\eta^2}{a_i^2(\lambda) + \eta^2} \rho_0 \quad (62)$$

and its first derivative with respect to η^2 is computed as:

$$\begin{aligned} \frac{d\rho_{reg}(\lambda_i)}{dn^2} &= \rho_0(\lambda_i)(a_{ii}^2(\lambda_i) + \eta^2)^{-1} \\ &\quad - [a_{ii}(r_{rs}(\lambda_i) - S_{col}(\lambda_i)) + \rho_0(\lambda_i)](a_{ii}^2(\lambda_i) + \eta^2)^{-2} \end{aligned} \quad (63)$$

and its second derivative with respect to η^2 is computed as:

$$\begin{aligned} \frac{d^2\rho_{reg}(\lambda_i)}{(dn^2)^2} &= -2\rho_0(\lambda_i)(a_{ii}^2(\lambda_i) + \eta^2)^{-2} \\ &\quad + 2[a_{ii}(r_{rs}(\lambda_i) - S_{col}(\lambda_i)) + \rho_0(\lambda_i)](a_{ii}^2(\lambda_i) + \eta^2)^{-3} \end{aligned} \quad (64)$$

These formulations allow for rapid integration into an algorithm because its functions can be performed while inverting the image. Figure 33 shows how a typical curvature graph looks like.

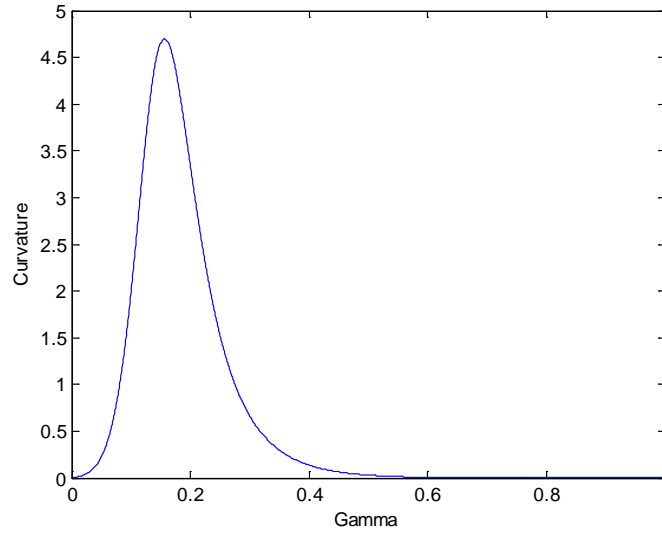


Figure 33: Typical Curvature Graph of the Regularization Algorithm

3.5.3 Single Regularization Parameter

The implementation of this algorithm into HyCIAT also includes and additional capability of inverting the whole image using a single regularization parameter selected by the user. This additional functionality is called Single regularization parameter

Recalling, regularization algorithm for each pixel,

$$\rho_{reg}(\lambda) = \frac{a_i^2(\lambda)}{a_i^2(\lambda) + \eta^2} \frac{r_{rs}(\lambda_1) - S_{col}(\lambda_i)}{a_i(\lambda)} + \frac{\eta^2}{a_i^2(\lambda) + \eta^2} \rho_0 \quad (65)$$

where ρ_0 is the spectral signature of individual objects of interest and η^2 is expressed as follows:

$$\eta^2 = \frac{\gamma}{1-\gamma} \text{ with } \gamma \in [0,1). \quad (66)$$

where γ , in this additional functionality, is a constant from 0 to 1 selected by the user.

This additional capability is convenient for studying the effect of the automatic procedure for selecting the regularization parameter for each pixel. This functionality was used to produce baseline results by setting γ to 0 and then classifying results. By setting γ to 0 and then classifying the image the effect of the automatically selection of the regularization parameter can be studied.

3.6 Classification Algorithms

After the inversion of the image using γ_{opt} and with the corresponding optimum bottom, the final image theoretically is a HSI reconstruction of the main image without the effect of the water column. This final image is called P_{reg} and, since is an HSI, conventional classification method can be used to classify the image.

In this project three classification methods were employed, two of them are common and one of them is an extension of the spectral unmixing algorithms explained in section 2.1. The first method, employed by Rodríguez-Díaz on [6], is the Minimum Euclidean Distance, the second method employed in this project is called Minimum Spectral Angle:

- **Minimum Euclidean Distance Classifier** starts by calculating the Euclidean distance between and inverted pixel P_{reg} with stored spectral signature P_{0i} . P_{0i} corresponds to the endmember i , stored in the endmember matrix. The mathematical expression for this classifier is the following:

$$g_i(P_{reg}) = (P_{reg} - P_{0i})^T (P_{reg} - P_{0i})$$

Choose class i is and only if an only if:

$$(67)$$

$$g_i(P_{reg}) \leq g_j(P_{reg}) \text{ for all } j = 1, 2, \dots, m$$

- **Minimum Spectral Angle Classifier** calculates the spectral angle between and inverted pixel P_{reg} with stored spectral signature P_{0i} in the following way:

$$g_i(P_{reg}) = \cos^{-1} \frac{P_{reg}^T P_{0i}}{\|P_{reg}\| \|P_{0i}\|}$$

(68)

Choose class i if and only if:

$$g_i(P_{reg}) \leq g_j(P_{reg}) \text{ for all } j = 1, 2, \dots, m$$

The third classifier employed in this project is called:

- **Maximum Endmember Value Classifier:** The algorithm will calculate the abundances of each endmember and will assign the pixel to the endmember that yields the highest abundance value. The mathematical expression of this classifier is the following:

$$G = \text{Unmix}(A, P_{reg})$$

Choose class i iff:

(69)

$$g_i(P_{reg}) \geq g_j(P_{reg}) \text{ for all } j = 1, 2, \dots, m$$

Where: A is the endmember matrix, G is a vector containing the individual abundances of each endmember, m is the number of endmembers and P_{reg} is the regularized pixel.

4 Software Development and Implementation

All the existing algorithms were carefully studied and improved by adding functionalities that make the Hyperspectral Coastal Image Analysis Toolbox (HyCIAT) more usable. Important new functions were developed and initially tested outside HyCIAT and then integrated into the toolbox. Additional tools were also included to have a unified system that can manage the dataset obtained for this project explained in section 4.3. Special tools were created for: Region of Interest (ROI) selection, obtaining spectral signature, obtaining calibration vectors, extracting data from each ROI, calibrating the image (Convert to Reflectance) using a calibration vector, and masking bad pixels. HyCIAT, now, can be also used for: data analysis, endmembers studies, unmixing studies, underwater classification and statistical analysis just to name a few applications.

There were two main software development aspects on this project: 1) Updating and enhancement of HyCIAT from MATLAB 2007 to MATLAB 2013, and 2) Recoding, Experimentation and Integration of the regularization algorithm into HyCIAT (See section 1). Section 4.1 will explain the first development aspect and section 4.2 will explain the second development aspect. Then, section 4.3 will described additional tools and changes implemented to enhance HyCIAT usability.

4.1 Updating and Enhancement of HyCIAT Underwater Unmixing Functions

HyCIAT underwater unmixing functions were enhanced and updated in several ways. The toolbox didn't work properly on MATLAB 2013a. After all the main functionalities were restore, it was observed that the obtained results were not the same as the ones published by Torres-Madroñero on [1]. The differences were due to changes in some default parameters in the `lsqnonlin` function implemented after MATLAB version 2008b. These parameters were identified and are explained in section 4.1.1. Sections from 4.1.2 to 4.1.4 will explained some extra tools and functionalities that were added to the underwater unmixing toolbox to increase its usability.

4.1.1 `lsqnonlin` Optimization Functions Default Parameters

HyCIAT was developed by Torres-Madroñero on [1] based on the algorithms presented by Lee *et al.* on [2], [3]. The toolbox was developed in MATLAB 2007 and after MATLAB 2008b some MATLAB native functions, that are used in it, change their default parameters. This caused that results published on [1] and the ones obtained from MATLAB 2013a were different, see figure 34.

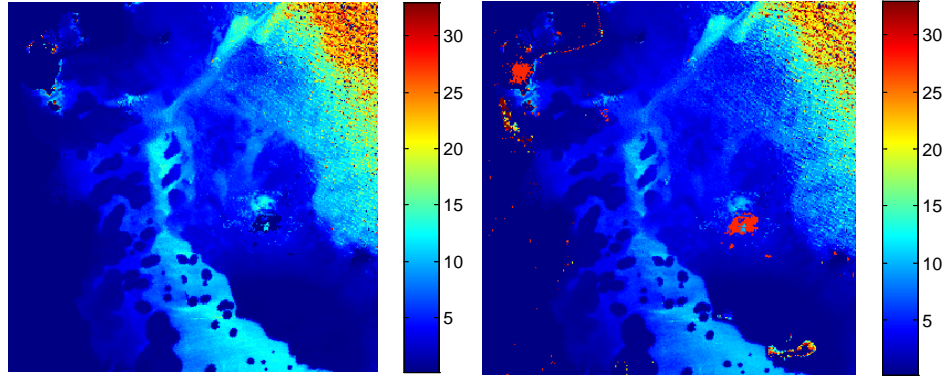


Figure 34: Result of the same parameters between two MATLAB versions.

Last figure shows obtained depth in meters, from the same image, using the Lee's algorithm developed and published on [1] without modifying its defaults parameters. The image on the left was obtained by using MATLAB 2007 and the image on the right by using MATLAB 2013a. figure 35 will show the difference, in meters, of the two images. It can be observed that in some large regions the results have up to 30m of difference.

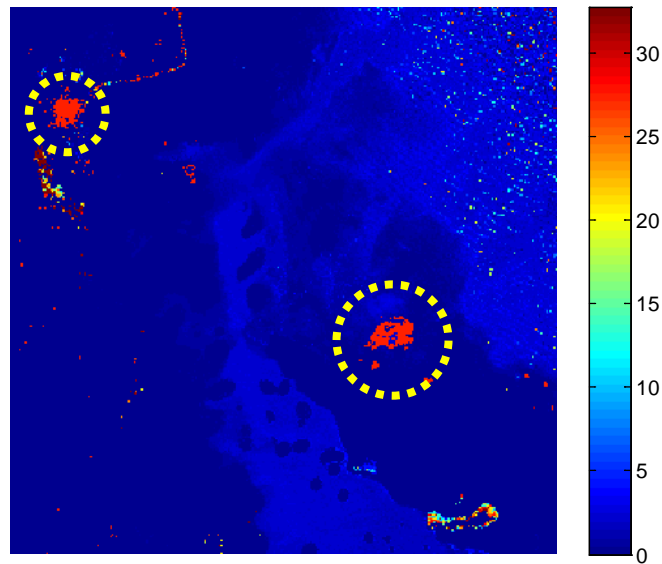


Figure 35: Difference of the two images show in figure 34

The following Table, lists the parameters that their default values changed from MATLAB version 2007 to 2013a.

Table 6: lsqnonlin parameters default value between MATLAB versions 2007 and 2013a

Parameter Name	Default value: 2007	Default Value: 2013a
DiffMaxChange	$1e - 1$	inf^{10}
DiffMinChange	$1e - 8$	0
PrecondBandWidth	0	inf

It was found that PrecondBandWidth which is an input parameter of the `lsqnonlin` function was affecting results. On MATLAB 2007 this parameter was set to 0 and after MATLAB version 2008b this parameter was change to ' inf '. Therefore, this value was fixed to 0 before any optimization is performed on the current version of HyCIAT. The following results are obtained after changing this parameter:

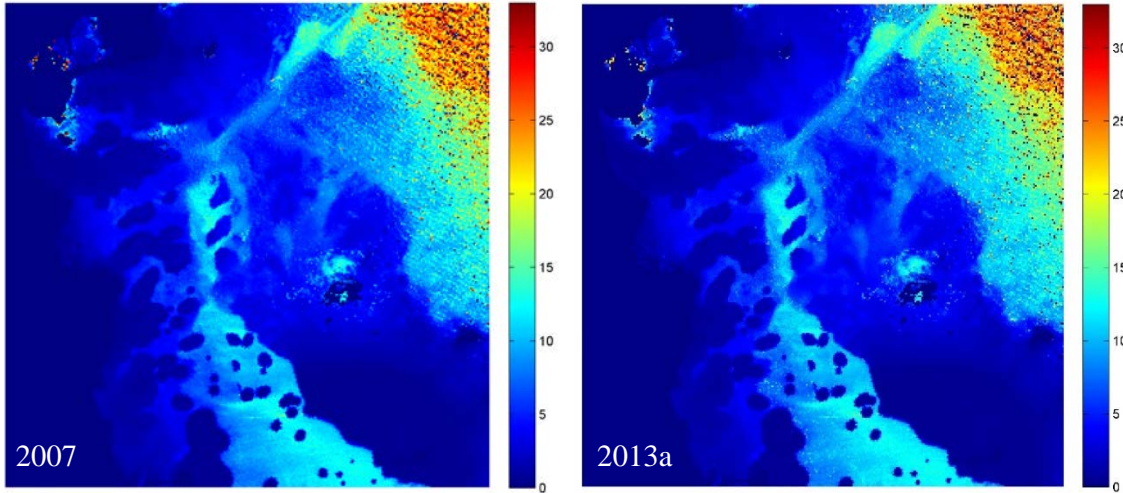


Figure 36: Same result as figure 34 but with modified parameters

For demonstration purposes, the difference between the two images showed in the last figure is calculated and showed on figure 37. It can be observed that there are some differences up to 30m per pixel but they are not concentrated on regions of the image, instead there are on random pixels. It is important to consider that the solution of the optimization problem is not necessarily unique. For more information of the MATLAB `lsqnonlin` function refer to [31].

¹⁰ Value inf represents infinity on the MATLAB syntax. [30]

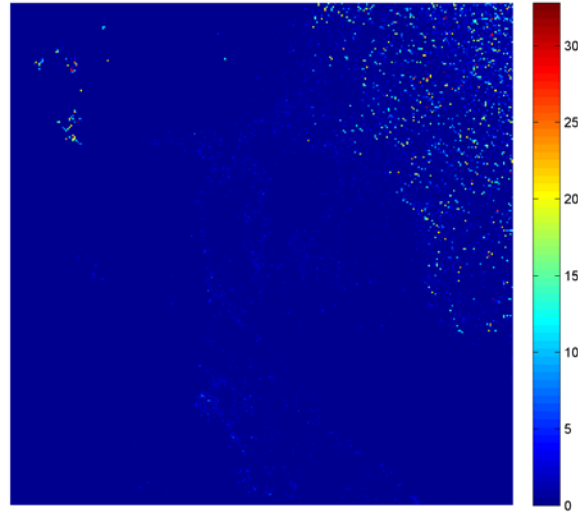


Figure 37: Difference of the two images showed in figure 36

The initial parameters window, showed on the next figure, was modified so that the *PrecondBandWidth* parameter value can be changed as the researcher see fit. The default value for the parameter will be *inf*.

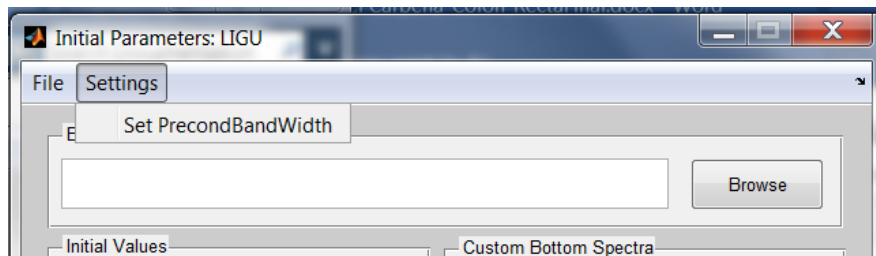


Figure 38: Modification for default Parameter *PrecondBandWidth*

To change the parameter, the user must select Set *PrecondBandWidth* option from the Settings menu. The form showed in figure 39 will appear. From there the use can select either '*inf*' or '*0*' from the drop-down menu. To save the parameter, the user must click save button otherwise the system will not save the modified value.

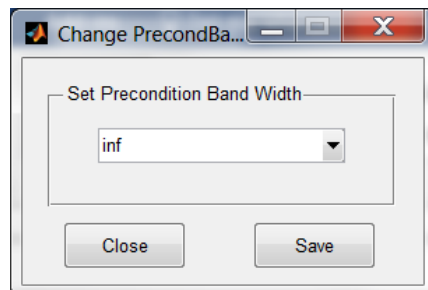


Figure 39: Independent interface to change the *PrecondBandWidth* parameter

4.1.2 HyCIAT Spectral Region for Unmixing

Lee's equation was modified by Goodman on [4] to add an extra layer of processing by extending the algorithm capabilities into spectral unmixing of the resulting R_{rs} with the given endmembers. This spectral unmixing was performed in a specific region of the spectrum which, on the first version of HyCIAT, this specific region, corresponds to the one between 545 nm to 675 nm. When using the spectral unmixing algorithms on the obtained dataset some endmembers could not be detected successfully because certain features of its signatures were discarded since they were on parts of the spectrum outside the one from 545 nm to 675 nm that was being used. By studying the algorithms, it was found that these regions were embedded in the code not allowing the user to modify these regions conveniently. Since different unmixing regions yield different results, the initial parameter interface was modified to allow the user change these regions as it see fit. Therefore, adding an extra layer of study that can be conducted using this toolbox, see next figure.

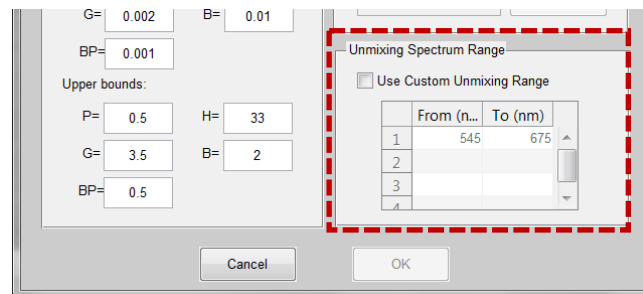


Figure 40: Functionality to select a region to perform the unmixing

Up to four regions can be selected. Each region can be specified by writing the wavelength of the starting band in the “From (nm)” column and writing the band of the final one in the “To (nm)” column. For example, if the region wanted to be used for unmixing is from 400nm to 900nm the user must configure the interface in the following way:

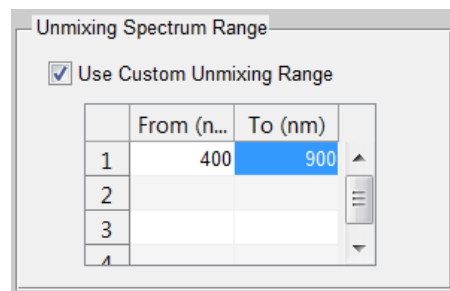


Figure 41: Configuring a custom unmixing range in a single section of the spectrum

In another example, if the user if the region wanted to be used for unmixing is from 400 to 650nm and from 700 to 900 the user must configure the interface in the following way:

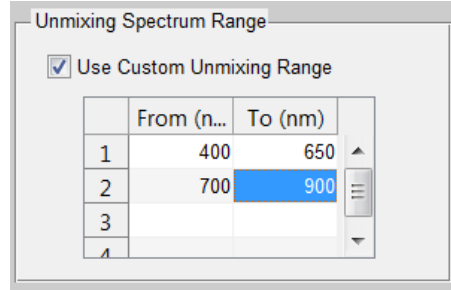


Figure 42: Configuring a custom unmixing range in multiple section of the spectrum

4.1.3 HyCIAT Default Bottom Spectral Signature

Recalling equation (6), Lee's equation that state that the Remotely Sensed Reflectance is a function of absorption, backscattering, bottom albedo, depth, the subsurface solar zenith angle, the subsurface viewing angle from nadir and the azimuth angle.

$$R_{rs} = f[a, b_b, \rho, H, \theta_w, \theta, \varphi]$$

The variables a and b in the un-mixing algorithms are retrieved by the optimization algorithm. H can be retrieved or given, meanwhile θ_w, θ and φ are given. The bottom albedo ρ as defined by the Lee's model, is a representative spectral signature of the bottom normalized at 550 nm. In [1]–[5] the spectral signature of sand, on their respective environments of study, was used for ρ . The toolbox stored this value in a constant saved in a “.mat”¹¹ file causing an inconvenience when the user wants to change this variable. To assess this problem, the initial parameters interface was modified to allow the user to input its own bottom spectral signature when needed¹². This functionality adds another layer of studies by allowing the researcher to input its own bottom to the algorithm. The following figure shows the Custom Button Spectra section of the interface. This section is used to input custom button spectra to the algorithm.

¹¹ “.mat” is a file extension used for files that contain MATLAB formatted data. Data can be loaded and or save from and or to files with this extension using the LOAD and SAVE functions respectively.

¹² The interface still loads up with the default variables published on [1].

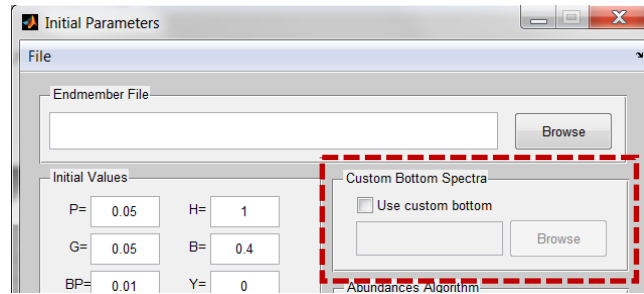


Figure 43: Added functionality: Custom bottom

After pressing the Browse button, this functionality will bring up another interface after (see next figure) that assists the user in analyzing the opened spectrum and normalized it by using the measured value in a certain band of it. This is stored in a special variable that will be used during the underwater unmixing process as the known bottom.

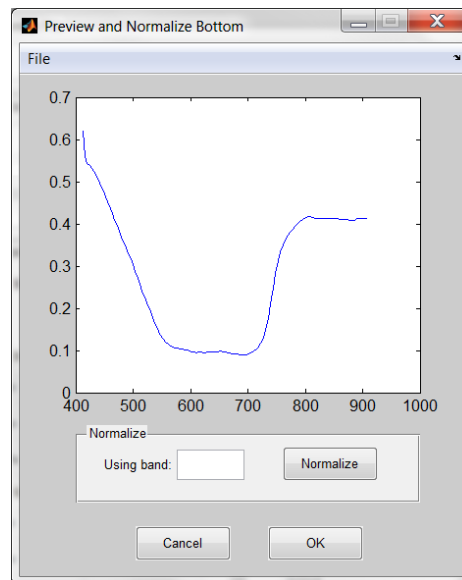


Figure 44: Interface to assist the user to analyze and modify its own custom bottom

4.1.4 Other Functionalities

On the first version of HyCIAT the initial parameter window the Lower and Upper bounds were programmed in a way was not very clear for the user to know which value correspond to which variable (see figure 45-A). This problem was solved by modifying the interface to include individual textboxes and labels for every variable on both bounds (see figure 45-B).

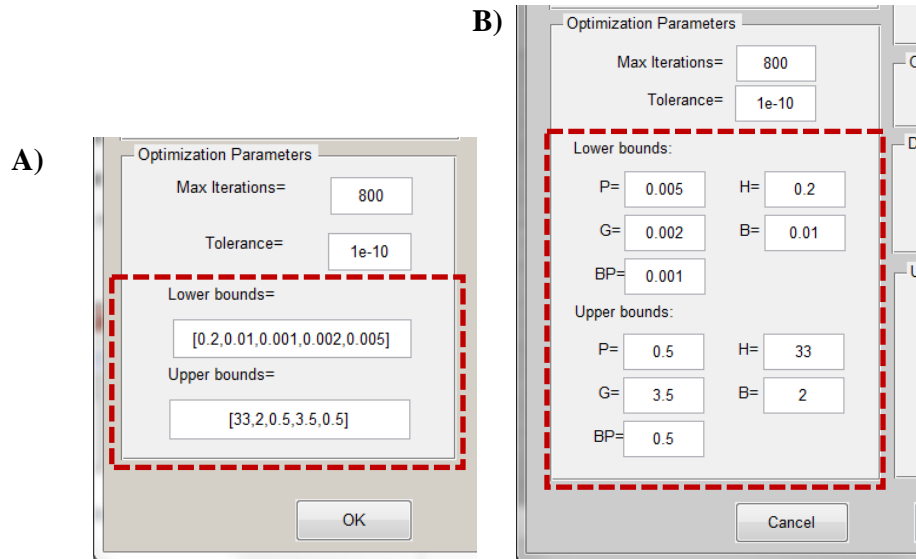


Figure 45: Interface modification on the Optimization Parameters section

Another new functionality was added to the initial parameter interface that save the configured parameters including custom bottoms, custom regions of the spectrum for the unmixing, initial values and bounds. These files can later be opened and it will configure the interface in the same way that it was saved.



Figure 46: Load and save configuration menu

4.2 Regularization Algorithm Development

The regularization algorithms were proposed by Luis O. Jiménez and former student Eladio Rodríguez-Díaz. Rodríguez-Díaz has a thesis on this topic from the University of Puerto Rico Mayagüez campus [6]. This algorithm was carefully studied and implemented in MATLAB 2013a. Unfortunately, the code developed before was lost, therefore the algorithm was programmed from the beginning into multiple functions outside HyCIAT. The algorithms were developed while testing them. On early development stages, testing was oriented to identify all parameters and inputs that the algorithms need. Variation that could, somehow, improve the algorithm results were identified. See table 7 for the identified parameters that are needed and table 8 for parameters identified that are optional.

Table 7: Inputs Parameter of the Regularization Algorithm

Parameter Name	Description
Pixels	The HSI opened in HyCIAT.
Regularization Parameter Resolution	The resolution that the algorithm will construct the γ vector from 0 to 1. Is a mandatory input. During the testing phase, it was observed that this value affects considerably the results.
Endmembers for Inversion	Endmembers for inversion are mandatory and is a very important parameter during the inversion of the image (See section 2.6)
Maximum Curvature Retrieval Algorithm	Since there are there are two methods to retrieve the Maximum Curvature (see section 3.5), this is also a major parameter that impacts significantly the result. The default parameter is 'Derived Equations'.
Classifiers	This version of the toolbox has three different classification algorithms implemented: Minimum Euclidean Distance, Minimum Spectral Angle and Maximum Endmember Abundance Value. The default classifier is Minimum Euclidean Distance. (See section 3.6)
Optical Properties	<p>Optical properties are very important since they are not retrieved by the algorithm. Consequently, they must be given. Optical properties impact result significantly. (See section 3.4 for the methodology implemented on this project to retrieved the optical properties)</p> <p>The implemented interface has the capacity to receive a single optical properties vector for the whole image or a 3-Dimensional Matrix (one vector for every pixel) for both, a and b, properties.</p>
Regularization Parameter Selection Criteria	There are two criteria to select the Regularization Parameter implemented on this project. (For details see section 2.6.1). Both methods yield different results. The default value is 'Gamma of Minimum Error'
Other inputs	<p>There are another two extra parameters that the algorithm needs: Bathymetry (H) and zenith angle.</p> <p>For H, the algorithm has the capacity of managing either a single value for the whole image or a 2-Dimensional matrix of the same spatial size as the original image with the depth at each pixel.</p>

Table 8: Optional Input Parameters for the Regularization Algorithm

Optional Parameter Name	Description
Endmembers for Classification	Different endmembers can be input for classifying the image after the regularization is performed. During preliminary test, better results were obtained by processing the image with a reduced set of endmembers and then classifying the image using the complete set of endmembers. ¹³
Subset of the spectrum	The algorithm includes functionalities so that the user can select specific region of the spectrum to perform the inversion and or another specification to perform the classification. ¹⁴

All the parameters showed in tables 7 and 8, and their descriptions, were considered when designing the final interface. The next section will describe how the actual algorithm was coded. After that, section 4.2.2 will described the final implementation into HyCIAT through an interface that offer the researcher multiple tools to modify parameters as it sees fit. After the regularization algorithm finish processing a final form will present results and contain several visualization tools that help in the analysis of results, this form will be described on section 4.2.3.

4.2.1 General Functional Specifications

An interface was designed to allow the user to process any image supported by HyCIAT using the regularization algorithm. The interface includes functionalities and tools to manipulate any parameter described in tables 7 and 8 as the researcher sees fits. The code can be divided in to five mayor components: **Regularization Main Menu, Interfacing Function, Regularization Function, Classification Function and Result GUI**. Regularization Main Menu is the main window were the user can configure all the parameters needed to run the algorithm, including the optional parameters. After the user press the ‘Ok’ button, the algorithm calls the Interfacing Function that will receive all the Handles Structure¹⁵ from the Regularization Main Menu. This Interfacing Function process the *initial parameters* and calls the corresponding *Regularization Function*. After the image is regularized the same function process the *classification parameters*

¹³ Note: if the user does not input different endmember for classifying the image the endmember used to process the image will be used also to classify it.

¹⁴ Note: if the user does not select a region to be used for processing and classifying, the whole spectrum of the image opened will be used.

¹⁵ Handles Structure is a MATLAB structure usually used to store the pointers of every graphical component in an interface developed using GUIDE.

and call the corresponding *Classification Function*. When the classification is performed, the Interfacing Function saves all the results into a single file and pass the file path of it to the Result GUI so that it can be opened and reviewed. At the end, the Regularization Main Menu verifies that there were no errors during execution, and close itself. If the execution stops due to an unexpected error the interface will show a report of it and will remain opened with the last configuration loaded. Once the result GUI is opened it will remain opened until the user closes it. Figure 47 showed a sequence diagram showing the interaction among the mentioned components.

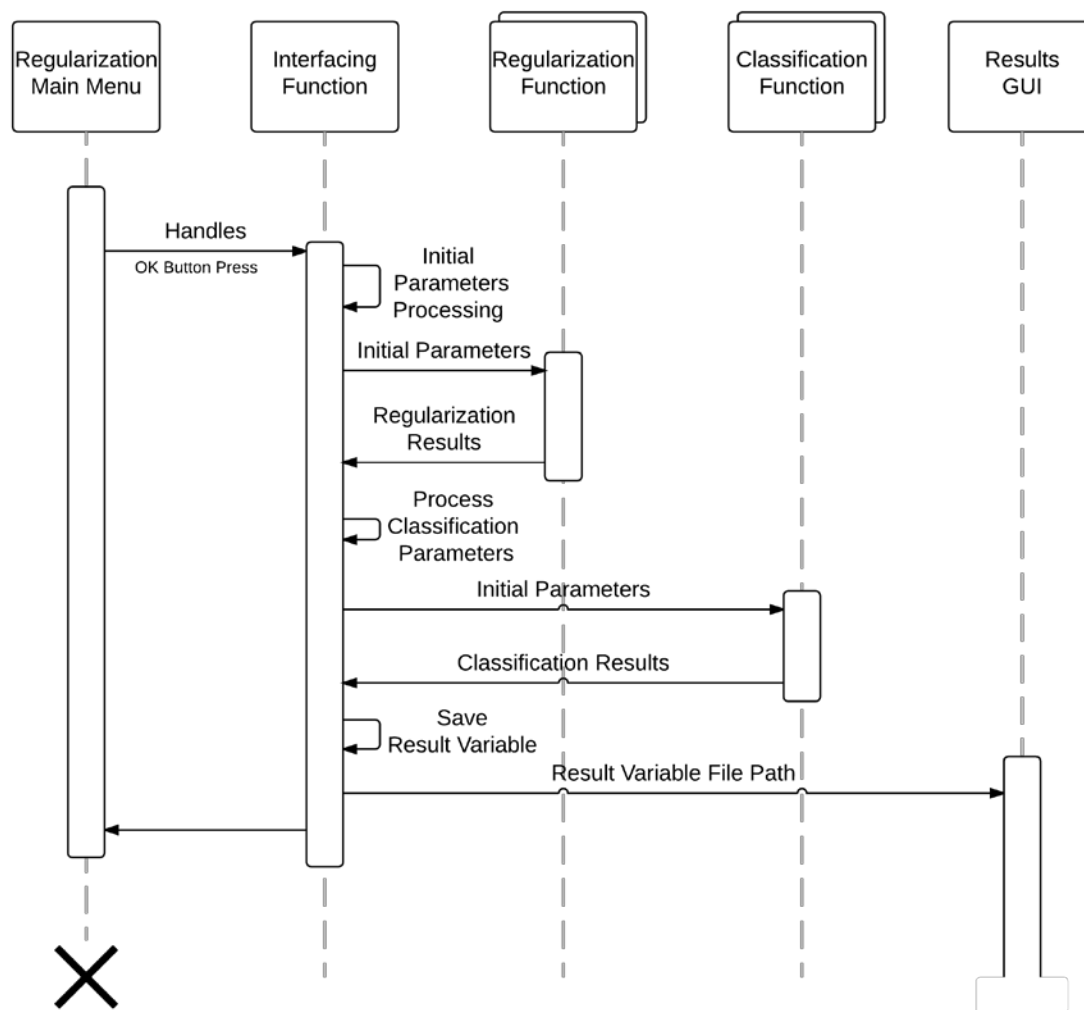


Figure 47: Regularization Menu Sequence Diagram

The Interface function is responsible to read and prepared the input parameters, to call the corresponding Regularization Function, to compile and save the result variable and finally pass the result variable file path to the Results GUI. The regularization function takes by parameters: Pixels, Depth (H), Zenith Angle (θ_w), Optical Properties (a, b), Endmembers and Regularization Parameter Resolution (RPR). The RPR is used to construct a vector from 0 to 1 in RPR steps that will hold all the values that γ will have during the inversion process. This vector is constructed inside the regularization function before starting to invert the image. Figure 48 showed the important inputs and outputs of the regularization algorithm.

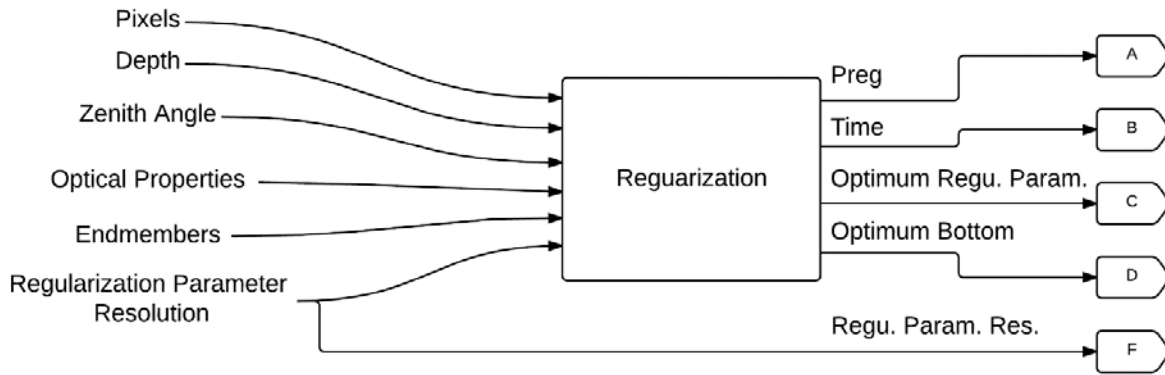


Figure 48: Regularization Algorithm Block Diagram 1

As can be observed in the previous figure, the regularization function outputs the following variables: P_{reg} , Time, Optimum γ , Optimum Bottom. The next stage in the algorithm is classification. Variables used on the classification stage is P_{reg} and Classification Endmembers. The user has the option of giving different endmembers to classify P_{reg} . If the user does not input a new set of endmembers the ones used on the regularization algorithm will be used to classify the image too. As can be observed in figure 49 the outputs of the classification algorithms are: Classification Maps and Performance Matrices. Classification maps is a two-dimensional matrix per classifier that each pixel is assigned a number from 0 to the number of endmember that represent the class to which each pixel was assigned to. Performance Matrices is a matrix that summarize how the classification perform on every endmember. This last result variable is conditioned if the endmembers contains testing regions or not.

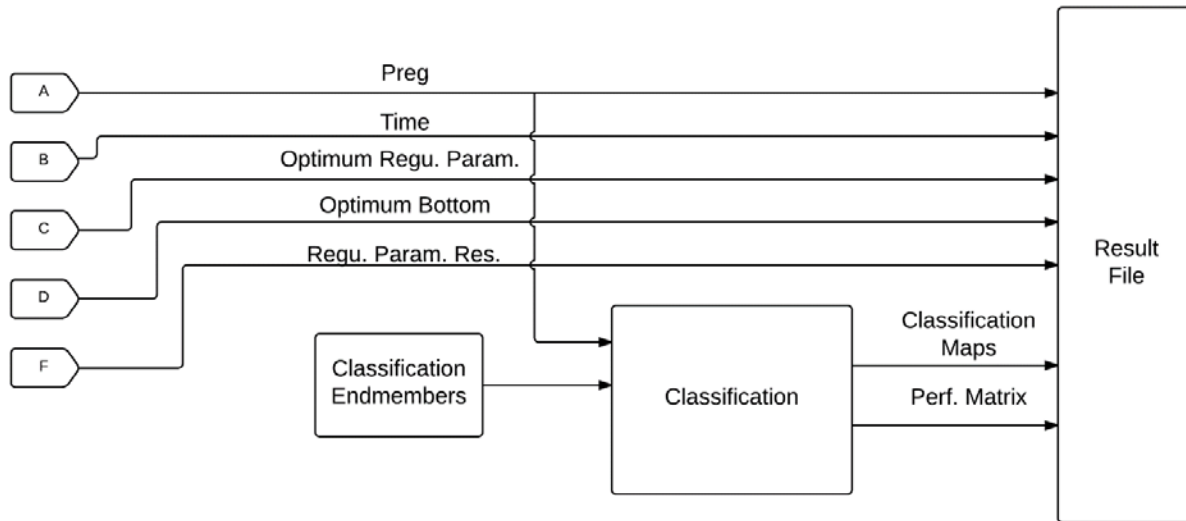


Figure 49: Regularization Algorithm Block Diagram 2

All the results, including the ones from the regularization algorithm, will be saved on the Result File. See table 9 for the summary of every variable. After these operations are performed successfully the file path of the result file is then sent to the result windows so that they can be shown and analyzed. Only results 1, 2 and 5 to 7 will be showed on the result GUI (See table 9).

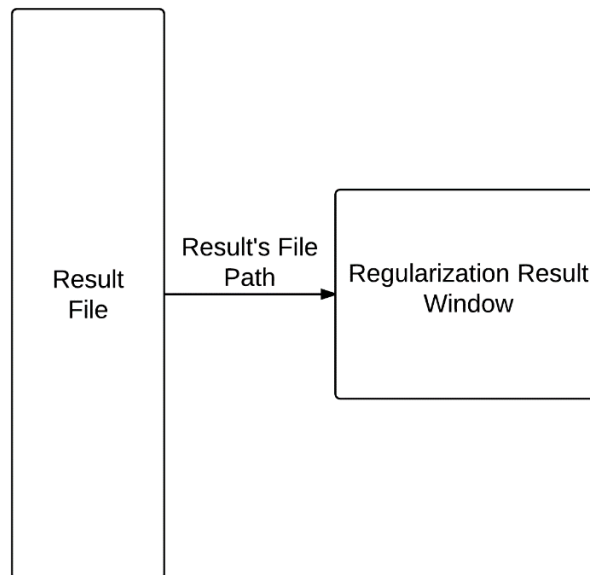


Figure 50: Regularization Block Diagram 3

Table 9: Result File Variables Descriptions

Number	Name	Description
1	P_{reg}	Main result of the regularization algorithm. In theory, this value represents the hyperspectral response of the bottom without the effect of the water column. This value is used to classify the bottom using a given Endmembers set.
2	Time	The time in minutes it takes the algorithm to invert the processed region of the HSI
3	Optimum Regularization Parameter	This variable is a matrix of the same size as the processed region of the image. It will contain the optimum regularization parameters (γ) used to invert each pixel in the image.
4	Optimum Bottom	This variable is a matrix of the same size as the processed region of the image. It will contain the optimum bottom (ρ_0) used to invert the image.
5	Regularization Parameter Resolution	The resolution used to construct the vector of values that will have (γ) during the inversion process.
6	Classification Maps	Is a two-dimensional matrix per classifier that each pixel has an assigned number from 0 to the number of endmembers that represent the class to which each pixel was assigned to.
7	Performance Matrix	It is a matrix that summarizes how the classification performs on every endmember. This variable will be present only if the endmembers contain testing regions.

The regularization algorithm has a unique sequence of steps; a pseudo code was presented on section 2.5.2 and was coded in the same way. Figure 51 presents a general operation flowchart of the regularization function. Basically, the algorithm first calculates the Optimum Regularization Parameter and the Optimum Bottom following the explanation on section 2.6. Then it uses this value to invert again the image and classify it using any classifier that the researcher sees fit. The classification stage is performed outside the regularization function for convenience and for future enhancement of the code.

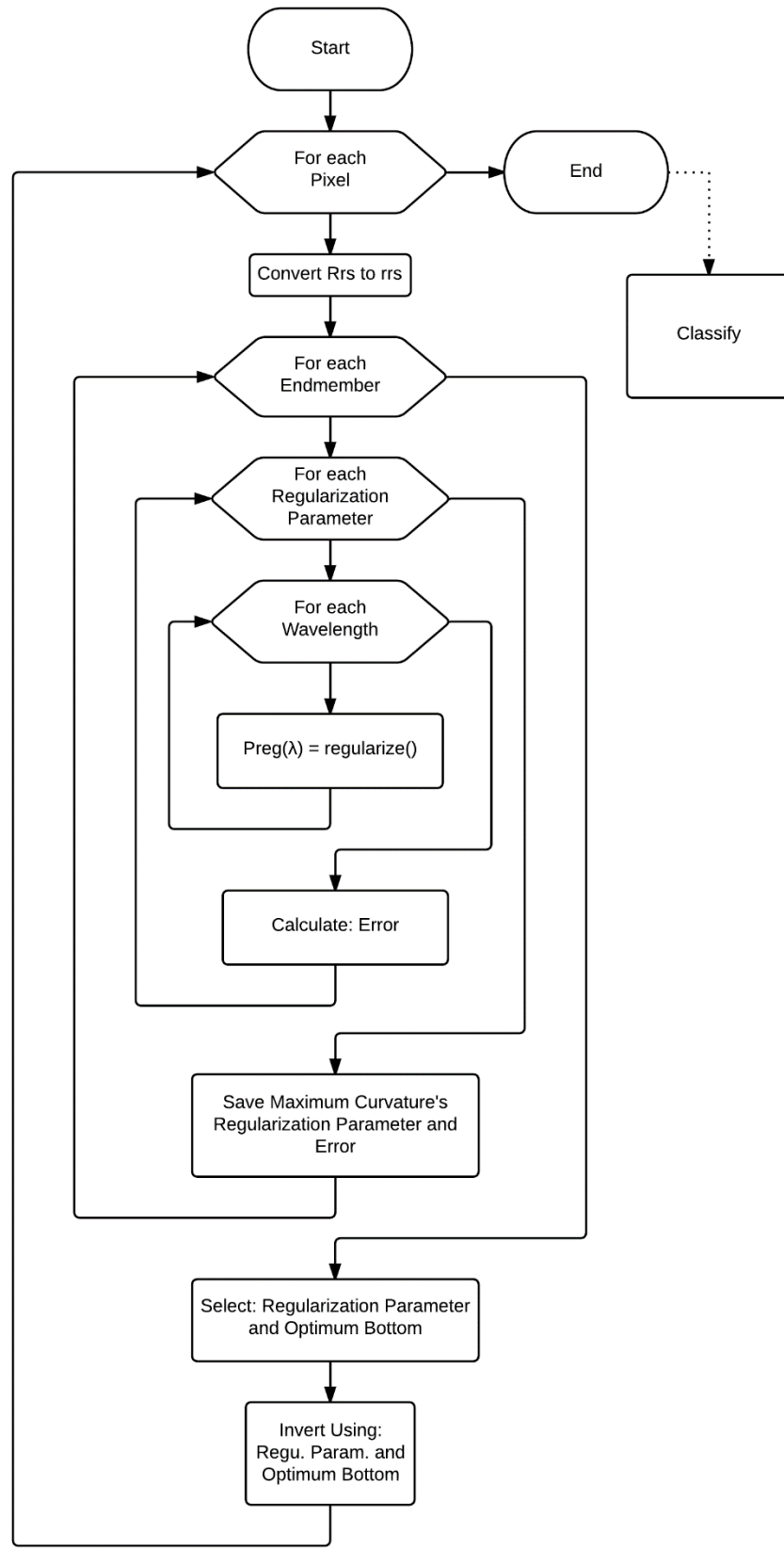


Figure 51: Regularization Function General Operation Flowchart

4.2.2 Integration into HyCIAT

The Regularization Menu can be opened directly on HyCIAT main interface on the classification menu as showed in the next figure:

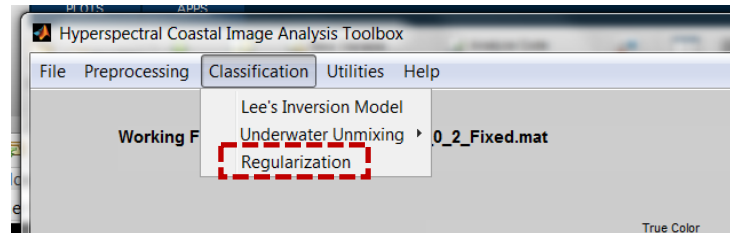


Figure 52: Opening Regularization Menu from HyCIAT GUI

After clicking Regularization option on the menu, the Regularization main interface will open, see figure 53:

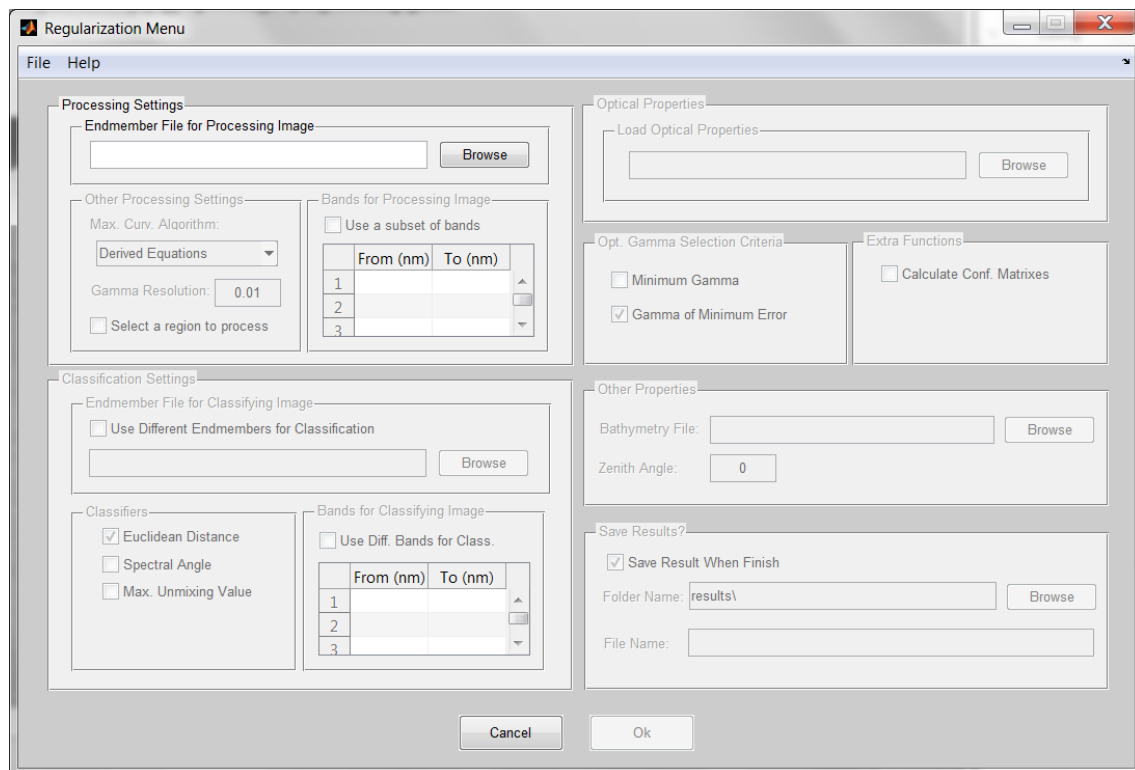


Figure 53: Regularization Main Menu

The Regularization Menu contains the necessary functionalities to manipulate every parameter described on tables 7 and 8. This menu will open with almost all the functionalities disabled for control purposes. Once all the necessary parameters are configured the 'Ok' button will be enabled. On the next sections, all the panels and functionalities will be described.

4.2.2.1 Processing Settings Panel

From top to bottom and left to right the first panel that is encountered is the Processing Settings (see figure 54). In this panel is where the endmembers that are going to be used to process the image. By loading the Endmember File for Processing Image will enable the controls for the rest of the parameters on the main window.

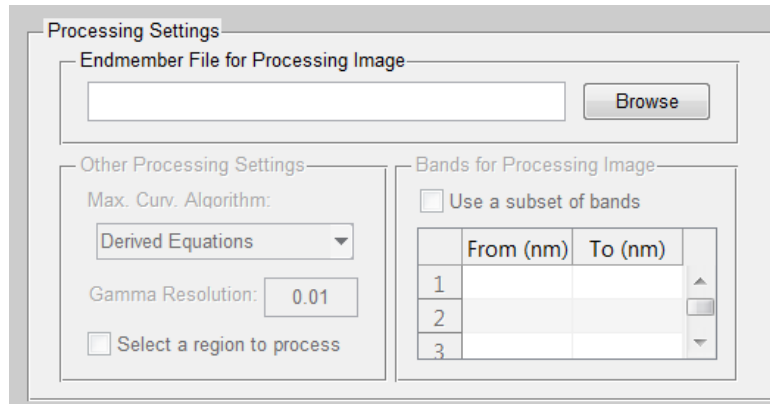


Figure 54: Processing Settings Panel from the Regularization Menu

Another panel inside the Processing Settings is the Other Processing Settings panel, this is where the user can select the Maximum Curvature calculation algorithm from a drop-down menu. Also, the user can specify the resolution of the γ vector used. And last the user can mark if only a region of the image is wanted to be process. This last functionality is used when the researcher only wants to process a certain region of the image instead of processing it completely. There exist three different Maximum Curvature selections: Derived Equation, Numerical Approximation and Single Regularization Parameter. They are explained on section 3.5. When Single Regularization Parameter is selected, the textbox called: Gamma Resolution changes to: Single Gamma.

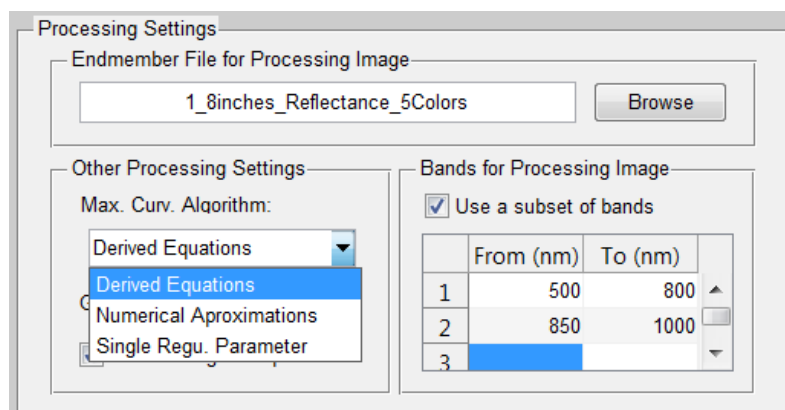


Figure 55: Maximum Curvature Algorithm Selection

The last panel in the Processing Settings is the one named ‘Bands for Processing Image’ this is where the user can select a subset of the bands to be used to process the image. The checkbox controls the Table. For example, if the main image contains bands from 500 to 1000 *nm* and the user does not want to include the bands between 800 and 850 *nm*, the user must first check ‘Use a subset of bands’ and fills the table as bellow¹⁶:

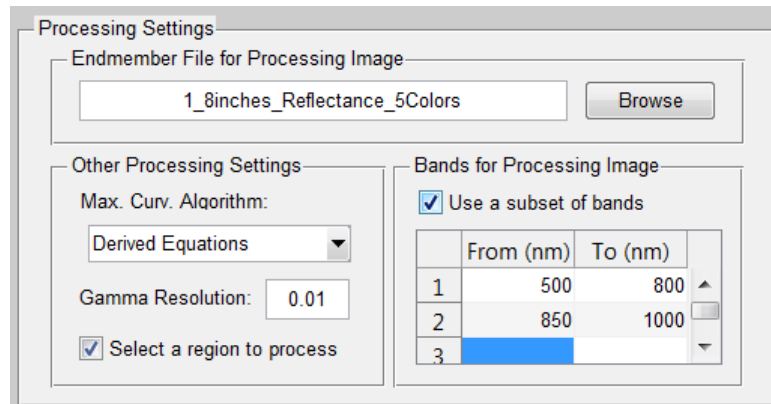


Figure 56: Subset of bands for processing example.

4.2.2.2 Classification Settings Panel

The next panel is the one named ‘Classification Settings’ (see figure 57). This is where the user can manipulate the parameters of the classification stage. There are a couple of important things to discuss of this Panel:

- The Endmembers for Classification are not mandatory. If Classification Endmembers are not specified on this panel the Processing Endmembers are going to be used for classification
- The toolbox come with three different classification algorithms, they are presented and described in section 3.6
- To specify a subset inside the specified processing subset the user must check ‘Use Diff. Bands for Class.’ and enters the corresponding region. For example, if the user only wants to use the bands from 400 to 650 *nm*, the Table must be filled as showed in figure 58. It is important to know that this subset will be based on the selected processing subset described in the last section.

¹⁶ Note: up to 4 different regions can be specified. If the user doesn’t select a subset of bands the whole image’s spectrum will be use

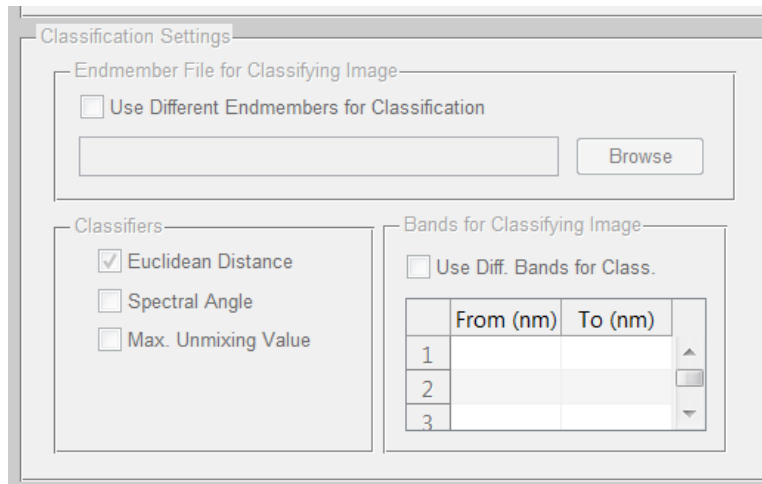


Figure 57: Classification Settings Panel from the Regularization Menu

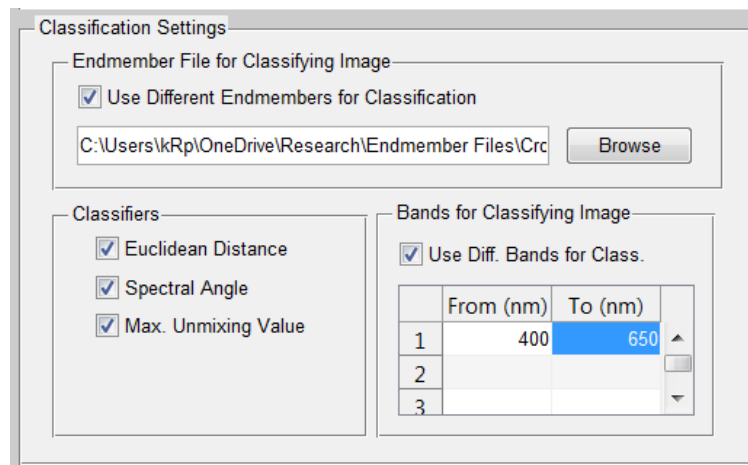


Figure 58: Selecting a subset of bands for classification example

4.2.2.3 Optical Properties, Optimal Gamma Selection and Extra Functions Panels

The next panel is the 'Opt. Gamma Selection Criteria'. The complete name is the Optimum Gamma Selection Criteria. There are two methods of selecting this important value, see section 2.6.1.

Finally, the last panel is the 'Extra Functions' (See figure 59) which contains only one functionality and is the Calculate Performance Matrices. If endmembers were selected using the **ROI Tools** (ROI Tools will be shortly explained on section 4.3) and testing regions were selected the algorithm will calculate automatically the performance matrices based on the classification results.

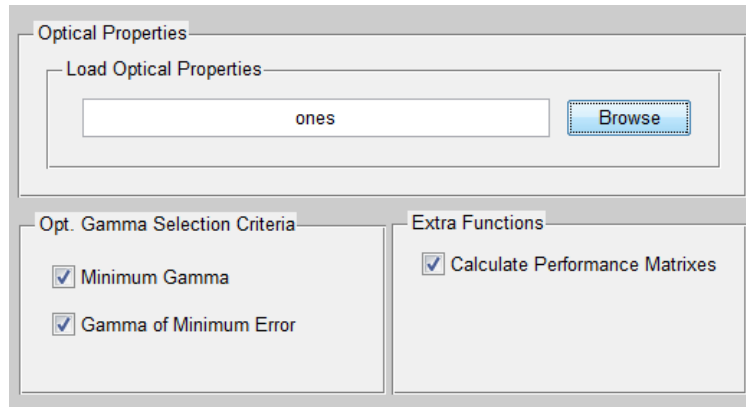


Figure 59: Optical Properties, Opt. Gamma Selection Criteria and Extra Functions Panels

4.2.2.4 Other properties and Save Results Panels

Other Properties Panel is used to configure two additional properties that the Regularization Algorithm needs: Bathymetry (H) and Zenith Angle(θ). The last panel of the Regularization Menu is Save Results (See figure 60). The GUI will upload with this value checked by default. If the user doesn't want the result to be automatically saved before the result windows opens it must uncheck the checkbox named Save Result When Finish. Also, in this panel, the user can configure the filename that the result file will have. The GUI creates a result file name automatically based on the time that the endmembers were input, opened Endmembers file name and Regularization Parameters Vector Resolution (Gamma Resolution).

For example: **Results_201410261651_1_8inches_Reflectance_5Colors_Gamma0_01**

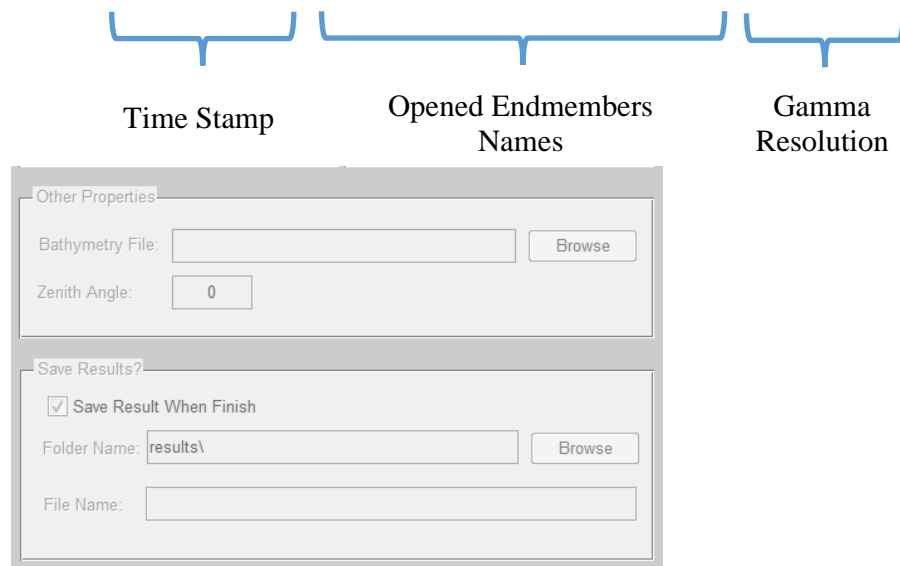


Figure 60: Other Properties and Save Results Panels from the Regularization Menu

4.2.3 Regularization Result Analysis GUI

The regularization algorithm saves all result variables on a file when it finishes. The file path of this result file is then passed to the result GUI that will display all results. The result GUI is designed to assist the user in the visualization and analysis of the results. The Result GUI consists of five main parts as can be observe in figure 61 and will be described in the next section.

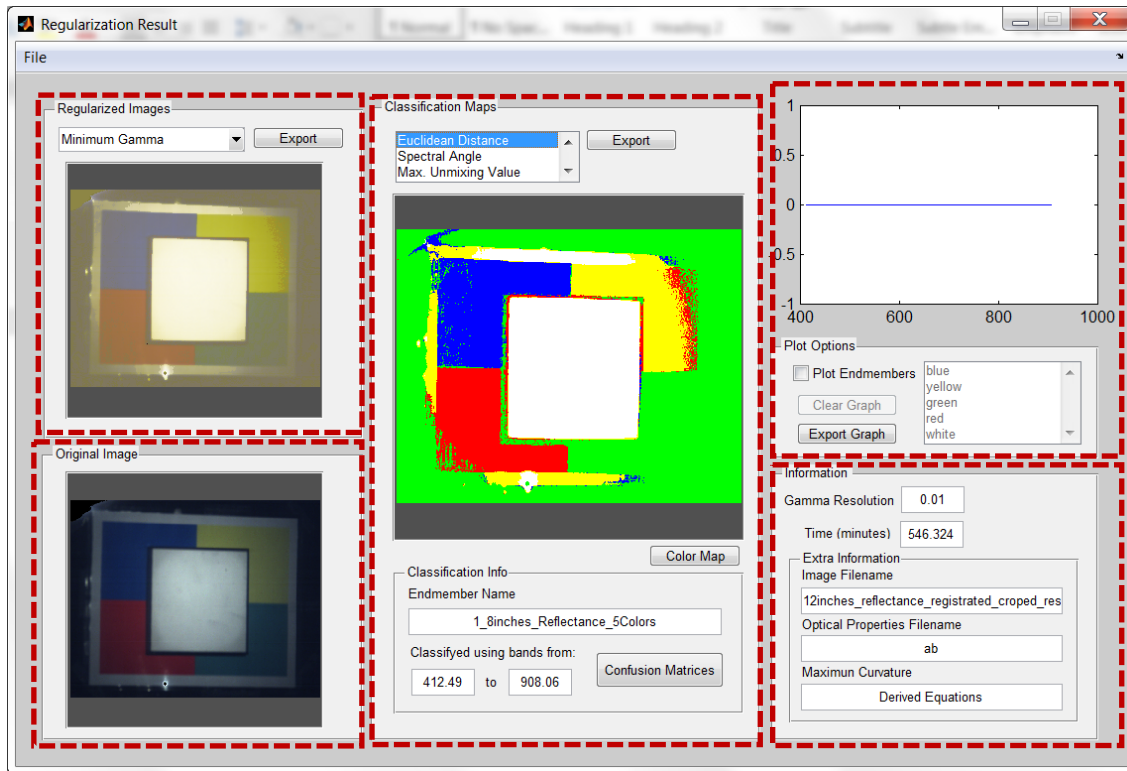


Figure 61: Regularization Result GUI

4.2.3.1 Regularized Images

The regularized images are the resulting P_{reg} . Described in other words, the regularized images are the inverted images or the reconstructed bottoms. They can vary based on the selected Optimum Gamma Selection criteria. The panel includes a dropdown menu from which the user can toggle between both results. The panel also includes an Export button that by pressing it the image displayed will open in a separated figure so that it can be copied and exported to other programs.

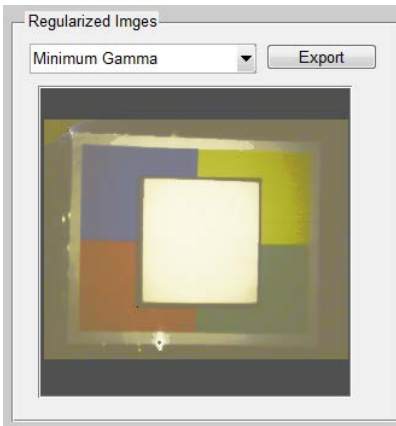


Figure 62: Regularized Images Panel Form Regularization Result GUI

4.2.3.2 Original Image

The original image is the true color RGB representation of the opened image before processing it. This was added to the GUI for comparison purposes.

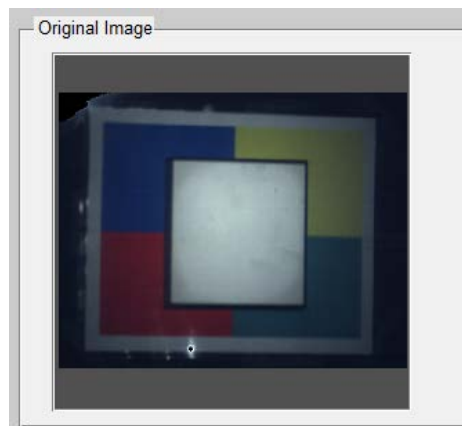


Figure 63: Original Images Panel from the Regularization Result GUI

4.2.3.3 Classification Maps

The classification maps will present the actual classification by coloring each class based on a custom color map. This map is saved on a variable called '**colormap.mat**' and can be changed to be adjusted to different classification maps by pressing the Color Map button. On the panel, it can be found a menu that will list all the classification algorithms applied to the image so that the user can toggle among them to see differences. It features an export button that by pressing it the classification map displayed will open in a separated figure so that it can be copied and exported to other programs.

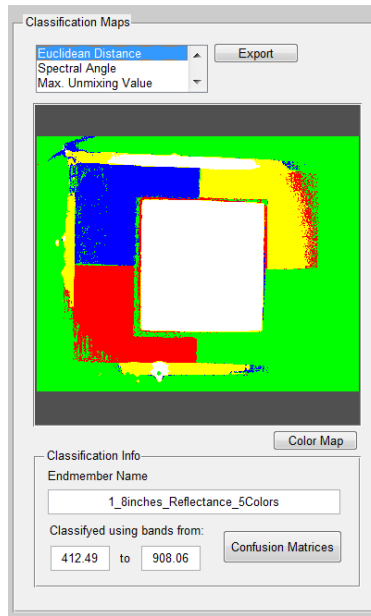


Figure 64: Classification Maps Panel Form Regularization Result GUI

Also at the bottom of the panel there is another panel called ‘Classification Info’ that will show up the filename of the endmembers used and the minimum and the maximum wavelength of the region used to classify the image. It also contains a button that, if the classification was performed with trainings regions, will open another GUI that will show up the performance matrices. These matrices can be used to compare numerically each classification, also they can be copied and passed on any spreadsheet software like Microsoft Excel. As can be observed in figure 65, the Performance Matrices GUI contains the same drop down menu and list to toggle between results as the Regularization Result GUI.

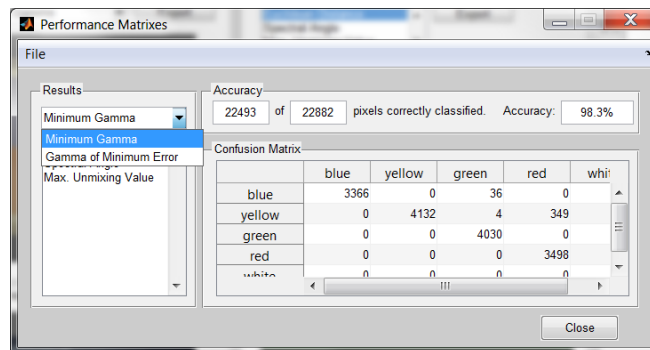


Figure 65: Performance Matrices GUI.

The color map applied to the classification maps can be modified on the following interface that appears after pressing the Color Map button:

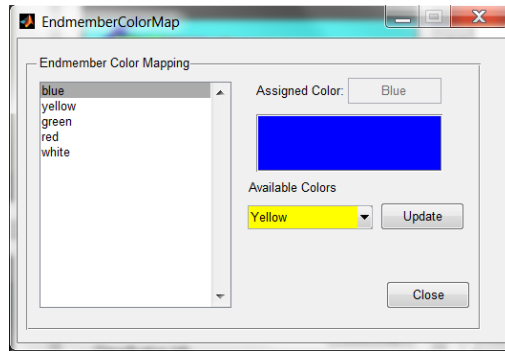


Figure 66: Update Color Map Interface

To update the color assigned to each class, first the user selects the endmember from the list, then selects the wanted color from the available ones on the Available Colors drop down menu and finally pressing the Update button. The selected color map configuration will be updated, changed on the Regularization Result interface and saved as default colormap on the **'colormap.mat'** variable.

4.2.3.4 Plot and Plot Options

The Plot and Plot Options is a very useful feature that allows the user to visually compare any pixel selected with the available endmembers. The plot will show the reflectance vs wavelength plot of any selected pixel either on the Regularized Image or on the Classification Map image. By clicking any pixel, the interface will show the following information: Column Number, Row Number and the Class that the selected pixel was assigned to. Endmembers can be plotted on top of the resulting reflectance for comparison purposes. Multiple endmembers can be selected and plot by holding down the **Ctrl** key (See figure 67 and 68).

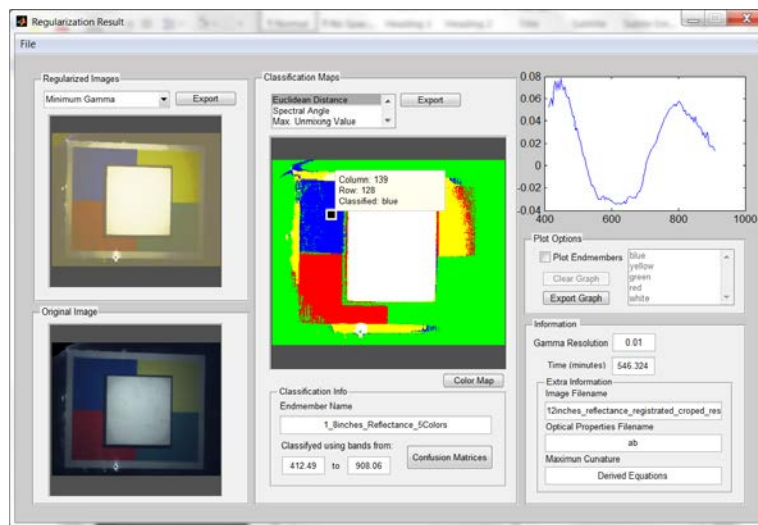


Figure 67: Regularization Result GUI with a Reflectance plot of a certain pixel

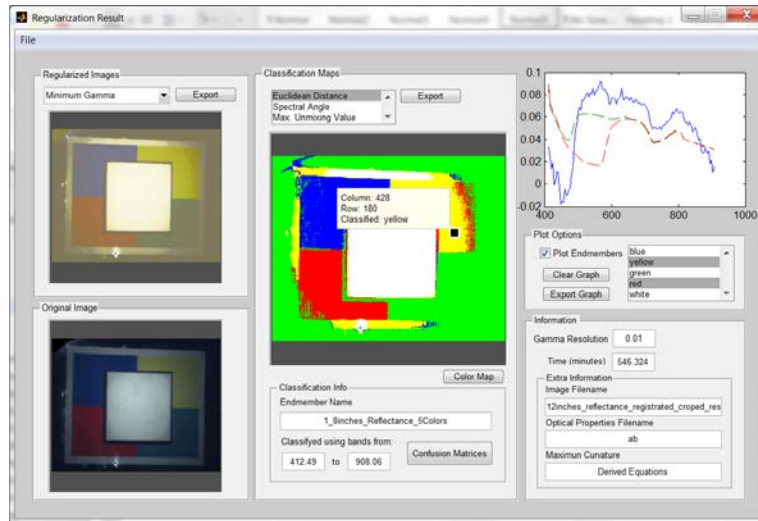


Figure 68: Regularization Result GUI with multiple endmembers plotted

4.2.3.5 Information

The last panel is the Information Panel. This panel shows the selected Resolution of the Regularization Parameter's Vector, the time it took the algorithm to process, the image name, the Optical Properties filename and the algorithm selected to calculate the derivative of the maximum curvature function.

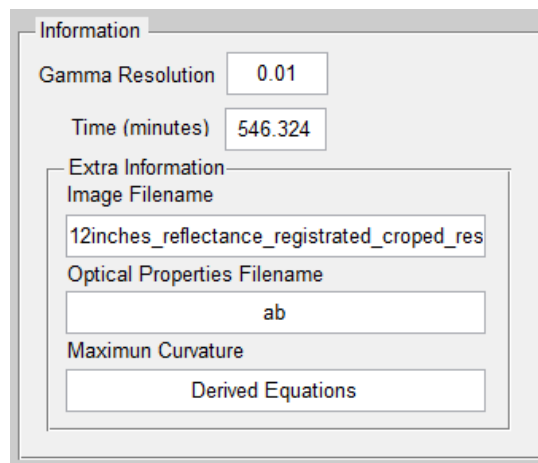


Figure 69: Information panel from the Regularization Result GUI

4.3 Additional tool: Region of Interest Tools

Region of Interest Tools is a GUI that integrates several functionalities needed to create components and parameters derived from region of interest (**ROI**¹⁷). With this tool, the user can:

- Visualize, create and manipulate ROIs.
- Create Endmembers Files for the Underwater Unmixing Algorithm and the Regularization algorithm with their respective testing regions.
- Extract data directly form ROIs, in known data formats, for external studies.
- Mask Saturated Pixels based on a certain region of the image.
- Export a real color image from the opened HSI that can include the selected regions of interest and its testing regions
- Export Reflectance vs Wavelength graph of the selected endmembers and pixels.

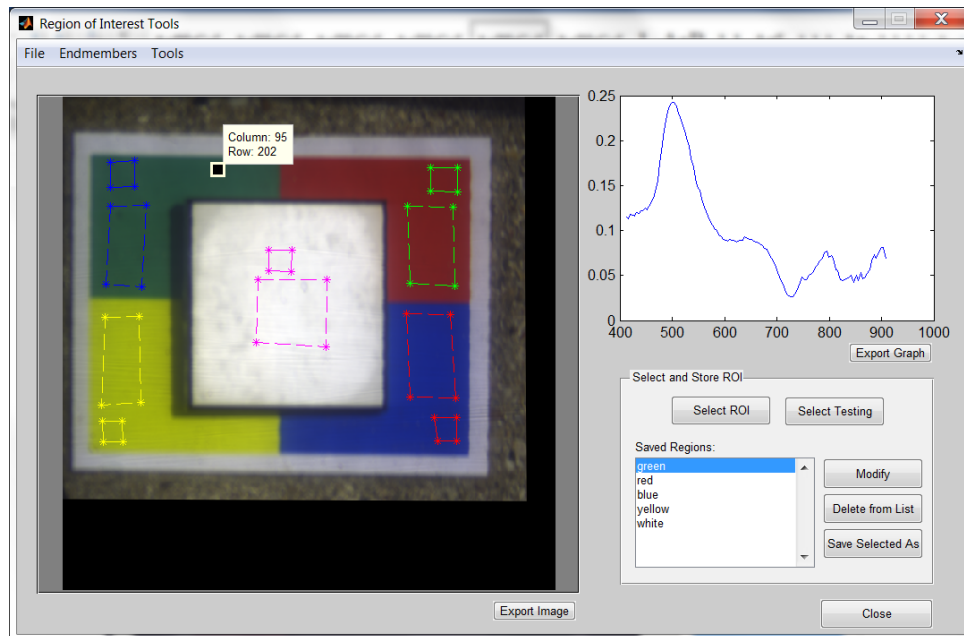


Figure 70: Region of Interest Tool GUI

¹⁷ Explained on Page 24.

5 Results

This section summarizes the obtained results and is divided in three main sections. The first section is 5.1 Underwater Linear Unmixing with AVIRIS Data, the data presented on this section was used to measure the difference of the obtained results between the two versions of the toolbox. The second section is 5.2 Underwater Linear Unmixing with Real Controlled Data. This section shows the obtained results from the underwater unmixing algorithms when applied to the new dataset. These results were used to measure the impact of the additional functionalities included to the unmixing algorithms. The second section is 5.2 Regularization Algorithm; this section shows the obtained result from the regularization algorithm applied to the new dataset. These results were used to validate the functionality and to establish a baseline results for future studies using the Regularization algorithm.

5.1 Underwater Linear Unmixing with AVIRIS Data

One of the main objective of this project was to Update HyCIAT from MATLAB 2007 up to MATLAB 2013a. After restoring functionality, it was observed that results between both versions were not similar. It was discovered that some default parameters, of MATLAB's `lsqnonlin` native function, change across platforms versions, see section 4.1.1. Parameters were modified so that both versions (2007 and 2013) had the same default parameter of the mentioned function. To test the impact of the parameter that was modified, results were produced in the following manner: **Without Modifying Parameter**¹⁸ and **With Parameter Modifications**¹⁹. The two images showed on figure 71 and published on [1], were selected to be processed on both version of the toolbox with and without parameter modifications without bathymetry using LIGU and CIUB algorithms. Unmixing results include per image: 5 optical parameters in some cases and 4 in others, plus one abundance map per endmembers given to the algorithms. The endmembers were sand, coral, and algae. The result set consists of more than 50 images, therefore the results obtained from **Image A**, shown in figure 71, will be showed on section 9.1 (Appendix). Image A and Image B are part of a set of hyperspectral images obtained from Kaneohe Bay Hawaii on 2000 using AVIRIS. Images were atmospherically corrected, subset from 224 bands to 42 in the 400 to 800 nm range and the land was masked before being process by the unmixing algorithms. [1]

¹⁸ Without Modifying Parameters, it means that the images were processed on the current version of the toolbox (2013) without modifying the default value of the identified parameter.

¹⁹ With Parameter Modifications, it means that the default value of the identified parameter of the optimization function was set to the same value that has on the previous version of the toolbox (2007).

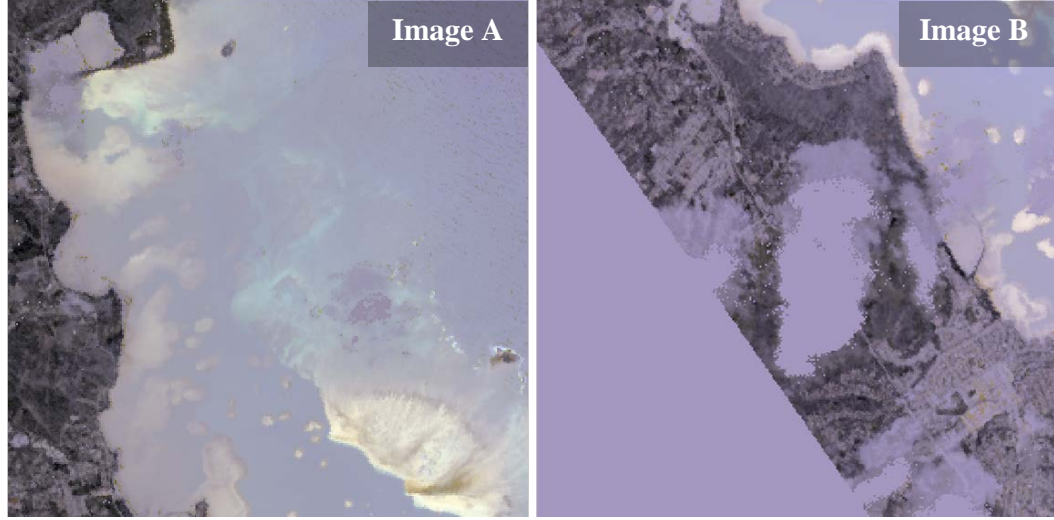


Figure 71: AVIRIS Images: A and B selected from [1]²⁰ to be processed

The calculated Sum of Squared Errors (SSE) was used as the mathematical foundation between results obtained from HyCIAT 2013 and from HyCIAT 2007. SSE results was used to perform a comparative analysis between the both results and measure the impact of the modified parameter. The SSE is obtained first by processing the image on the original version of the toolbox. Second, the same image will be process on the newer version of the toolbox without modifying the default parameters of the optimization function. Then, the SSE of the resulting optical properties and abundances will be calculated using the following formula:

$$\text{SSE of result } Val = \sum_{i=1}^n (Val_{i_{2007}} - Val_{i_{2013}})^2 \quad (70)$$

where, n is the number of pixels, and Val_i is the corresponding obtained result for each optical properties and abundances of pixel i . Val can represent: Depth, Bottom Reflectance, Backscattering, Absorption, Phytoplankton, Sand, Coral and Algae. Then this process will be repeated with the results obtained from HyCIAT 2013 with the default parameters configured as in HyCIAT 2007. The result is an SSE number for each underwater unmixing algorithm results from: HyCIAT 2013 without modified parameters and HyCIAT 2013 with modified parameters, refer to table 10. Finally, two additional quantities were calculated to perform a comparative analysis with the obtained SSEs. One of them is the Individual Similarity. This quantity will be used to determine which individual

²⁰ Images obtained from Kaneohe Bay Hawaii on 2000 using AVIRIS²⁰. In [1], image were atmospherically corrected, subset from 224 bands to 42 and the land was masked before being process by the unmixing algorithms. The images were processed with bathymetry data that comes from a survey of the Hawaiian Islands conducted around 2000 compiled for US Naval Oceanographic Office, US Geological Service and US Army Corps of Engineers Honolulu District. This data was provided by Torres-Madroñero along with the existing version of HyCIAT.

results from 2013 were more like the obtained ones from HyCIAT 2007. The individual similarity is calculated by dividing the obtained individual SSE with parameter modifications by the obtained individual SSE without parameter modification. The second quantity is the Total Similarity that will be used to calculate how similar results obtained from HyCIAT 2013 are like the results obtained from HyCIAT 2007. The total similarity sums all the obtained individual SSE with parameter modifications and divide it by the sum of all the obtained individual SSE without parameters modifications. The individual similarity and total similarity will be calculated using equations 71 and 72 respectively:

$$\text{Individual Similarity} = 1 - \frac{SSE \text{ Mod}}{SSE \text{ UnMod}} \times 100\% \quad (71)$$

$$\text{Total Similarity} = 1 - \frac{\text{Total } SSE \text{ Mod}}{\text{Total } SSE \text{ UnMod}} \times 100\% \quad (72)$$

Where *SSE Mod* corresponds to the values on the Modified Parameters column and *SSE UnMod* corresponds to the values on the Unmodified Parameters column. The following table present the calculated SSE of each individual result (SSE Modified Parameter and SSE Unmodified Parameter columns) with its calculated Individual Similarity and the Total Similarity. Refer to Appendix Section 9.2 for more resulting SSE comparison tables.

Table 10: Result's SSE Differences LIGU of Image A without Bathymetry

Result Name	SSE Modified Parameter (SSE Mod)	Calculated SSE Unmodified Parameter (SSE UnMod)	Individual Similarity
Depth	71555.72	604876.09	88.17%
Bottom Reflectance	174.58	312.56	44.14%
Backscattering	0.26	0.74	65.31%
Absorption	206.33	264.22	21.91%
Phytoplankton	8.49	35.04	75.77%
Sand	172.86	371.38	53.45%
Coral	153.40	226.48	32.27%
Algae	169.95	394.59	56.93%
Total SSE	72441.58	606481.09	
Total Similarity	88.06%		

The following graphs compares the obtained similarities of each results after modifying the identified parameter. For interpretation purposes, please keep in mind that: **100%** means that results obtained from HyCIAT 2013 with parameter modification were absolutely like the ones obtained

in HyCIAT 2007 by modifying parameters. **0%** means that results obtained from HyCIAT 2013 with parameter modification were absolutely similar to the ones obtained from HyCIAT 2013 without parameter modification. **Negative Values** means that results obtained from HyCIAT 2013 did not become similar that the ones obtained from HyCIAT 2013 without modifying parameters.

5.1.1 Obtained Similarity of AVIRIS – Image A using LIGU algorithm:

- Total Improvement: 88.06%

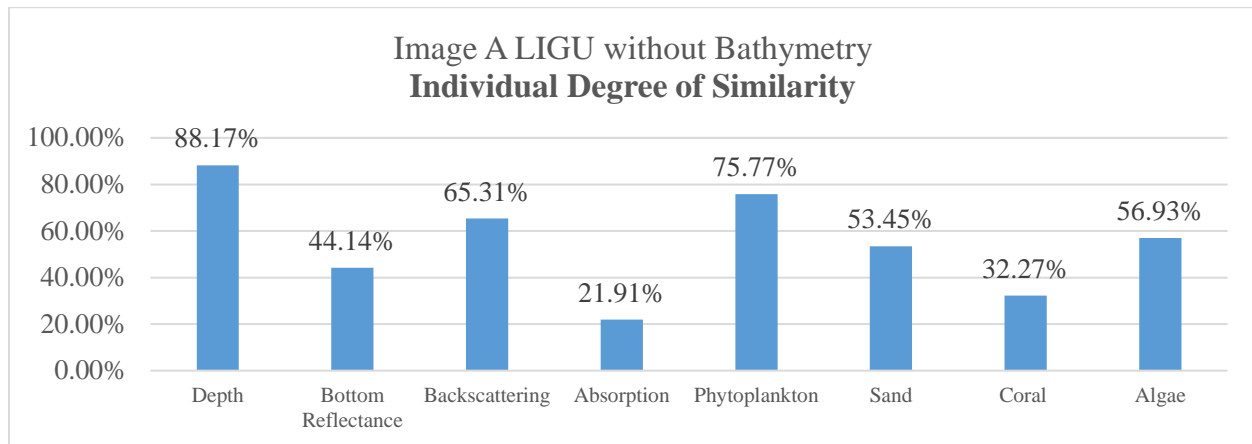


Figure 72: Improvement by modifying parameters – Image A LIGU without Bathymetry

5.1.2 Obtained Similarity of AVIRIS – Image B using LIGU

- Total Improvement: 6%

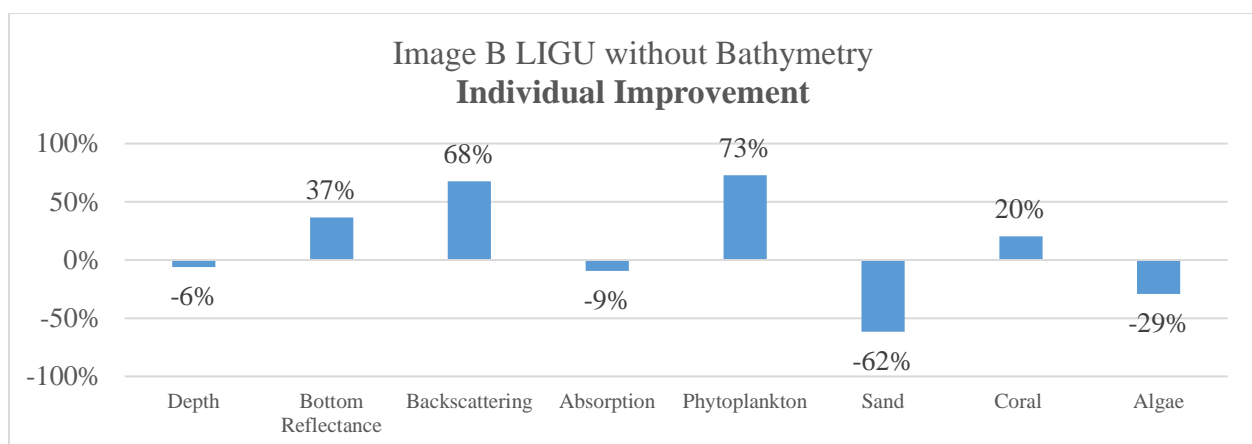


Figure 73: Improvement by modifying parameters – Image B LIGU without Bathymetry

5.1.3 Obtained Similarity of AVIRIS – Image A using CIUB algorithm

- Total Improvements: 36.54%

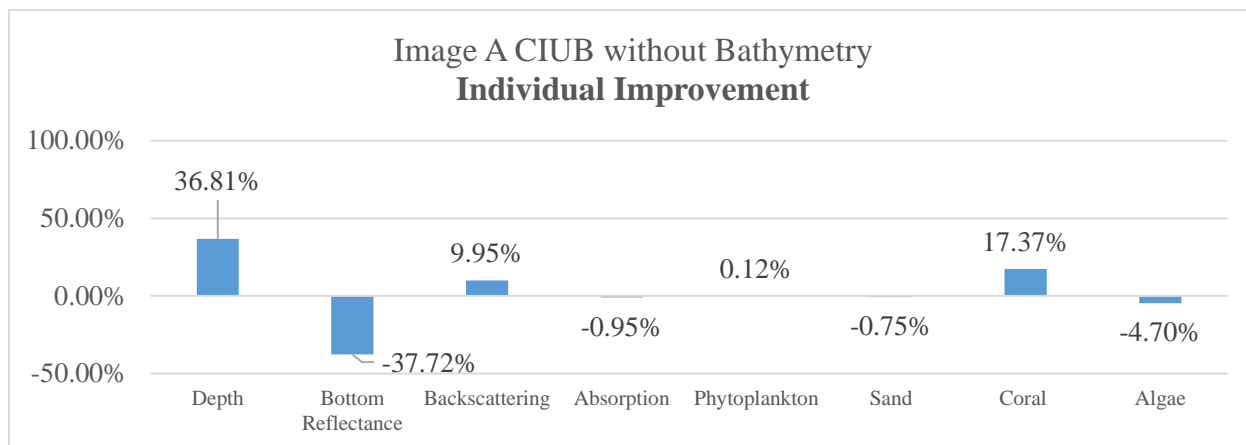


Figure 74: Improvement by modifying parameters – Image A CIUB without Bathymetry

5.1.4 Obtained Similarity of AVIRIS – Image B using CIUB algorithm

- Total Improvements: 3.54%

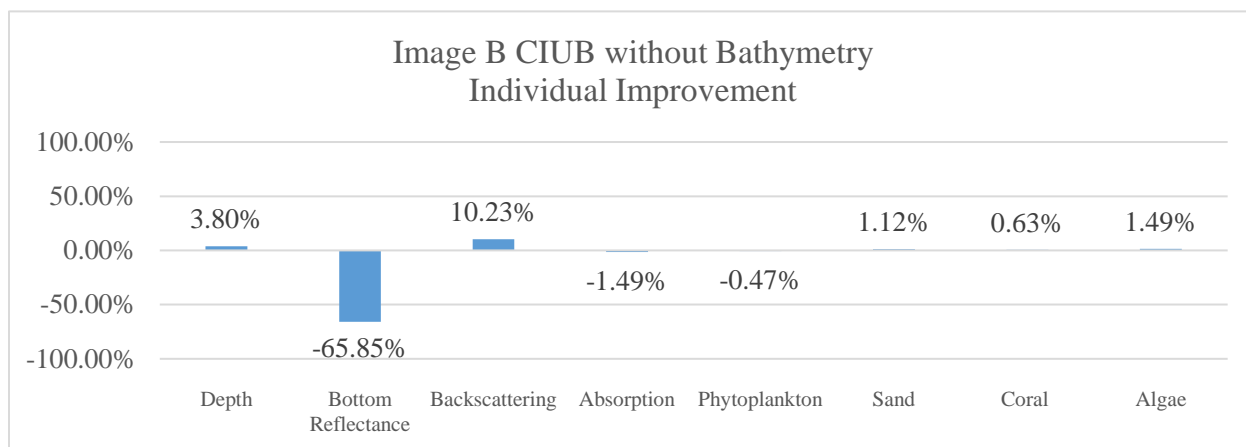


Figure 75: Improvement by modifying parameters – Image B CIUB without Bathymetry

5.2 Underwater Linear Unmixing applied to Real Controlled Data

Recall from section 4.1 two functionalities were added to the underwater unmixing algorithms. These functionalities are called: Custom Unmixing Range and Custom Button, refer to sections 4.1.2 and 4.1.3. The validation of these enhanced features of the underwater unmixing algorithms was performed using the following two images: 12.0 in without TiO_2 and 12.0 in with 0.5 g of TiO_2 (Recall that TiO_2 is being used to simulate turbid waters, see section 3.1 for image details). These

images were processed on HyCIAT 2007 and on HyCIAT 2013 so that a comparative analysis between results can be performed. Furthermore, HyCIAT 2013 will be configured in different ways, this will allow us to measure the impact of the modifications performed to the toolbox. Next table summarizes the different configurations used. From now on each configuration will be referenced by the Configuration Name:

Table 11: Configuration Descriptions

Configuration Name	Description
Baseline	Images processed in HyCIAT 2007.
2013-1	HyCIAT 2013 configured as HyCIAT 2007.
2013-2	HyCIAT 2013 configured with extended unmixing ranges
2013-3	HyCIAT 2013 configured with a custom sand spectral signature.
2013-4	HyCIAT 2013 configured with extended unmixing ranges, custom sand spectral signature and PrecondBandWidth parameter set to 0.

To quantify unmixing results, the testing regions presented on section 3.3 were used as “pure pixel” of each class. The fractional abundance result of a pure pixel on the unmixing algorithm should be one on the training region selected for that class. This means that, after processing the blue region, the endmember “Blue” should yield a fractional abundance of 1 on its testing region and 0 on others. The accuracy of each endmember over its testing region will be calculated with the following formula:

$$Acc_i = \frac{\sum_j^P x_{i,j}}{\sum_j^P T_{i,j}} \times 100 \quad (73)$$

where: Acc_i is the accuracy of the i^{th} endmember, $x_{i,j}$ is the obtained abundance for the i^{th} endmember on the j^{th} pixel of the particular testing region, P is the amount of pixel enclosed by the testing region and $T_{i,j}$ is the theoretical abundance value of the endmember that the testing region pertains to i . Since the testing region selected represents “pure pixels”, $T_{i,j}$ is equal to 1.

5.2.1 LIGU Results from the 12.0 in without TiO₂ Image and 5 Colors Endmembers

This section will show results obtained from the 12.0 in image without TiO₂ using LIGU algorithm. In this case, five endmembers representing: Blue, Yellow, Green, Red and White regions from the 1.8 in hyperspectral image without TiO₂ were used as input to the algorithm (See next figure, refer to section 3.3 for more information on the endmembers selected). The obtained accuracies from each configuration are showed on Table 11.

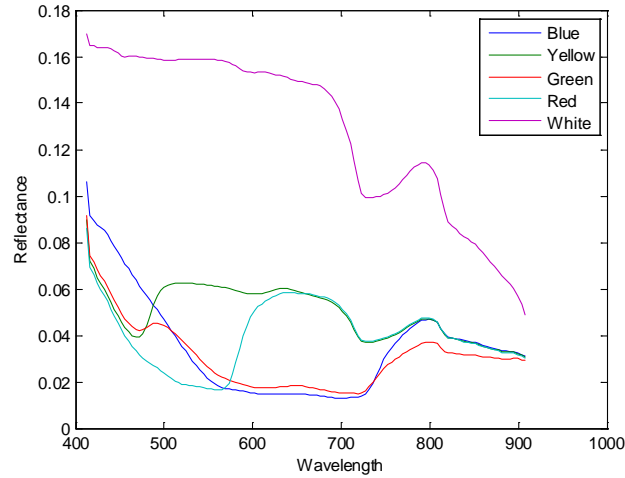


Figure 76: Endmember used for the 5 colors underwater unmixing processing

Table 12: LIGU results from the 12.0 in image without TiO₂ and 5 color endmembers

Configurations	Overall Accuracy	Endmembers				
		Blue	Yellow	Green	Red	White
Baseline	19.87%	0.00%	0.00%	0.00%	0.00%	99.35%
2013-1	20.00%	0.00%	0.00%	0.00%	0.00%	100.00%
2013-2	20.00%	0.00%	0.00%	0.00%	0.00%	100.00%
2013-3	49.88%	93.53%	0.00%	0.02%	55.88%	100.00%
2013-4	49.89%	93.53%	0.00%	0.02%	55.88%	100.00%

5.2.2 LIGU Results from the 12.0 in without TiO₂ Image and 4 Colors Endmembers

This section will show results obtained from the 12.0 in image without TiO₂ using LIGU algorithm with 4 endmembers that correspond to: Blue, Yellow, Green and Red regions extracted from the 1.8 in image without TiO₂, (see next figure and refer to section 3.3 for more information on the endmembers selected). Table 12 shows the obtained accuracy from LIGU with the 12.0 in without TiO₂ image and 4 color endmembers.

Table 13: LIGU results from the 12.0 in without TiO₂ image and 4 color endmembers

Configurations	Overall Accuracy	Endmembers			
		Blue	Yellow	Green	Red
Baseline	25.00%	0.00%	100.00%	0.00%	0.00%
2013-1	25.00%	0.00%	100.00%	0.00%	0.00%
2013-2	40.63%	62.53%	100.00%	0.00%	0.00%
2013-3	74.94%	100.00%	100.00%	0.00%	99.75%
2013-4	74.94%	100.00%	100.00%	0.00%	99.75%

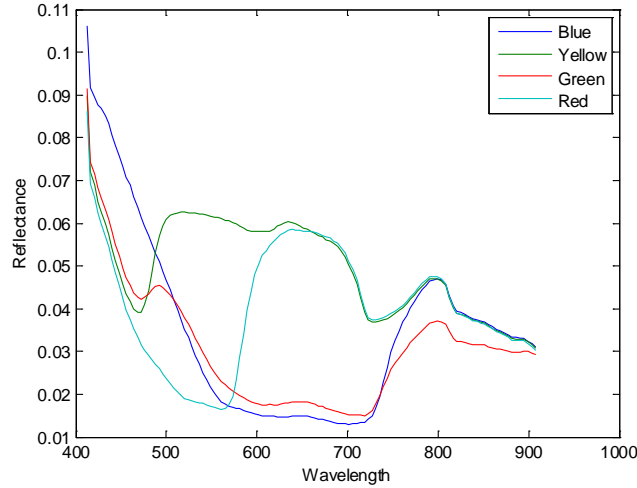


Figure 77: Endmembers used for 4 colors underwater unmixing processing

5.2.3 CIUB Results from the 12.0 in without TiO₂ Image and 5 Colors Endmembers

This section shows the obtained results from the 12.0 in image without TiO₂ using CIUB algorithm. The same five endmembers showed on section 5.2.1 representing the Blue, Yellow, Green, Red and White regions were used as input to the algorithm. These endmembers were extracted from the 1.8 in without TiO₂ image. Table 13 summarize the obtained results:

Table 14: CIUB results from the 12.0 in without TiO₂ image and 5 color endmembers

Configurations	Overall Accuracy	Endmembers				
		Blue	Yellow	Green	Red	White
Baseline	21.18%	0.55%	0.00%	5.36%	0.00%	100.00%
2013-1	20.36%	0.00%	0.00%	1.78%	0.00%	100.00%
2013-2	20.64%	3.18%	0.00%	0.00%	0.00%	100.00%
2013-3	20.64%	3.18%	0.00%	0.00%	0.00%	100.00%
2013-4	26.20%	31.00%	0.00%	0.00%	0.00%	100.00%

5.2.4 CIUB Results from the 12.0 in without TiO₂ Image and 4 Colors Endmembers

This section shows the obtained results from the 12.0 in image without TiO₂ using CIUB algorithm. The same endmembers, showed in section 5.2.2, that corresponds to the Blue, Yellow, Green and Red regions were used as input to the algorithm. These endmembers were extracted from the 1.8 in without TiO₂ image. Table 14 summarize the obtained results:

Table 15 CIUB results from the 12.0 in without TiO₂ image and 4 Color Endmembers

Configuration	Overall Accuracy	Endmembers			
		Blue	Yellow	Green	Red
Baseline	25.51%	2.05%	100.00%	0.00%	0.00%
2013-1	25.04%	0.16%	100.00%	0.00%	0.00%
2013-2	35.75%	43.00%	100.00%	0.00%	0.00%
2013-3	36.45%	45.82%	100.00%	0.00%	0.00%
2013-4	36.44%	45.75%	100.00%	0.00%	0.00%

5.2.5 LIGU Results from the 12.0 in with 0.5 g TiO₂ Image and 4 Colors Endmembers

This section presents the obtained result from underwater unmixing algorithm LIGU using the 12.0 in 0.5 g TiO₂ image and the 4 colors endmembers as input. The selected image, that contains 0.5 g of TiO₂, was processed using Custom Bottom and Custom Unmixing Range functionalities with 4 color endmembers (Refer to section 4.1 for more information). This configuration corresponds to the one named 2013-3 described on table 10 and was selected because is the one that demonstrated to produce better overall accuracy (refer to section 5.2.1 to 5.2.4). The next table summarize the obtained accuracies from the 12.0 in with 0.5 g TiO₂ image processed using LIGU:

Table 16: LIGU results from the 12.0 in with 0.5 g TiO₂ image and 4 colors endmembers

Configuration	Overall Accuracy	Endmembers			
		Blue	Yellow	Green	Red
Baseline	26.25%	0.00%	59.14%	0.00%	45.85%
2013-3	43.00%	0.03%	82.25%	0.00%	89.70%

5.2.6 CIUB Results from the 12.0 in with 0.5 g of TiO₂ Image and 4 Colors Endmembers

This section presents the obtained result from underwater unmixing algorithms using the 12.0 in with 0.5 g of TiO₂ image processed on CIUB. It is important to mention that a single configuration was used. The selected image was processed using Custom Bottom and Custom Unmixing Range functionalities with 4 color endmembers. Again, this configuration corresponds to the one named 2013-3 described on table 10 and was selected because is the one that produced better overall accuracy in the previously presented results (refer to section 5.2.1 to 5.2.4). The next table summarize the obtained accuracies from the 12.0 in with 0.5 g of TiO₂ image processed using CIUB:

Table 17: CIUB results from the 12.0 in with 0.5 g of TiO₂ Image and 4 Colors Endmembers

Configuration	Overall Accuracy	Endmembers			
		Blue	Yellow	Green	Red
Baseline	25.00%	0.00%	100.00%	0.00%	0.00%
2013-3	27.22%	0.00%	100.00%	0.00%	8.88%

5.3 Regularization Algorithm

The regularization algorithm was programmed and implemented into HyCIAT as one of the main objective of this work (Refer to section 4.2 for the implementation). To validate the functionality of this algorithm, images 12.0 in without TiO₂ and 12.0 in with 0.5 g of TiO₂ (See Section 3.2 for image details) were processed using endmembers obtained from the 1.8 in without TiO₂ image (endmembers extraction procedure is presented on Section 3.3). The regularization algorithm has several input parameters that affect its results. One of them is the gamma resolution. The gamma resolution sets the number of concrete steps between 0 and 1 that the vector γ can have. For example, if gamma resolution is set to 0.1 the vector will be:

$$\gamma = [0.0, 0.1, 0.2, 0.3, 0.4, 0.5, 0.6, 0.7, 0.8, 0.9, 1.0]$$

Different gamma resolutions yield different results; therefore, two gamma resolutions were selected for this project: 0.1 and 0.01. For each gamma resolution, there are two different ways of selecting the optimum gamma per pixel: **Gamma of Minimum Error** and **Minimum Gamma** (See section 2.6.1 for theoretical background); also, two methods of calculating the maximum curvature: **Numerical Approximations** and **Derived Equations** (See Section 2.6). After processing, regularized images were classified with the three classification algorithms included in the toolbox (Minimum Euclidean Distance, Minimum Spectral Angle and Maximum Endmember, see section 3.6). Summarizing, two images were selected to be processed using: two different gamma resolutions, two different maximum curvature algorithms, two different ways of retrieving the optimum γ per pixel and classified using three different classifiers. This constitutes a total of 48 unique results that were evaluated using testing regions selected and showed on section 3.3. Results will be compare and analyzed based on the classification accuracy over the selected testing regions calculated in the following way:

$$\frac{\text{Pixel Correctly Classified}}{\text{Ammout of pixels enclosed on the training regions}} \times 100 \quad (74)$$

For standardizing results, the input parameters were set for both images in the following way:

- **Endmembers:** In this case five endmembers representing the Blue, Yellow, Green, Red and White regions from the 1.8 in without TiO₂ image (showed on section 3.3)
- **Bands for Processing:** Full Image's spectrum
- **Endmembers for classifying:** Same as for Processing
- **Band for Classifying:** Full Image's spectrum
- **Optical Properties:** Average of all the empirically derived α and β vectors, one per each colored region (Refer to section 3.4).
- **Bathymetry File:** Depth of the tank in meter, in this case 12.0 in = 0.3048m.

Finally, for visualization, each endmember was given the color that it represents on the classification maps. For example, the red endmember is colored red on the classification maps showed as results. The following sections summarized the obtained results from the Regularization. For a comprehensive set of result including classification maps and performance matrices refer to Appendix sections: 9.4 and 9.5.

5.3.1 Regularization Baseline Results

To create baseline results, images were classified with the proposed classification algorithms before being process by the Regularization algorithm. The following images were used to produce baseline results: 0", 12.0 in without TiO₂, 12.0 in with 0.5 g of TiO₂, 12.0 in with 1.0 g of TiO₂, 12.0 in with 1.5 g of TiO₂ and 12.0 in with 2.0g of TiO₂ (Refer to section 3.1 for more image information). The following graphs summarized the obtained classification accuracy before regularization. To calculate the Classification Accuracy, the selected testing regions showed on section 3.3 were used.

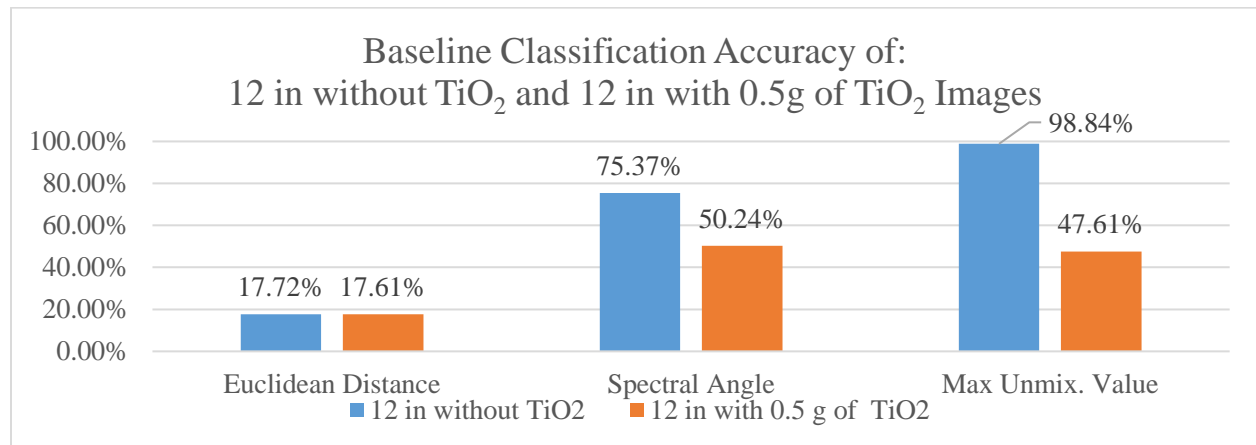


Figure 78: Baseline Classification Accuracy

5.3.2 Numerical Approximation Classification Results after Regularization

Numerical Approximations is one of the algorithm implemented to calculate the point of maximum curvature which from now on will be referred as **NA** on this document. NA uses the method of forward difference to calculate the derivative of a vector of concrete values. Refer to section 3.5.2 for the theoretical background. The following two sections will show the obtained result from 12.0 in without TiO₂ and 12.0 in with 0.5 g of TiO₂.

5.3.2.1 12.0 in without TiO₂ Image Classification Results after Regularization

There are two methods of selecting the optimum γ : Gamma of Minimum Error and Minimum Gama and their results will be compared side by side throughout this section. Results obtained using a gamma resolution of 0.1 and 0.01 will be showed on figures 80 and 81 respectively. Baseline results were also included on these graphs for comparison purposes. The reader must keep in mind that the baseline results were obtained by classifying the images without any being processed with the regularization algorithm.

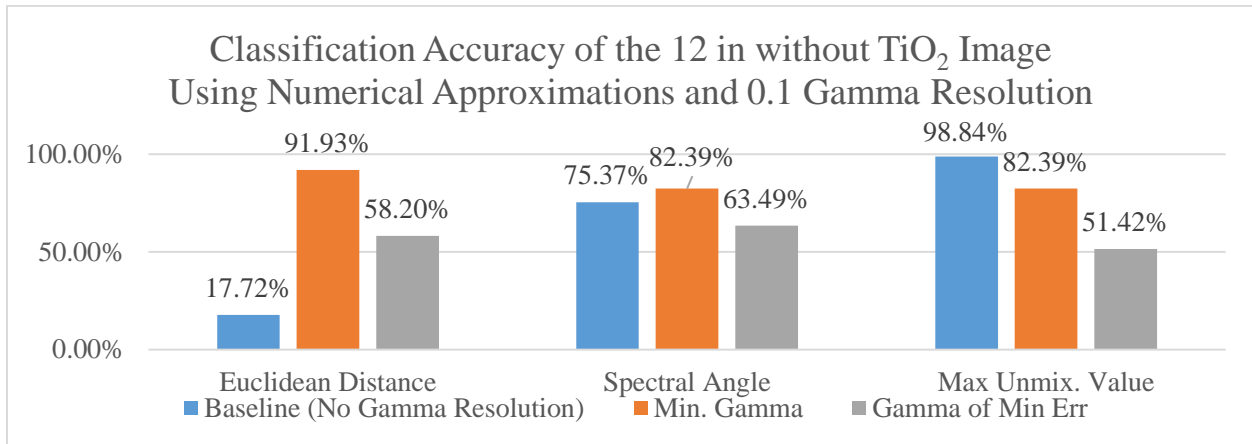


Figure 79: Classification Accuracy of the 12.0 in without TiO₂ Image using NA & 0.1 Gamma Res

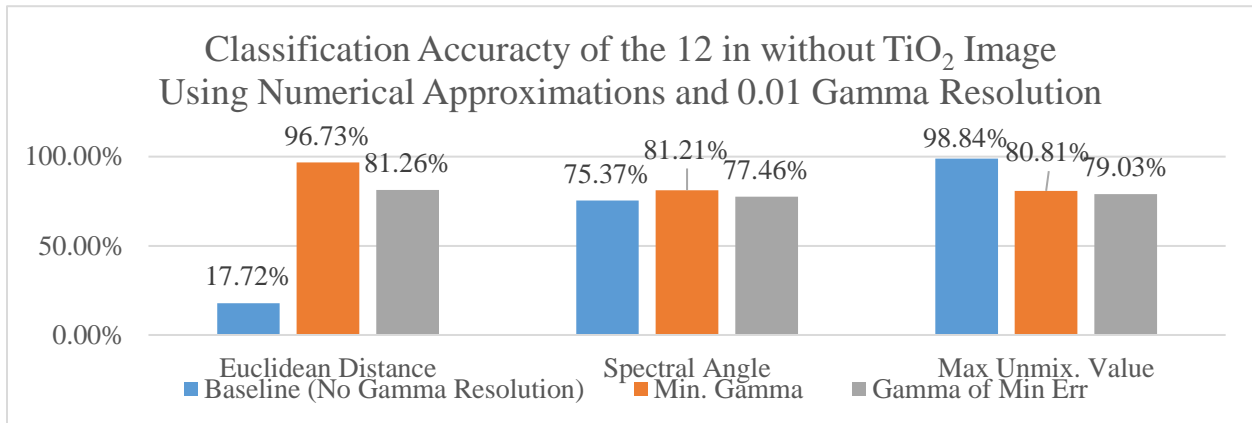


Figure 80: Classification Accuracy of the 12.0 in without TiO₂ using: NA & 0.01 Gamma Res

5.3.2.2 12.0 in with 0.5 g of TiO₂ Classification Results after Regularization

Figures 82 and 83 summarize the obtained classification accuracy after Regularization from the 12.0 in with 0.5 g of TiO₂ image using NA and Gamma Resolution of 0.1 and 0.01 respectively. Baseline results will be included for comparison purposes.

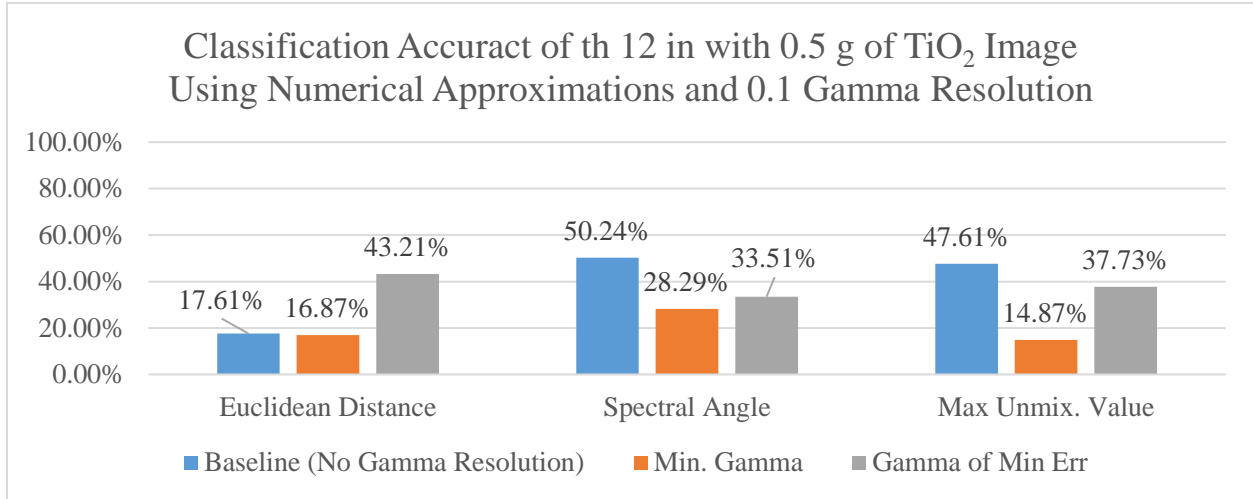


Figure 81: Classification Accuracy of the 12 in 0.5 g of TiO₂ Image using: NA & 0.1 Gamma Res

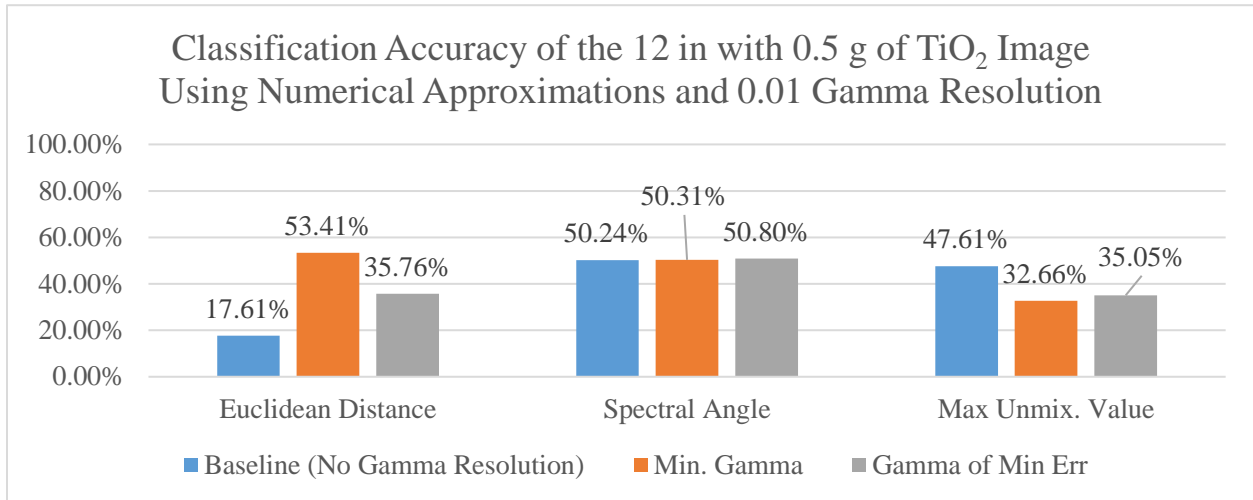


Figure 82: Classification Accuracy of the 12 in 0.5 g TiO₂ Image using NA & 0.01 Gamma Res

5.3.3 Derived Equations Classification Results after Regularization

Derived Equations is another algorithm implemented to calculate the point of maximum curvature which from now on will be referred as **DE**. DE, uses mathematically derived equations to calculate the derivative of the error curves. These equations are presented on section 3.5.3 for the theoretical background. The following two sections will show the obtained results from the 12.0 in without TiO₂ and 12.0 in with 0.5 g of TiO₂.

5.3.3.1 12.0 in without TiO₂ Classification Results After Regularization

Next graphs summarize the obtained classification accuracy after Regularization from the 12.0 in without TiO₂ image processed using Derived Equations with Gamma Resolution of 0.1 and 0.01 on figure 84 and 85 respectively.

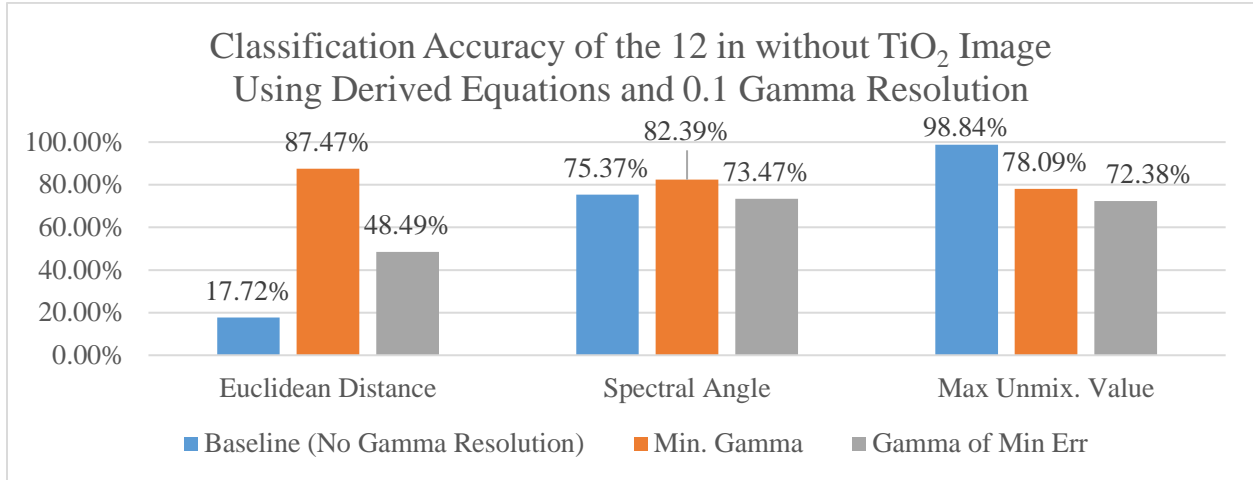


Figure 83: Classification Accuracy of the 12 in without TiO₂ Image using DE & 0.1 Gamma Res

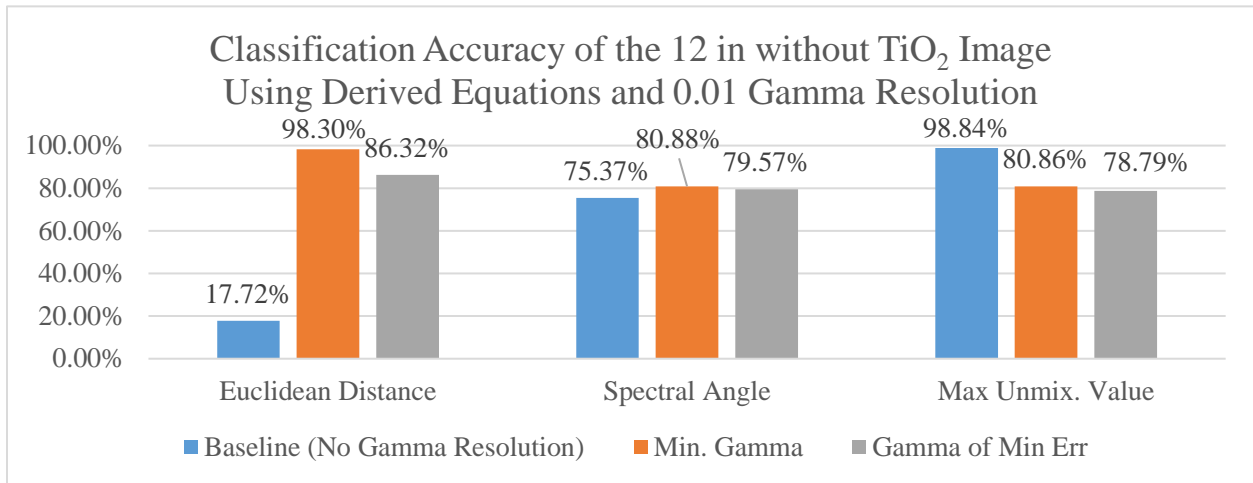


Figure 84: Classification Accuracy of the 12 in without TiO₂ Image using DE & 0.01 Gamma Res

5.3.3.2 12.0 in with 0.5 g of TiO₂ Classification Result after Regularization

Next graphs summarize the obtained classification accuracy after Regularization from the 12.0 in with 0.5 g of TiO₂ image using Derived Equations and with Gamma Resolution of 0.1 and 0.01 on figure 86 and 87 respectively.

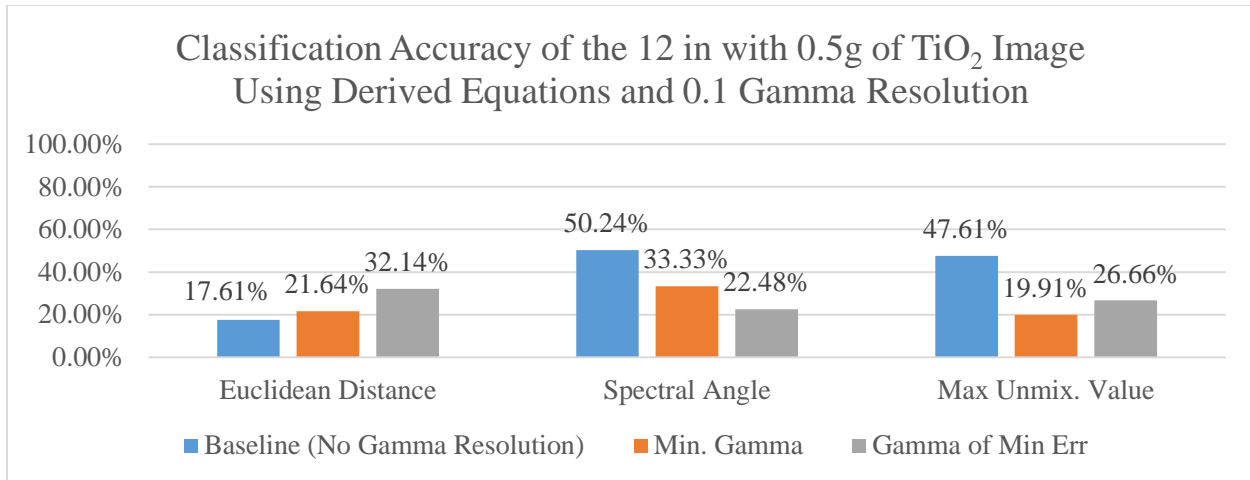


Figure 85: Classification Accuracy of the 12 in 0.5 g of TiO₂ Image using DE & 0.1 Gamma Res

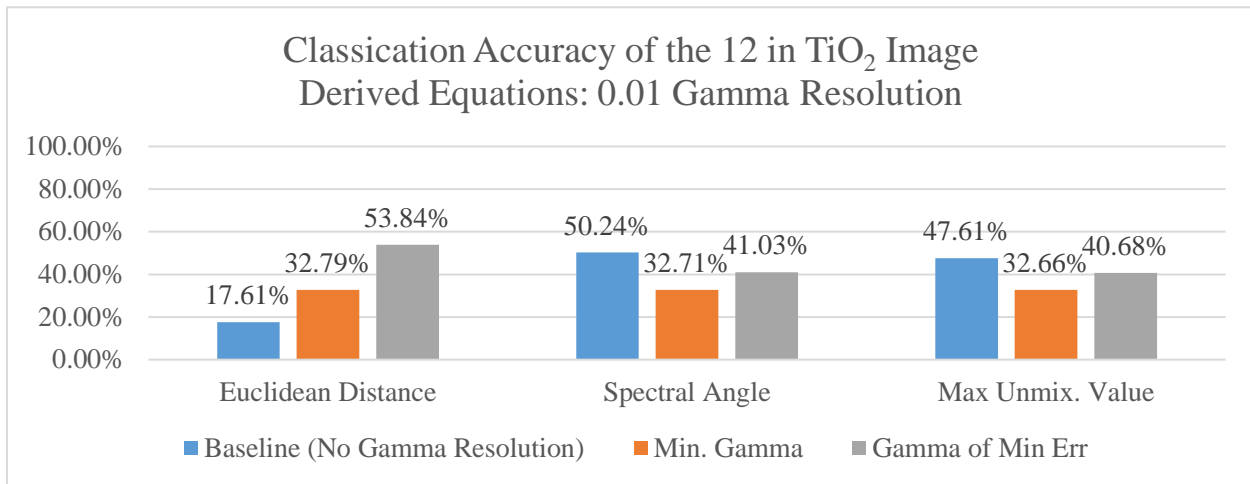


Figure 86: Classification Accuracy of the 12 in 0.5 g of TiO₂ Image using DE & 0.01 Gamma Res

5.3.4 Example with Reduced Bands using SVD Algorithm – Derived Equations

As an example, the 12.0 in without TiO₂ image was processed using a band reduction algorithms. The bands were reduced from more than 120 to 40 bands using Single Value Decomposition (SVD) feature reduction algorithm present on HIAT²¹. Reducing the number of spectral features makes the regularization algorithm perform faster. SVD40 will be added to the images with reduced bands for identification. To have an accurate comparison, baseline results were produced by classifying the mentioned image without being process by the regularization

²¹ Stands for Hyperspectral Image Analysis Toolbox. HIAT Is a legacy toolbox, originally developed and maintained at LARSIP laboratory, which includes a comprehensive set of algorithms for the studies of Hyperspectral Images, for more information refer to: [32]–[34]. HIAT can be downloaded following reference: [35]

algorithm. The endmembers' spectral features were also reduced from 120 to 40 bands. Figure 88 shows the obtained accuracy from the 12 in without TiO_2 .

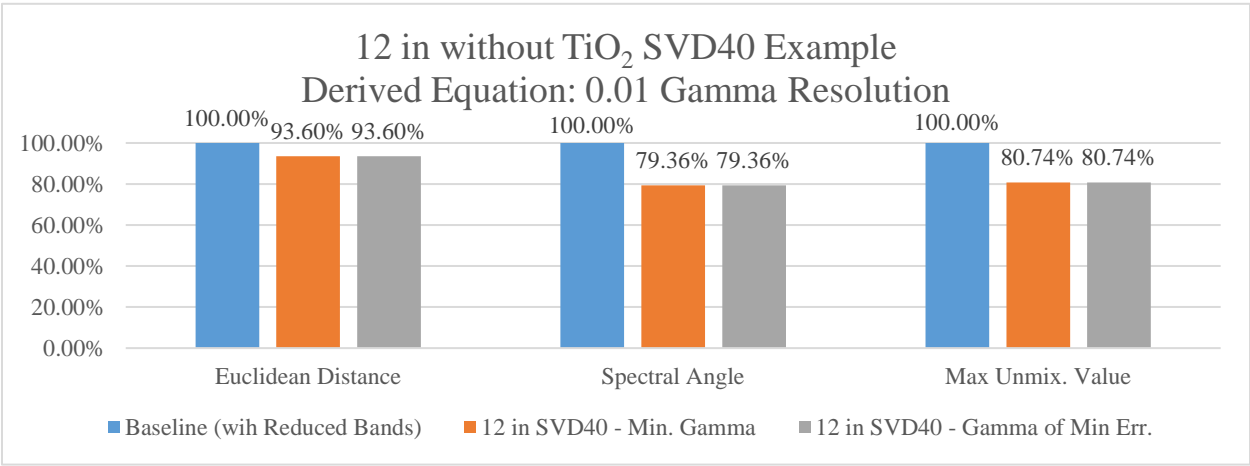


Figure 87: Example with Reduce Bands Obtained Accuracy after Regularization

6 Discussion of Results

After updating HyCIAT a huge amount of data was produced as results. The most important ones are going to be summarized and discussed on this section. Refer to section 4 for a complete description of the software development employed for: 1) the enhancement made to the underwater unmixing algorithm, 2) the integration of the regularization algorithm and 3) the integration of a new tool that increase the toolbox functionality. Refer to section 6 for a summary of results and section 9 (Appendix) for a detailed set of results.

6.1 Underwater Linear Unmixing with AVIRIS Data

The underwater unmixing algorithms available at HyCIAT uses optimization algorithms to perform the inversion of pixels and retrieve the optical water properties (see section 2 for information on the unmixing algorithms). The function used on the toolbox's algorithms is `lsqnonlin` which solves optimization problem using nonlinear least squares fitting. The default parameters of the mentioned function changed across MATLAB platform versions causing dissimilar results between them. The default parameters called *PrecondBandWidth* was identified as the one that produced the mayor discrepancies between results obtained on both versions of the toolbox. Therefore, the effect of *PrecondBandWidth* was studied by processing the selected images from AVIRIS (refer to section 6.1 for image details) on both versions of the toolbox without bathymetry. On HyCIAT 2013, images were processed with and without modifying the *PrecondBandWidth* default value. Please recall that “**without modified parameters**” means that the images were processed on MATLAB 2013a without modifying the default value that *PrecondBandWidth* had which is `inf`. Also, recall that “**with modified parameters**” means that the default value of *PrecondBandWidth* was set to 0 on MATLAB 2013a, which is the value that the parameter had on MATLAB 2007. To measure how results obtained from HyCIAT 2013 are similar to the results obtained on HyCIAT 2007, a comparative analysis was performed using the calculated **Sum of Squared Errors (SSE)**, refer to equation 70) between them. The reader must keep in mind that when a result **increase in similarity** means that the obtained result from HyCIAT 2013 with modified parameter was more **similar** to the results obtained on HyCIAT 2007 than the ones obtained from HyCIAT 2013 without modified parameter. At the other hand, when a result **decrease in similarity** means that the obtained result from HyCIAT 2013 with modified parameter was more **dissimilar** to the results obtained on HyCIAT 2007 than the obtained results from HyCIAT 2013 without modified parameter.

Analyzing results, it can be observed on figure 88 that up to an 88% increase in similarity was achieved by modifying parameters. However, this elevated percentage was observed in a particular case that correspond to AVIRIS Image A processed in LIGU. The second highest increase in similarity was also AVIRIS Image A processed with CIUB with a 36% increase in similarity. The similarity of the other two results, one did not increase significantly and the other one was dissimilar. Let's consider the result that corresponds to AVIRIS Image B processed with LIGU, the obtained similarity was negative. That means that, in that case, result from HyCIAT 2013 with modified parameters were 6% more different than the ones obtained without modifying parameters.

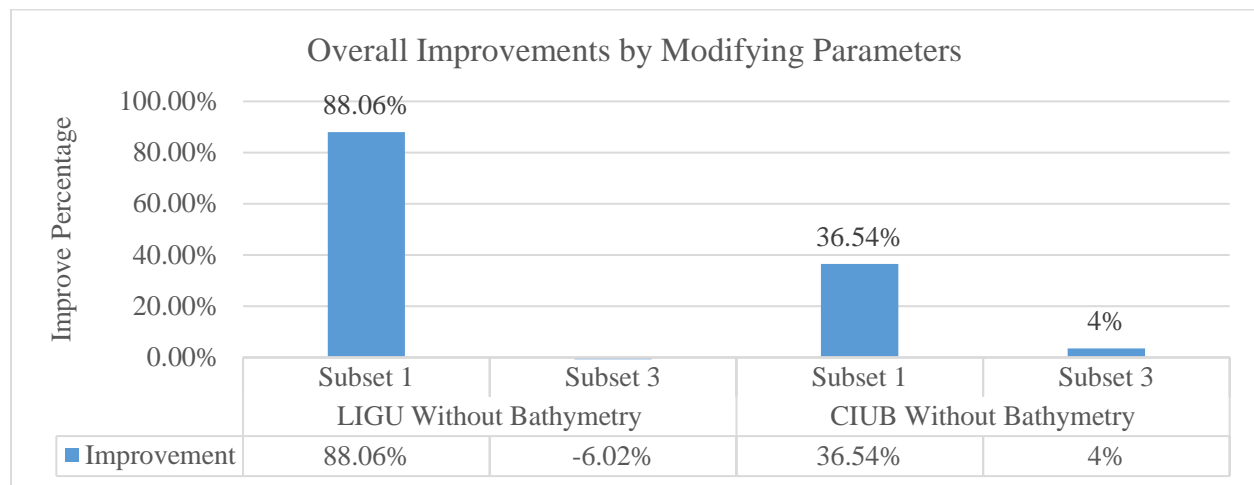


Figure 88: Overall similarity improvement by Modifying Parameters

It is also important to mention that when analyzing the obtained results, it was found that, in some cases, the individual improvements were significant. Next figure presents the calculated degree of similarity from results obtained from AVIRIS Image A processed in CIUB. It can be observed that Depth increase in similarity in a 36.81% follow by the abundance estimation of coral that increase in similarity in a 17.31%. Also, it can be observed that bottom reflectance decreases in similarity in a 37.72%. Another set of results were the individual results were significant is AVIRIS Image B processed in CIUB. It can be observed that also the Bottom Reflectance decrease in similarity and the rest of the parameters did not change significantly.

Therefore, analyzing the obtained result, it is deduced that the overall similarity of results between both versions of the toolbox did not increase significantly when using AVIRIS data while modifying the identified parameter. Due to this, the initial parameters form was updated to include a mechanism to modify the *PrecondBandWidth* parameter as the researcher see fit, see section 4.1.1.

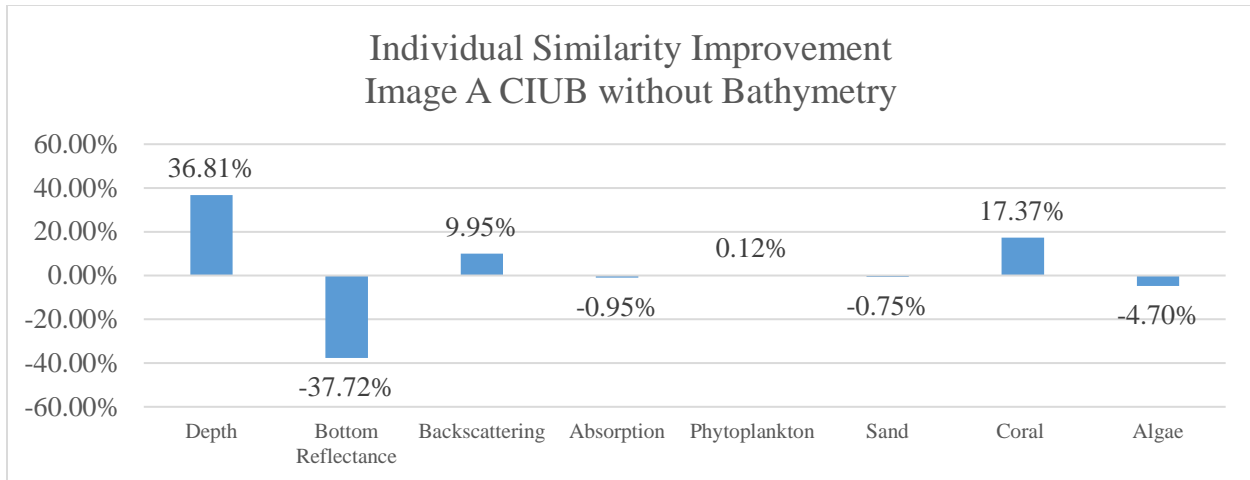


Figure 89: Similarity Improvement: Image A CIUB without Bathymetry

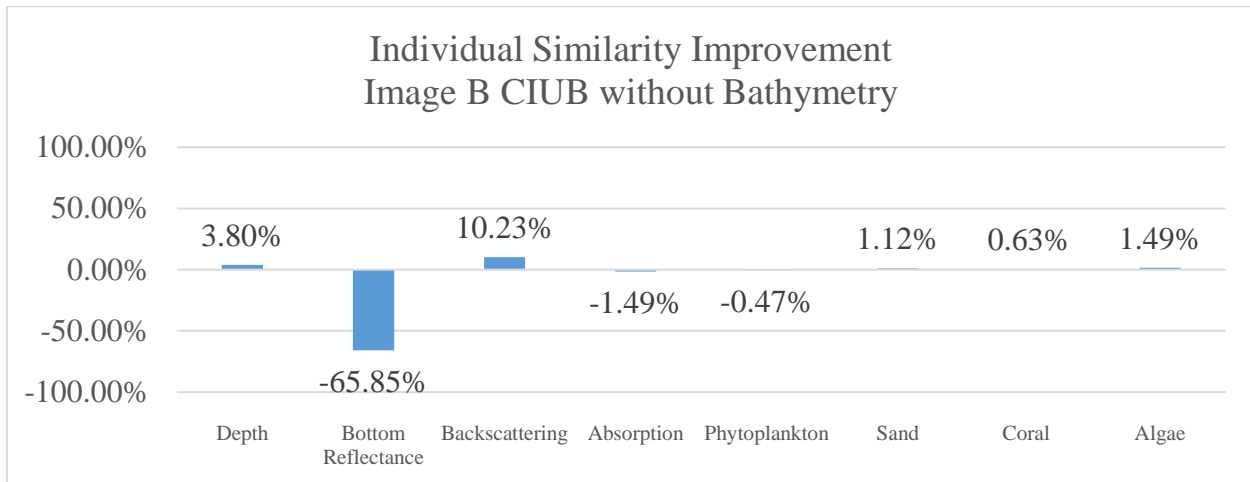


Figure 90: Similarity Improvement: Image B CIUB without Bathymetry

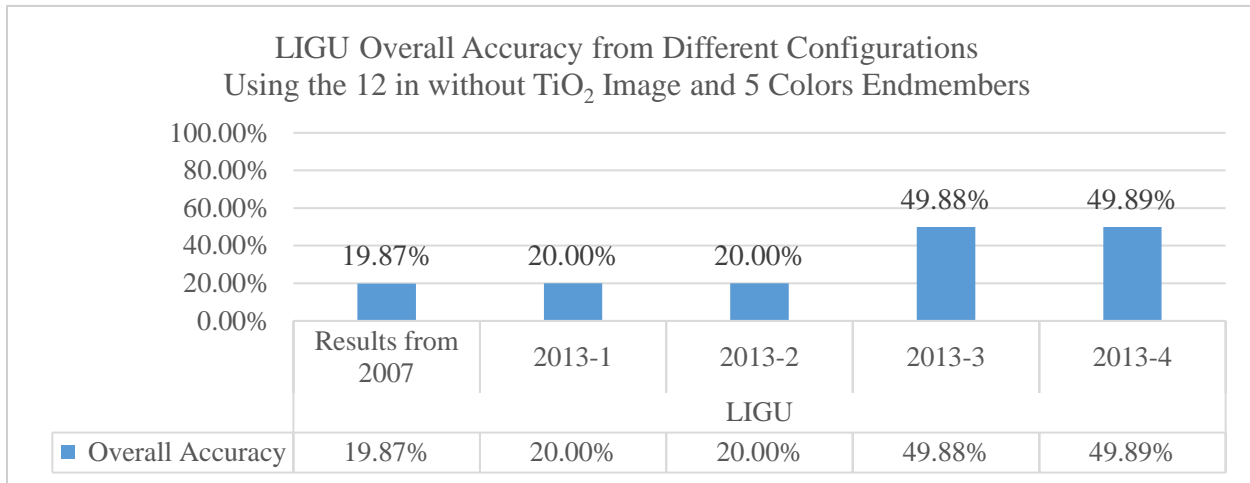
6.2 Underwater Linear Unmixing with Real Controlled Data

In another part of this project, the underwater unmixing algorithms were tested using the obtained image database on this project, refer to section 3.1 for a detailed explanation on them. Those images were used to validate the additional enhancement made to the underwater unmixing algorithms. There are two main modifications: **Custom Unmixing Range** and **Custom Bottom**. Custom Unmixing Range functionality allows the researcher to input a custom range of the spectrum where the algorithm will perform the unmixing, refer to section 4.1.2. Custom Bottom functionality allows the researcher to input its custom bottom to the Lee's equation. Recall that 5 different configurations, described on the next table, were used to reproduce results to measure the impact of the included modifications:

Table 18: Configuration Descriptions

Configurations Name	Description
Baseline	Images processed in HyCIAT 2007.
2013-1	HyCIAT 2013 configured as HyCIAT 2007.
2013-2	HyCIAT 2013 configured with extended unmixing ranges
2013-3	HyCIAT 2013 configured with a custom Sand spectral signature.
2013-4	HyCIAT 2013 configured with extended unmixing ranges, custom Sand spectral signature and <i>PrecondBandWidth</i> parameter set to 0.

To quantify unmixing results, the testing regions presented on section 3.3 were used as “pure pixel” of each class. The individual accuracy of each endmember over its testing region was calculated with equation 73 (Refer to section 5.2 for explanation). The overall accuracy of each configuration is calculated by averaging the obtained individual accuracies of each endmember given to the underwater unmixing algorithm. Results shows an increment in accuracy with the modification performed to the algorithms. It can be observed, on figure 91 that the obtained overall accuracy increases in around 29 % for configurations 2013-3 and 2013-4 by comparing it to the Results from HyCIAT 2007. The following two figure, 91 and 92 shows the Overall Accuracy results for images processed with LIGU using 5 colors endmembers and 4 colors endmembers.

**Figure 91: LIGU overall accuracy using the 12 in without TiO₂ Image and 5 color endmembers.**

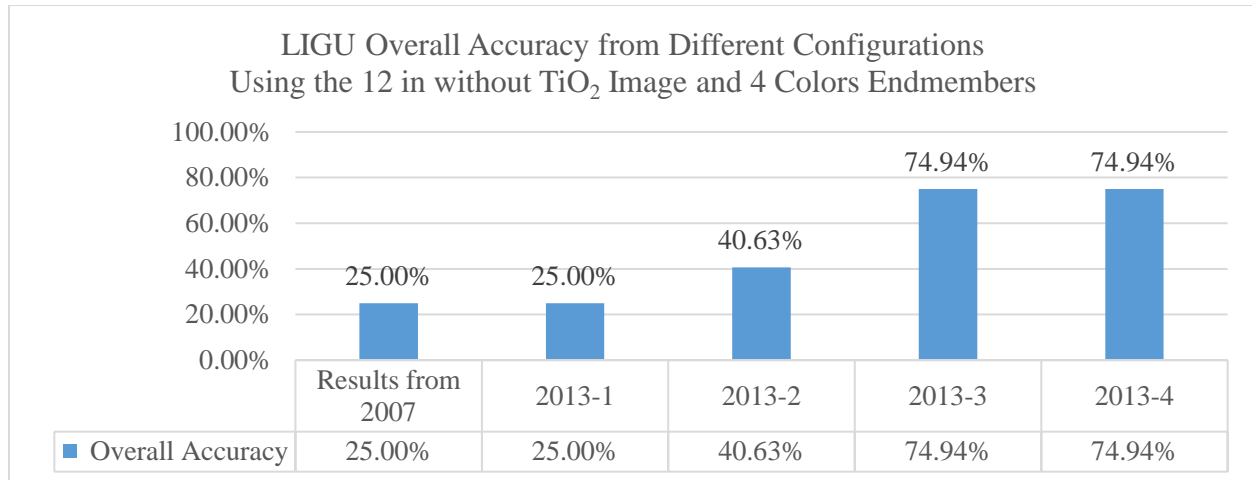


Figure 92: LIGU overall accuracy using the 12 in without TiO₂ Image and 4 color endmembers.

There are several things that need to be discussed from the last two graphs. 1) It can be observed that the additional functionalities have a positive impact on obtained results. A 29% increase in accuracy was obtained with configuration 2013-3 where the overall accuracy came up to 49.88% when combining the new functionalities. 2) Results also show that by reducing the number of endmembers from 5 to 4 the accuracy increase. Accuracy improves close to a 25% on configuration 2013-3 by reducing the number of endmembers. On this case, the overall accuracy increases from 49.88% to 74.94% and comparing results from 2013-3 of figure 92 with Results from 2007 close to a 50% increase in accuracy was obtained. This establishes the trend that by reducing the amount of endmember more accuracy can be obtain from the underwater algorithms. 3) When using only the Custom Unmixing Range functionality with 5 Colors endmembers results did not increase. But, it also can be observed that when eliminating one endmember results improves in around 15%. 4) The accuracy obtained on configuration 2013-1²², is almost similar as the accuracy obtained from Results from 2007. Both accuracies stay close to 20% when unmixing with 5 colors and close to 25 % when unmixing with 4 colors. This stablish the fact that results are not affected by updating the toolbox when configured in the same way. 5) LIGU results doesn't change by modifying the identified parameter of the optimization function. Both overall accuracies were around 49.88% using 5 Colors endmembers and 74.49%. when using 4 Colors endmembers. This is a restatement of fact presented on the section 6.1 where it was evidenced that the *PrecondBandWidth* parameter do not significantly affect the majority of the obtained results.

²² Recall that 2013-1 represent the results obtained from HyCIAT 2013 configured as HyCIAT 2007, see table 18.

In contrast, as can be observed on the next two figures (figures 93 and 94) the obtained accuracies from CIUB was not as high as LIGU when unmixing over the testing regions. The obtained overall accuracy, with 5 colors endmembers, from HyCIAT 2007 was 21.18% and when processing the same image on HyCIAT 2013 with the same parameter as 2007 (configuration 2013-1) was 20.36%. Again, restating the fact that results are not affected by updating the toolbox when they are configured in the same way. Looking at other configurations, an accuracy increment of 0.28% was obtained when increasing the unmixing range (2013-2) and an additional 5.5% overall accuracy increment was obtained when modifying the optimization function parameter (2013-4). When contrasting the next two figure it can be observed that result didn't improve significantly when reducing the number of endmember. Looking at figure 94 close to an accuracy increment of 10% was obtain with the enhanced features. Accuracy did not increase when modifying the default parameters of the optimization function. By observing CIUB results, it can also be said that updating the toolbox did not have an adverse impact on result. Again, restating the fact that results are not affected by updating the toolbox when configured in the same way.

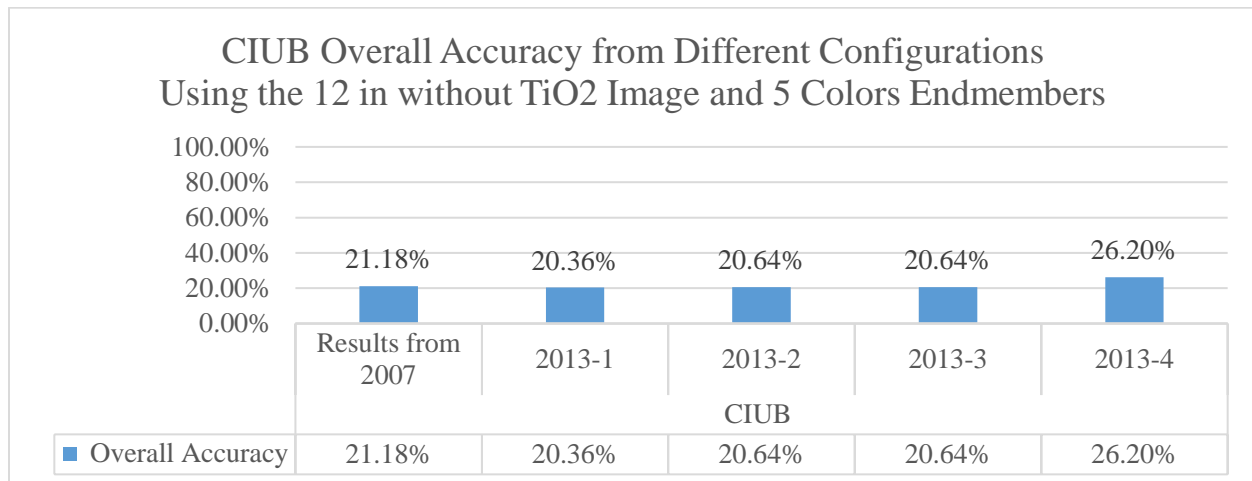


Figure 93: 12.0 in CIUB 5 Colors Blue Individual Accuracy

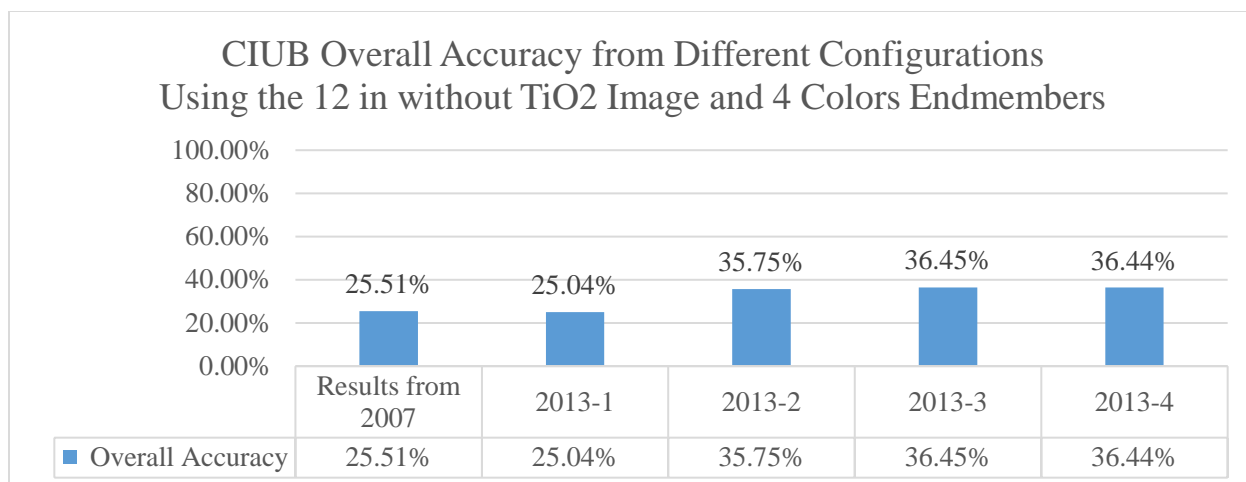


Figure 94: 12.0 in CIUB 4 Colors – Blue Individual accuracy

Analyzing individual results, it can be observed that close to a 94% of accuracy was achieved by calculating fractional abundances of the Blue endmember with LIGU on the 12.0 in without TiO₂ image with 5 colors endmembers, see figure 95. Additionally, the accuracy increases considerably just by reducing the number of endmembers from 5 to 4 as can be appreciated on figure 96. On that figure, it can be observed up to 62.53% in accuracy increment was achieved by just adjusting the unmixing range and a 100.00% in accuracy was obtained by combining the custom unmixing range and the custom bottom functionalities on the 12.0 in without TiO₂ image processed with 4 Colors Endmembers. The results obtained with the Blue endmember is being highlighted because is the one that obtained the major improvement with the proposed algorithm enhancements.

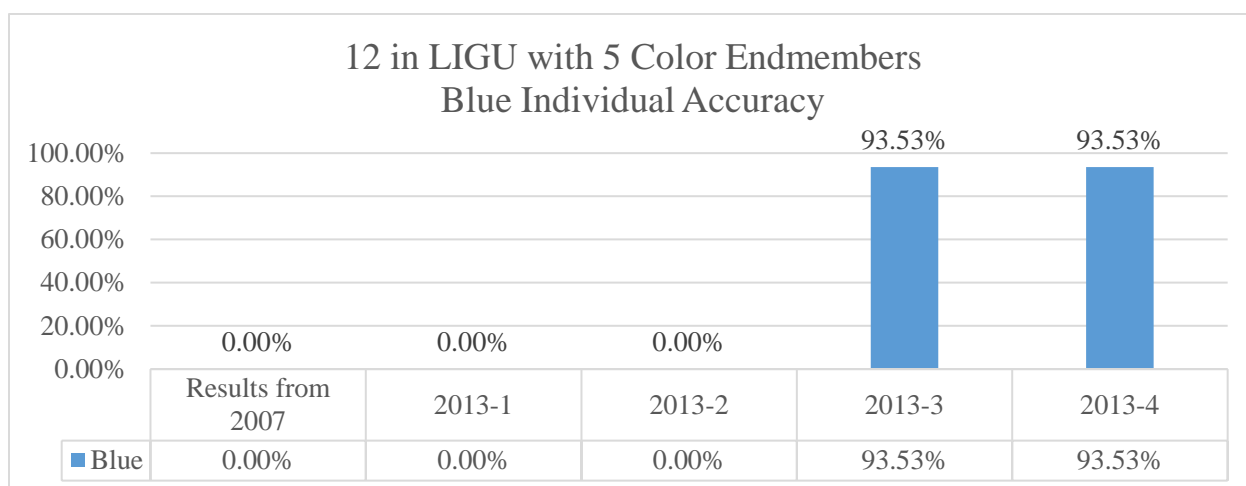


Figure 95: 12.0 in LIGU 5 Colors – Blue Individual accuracy

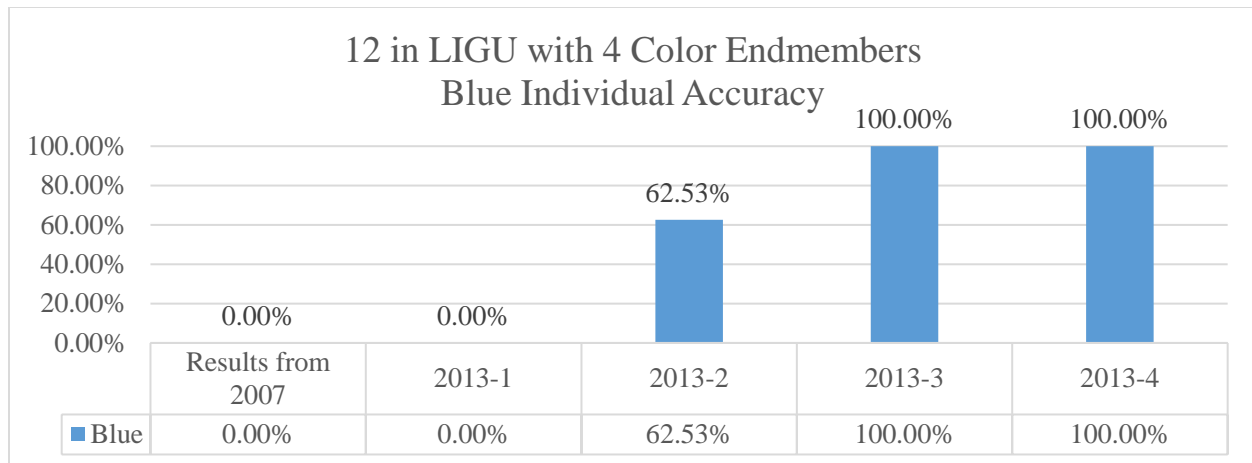


Figure 96: 12.0 in LIGU 4 Colors – Blue Individual accuracy

In contrast, it is important to mention that accuracy was constantly zero over the Green testing regions by processing the image with 5 Colors Endmembers, as can be observed in figure 97. This accuracy was also obtained even when reducing the amount endmember to 4, as can be observed in figure 98.

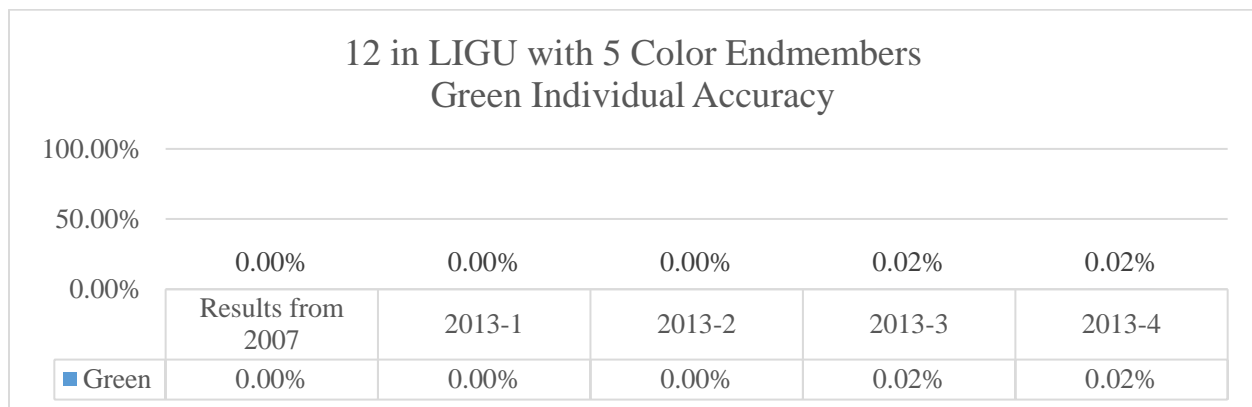


Figure 97: 12.0 in LIGU 5 Colors – Green Individual accuracy

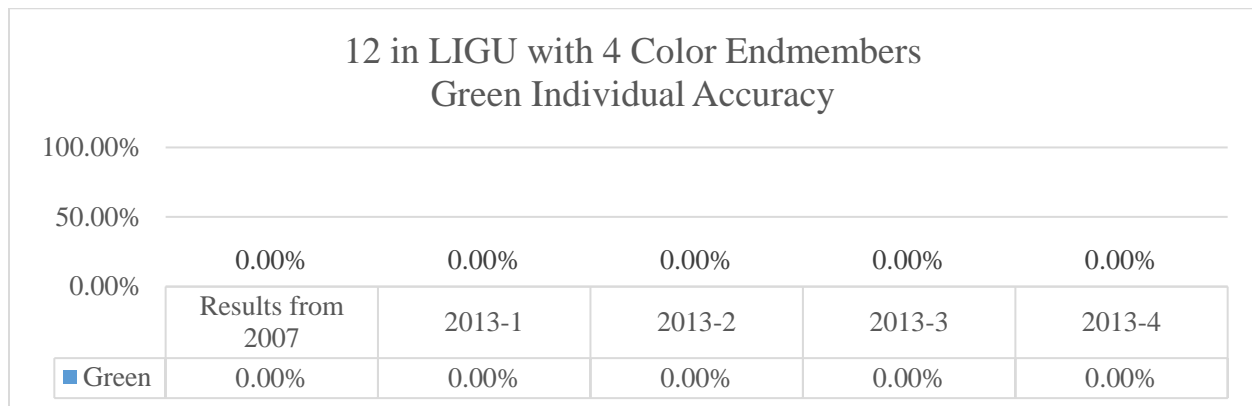


Figure 98: 12.0 in LIGU 4 Colors – Green Individual accuracy

This is due to the similarity that green and blue endmembers have between each other, see figure 99. The algorithm does not discriminate between the green endmember correctly from the blue endmembers. The same figure shows the fractional abundances of the Blue endmember obtained from 12.0 in without TiO_2 image processed in LIGU with 5 color endmembers. It can be observed high abundance of blue over the region that pertain to the green color.

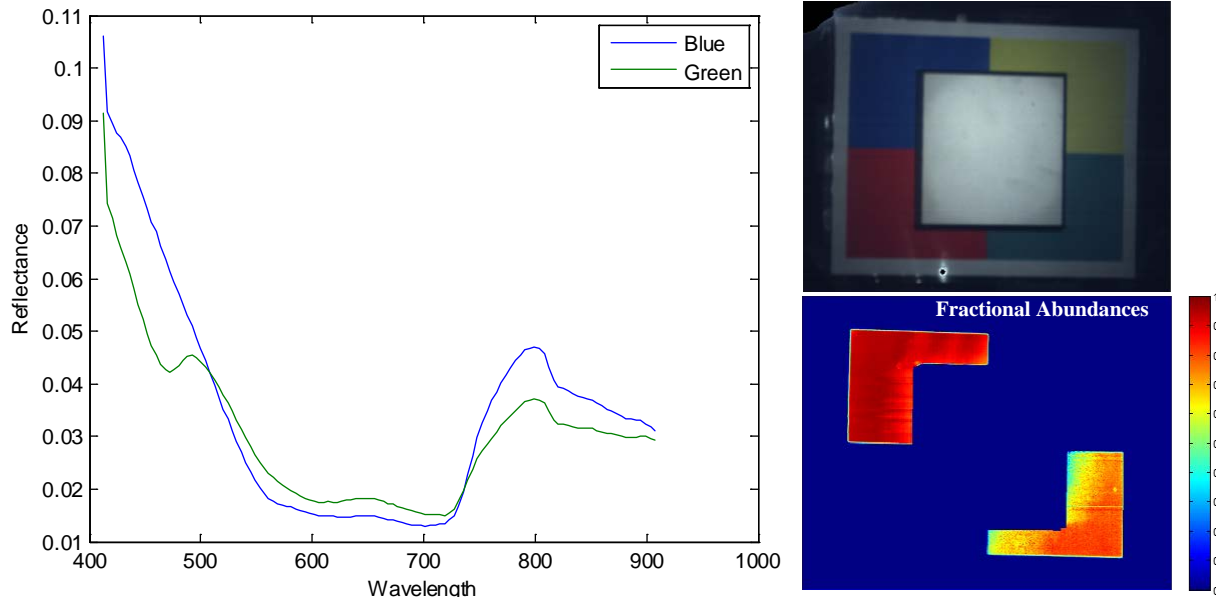


Figure 99: Blue and Green Endmember Spectral Signature and unmixing results

6.2.1.1 Underwater Unmixing of the 12 in with 0.5 g of TiO_2

In another part of the project, Titanium Dioxide (TiO_2) was used as light scattering agent in the water to decrease the visibility of the bottom of the tank. Obtained images with TiO_2 were processed on both versions of the toolbox. In HyCIAT 2013 images were processed using custom bottom and custom unmixing range functionalities. This configuration corresponds to the one named 2013-3 described on table 10 and was selected because is the one that demonstrated to produce better overall accuracy (refer to section 5.2.1 to 5.2.4). Result shows that when processing the 12.0 in 0.5 g TiO_2 image with LIGU a 23% accuracy increment over the yellow testing region and a close to a 44% accuracy increment over the red resting region were obtained, see figure 100.

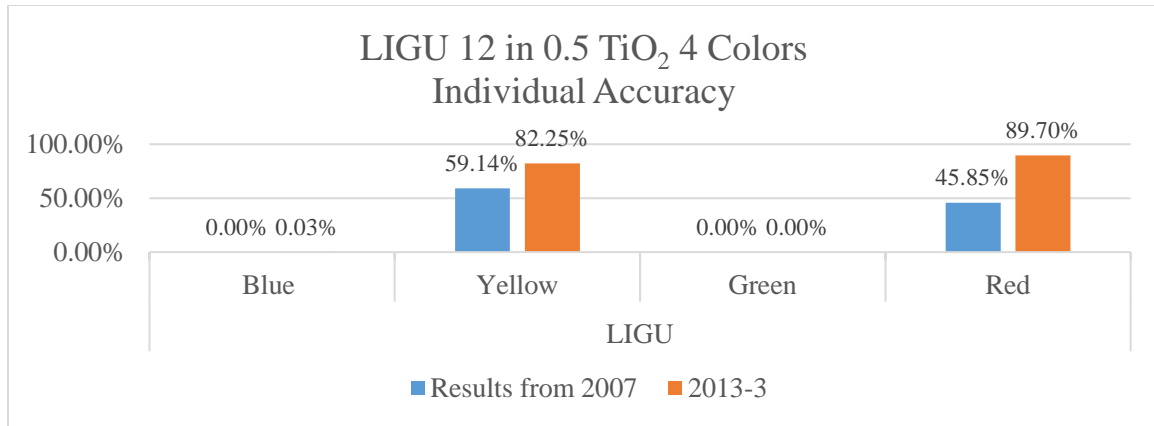


Figure 100: 12.0 in 0.5 g TiO₂ LIGU 4 Colors –Individual accuracy

In contrast by processing the same image with CIUB on both versions of the toolbox only the accuracy of the red color increased to 8.88% as can be observed in the next figure:

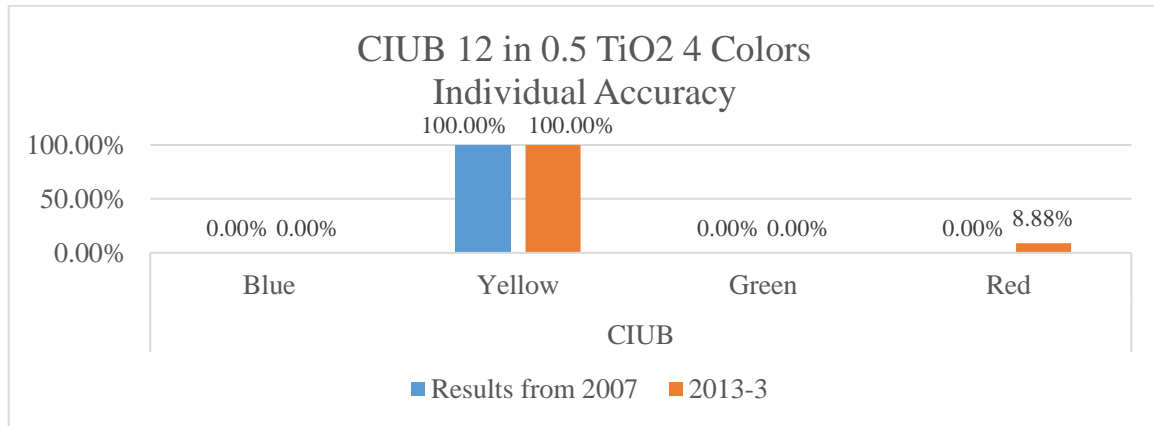


Figure 101: 12.0 in 0.5 g TiO₂ LIGU 4 Colors –Individual accuracy

6.3 Regularization Algorithm

The final part of the project is the recoding, integration and validation of the Regularization algorithm. Refer to section 4.2 for the complete description on the implementation of this algorithm. Figure 102, shows the obtained classification accuracy of baseline results. Baseline results were produced by classifying the obtained images with the proposed classification algorithms before being process by the Regularization algorithm, refer to section 5.3.1. Analyzing the baseline results showed on figure 102, the classification accuracy of the Euclidean Distance classifier the Dry image was 100% but, by adding 12.0 of water the classification decreases down to 17.70% and stays at 17.61% even when adding multiple quantities of TiO₂. In the Spectral Angle classifier, the accuracy also was 100% on the Dry image and, by adding 12.0 in of water and multiple quantities of TiO₂ its

classification accuracy decreases, see figure 102. It's important to point out that, even though the accuracy decreases by adding water and TiO₂, the Spectral Angle classifier performed better than the other two classifiers in the majority of the obtained images. A case, on the 12.0 in without TiO₂ image the Maximum Unmixing Value classifier performed excellent achieving a classification accuracy of almost 99% over testing regions.

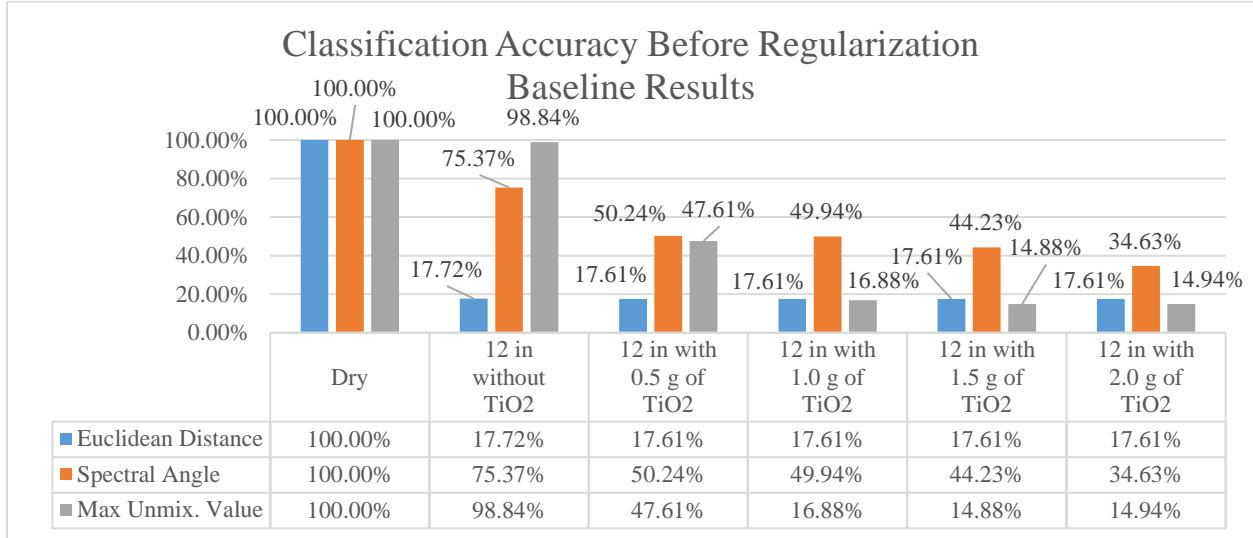


Figure 102: Comparative graph of baseline result with multiple TiO₂ concentrations

As mentioned before, two gamma resolutions were selected for this project: 0.1 and 0.01. For each gamma resolution, there are two different ways of selecting the optimum γ per pixel: Gamma of Minimum Error and Minimum Gamma. Finally, two methods of calculating the maximum curvature: Numerical Approximations and Derived Equations were implemented. All these variations were tested in the selected images (12.0 in without TiO₂ and 12.0 in with 0.5 g of TiO₂).

Obtained classification accuracy after Regularization of the 12.0 in without TiO₂ image using Numerical Approximation are showed on figure 103. The most notable improvement is on the Euclidean Distance classifier where accuracy increase from a 17% to and 91.93% using gamma resolution of 0.1 and increase again up to a 96.73% using gamma resolution of 0.01 establishing the tendency that accuracy improve by increasing the gamma resolution.

Figure 104 shows classification accuracy after Regularization of the 12.0 in without TiO₂ image using Derived Equations. Also, as can be observed in the same figure, the most notable improvement was on the Euclidean Distance classifier where accuracy increase from 17.72% to 87.47% with a gamma resolution of 0.1 and ramp up to 98.30% with a gamma resolution of 0.01. This confirms the tendency accuracy increases with the increment of gamma resolution. This behavior is observed

only in Euclidean Distance and on Spectral Angle. Again, Maximum Unmixing Value baseline result was not outperformed by the rest of the experiments.

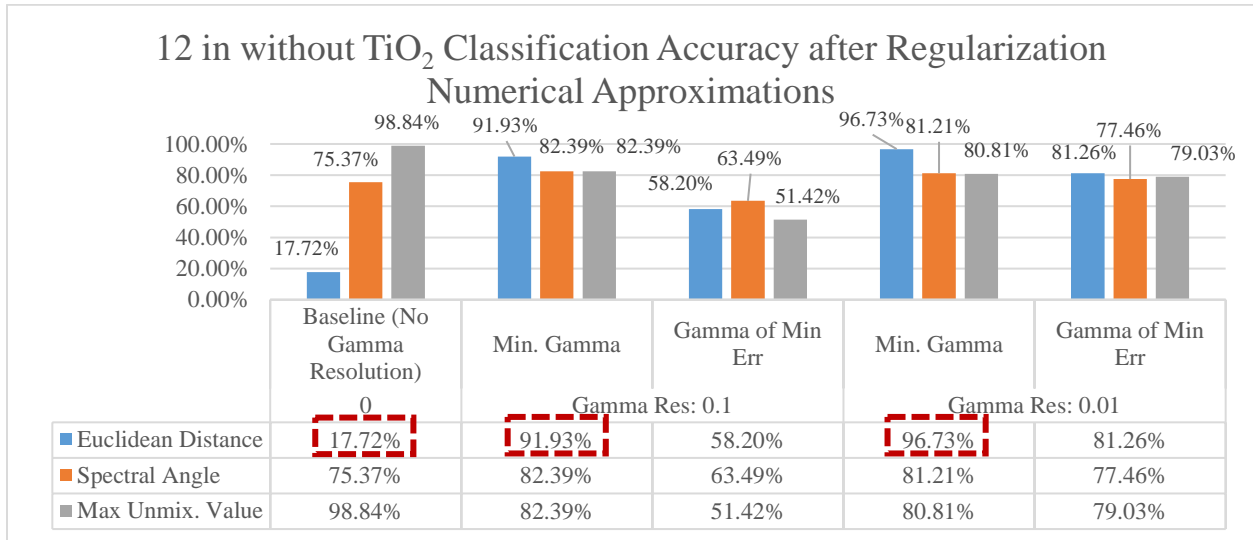


Figure 103: 12.0 in Image Numerical Approximation Results Comparison with Baseline Results

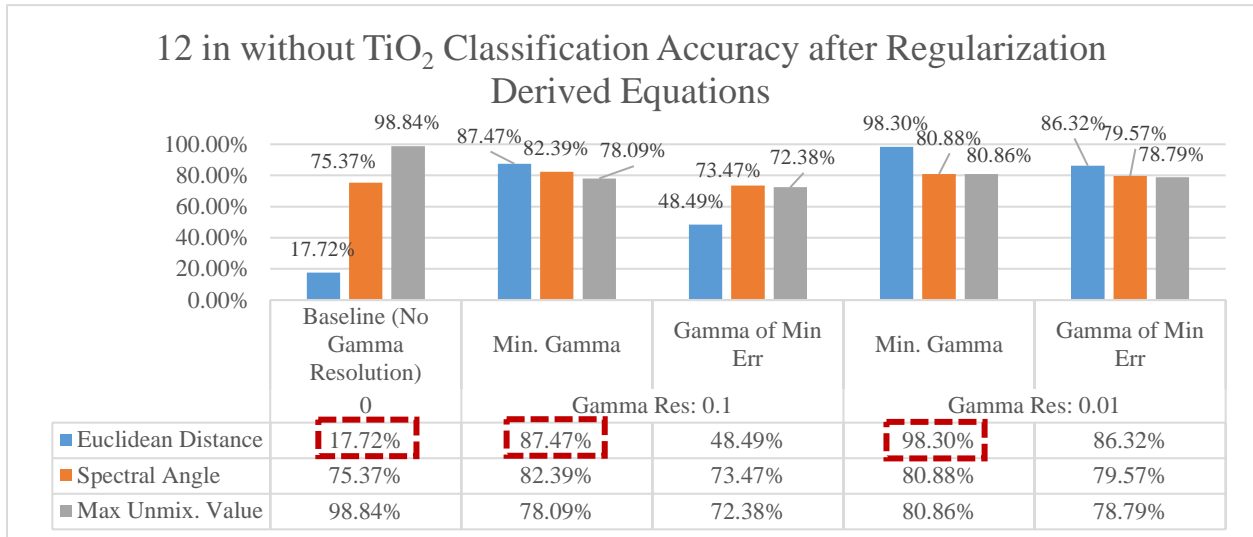

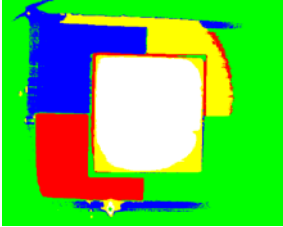
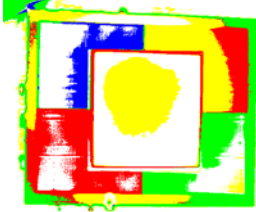
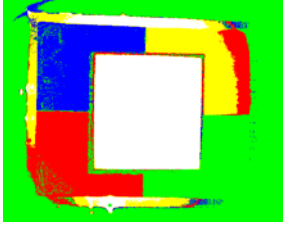



Figure 104: 12.0 in Image Derived Equations Results Comparison with Baseline Results

Each class on the classification map were colored with the color that the class represents. This facilitate the analysis of results. Table 19 compares visually the classification maps obtained from regularized images using Minimum Gamma and Gamma of Minimum Error and classified with Euclidean Distance. Also, for this results, Numerical Approximations were used on the for processing the image and gamma resolution was set to 0.1 and 0.01.

Table 19: Euclidean Distance Classification after Regularization of the 12.0 in image

Real Image		
Classification Algorithm	Classification Maps	
	Minimum Gamma	Gamma of Minimum Error
Minimum Euclidean Distance	Gamma Resolution:	0.1
	 <p>Accuracy = 91.93%</p>	 <p>Accuracy = 58.20%</p>
Minimum Euclidean Distance	Gamma Resolution:	0.01
	 <p>Accuracy = 96.73%</p>	 <p>Accuracy = 81.26%</p>

It can be observed, on the last table, that Minimum Gamma methodology could separate each class almost perfectly with Euclidean Distance. When using Gamma of Minimum Error some features in the classification map start to appear and the algorithm misclassifies some pixels. By increasing the gamma resolution to 0.01 the algorithm has more values to select the optimum γ making calculations more precise therefore increasing accuracy. Visually and statically it can be observed that with a resolution of 0.01 the regions are more defined on the obtained classification maps. For a complete set of results refer to Appendix sections 9.4 and 9.5.

Titanium Dioxide was added to the water as a light scattering agent that difficult the visibility of the bottom. This poses a big challenge while classifying because most the light reflected from the bottom is scattered by the chemical compound suspended in the water and does not reach the camera. Figure 105 compares visually multiple images where the effect of the TiO_2 can be observed. Figure 106 shows the obtained endmembers from the testing regions of figure 105. Figure 107

shows the obtained classification accuracy from the 12.0 in with 0.5 g of TiO_2 image regularized using Numerical Approximations. The most notable results also were obtained when using Euclidean Distance where baseline accuracy of 17.61% increase to 53.41% when using a gamma resolution of 0.01. It can be observed that results were not as good as the one obtained from the 12.0 in without TiO_2 image. But the accuracy obtained on regularized images tends to be higher than the accuracy obtained on the baseline.

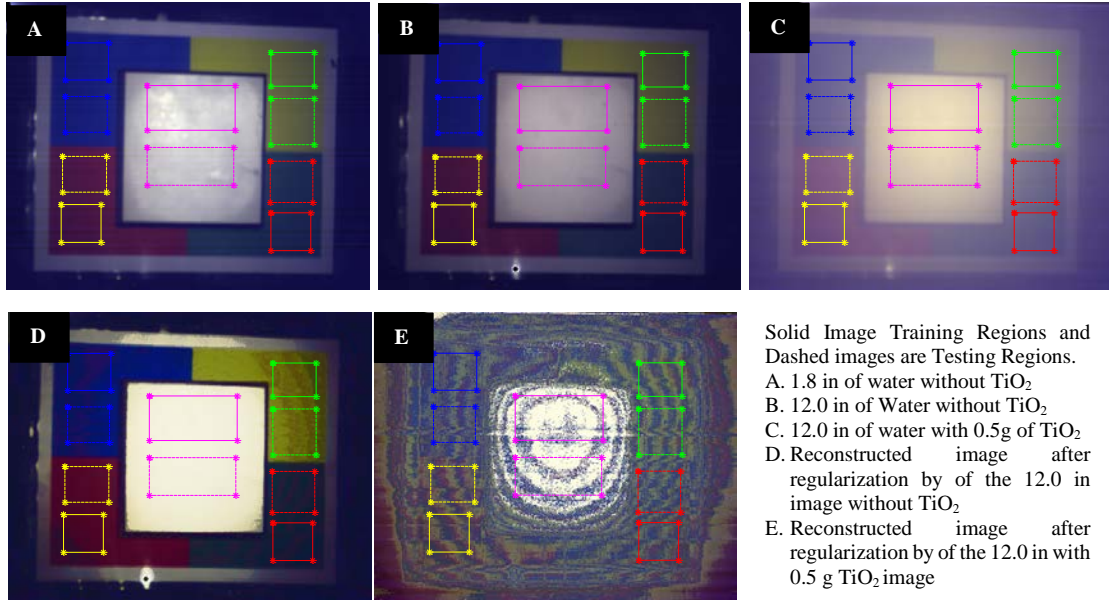


Figure 105: Multiple measure HSI images and Reconstructed ones with Regularization

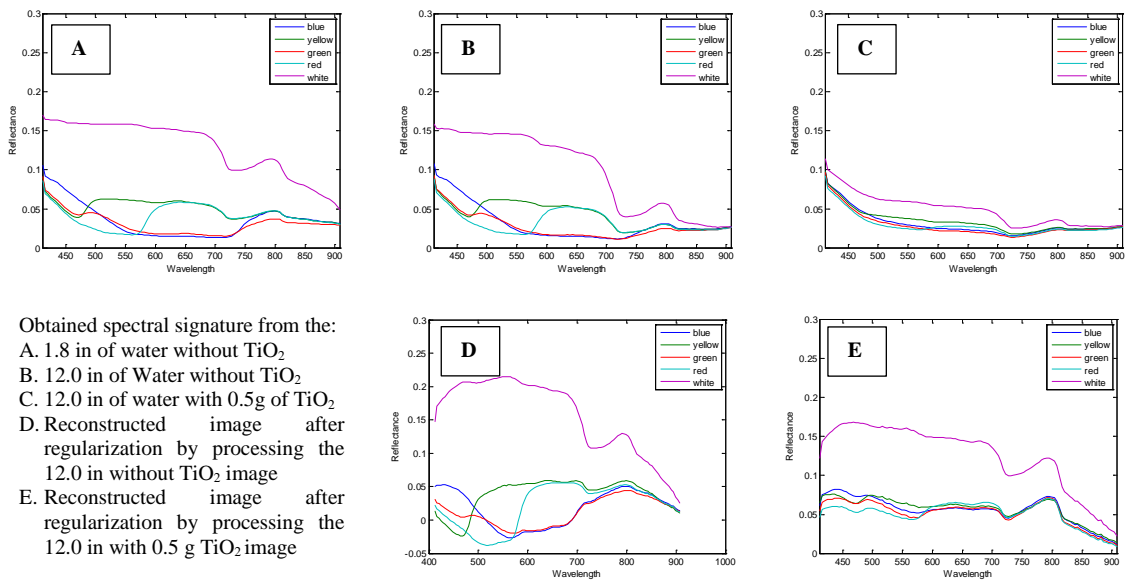


Figure 106: Obtained spectral signature from the training regions showed on figure 106

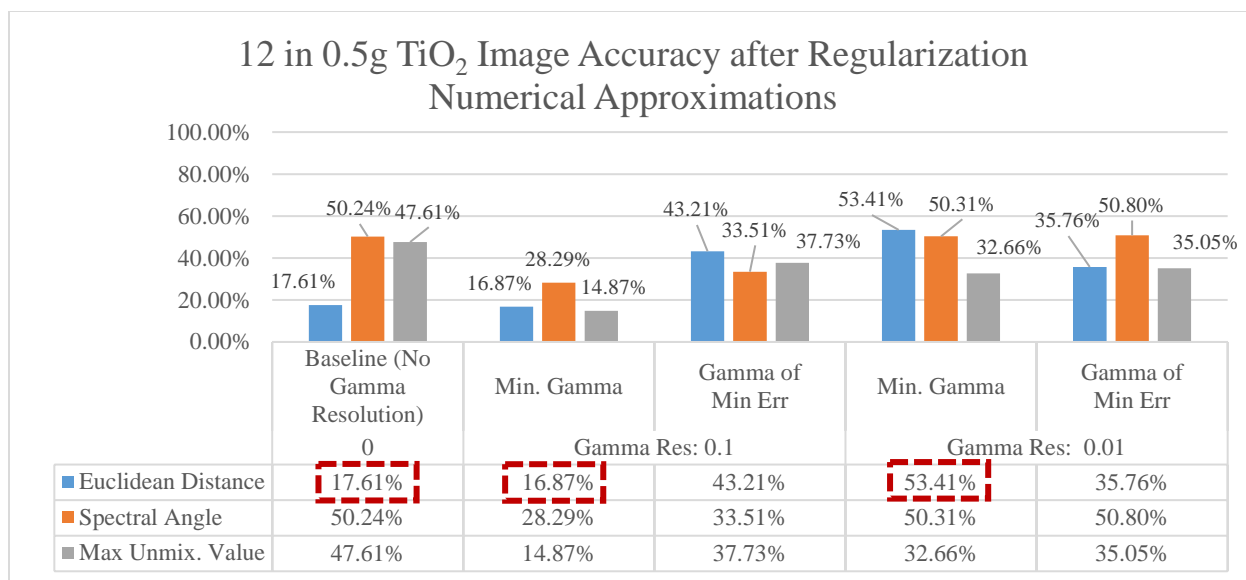


Figure 107: 12.0 in 0.5 g TiO₂ Image Numerical Approximations Results Comparison

Last figure showed the accuracy obtained using Numerical Approximations, next figure showed the obtained accuracy from the 12.0 in with 0.5 g of TiO₂ image regularized using Derived Equations. It can be observed that results were not very good, but both tendency of increasing accuracy after regularizing the image and after incrementing the gamma resolution from 0.1 to 0.01 prevails on results obtained from the Euclidean Distance classifier.

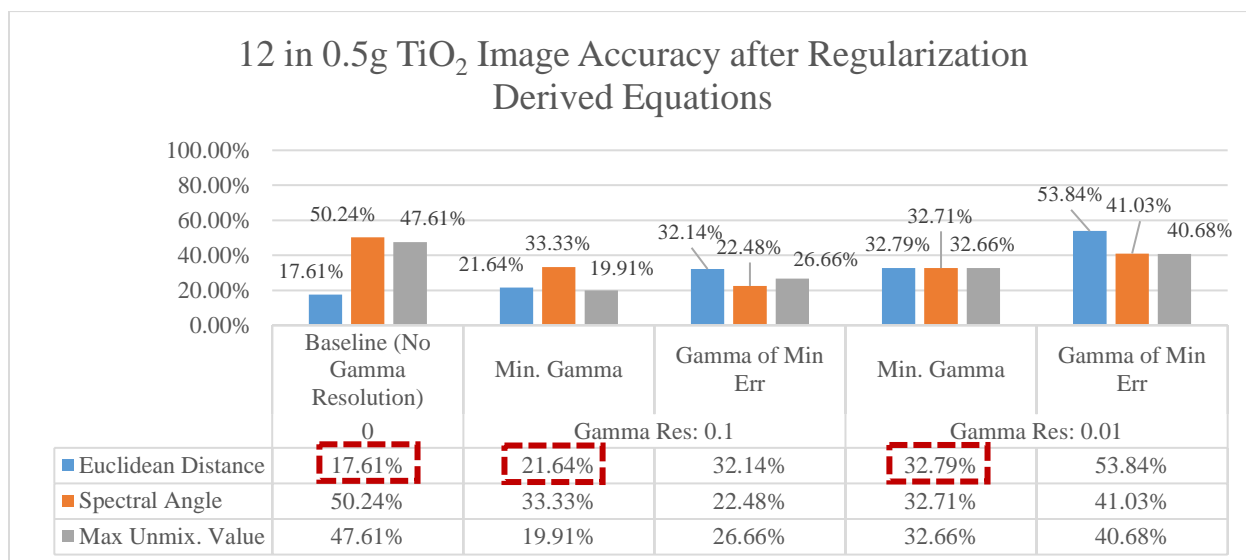


Figure 108: 12.0 in 0.5 g TiO₂ Image Derived Equations Results Comparison

For comparison purposes the following 4 figures shows the Classification Improvement for each presented result. To interpret them the reader must keep in mind that a positive value means that the

classification accuracy improves after regularization. At the other hand, negative values mean that the classification accuracy did not improve after regularization. From these figures, it can be observed that Euclidean Distance (**ED**) classifier benefits more, than the other two, from the Regularization algorithm. Euclidean Distance results in an 80.58% increase in accuracy for 12.0 in image and a 36.23% in the 12.0 in 0.5 g TiO₂ image with a gamma resolution of 0.01. Also, this graph reflects clearly that the Maximum Unmixing Value (**MUV**) classifier baseline results were not outperformed on any of results obtained after Regularization. Spectral Angle (**SA**) classifier did not improve significantly as ED because it performed relatively well while producing baseline results.

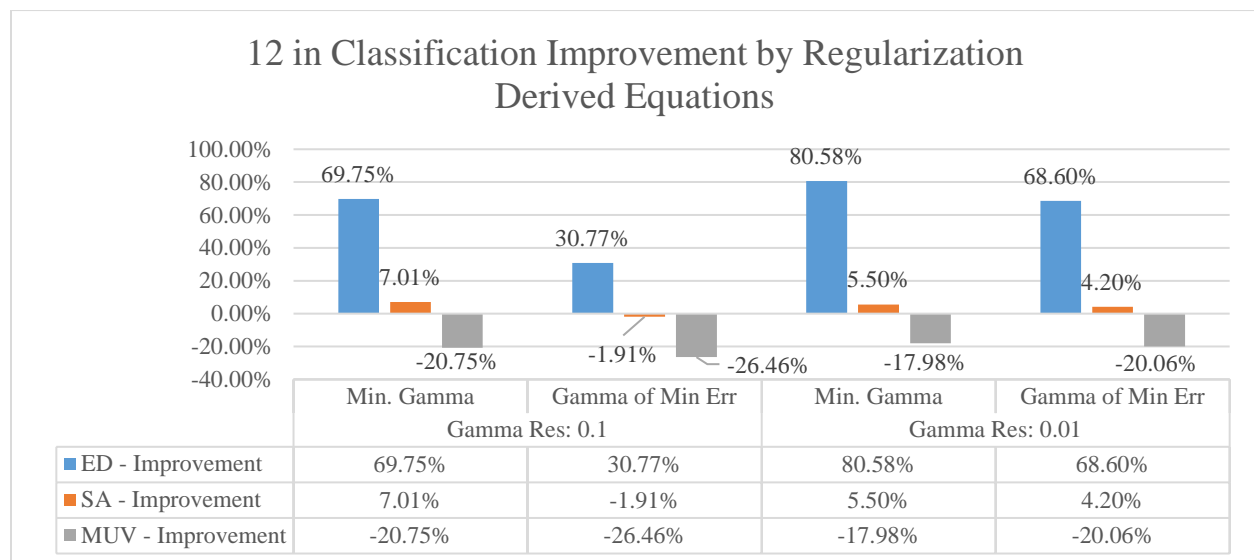


Figure 109: 12.0 in Improvement by Regularization – Derived Equations

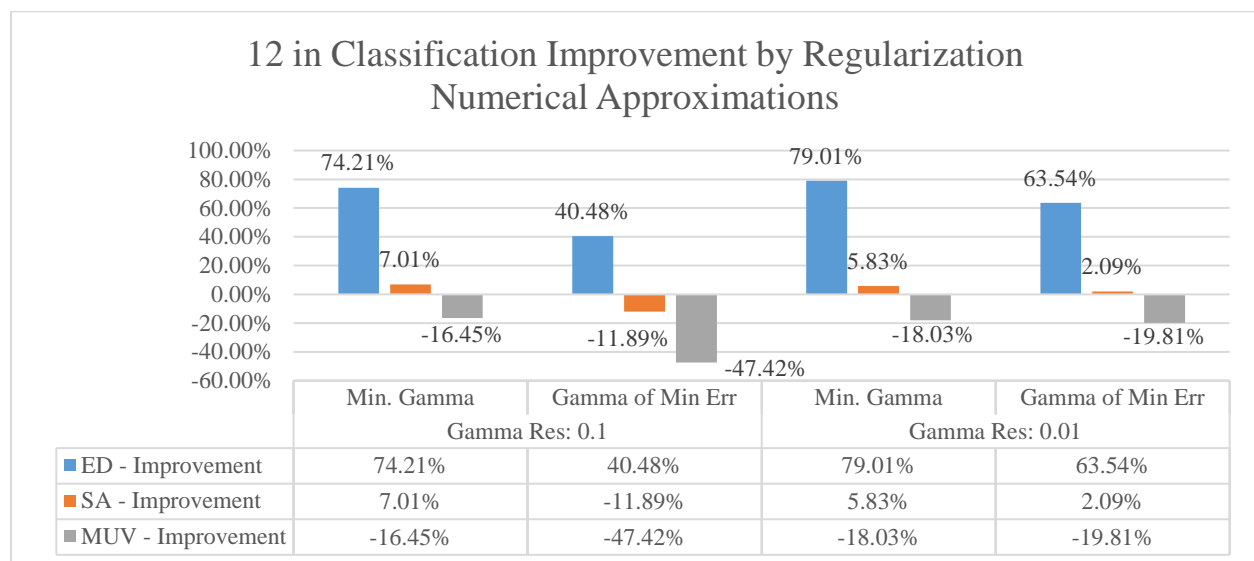


Figure 110: 12.0 in Improvement by Regularization – Numerical Approximations

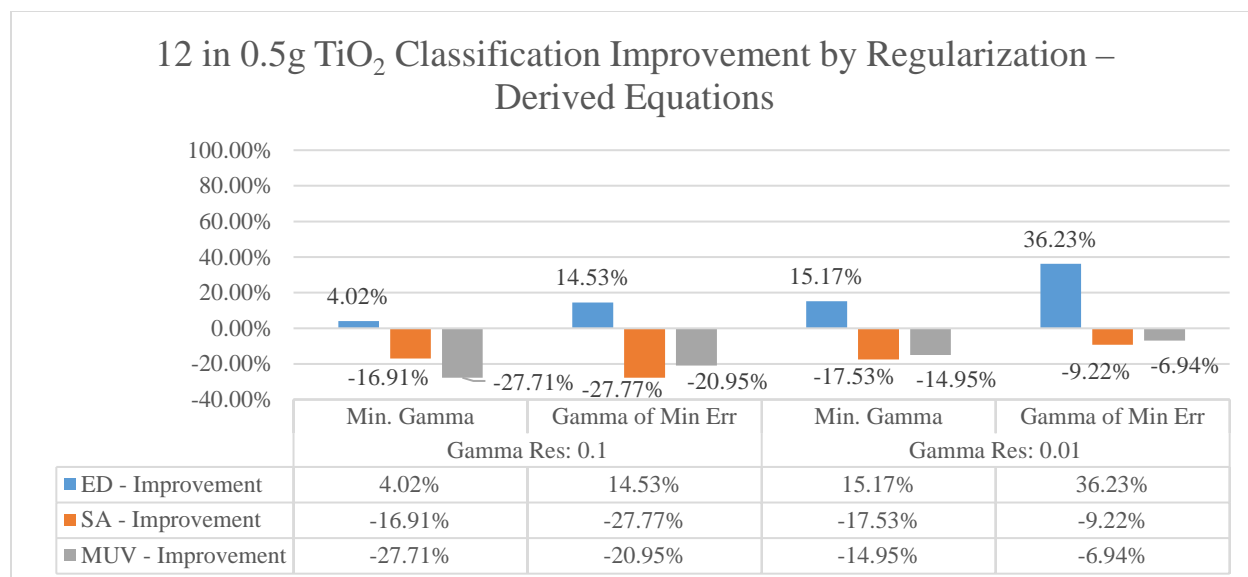


Figure 111: 12.0 in 0.5 g TiO₂ Improvement by Regularization – Derived Equations

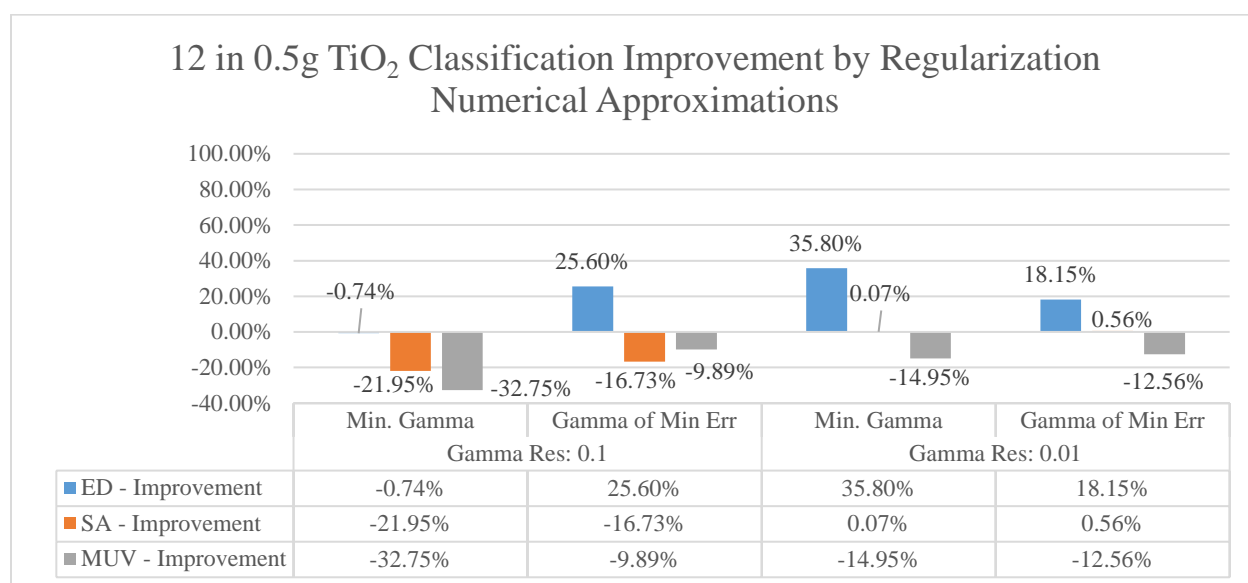


Figure 112: 12.0 in 0.5 g TiO₂ Improvement by Regularization – Numerical Approximations

Finally, analyzing all the Regularization results, there are some important facts that must be discussed:

1. Regularization increase the classification accuracy in the majority of presented cases.

14 out of 24 of the 12.0 in image demonstrate improvement after regularization. When adding Titanium Dioxide (TiO₂), the overall results did not improve significantly and this is due to the light scattering of the compound that limits the amount of information from the bottom that reach the

camera. Also, light intensity variation due to the lamp used on the experiment affect result considerably, see figure 113.



Figure 113: Circular light pattern created by the lamp over the water with TiO_2

2. There is a tendency that the accuracy improves by increasing the gamma resolution

18 out of 24 presented cases showed an improvement in accuracy by increasing the resolution from 0.1 to 0.01. It is important to mention that from the obtained data it was observed that a bigger gamma resolution makes the regularization algorithms more sensitive to intensity variations on the measured signals. In the presented experiment, these intensity variations were induced by the lamp used, that drawback will be discussed in item 5 of this list.

3. Minimum Gamma performed better than Gamma of Minimum Error

In 14 of the 24 cases presented Minimum Gamma obtained a higher classification accuracy after regularization. In all the obtained result of the 12.0 in without TiO_2 image Minimum Gamma outperformed Gamma of Minimum Error and in contrast on the 12.0 in with 0.5 g of TiO_2 image most the presented cases it was the opposite. Also, as an attribute, Minimum Gamma is less sensitive to light intensity variation on the obtained images, as observed in section 9.4 when the classification maps are compared.

4. Both methods to calculate the point of maximum curvature: Derived Equation and Numerical Approximation perform similarly in an overall accuracy sense.

Both methods employed in the algorithm to calculate the point of maximum curvature yield similar classification accuracies. Derived Equation finish in an overall accuracy of 55.70% and Numerical Approximation finish with an overall accuracy of 56.62%. Leaving a 0.91% of difference in the overall accuracy.

5. The lamp used on the indoor experiment creates intensity variation on the surface of the water that induce error.

When studying, classification maps some circular patterns can be observed, see figure 114 for examples. The conventional lamp with a Tungsten light bulb, used in the performed experiments, does not project a uniform light pattern over the illuminated objects. Figure 115 shows the Dry image, observed the difference in the light intensity from the center of the white standard thorough its corners. Each corner of the standard is less bright than the center. The dry image give evidence that the projected pattern on our experiments is due to this.

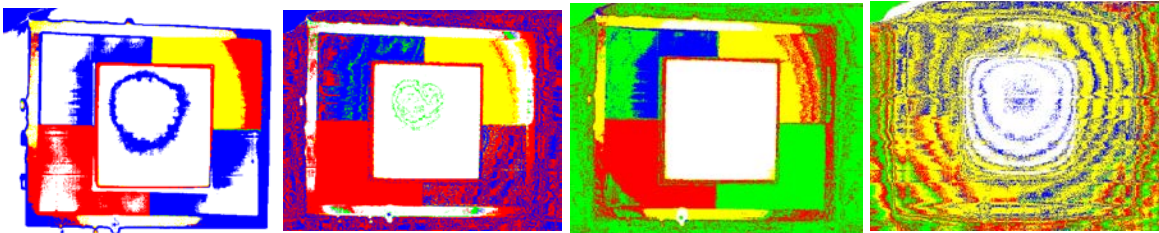


Figure 114: Example of the Circular Patterns obtained on the Classification Maps



Figure 115: Dry Image to observed the light intensity variation over the white standard

The applied methodology for calibrating the image is the following: divide all its pixel by a single calibration vector obtained from a white standard without the effect of water. This technique does not compensate for intensity variations projected by the lamp over our regions of interests. This is an issue since the designed preprocessing methodology obtains the endmembers used for processing image from the same data set. Figure 116 A shows 4 linearly selected regions from the center across the yellow region and B shows the average of all the pixels enclose on each selected region. It clearly demonstrates intensity variations and these variations affect the classification results.

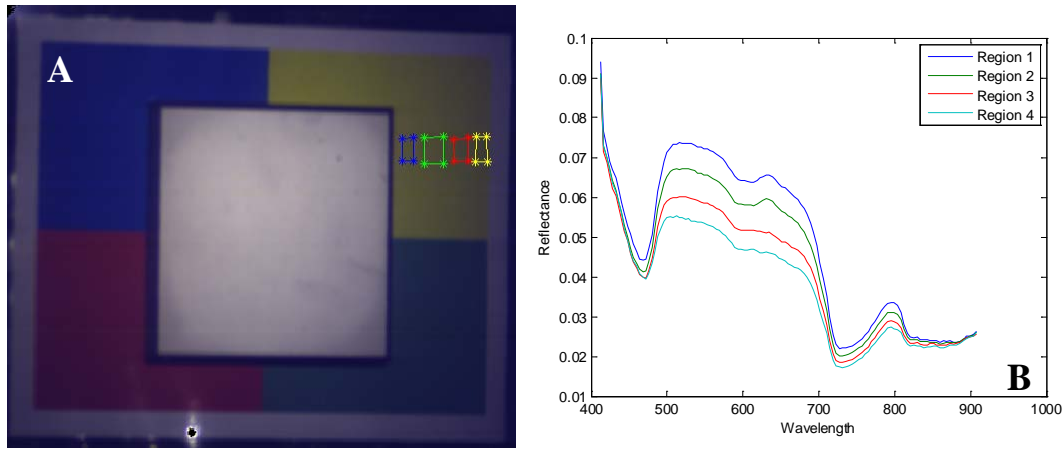


Figure 116: A Linearly Obtained Regions; B Spectral Signatures of those regions

6. Dimensionality reduction can become an important part of the algorithm

The 12.0 in image was reduced using Single Value Decomposition (SVD) dimensionality reduction algorithm. The number of spectral features were reduced from more 120 to 40. This reduction minimizes the time of processing the image. The image reduced was the 12 in without TiO_2 , this reduced image will be referred as SVD40 on the next graphs. Figures 117 and 118 shows the comparison between the obtained results using reduced bands images with additional ones previously showed. It can be observed that result stay almost the same with a slight decrease in accuracy of around 5% from Euclidean Distance. For Spectral Angle this difference is around 2% and for Maximum Unmixing Value this difference is less than 1%. From these results, it can be said that for Minimum Gamma classification accuracy is not impacted considerably by reducing the number of spectral bands.

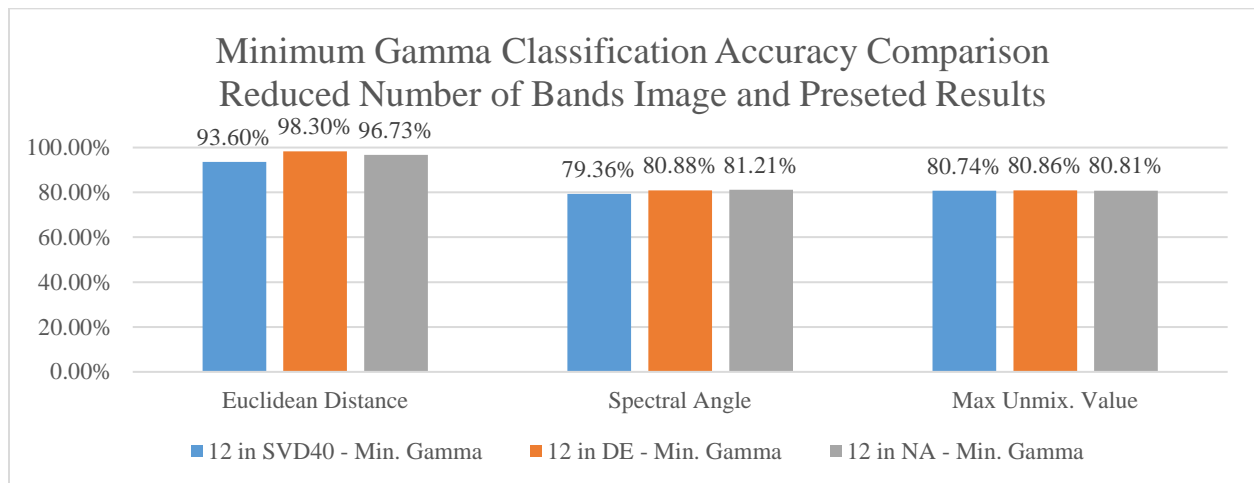


Figure 117: Reduced bands images result comparison – Minimum Gamma

In contrast, when processing reduced band images using Gamma of Minimum Error the classification accuracy was observed to increase, as shown in figure 118. For Euclidean Distance Classifier accuracy rises around 12% and in the other two classifiers remains basically unchanged. This establishes the tendency that even by reducing the number of spectral features the regularization algorithm has a positive impact on results.

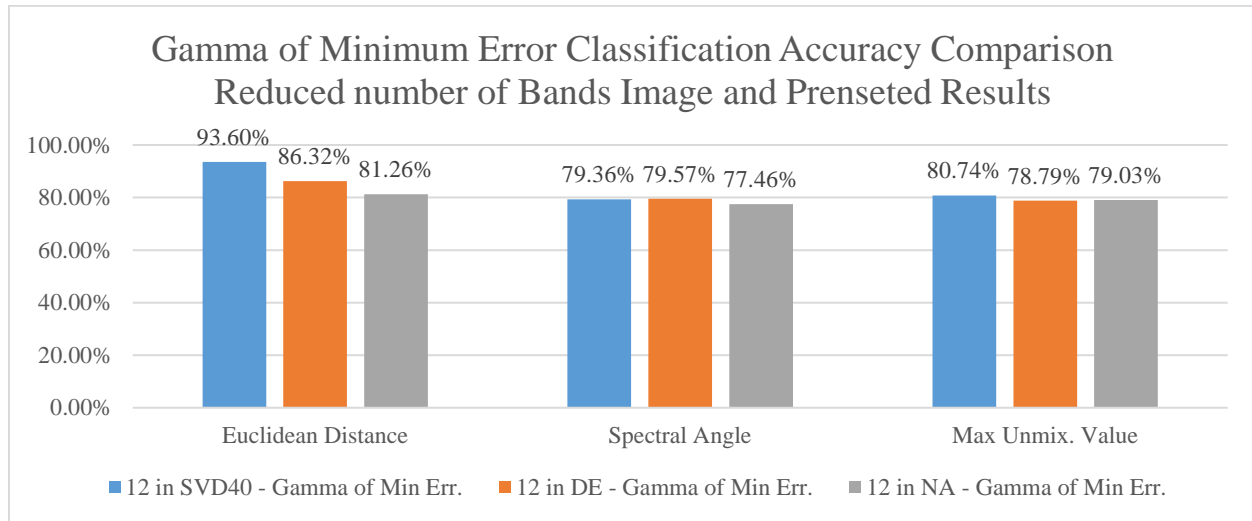


Figure 118: Reduced bands images result comparison – Gamma of Minimum Error

7 Conclusions & Future Work

In this section, the conclusions based on the importance of this toolbox and the algorithms within is presented. Also, another section will describe future research work that can be conducted to understand more benthic habitat, its simulations and to extend HyCIAT capabilities for a more complete and robust toolbox.

7.1 Conclusion

From the startup, this project was conducted to understand the underwater unmixing algorithms based on Lee's bio optical model that has been the point of study of several works at LARSIP. Lee's bio optical model combined with Underwater Unmixing and Bottom Classification using Regularization Techniques creates a very important tool set that could become the foundation of future software platforms designed for comprehensive studies of the underwater environment using remotely sensed data. This technology can be extended into different facets of environmental monitoring like health and ecological sustainability. Benthic environments are complex scenarios where its biodiversity and optical properties make it very interesting, very difficult and very important to study. HyCIAT integrates the algorithms into a single platform with tools and functionalities that provides the researcher with options to study multiple aspects of hyperspectral coastal images in a single interface. That is why it is important to maintain the operability of this toolbox.

With this work, HyCIAT was enabled to be used in MATLAB 2013. All modifications were verified to have a positive impact on results. Validation data was obtained based on an experimental procedure (documented on section 3.1) that can be used as a guideline for future indoor/outdoor hyperspectral imaging acquisition experiments with a controlled real benthic environment. This work also, gather a broad review of literature and explanations of all the algorithm in the toolbox that can be used as an important reference in future studies. Mathematical procedures were established for the empirically retrieval of optical properties: absorption and backscattering, coefficients of water, using Lee's equations and Hyperspectral Images of a real or simulated benthic environment. This project also, present a detailed explanation about the preprocessing steps followed that can benefit future studies. Moreover, this project presents a detailed explanation of the software implementation that can be used for reference of the delivered toolbox. And last, but not the least important aspects of the enhancement, this project establishes a baseline for future studies using HyCIAT.

This project and its results have been limited to the validation of different functionalities that the toolbox has, focusing on their applicability. Tools like custom bottom and custom unmixing range, implemented for the underwater unmixing algorithms, give the researcher the capability to manipulate parameters of the algorithms in a convenient way. Therefore, the obtained image database was intended to measure the impact of these new functionalities over the obtained results. That is why optical properties of the water column were out of scope when validating the Underwater Unmixing algorithms. These variables were neither being controlled nor measured when the experiment was conducted, therefore validation data for bottom reflectance, absorption, backscattering and phytoplankton were not available. Furthermore, the Regularization algorithm was developed and programmed in previous studies by Eladio Rodríguez-Díaz, and was reprogramed and integrated into HyCIAT in this version of the toolbox. Now, since this algorithm is designed to take high uncertainty on the measured signal, or in other words there is no need to have precise measurements of backscattering and absorption coefficients, the same data set was used to extract these parameters to test the implementation of the algorithm, its functionalities and therefore establishing baseline results.

Therefore, results show that HyCIAT 2013 produce similar results to those obtained in HyCIAT 2007. It has been demonstrated that default parameters of MATLAB's native optimization function do not have a considerable effect on the similarity of results obtained from both versions. For underwater unmixing, overall accuracy increases from 20% to 50% in one case and from 25% to 75% in others. The algorithms implemented are prone to confuse similar endmembers like Green and Blue as showed previously. This disadvantage can be mitigated with the custom unmixing range functionality in future studies. When simulating turbid waters, individual improvements were achieved up to 44%. For results obtained from the regularization algorithm, it can be highlighted an increase from 18% up to 98% of classification accuracy on an object submerged in 12.0 m of water and up to a 53% in individual classification accuracy on simulated turbid water. Circular patterns were observed on the obtained classification maps from the regularization algorithm. These patterns were caused by the nature of the experimental setup where the lamp was not projecting a uniform light pattern over our regions of interests. This can be corrected by either using an instrument capable of projecting uniform light patterns or by conducting the data acquisition experiment using the Sun as the light source.

In summary, HyCIAT has been updated and its functionality has been restored up to MATLAB 2013. Results from current version of the toolbox are similar than the ones produced in the previous

version of the toolbox. Additional tools were added to increase functionality and convenience with a positive impact on result. The regularization algorithm was coded on MATLAB 2013 and integrated into the toolbox. Regularization algorithm functionality was validated and demonstrate once again to have promising results and a high applicability to problems where there is high uncertainty on the measured signal. Therefore, objectives have been fulfilled.

7.2 Future Studies

The following are ideas for future studies that can be integrated into HyCIAT using this work as the starting point:

- The toolbox can be further enhanced by:
 - Including functionalities to save continuously the data or segment of the image to avoid losing data if the algorithm is forced to stop or accidentally stopped while processing.
 - Enable the functionality of forcing to stop and still obtain what the algorithm has processed so far. Perhaps the functionality of restarting from where it was left could be included.
 - Conduct time studies and further optimize the algorithms using MATLAB specials capabilities of efficiently managing matrices and vectors.
- The implemented regularization algorithm can be enhanced by:
 - Integrate the methods of thresholding the regularized images presented by Rodriguez-Dias on [6]. According to the authors, resulting data from this thresholding algorithm demonstrated to have a great capacity of discriminating a single class on the whole image in highly turbid waters.
 - Integrate Lee's equations for retrieving the optical properties of water: depth absorption and backscattering and pass them to the regularization algorithm.
- Conduct studies on the separability of endmembers among its wavelength features and develop an automatic algorithm that tells the researcher the 2 to 4 distinct custom regions for maximum spectral separability.
- Conduct exhaustive studies on all the functionalities that provides the recently implemented regularization interface. Including but not limited to the following:
 - Using Custom range for processing and a different range for classifying.

- The regularization interface contains functionalities so that the researcher can set a specific range to conduct the inversion and another range, within the established one for inversion, to classified the obtained the regularized image. This can be used to achieved more discrimination between similar endmembers.
 - Using a set of endmembers for processing and a different set for classifying
 - The regularization interface contains functionalities to regularize the image with a set of endmembers and perform the classification of the regularized image with another set of endmembers. This can be used, in example, for conducting studies on detection and classification of different types of algae. With these functionalities, the image can be regularized using a “generic” algae endmember and classified using the endmembers of different types of algae. The preliminary hypothesis, in this example, is that regularizing with a generic algae endmember will enhance the spectral features of the pixels that corresponds to algae on the image and the classification after regularization will be more precise.
- Conduct experiments to determine what is the best way of measuring the absorption and backscattering coefficients. This will help us understand the optical impact of these properties and how they impact our classification algorithms.
- Conduct an experiment of measuring the spectral signature of suspended sediments on the water column and how they can be simulated. This can be useful to extend the presented algorithms into detection and classification of materials suspended on water bodies.
- Investigate on how the algorithms for dimensionality reduction affect results and what is the set of bands, if any, that produces the best results. During this project, it was observed that in some results accuracy went up after reducing the number of bands of the image used.
- More future work can be found on the thesis by Torres-Madroño [1].

8 References

- [1] M. C. Torres Madronero, "Development of the Hyperspectral Coastal Image Analysis Toolbox (HyCIAT) with a focus on hyperspectral and lidar data fusion," M.E. Project, University of Puerto Rico, Mayagüez Campus, 2010.
- [2] Z. Lee, K. L. Carder, C. D. Mobley, R. G. Steward, and J. S. Patch, "Hyperspectral Remote Sensing for Shallow Waters. I. A Semianalytical Model," *Appl. Opt.*, vol. 37, no. 27, pp. 6329–6338, Sep. 1998.
- [3] Z. Lee, K. L. Carder, C. D. Mobley, R. G. Steward, and J. S. Patch, "Hyperspectral Remote Sensing for Shallow Waters. 2. Deriving Bottom Depths and Water Properties by Optimization," *Appl. Opt.*, vol. 38, no. 18, pp. 3831–3843, Jun. 1999.
- [4] J. A. Goodman, "Hyperspectral remote sensing of coral reefs: Deriving bathymetry, aquatic optical properties and a benthic spectral unmixing classification using AVIRIS data in the Hawaiian Islands," Ph.D. Dissertation, University of California, Davis, United States -- California, 2004.
- [5] A. Castrodad, "An algorithm for retrieval of Optical Properties, Bathymetry, and Benthic Cover in shallow waters from Hyperspectral Imagery," M.S. Thesis, University of Puerto Rico, Mayagüez Campus, 2005.
- [6] E. Rodríguez-Díaz, "Subsurface Detection of Underwater Targets by Inversion of Hyperspectral Imagery," M.S. Thesis, University of Puerto Rico, Mayagüez Campus, 2003.
- [7] E. Rodriguez-Diaz, L. O. Jimenez-Rodriguez, M. Velez-Reyes, F. Gilbes, and C. A. DiMarzio, "Subsurface detection of coral reefs in shallow waters using hyperspectral data," 2003, vol. 5093, pp. 538–546.
- [8] Ö. Ceyhan and A. Yalçın, "Remote sensing of water depths in shallow waters via artificial neural networks," *Estuar. Coast. Shelf Sci.*, vol. 89, no. 1, pp. 89–96, Sep. 2010.
- [9] P. R. C. Fearn, W. Klonowski, R. C. Babcock, P. England, and J. Phillips, "Shallow water substrate mapping using hyperspectral remote sensing," *Cont. Shelf Res.*, vol. 31, no. 12, pp. 1249–1259, Aug. 2011.
- [10] D. R. Lyzenga, "Passive remote sensing techniques for mapping water depth and bottom features," *Appl. Opt.*, vol. 17, no. 3, pp. 379–383, Feb. 1978.
- [11] R. K. Clark, T. H. Fay, and C. L. Walker, "Bathymetry calculations with Landsat 4 TM imagery under a generalized ratio assumption," *Appl. Opt.*, vol. 26, no. 19, p. 4036_1-4038, Oct. 1987.
- [12] E. Hochberg, "Capabilities of remote sensors to classify coral, algae, and sand as pure and mixed spectra," *Remote Sens. Environ.*, vol. 85, no. 2, pp. 174–189, May 2003.
- [13] E. Hochberg, "Spectral reflectance of coral reef bottom-types worldwide and implications for coral reef remote sensing," *Remote Sens. Environ.*, vol. 85, no. 2, pp. 159–173, May 2003.
- [14] S. R. Phinn, A. G. Dekker, V. E. Brando, and C. M. Roelfsema, "Mapping water quality and substrate cover in optically complex coastal and reef waters: an integrated approach," *Mar. Pollut. Bull.*, vol. 51, no. 1–4, pp. 459–469, Jan. 2005.
- [15] A. Minghelli-Roman and C. Dupouy, "Influence of Water Column Chlorophyll Concentration on Bathymetric Estimations in the Lagoon of New Caledonia, Using Several MERIS Images," *IEEE J. Sel. Top. Appl. Earth Obs. Remote Sens.*, vol. 6, no. 2, pp. 739–745, 2013.
- [16] S. Rosario-Torres, "Iterative algorithms for abundance estimation on unmixing of hyperspectral imagery," M.S. Thesis, University of Puerto Rico, Mayagüez Campus, 2004.
- [17] G. Casal, T. Kutser, J. A. Domínguez-Gómez, N. Sánchez-Carnero, and J. Freire, "Mapping benthic macroalgal communities in the coastal zone using CHRIS-PROBA mode 2 images," *Estuar. Coast. Shelf Sci.*, vol. 94, no. 3, pp. 281–290, Sep. 2011.
- [18] R. A. Schowengerdt, *Remote Sensing: Models and Methods for Image Processing*. Academic Press, 2006.

- [19] S. Bagheri, "Nearshore Water Quality Estimation Using Atmospherically Corrected AVIRIS Data," *Remote Sens.*, vol. 3, no. 12, pp. 257–269, Feb. 2011.
- [20] Z. Lee, K. L. Carder, R. F. Chen, and T. G. Peacock, "Properties of the Water Column and Bottom Derived from Airborne Visible Infrared Imaging Spectrometer (AVIRIS) Data," *J. Geophys. Res. - Oceans*, vol. 106, no. C6, pp. 11639–11651, 2001.
- [21] M. Janecek and W. W. Moses, "Optical Reflectance Measurements for Commonly Used Reflectors," *IEEE Trans. Nucl. Sci.*, vol. 55, no. 4, pp. 2432–2437, Aug. 2008.
- [22] N. G. Chorianopoulos, D. S. Tsoukleris, E. Z. Panagou, P. Falaras, and G.-J. E. Nychas, "Use of titanium dioxide (TiO₂) photocatalysts as alternative means for *Listeria monocytogenes* biofilm disinfection in food processing," *Food Microbiol.*, vol. 28, no. 1, pp. 164–170, Feb. 2011.
- [23] M. I. Cabrera, O. M. Alfano, and A. E. Cassano, "Absorption and Scattering Coefficients of Titanium Dioxide Particulate Suspensions in Water," *J. Phys. Chem.*, vol. 100, no. 51, pp. 20043–20050, Jan. 1996.
- [24] N. M. Ahmed and M. M. Selim, "Anticorrosive performance of titanium dioxide-talc hybrid pigments in alkyd paint formulations for protection of steel structures," *Anti-Corros. Methods Mater.*, vol. 57, no. 3, pp. 133–141, 2010.
- [25] J. G. Castaño, E. Velilla, L. Correa, M. Gómez, and F. Echeverría, "Ceramic insulators coated with titanium dioxide films: Properties and self-cleaning performance," *Electr. Power Syst. Res.*, vol. 116, pp. 182–186, Nov. 2014.
- [26] R. K. Gupta, B. Bills, M. DUBEY, D. Galipeau, and Q. H. Fan, "Light scattering behavior of oxide nanoparticles," in *2013 IEEE International Conference on Electro/Information Technology (EIT)*, 2013, pp. 1–5.
- [27] Y. Lan, Y. Lu, and Z. Ren, "Mini review on photocatalysis of titanium dioxide nanoparticles and their solar applications," *Nano Energy*, vol. 2, no. 5, pp. 1031–1045, Sep. 2013.
- [28] S. K. Kim, K. M. Kim, D. S. Jeong, W. Jeon, K. J. Yoon, and C. S. Hwang, "Titanium dioxide thin films for next-generation memory devices," *J. Mater. Res.*, vol. 28, no. 03, pp. 313–325, Feb. 2013.
- [29] The MathWorks, Inc, "Infer spatial transformation from control point pairs - cp2tform," *Infer spatial transformation from control point pairs*, 2014. [Online]. Available: http://www.mathworks.com/help/images/ref/cp2tform.html#inputarg_transformtype. [Accessed: 21-Aug-2014].
- [30] "Infinity - MATLAB Inf." [Online]. Available: <https://www.mathworks.com/help/matlab/ref/inf.html>. [Accessed: 18-Oct-2016].
- [31] "Solve nonlinear least-squares (nonlinear data-fitting) problems - MATLAB lsqnonlin." [Online]. Available: <https://www.mathworks.com/help/optim/ug/lsgnonlin.html>. [Accessed: 18-Oct-2016].
- [32] E. Arzuaga-Cruz *et al.*, "A MATLAB toolbox for Hyperspectral Image Analysis," in *Geoscience and Remote Sensing Symposium, 2004. IGARSS '04. Proceedings. 2004 IEEE International*, 2004, vol. 7, pp. 4839–4842 vol.7.
- [33] S. Rosario-Torres, M. Vélez-Reyes, S. D. Hunt, and L. O. Jiménez, "New developments and application of the UPRM MATLAB hyperspectral image analysis toolbox," 2007, vol. 6565, p. 65650E–65650E–12.
- [34] S. Rosario-Torres, M. Velez-Reyes, L. O. Jimenez-Rodriguez, and S. D. Hunt, *Introduction to Advanced Scientific Softwares and Toolboxes*. International Association of Engineers Press, 2007.
- [35] "Hyperspectral Toolbox Disclaimer." [Online]. Available: <http://www.censsis.neu.edu/software/hyperspectral/Hyperspecttoolbox.html>. [Accessed: 18-Oct-2016].

9 Appendix

9.1 Additional Results – Image A LIGU Unmixing Result

9.1.1 Without Bathymetry: without parameter modification

Table 20: Result LIGU w/o bathymetry and w/o Parameter Modifications

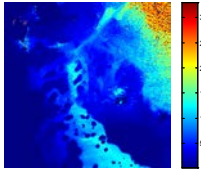
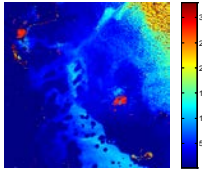
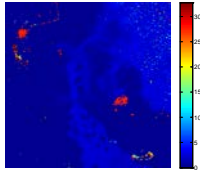
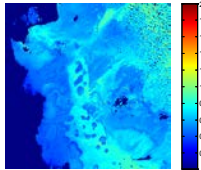
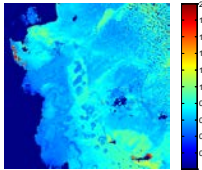
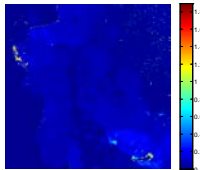
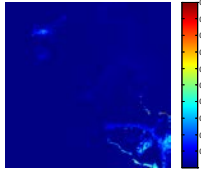
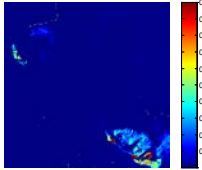
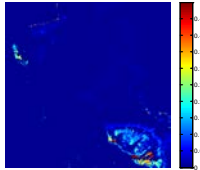
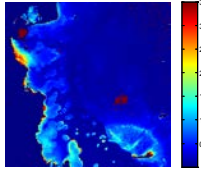
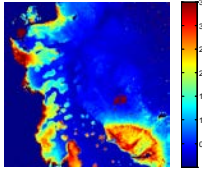
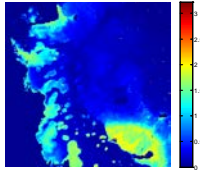
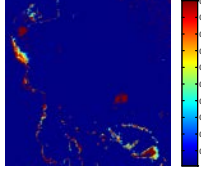
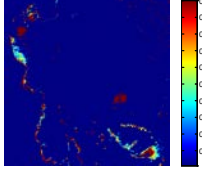
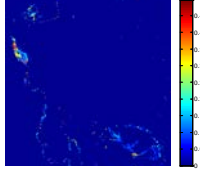
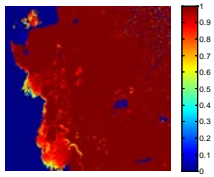
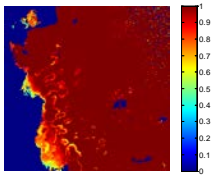
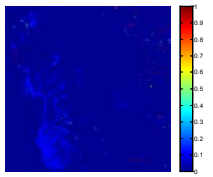
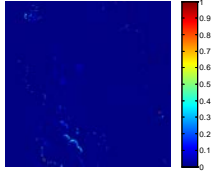
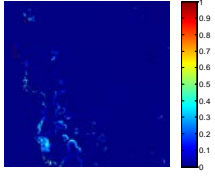
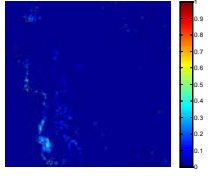
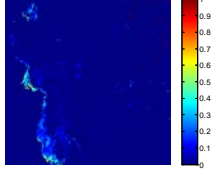
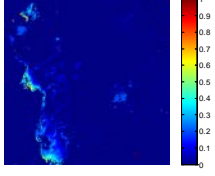
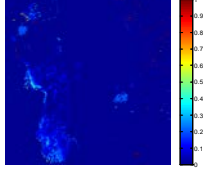
Results 2007	Results 2013	Difference
Depth		
		 $SSE = 604876.09$
Bottom Reflectance		
		 $SSE = 312.56$
Backscattering		
		 $SSE = 0.74$
Absorption		
		 $SSE = 264.22$
Phytoplankton		
		 $SSE = 35.04$

Table 20: Result LIGU w/o bathymetry and w/o Parameter Modifications

Results 2007	Results 2013	Difference
Sand		
		 $SSE = 371.38$
Coral		
		 $SSE = 226.48$
Algae		
		 $SSE = 394.59$

9.1.2 With Bathymetry: without parameter modifications

Table 21: Result LIGU with bathymetry and w/o Parameter Modifications

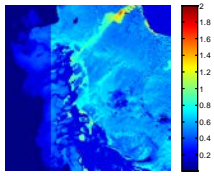
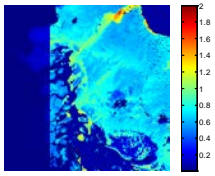
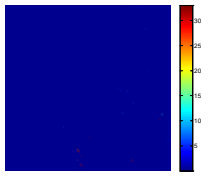
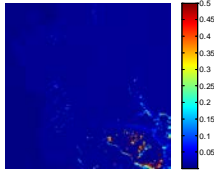
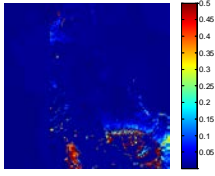
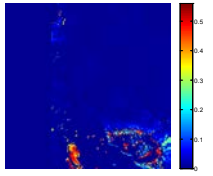
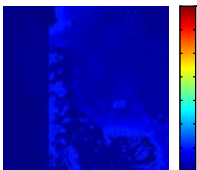
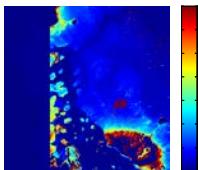
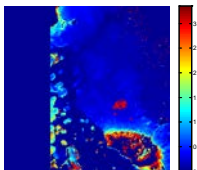
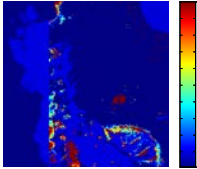
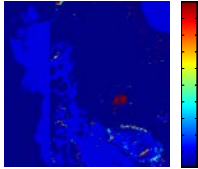
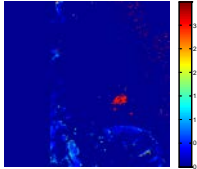
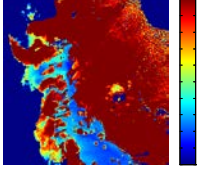
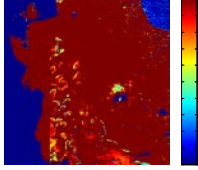
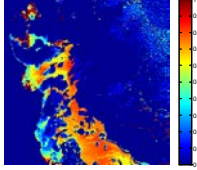
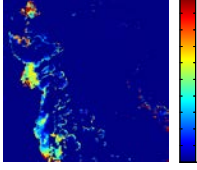
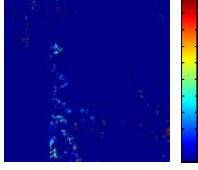
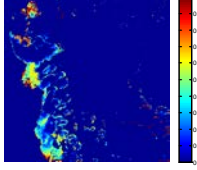
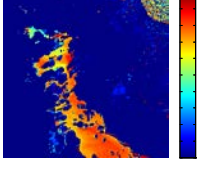
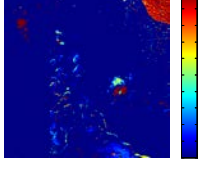
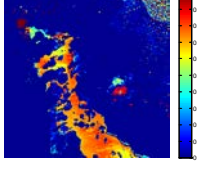
Results 2007	Results 2013	Difference
Bottom Reflectance		
		 $SSE = 26471.90$
Backscattering		
		 $SSE = 94.51$

Table 21: Result LIGU with bathymetry and w/o Parameter Modifications

Results 2007	Results 2013	Difference
Absorption		
		 $SSE = 7665.83$
Phytoplankton		
		 $SSE = 6910.40$
Sand		
		 $SSE = 879.86$
Coral		
		 $SSE = 637.34$
Algae		
		 $SSE = 441.48$

9.1.3 Without Bathymetry: with parameter modification

Table 22: Result LIGU w/o bathymetry and with Parameter Modifications: Water Properties

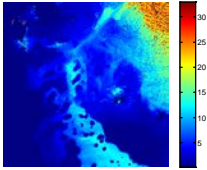
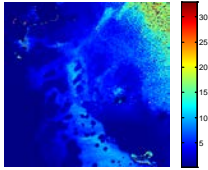
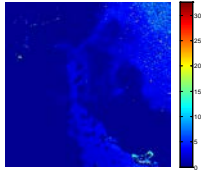
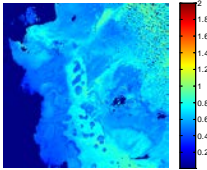
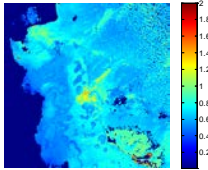
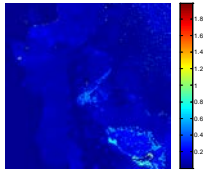
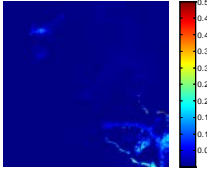
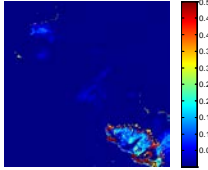
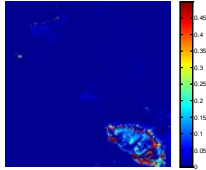
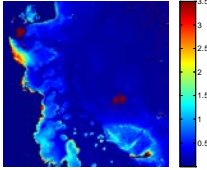
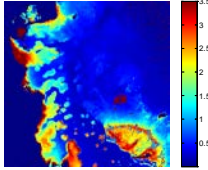
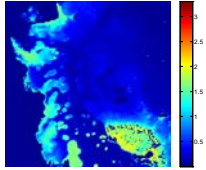
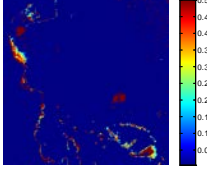
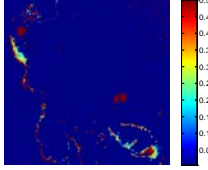
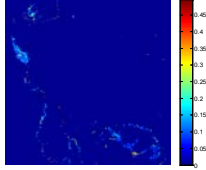
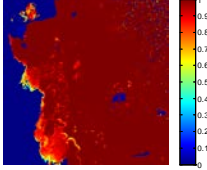
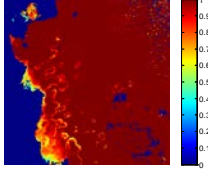
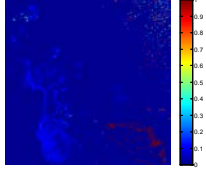
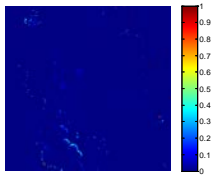
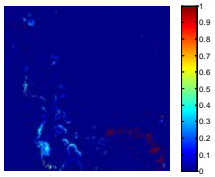
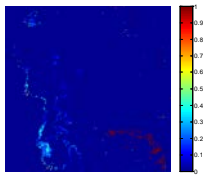
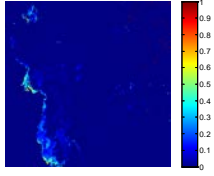
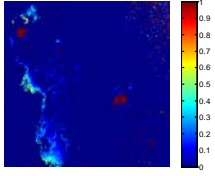
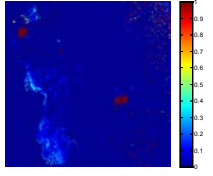
Results 2007	Results 2013	Difference
Depth		
		 $SSE = 71555.72$
Bottom Reflectance		
		 $SSE = 174.58$
Backscattering		
		 $SSE = 0.26$
Absorption		
		 $SSE = 206.33$
Phytoplankton		
		 $SSE = 8.49$
Sand		
		 $SSE = 172.86$

Table 22: Result LIGU w/o bathymetry and with Parameter Modifications: Water Properties

Results 2007	Results 2013	Difference
Coral		
		 $SSE = 153.40$
Algae		
		 $SSE = 169.95$

9.1.4 With Bathymetry: with parameter modifications

Table 23: Result LIGU with bathymetry and with Parameter Modifications: Water Properties

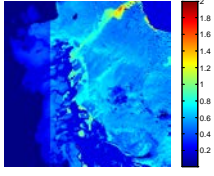
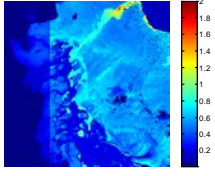
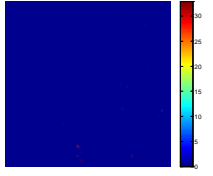
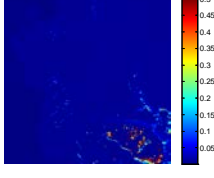
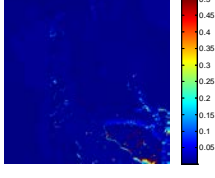
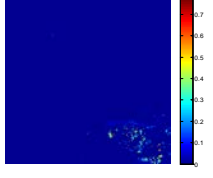
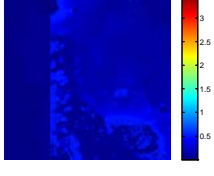
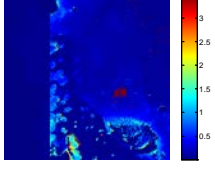
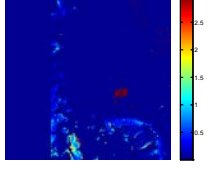
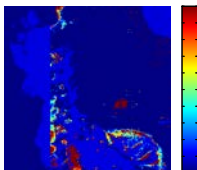
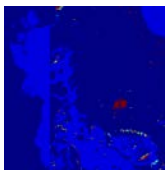
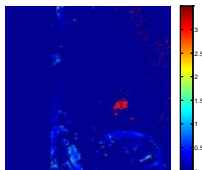
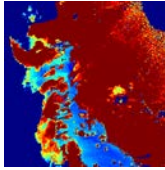
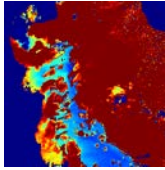
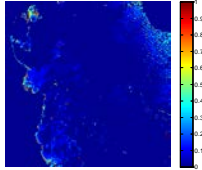
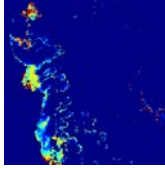
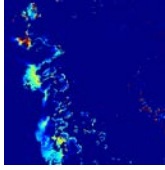
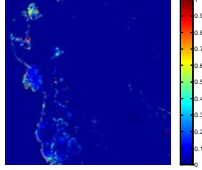
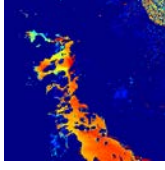
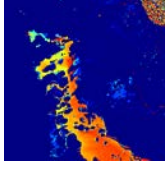
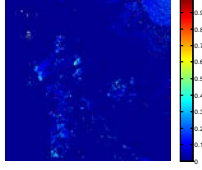
Results 2007	Results 2013	Difference
Bottom Reflectance		
		 $SSE = 26586.33$
Backscattering		
		 $SSE = 69.49$
Absorption		
		 $SSE = 7778.69$

Table 23: Result LIGU with bathymetry and with Parameter Modifications: Water Properties

Results 2007	Results 2013	Difference
Phytoplankton		
		 $SSE = 6896.11$
Sand		
		 $SSE = 908.99$
Cora		
		 $SSE = 655.81$
Algae		
		 $SSE = 441.49$

9.2 Extended Results – Underwater Linear Unmixing Results with Previous Data

9.2.1 LIGU Results Improvements: Image A without Bathymetry

The following Table shows the calculated SSE between results from HyCIAT 2013 and HyCIAT 2007 with and without parameters modifications. This data corresponds to result obtained from Image A using LIGU algorithm without Bathymetry.

Table 24: Result's SSE Differences LIGU of Image A without Bathymetry

Parameter Name	SSE Modified Parameter	SSE Unmodified Parameter	Individual Improvement
Depth	71555.72	604876.09	88.17%
Bottom Reflectance	174.58	312.56	44.14%
Backscattering	0.26	0.74	65.31%
Absorption	206.33	264.22	21.91%
Phytoplankton	8.49	35.04	75.77%
Sand	172.86	371.38	53.45%
Coral	153.40	226.48	32.27%
Algae	169.95	394.59	56.93%
Total	72441.58	606481.09	
Total Improvement	88.06%		

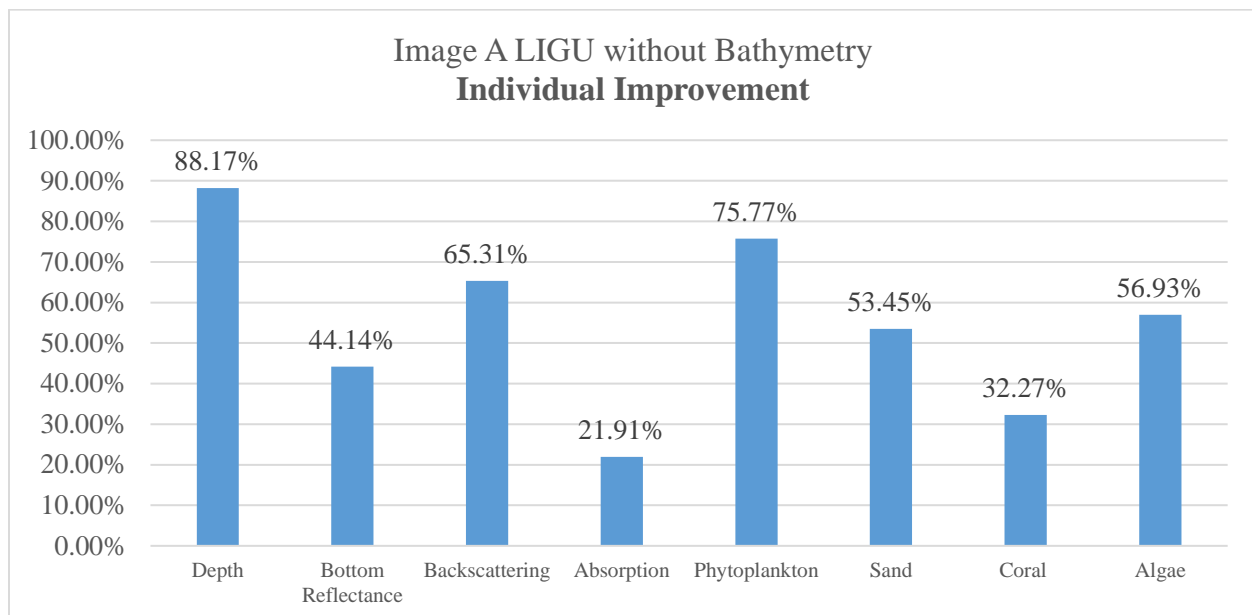


Figure 119: Improvement by modifying parameters – Image A LIGU without Bathymetry

9.2.2 LIGU Results Improvements: Image B without Bathymetry

The following Table shows the calculated SSE between results from HyCIAT 2013 and HyCIAT 2007 with and without parameters modifications. This data corresponds to result obtained from Image B using LIGU algorithm without Bathymetry.

Table 25: Result's SSE Differences LIGU of Image B without Bathymetry

Parameter Name	SSE Modified Parameter	SSE Unmodified Parameter	Individual Improvement
Depth	20167.7088	19003.8662	-6%
Bottom Reflectance	24.9852	39.3862	37%
Backscattering	0.023579	0.072877	68%
Absorption	84.6693	77.4388	-9%
Phytoplankton	3.9703	14.5735	73%
Sand	32.2958	19.9951	-62%
Coral	32.8194	41.1619	20%
Algae	35.7896	27.7195	-29%
Total	20382.26198	19224.21408	
Total Improvement	-6%		

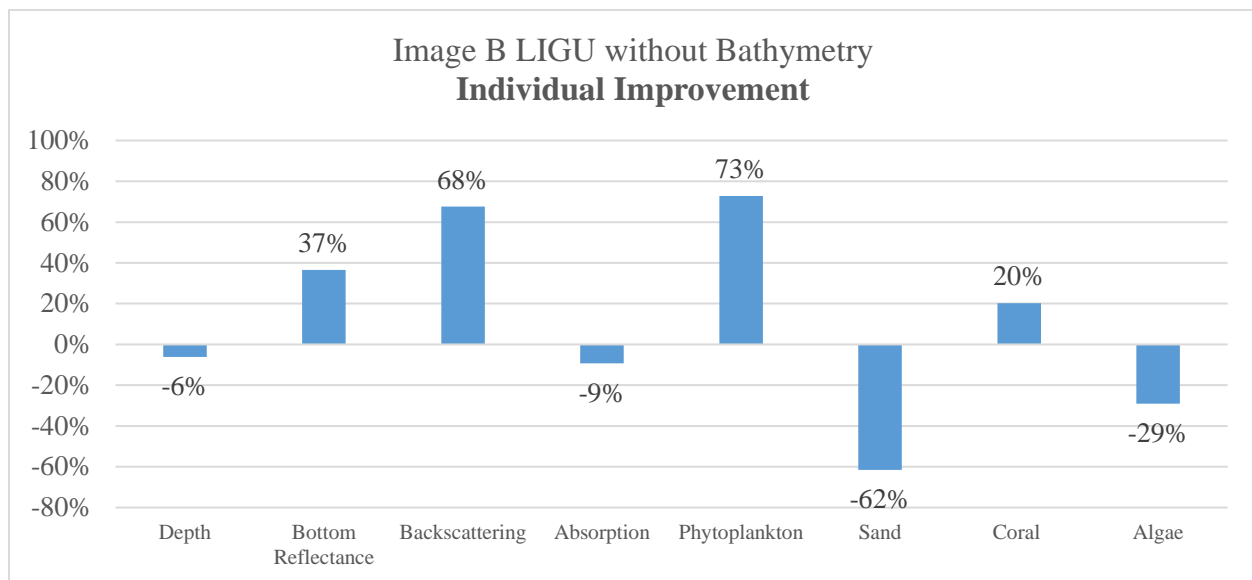


Figure 120: Improvement by modifying parameters – Image B LIGU without Bathymetry

9.2.3 LIGU Results Improvements: Image A with Bathymetry

The following Table shows the calculated SSE between results from HyCIAT 2013 and HyCIAT 2007 with and without parameters modifications. This data corresponds to result obtained from Image A using LIGU algorithm with Bathymetry.

Table 26: Result's SSE Differences LIGU of Image A with Bathymetry

Parameter Name	SSE Modified Parameter	SSE Unmodified Parameter	Individual Improvement
Bottom Reflectance	26586.33	26471.90	-0.43%
Backscattering	69.49	94.51	26.47%
Absorption	7778.69	7665.83	-1.47%
Phytoplankton	6896.11	6910.40	0.21%
Sand	908.99	879.86	-3.31%
Coral	655.81	637.34	-2.90%
Algae	441.49	441.48	0.00%
Total	43336.91	43101.32	
Total Improvement	-0.55%		

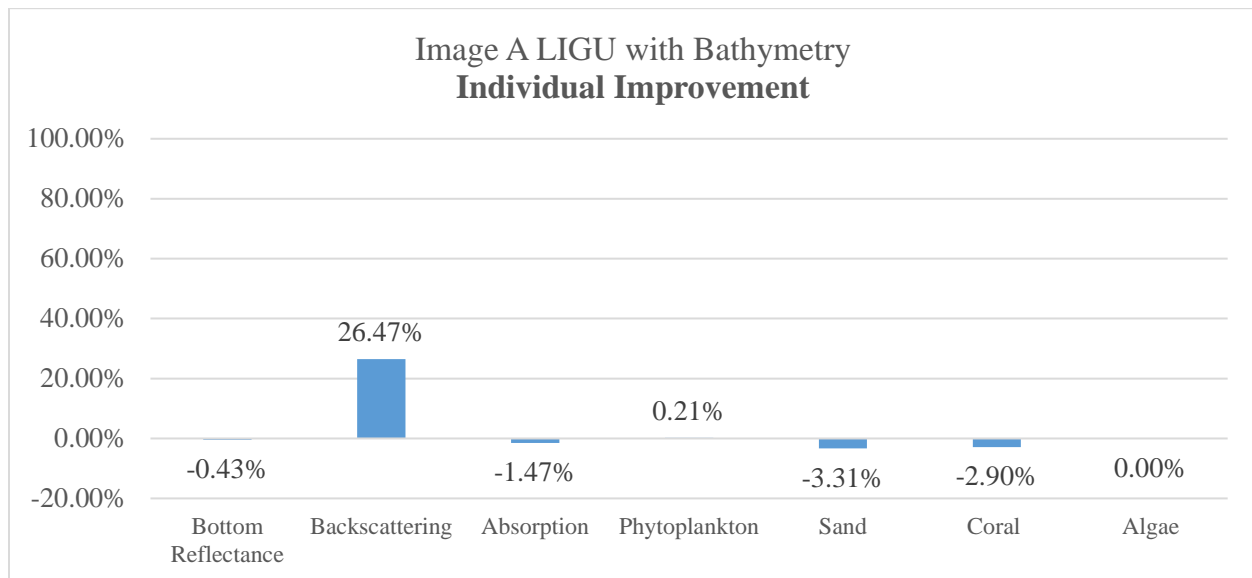


Figure 121: Improvement by modifying parameters – Image A LIGU with Bathymetry

9.2.4 LIGU Results Improvements: Image B with Bathymetry

The following Table shows the calculated SSE between results from HyCIAT 2013 and HyCIAT 2007 with and without parameters modifications. This data corresponds to result obtained from Image B using LIGU algorithm with Bathymetry.

Table 27: Result's SSE Differences LIGU of Image B with Bathymetry

Parameter Name	SSE Modified Parameter	SSE Unmodified Parameter	Individual Improvement
Bottom Reflectance	54.5947	55.1209	0.95%
Backscattering	7.0291	11.6431	39.63%
Absorption	919.7675	919.6687	-0.01%
Phytoplankton	404.5047	406.7838	0.56%
Sand	271.1028	273.0824	0.72%
Coral	238.8469	239.9439	0.46%
Algae	198.0625	199.2629	0.60%
Total	2093.9082	2105.5057	
Total Improvement	0.55%		

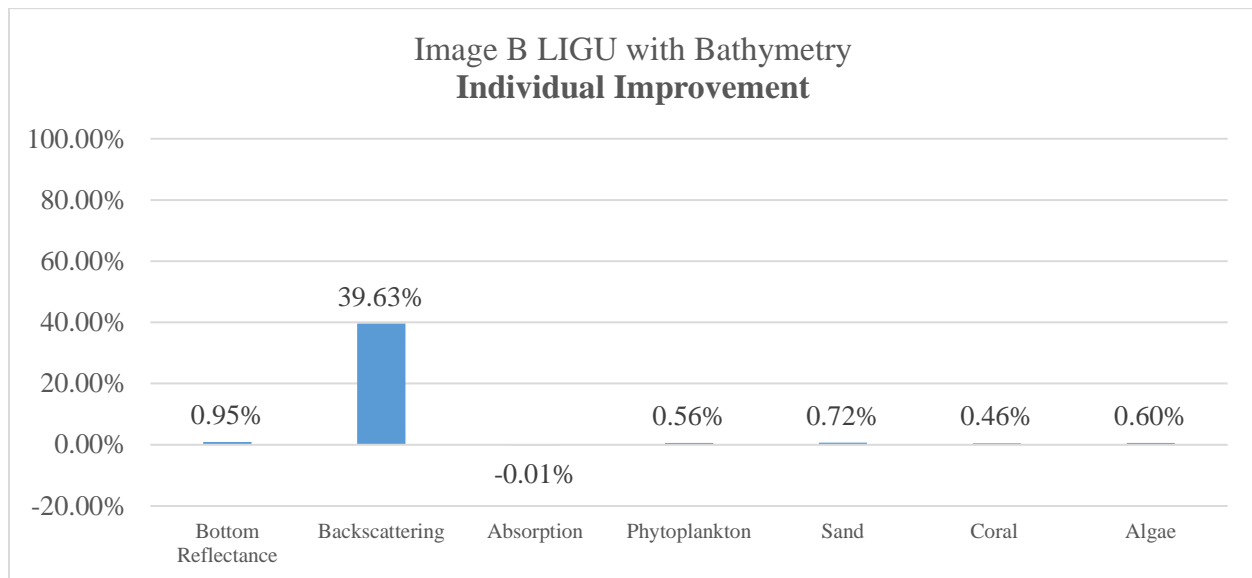


Figure 122: Improvement by modifying parameters – Image B LIGU with Bathymetry

9.2.5 CIUB Results Improvements: Image A without Bathymetry:

The following Table shows the calculated SSE between results from HyCIAT 2013 and HyCIAT 2007 with and without parameters modifications. This data corresponds to result obtained from Image A using CIUB algorithm without Bathymetry.

Table 28: Result's SSE Differences CIUB of Image A without Bathymetry

Parameter Name	SSE Modified Parameter	SSE Unmodified Parameter	Individual Improvement
Depth	2142385.82	3390652.15	36.81%
Bottom Reflectance	6298.11	4573.28	-37.72%
Backscattering	78.62	87.31	9.95%
Absorption	2341.66	2319.68	-0.95%
Phytoplankton	210.63	210.89	0.12%
Sand	3634.61	3607.65	-0.75%
Coral	5067.74	6132.78	17.37%
Algae	6003.54	5734.04	-4.70%
Total	2166020.72	3413317.79	
Total Improvement	36.54%		

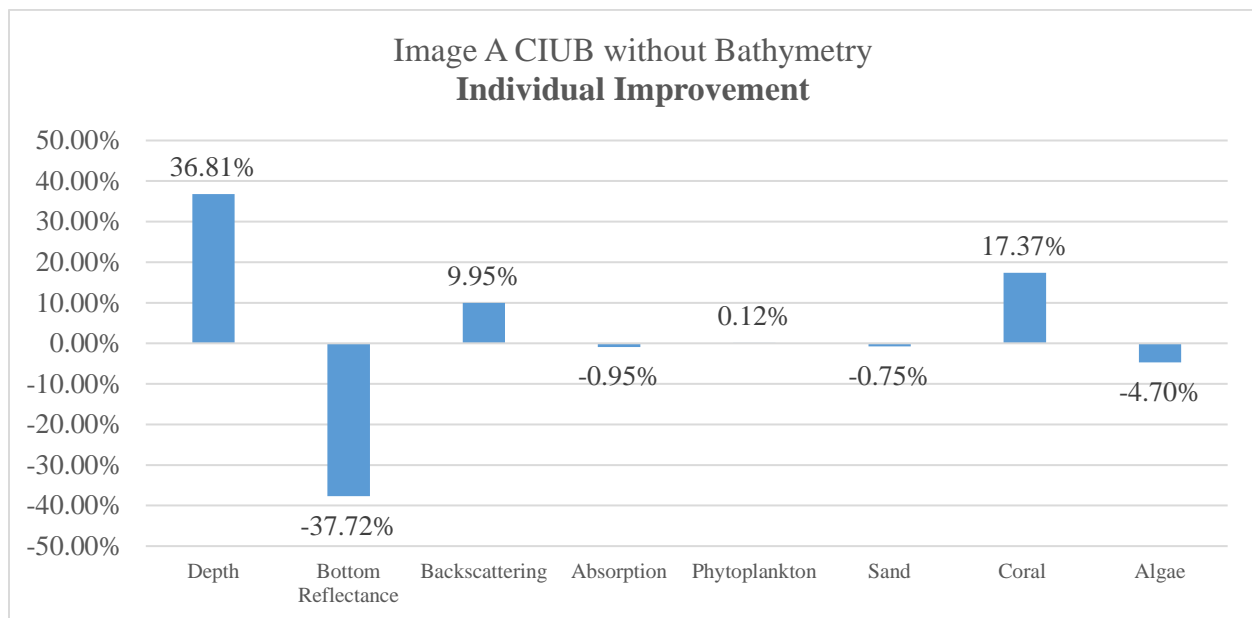


Figure 123: Improvement by modifying parameters – Image A CIUB without Bathymetry

9.2.6 CIUB Results Improvements: Image B without Bathymetry

The following Table shows the calculated SSE between results from HyCIAT 2013 and HyCIAT 2007 with and without parameters modifications. This data corresponds to result obtained from Image B using CIUB algorithm without Bathymetry.

Table 29: Result's SSE Differences CIUB of Image B without Bathymetry

Parameter Name	SSE Modified Parameter	SSE Unmodified Parameter	Individual Improvement
Depth	207551.2083	215752.5751	3.80%
Bottom Reflectance	1147.2801	691.7502	-65.85%
Backscattering	6.1631	6.8656	10.23%
Absorption	776.2343	764.8338	-1.49%
Phytoplankton	90.1098	89.6909	-0.47%
Sand	663.0366	670.5677	1.12%
Coral	242.2238	243.771	0.63%
Algae	894.7559	908.3273	1.49%
Total	211371.0119	219128.3816	
Total Improvement	3.54%		

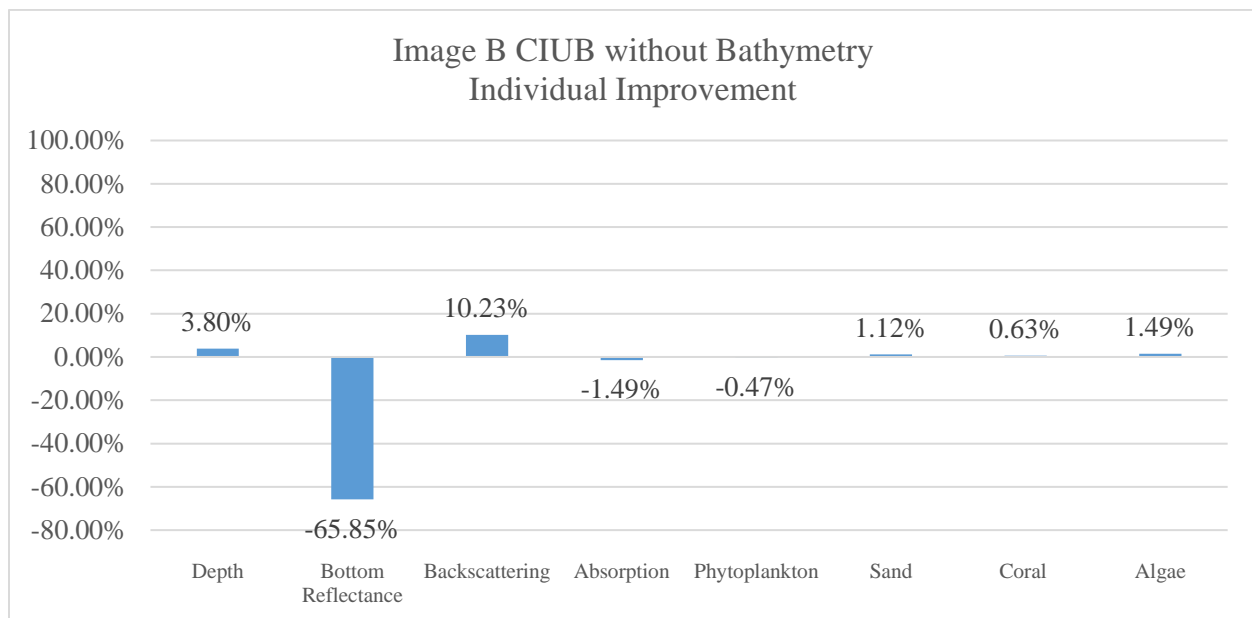


Figure 124: Improvement by modifying parameters – Image B CIUB without Bathymetry

9.2.7 CIUB Results Improvements: Image A with Bathymetry

The following Table shows the calculated SSE between results from HyCIAT 2013 and HyCIAT 2007 with and without parameters modifications. This data corresponds to result obtained from Image A using CIUB algorithm with Bathymetry.

Table 30: Result's SSE Differences CIUB of Image A with Bathymetry

Parameter Name	SSE Modified Parameter	SSE Unmodified Parameter	Individual Improvement
Bottom Reflectance	44776.61	44755.51	-0.05%
Backscattering	493.27	492.12	-0.23%
Absorption	4619.36	4600.93	-0.40%
Phytoplankton	7760.16	7773.34	0.17%
Sand	4704.26	4714.45	0.22%
Coral	4621.82	4607.52	-0.31%
Algae	5043.03	5086.89	0.86%
Total	72018.51	72030.76	
Total Improvement	0.02%		

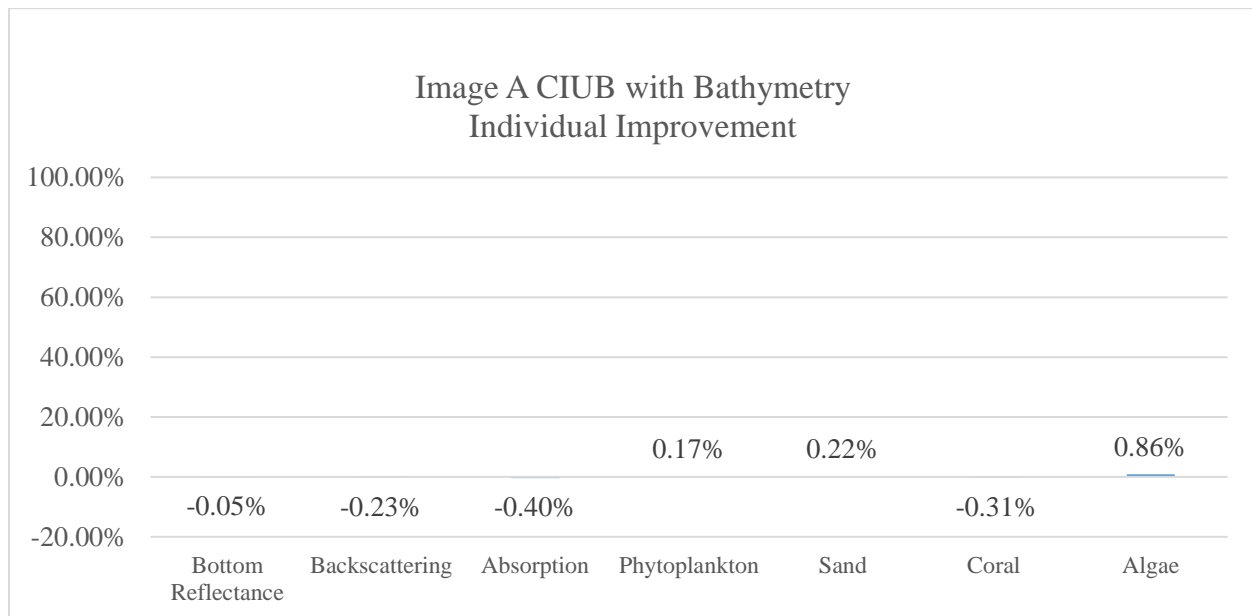


Figure 125: Improvement by modifying parameters – Image A CIUB with Bathymetry

9.2.8 CIUB Results Improvements: Image B with Bathymetry

The following Table shows the calculated SSE between results from HyCIAT 2013 and HyCIAT 2007 with and without parameters modifications. This data corresponds to result obtained from Image B using CIUB algorithm with Bathymetry.

Table 31: Result's SSE Differences CIUB of Image B with Bathymetry

Parameter Name	SSE Modified Parameter	SSE Unmodified Parameter	Individual Improvement
Bottom Reflectance	546.3297	545.7591	-0.10%
Backscattering	50.4385	50.7122	0.54%
Absorption	293.1214	296.9141	1.28%
Phytoplankton	958.2156	964.5725	0.66%
Sand	279.6945	280.7299	0.37%
Coral	150.7805	149.0381	-1.17%
Algae	294.4853	300.9449	2.15%
Total	2573.0655	2588.6708	
Total Improvement	0.60%		

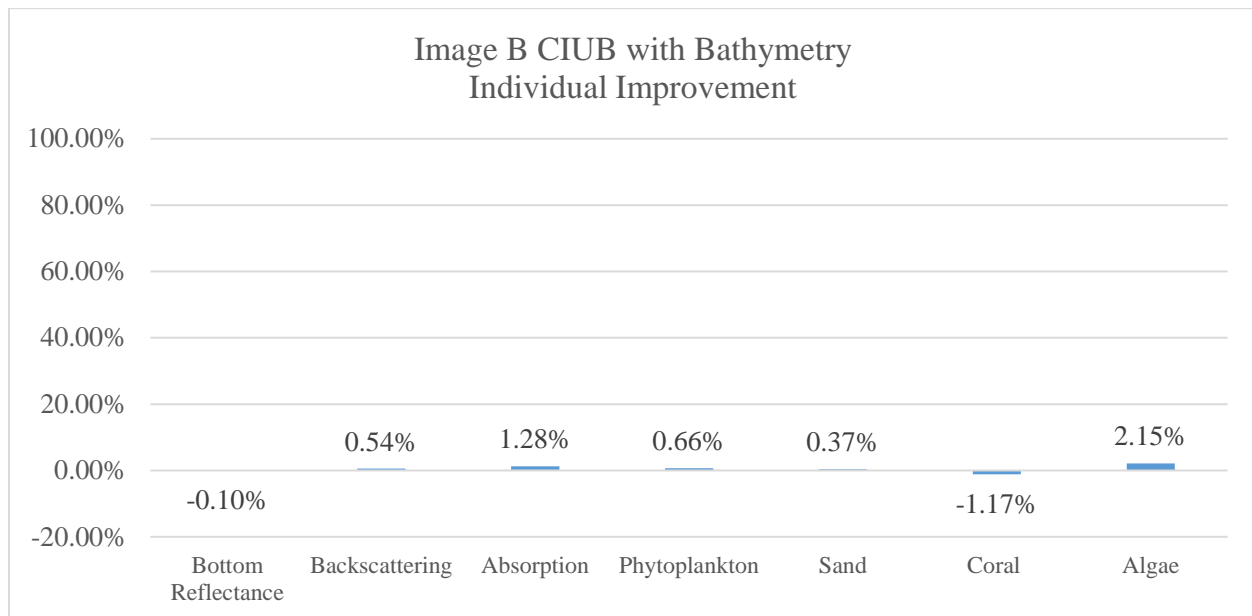


Figure 126: Improvement by modifying parameters – Image B CIUB with Bathymetry

9.3 Extended Results – Underwater Linear Unmixing with Real Controlled Data

9.3.1 LIGU 12.0 in Image with 5 Colors Endmembers

This section will show result obtained from the 12.0 in image using LIGU algorithm. In this case, five endmembers representing: Blue, Yellow, Green, Red and White regions from the 1.8” hyperspectral image were used as input to the algorithm (See next Figure). Obtained accuracy are showed on Table 33. Visual representation will be showed on Table 32 and at last, figure 129 will present the graph of the overall accuracy over testing regions.

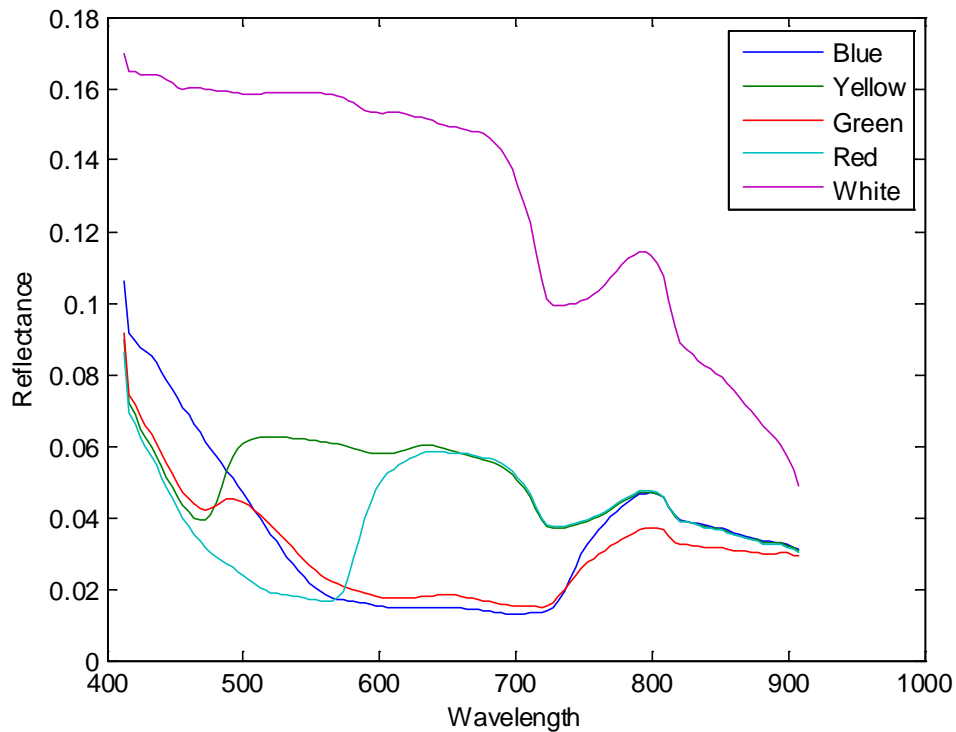


Figure 127: Endmember Used for the 5 Colors processing

The resulting images represent the fractional contribution of the particular endmember to the measured signal. Colors has been applied to the results to facilitate the visualization of them (see figure 128 for the color scale). For example, a pixel showed as blue means that that particular endmember did not contribute to the measured spectra whatsoever and, in contrast, a dark red pixel means that that particular endmember contributes in a 100% to the measured spectra. The optical water properties are out of scope of this work since they were not controlled by the time of the experiment.

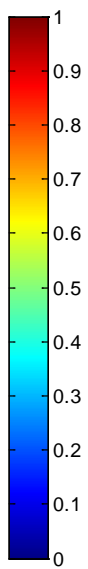


Figure 128: Enhanced color scale for reference.

Table 32: LIGU 5 Color Endmembers Results





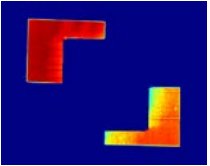
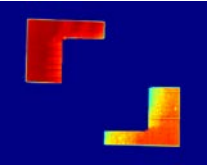










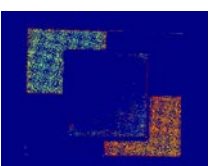

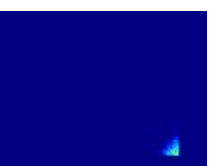
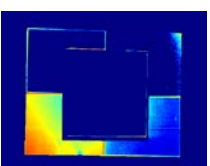
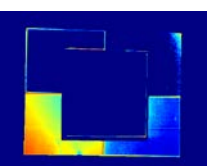
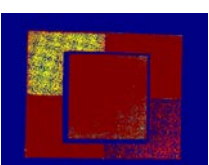
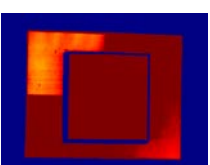
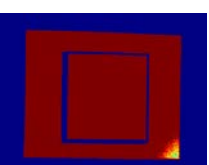
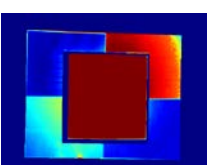
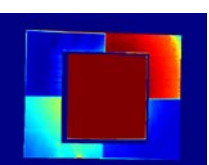
Real Image: 12.0 in				
	Configurations			
Baseline	2013-1	2013-2	2013-3	2013-4
Blue				
				
Accuracy = 0%	Accuracy = 0%	Accuracy = 0%	Accuracy = 93.53%	Accuracy = 93.53%
Yellow				
				
Accuracy = 0%	Accuracy = 0%	Accuracy = 0%	Accuracy = 0%	Accuracy = 0%
Green				
				
Accuracy = 0.0%	Accuracy = 0%	Accuracy = 0%	Accuracy = 0%	Accuracy = 0%
Red				
				
Accuracy = 0.00%	Accuracy = 0.00%	Accuracy = 0.00%	Accuracy = 55.86%	Accuracy = 55.88%
White				
				
Accuracy = 99.35%	Accuracy = 100.0%	Accuracy = 100.0%	Accuracy = 100.0%	Accuracy = 100.0%

Table 33: 12.0 in 5 Color Endmember LIGU Results

Configurations	Overall Accuracy	Endmembers				
		Blue	Yellow	Green	Red	White
Baseline	19.87%	0.00%	0.00%	0.00%	0.00%	99.35%
2013-1	20.00%	0.00%	0.00%	0.00%	0.00%	100.00%
2013-2	20.00%	0.00%	0.00%	0.00%	0.00%	100.00%
2013-3	49.88%	93.53%	0.00%	0.02%	55.88%	100.00%
2013-4	49.89%	93.53%	0.00%	0.02%	55.88%	100.00%

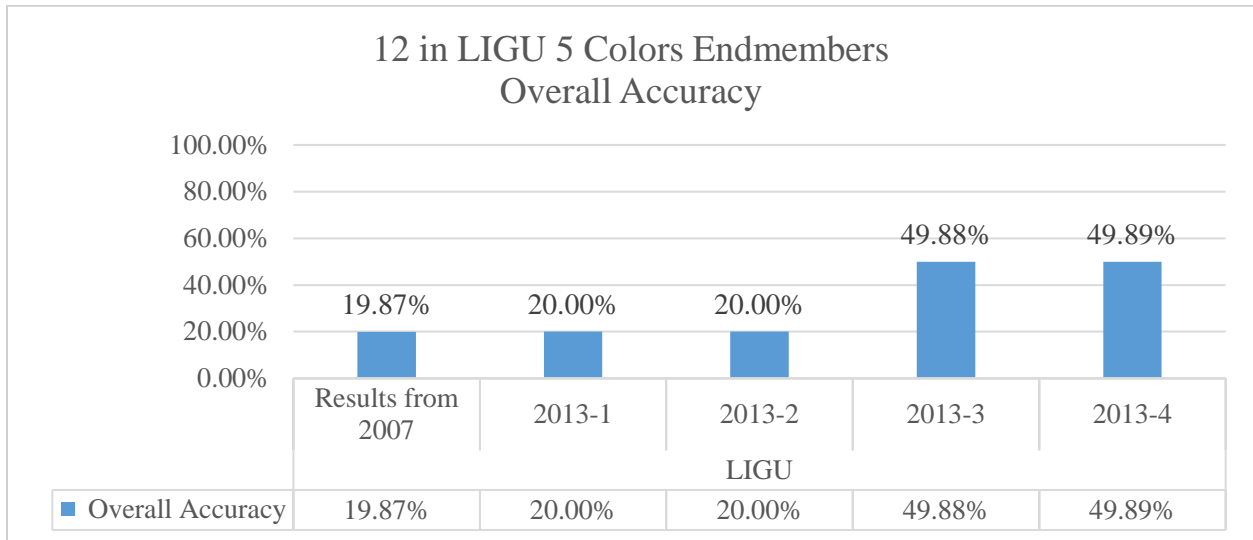


Figure 129: 12.0 in LIGU 5 Colors Overall accuracy graph

9.3.2 LIGU 12.0 in Image with 4 Colors Endmembers

This section will show results obtained from the 12.0 in image using LIGU algorithm with 4 endmembers that correspond to: Blue, Yellow, Green and Red regions from the 1.8" image. Next figure shows the endmembers used. Table 35 shows the obtained accuracy from LIGU with the 12.0 in image with 4 color endmembers. Visual representations are presented on Table 34 and graph comparing the obtained overall accuracy of each configuration is showed on figure 131.

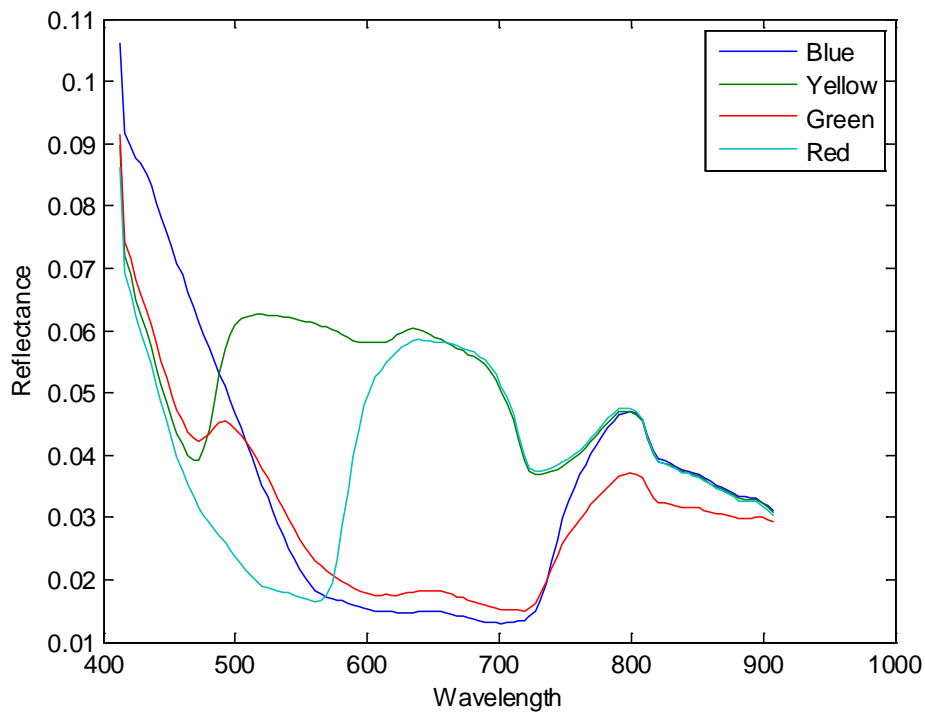


Figure 130: Endmembers used for 4 Colors processing

Table 34: LIGU 4 Color Endmembers Results

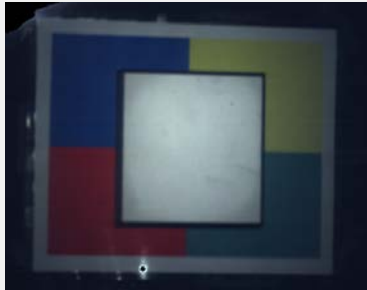


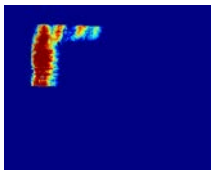
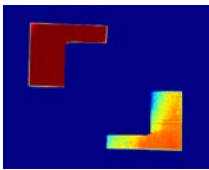
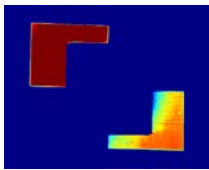
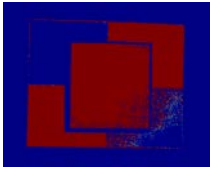
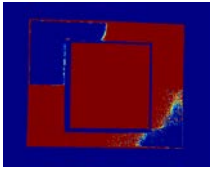
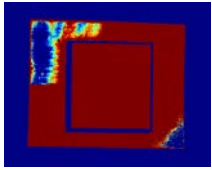
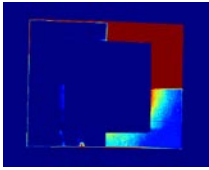
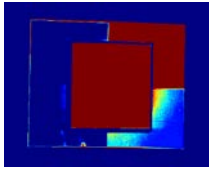





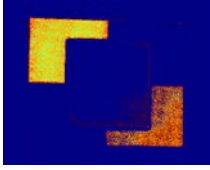
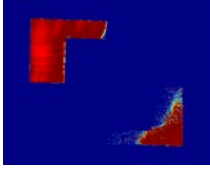
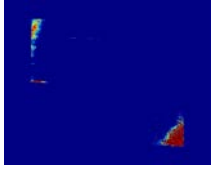
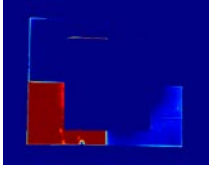
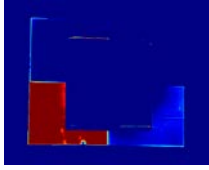
Real Image: 12.0 in					
Configurations					
Baseline	2013-1	2013-2	2013-3	2013-4	
Blue					
 Accuracy = 0.00%	 Accuracy = 0.00%	 Accuracy = 62.52%	 Accuracy = 100.00%	 Accuracy = 100.00%	
Yellow					
 Accuracy = 100.0%	 Accuracy = 100.0%	 Accuracy = 100.0%	 Accuracy = 100.0%	 Accuracy = 100.0%	
Green					
 Accuracy = 0.00%	 Accuracy = 0.00%	 Accuracy = 0.00%	 Accuracy = 0.00%	 Accuracy = 0.00%	
Red					
 Accuracy = 0.00%	 Accuracy = 0.00%	 Accuracy = 0.00%	 Accuracy = 99.75%	 Accuracy = 99.75%	

Table 35: 12.0 in 4 Color Endmember LIGU Results

Configurations	Overall Accuracy	Endmembers			
		Blue	Yellow	Green	Red
Baseline	25.00%	0.00%	100.00%	0.00%	0.00%
2013-1	25.00%	0.00%	100.00%	0.00%	0.00%
2013-2	40.63%	62.53%	100.00%	0.00%	0.00%
2013-3	74.94%	100.00%	100.00%	0.00%	99.75%
2013-4	74.94%	100.00%	100.00%	0.00%	99.75%

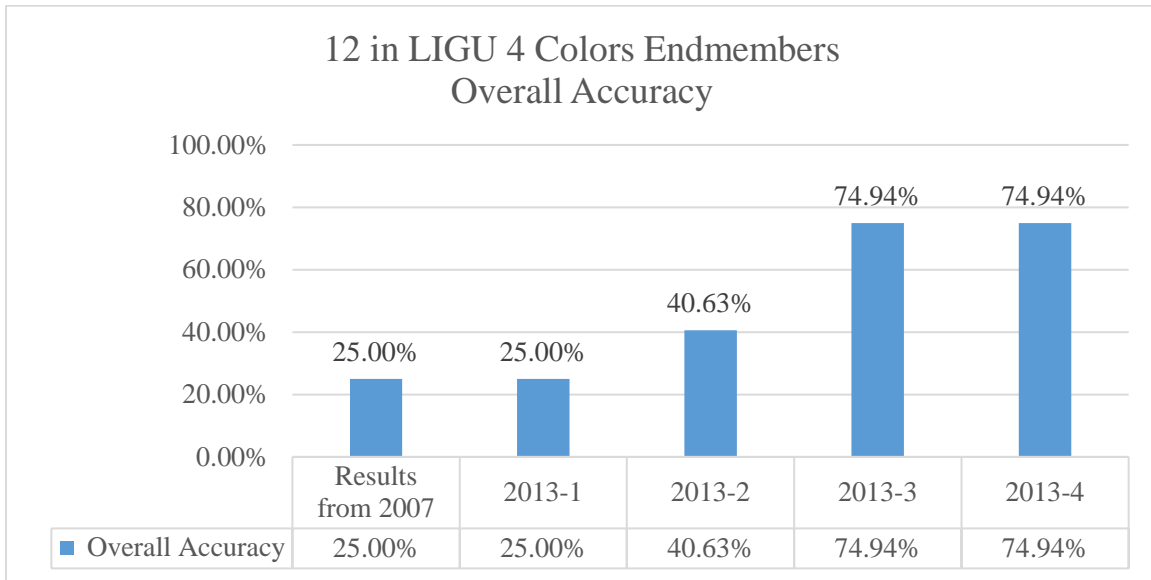


Figure 131: 12.0 in LIGU 4 Colors Overall accuracy graph

9.3.3 CIUB 12.0 in Image with 5 Colors Endmembers

This section shows obtained result from the 12.0 in image using CIUB algorithm. The same five endmembers representing the Blue, Yellow, Green, Red and White regions from the 1.8” hyperspectral image presented on section 9.3.1 were used as input to the algorithm. Each result will be compared visually on Table 37. Table 36 summarized the obtained results. figure 132 shows the obtained overall accuracy for each configuration used.

Table 36: 12.0 in 5 Color Endmember CIUB Results

Configurations	Overall Accuracy	Endmembers				
		Blue	Yellow	Green	Red	White
Baseline	21.18%	0.55%	0.00%	5.36%	0.00%	100.00%
2013-1	20.36%	0.00%	0.00%	1.78%	0.00%	100.00%
2013-2	20.64%	3.18%	0.00%	0.00%	0.00%	100.00%
2013-3	20.64%	3.18%	0.00%	0.00%	0.00%	100.00%
2013-4	26.20%	31.00%	0.00%	0.00%	0.00%	100.00%

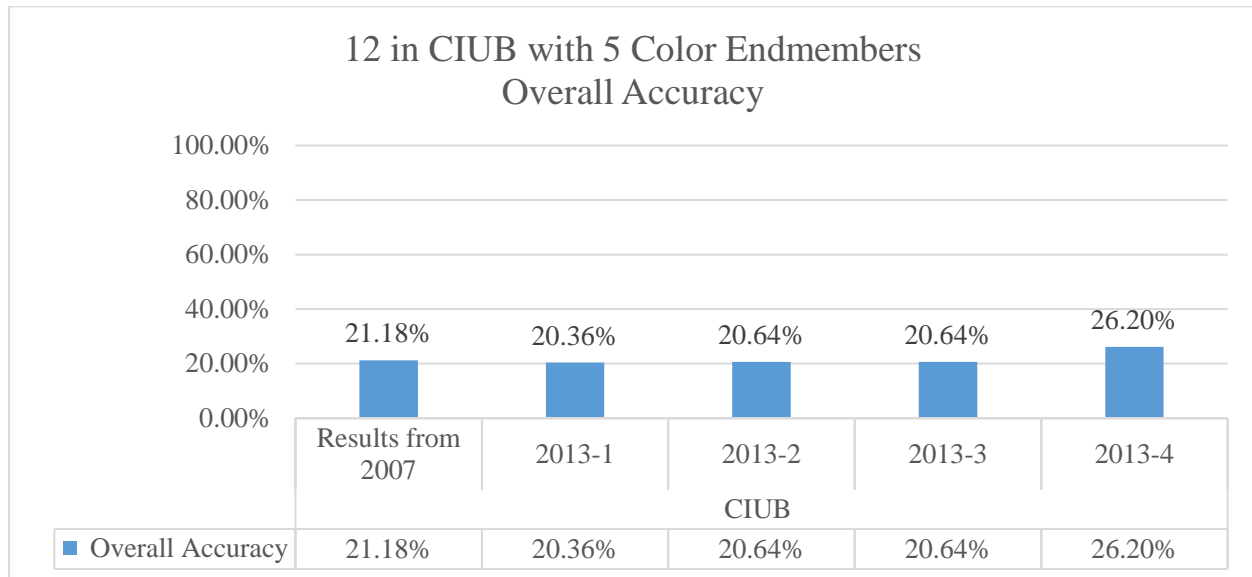



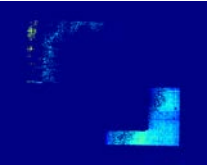
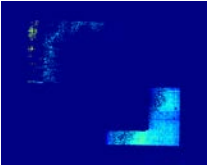
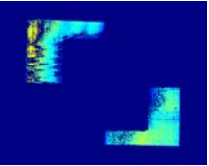





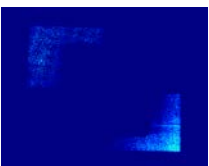
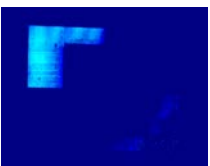



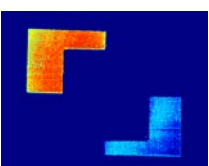
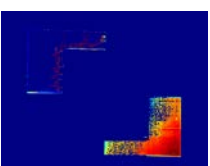
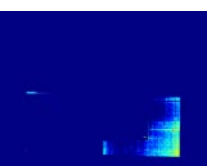
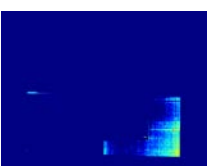
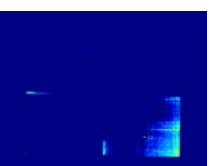
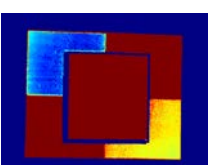
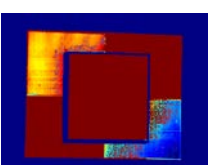
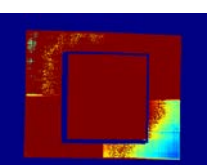
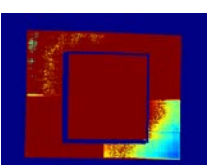
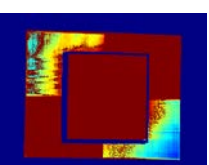


Figure 132: 12.0 in CIUB 5 Colors Overall accuracy graph

Table 37: CIUB 5 Color Endmembers Results

Real Image: 12.0 in				
	Configurations			
Baseline	2013-1	2013-2	2013-3	2013-4
Blue				
				
Accuracy = 0.55%	Accuracy = 0.00%	Accuracy = 3.18%	Accuracy = 3.18%	Accuracy = 31.00%
Yellow				
				
Accuracy = 0.00%	Accuracy = 0.00%	Accuracy = 0.00%	Accuracy = 0.00%	Accuracy = 0.00%
Green				
				
Accuracy = 5.36%	Accuracy = 1.78%	Accuracy = 0.00%	Accuracy = 0.00%	Accuracy = 0.00%
Red				
				
Accuracy = 0.00%	Accuracy = 0.00%	Accuracy = 0.00%	Accuracy = 55.86%	Accuracy = 55.88%
White				
				
Accuracy = 100.0%	Accuracy = 100.0%	Accuracy = 100.0%	Accuracy = 100.0%	Accuracy = 100.0%

9.3.4 CIUB 12.0 in Image with 4 Colors Endmembers

This section shows obtained result from the 12.0 in image using CIUB algorithm with 4 endmembers that corresponds to the Blue, Yellow, Green and Red regions from the 1.8 hyperspectral image previously showed on section 9.3.2. Each result will be compared visually on Table 39. Table 38 summarized the obtained results. Figure 133 show the obtained overall accuracy for each configuration used.

Table 38: 12.0 in 4 Color Endmember CIUB Results

Configuration	Overall Accuracy	Endmembers			
		Blue	Yellow	Green	Red
Baseline	25.51%	2.05%	100.00%	0.00%	0.00%
2013-1	25.04%	0.16%	100.00%	0.00%	0.00%
2013-2	35.75%	43.00%	100.00%	0.00%	0.00%
2013-3	36.45%	45.82%	100.00%	0.00%	0.00%
2013-4	36.44%	45.75%	100.00%	0.00%	0.00%

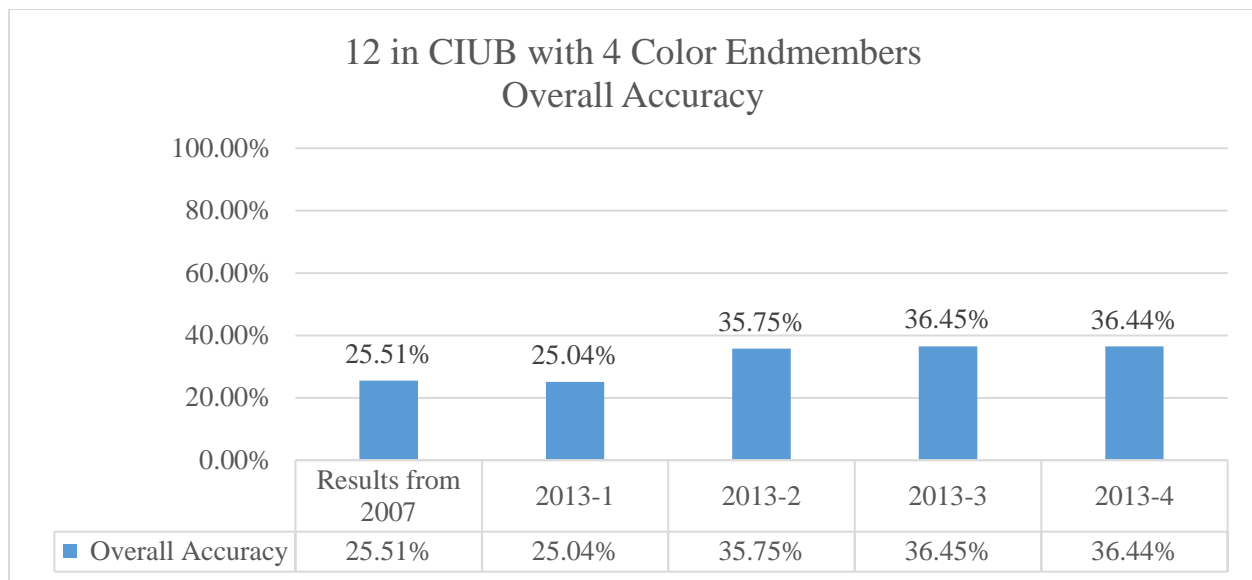
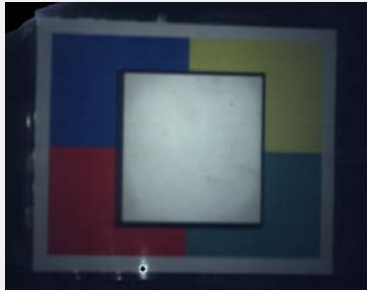


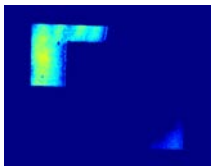
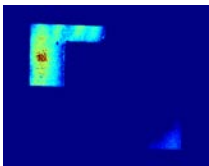
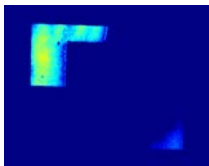
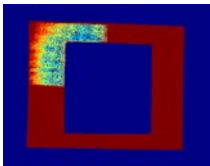
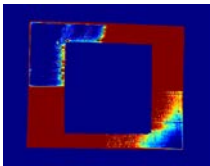
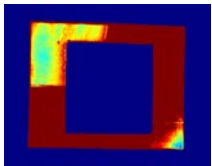
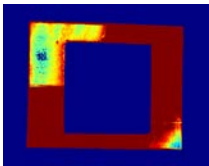
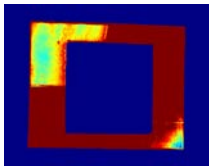
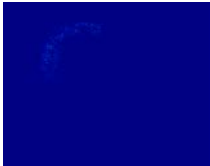




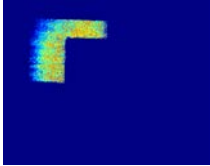
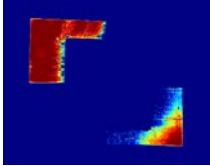
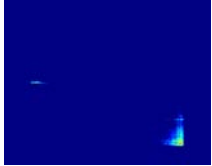
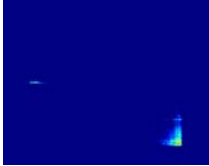
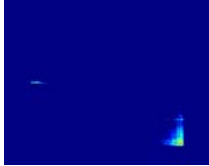


Figure 133: 12.0 in CIUB 4 Colors Overall accuracy graph

Table 39: CIUB 5 Color Endmembers Results

Real Image: 12.0 in					
Configurations					
Baseline	2013-1	2013-2	2013-3	2013-4	
Blue					
					
Accuracy = 2.05%	Accuracy = 0%	Accuracy = 43.00%	Accuracy = 45.82%	Accuracy = 45.75%	
Yellow					
					
Accuracy = 100.00%	Accuracy = 100.00%	Accuracy = 100.00%	Accuracy = 100.00%	Accuracy = 100.00%	
Green					
					
Accuracy = 0.00%	Accuracy = 0.00%	Accuracy = 0.00%	Accuracy = 0.00%	Accuracy = 0.00%	
Red					
					
Accuracy = 0.00%	Accuracy = 0.00%	Accuracy = 0.00%	Accuracy = 0.00%	Accuracy = 0.00%	

9.3.5 LIGU 12.0 in 0.5 g TiO₂ Image with 4 Colors Endmembers

This section presents the obtained result from underwater unmixing algorithms using the 12 in 0.5 g of TiO₂ image using LIGU. Titanium Dioxide images were processed using Custom Bottom and Custom Unmixing Range functionalities with 4 color endmembers. This configuration was selected because is the one that was demonstrated to produce better overall accuracy. Table 40 summarizes the obtained accuracies and the graph of each individual accuracy is presented on figure 134. Table 41 shows the graphical representation of these results.

Table 40: 12.0 in 0.5 TiO₂ 4 Colors Endmembers LIGU Results

Configuration	Overall Accuracy	Endmembers			
		Blue	Yellow	Green	Red
Baseline	26.25%	0.00%	59.14%	0.00%	45.85%
2013-3	43.00%	0.03%	82.25%	0.00%	89.70%

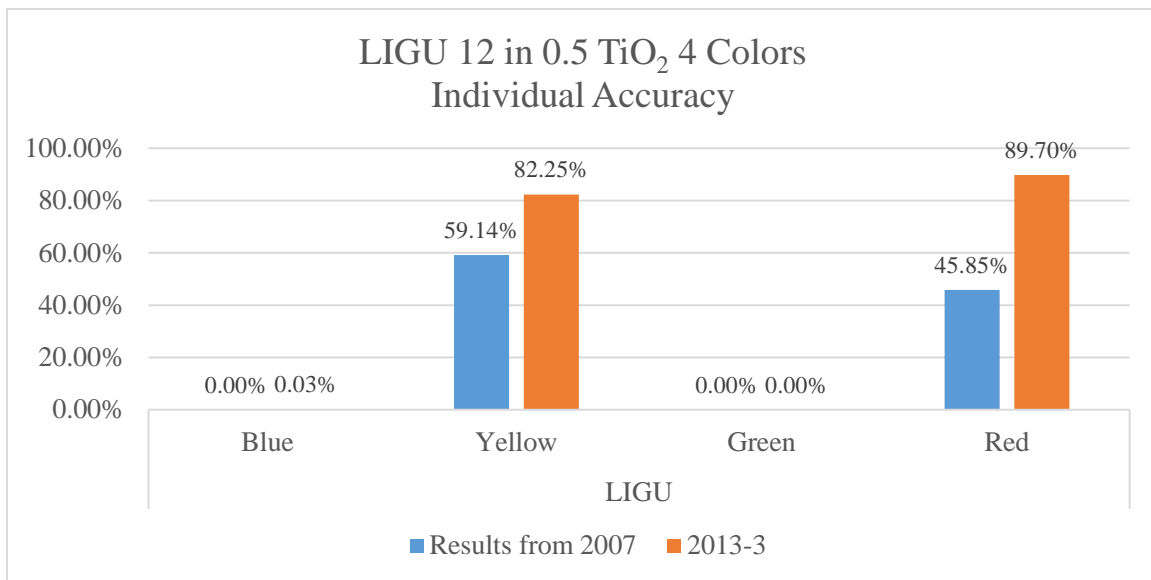


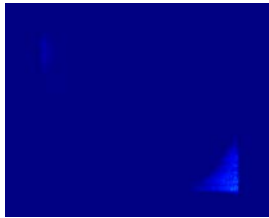
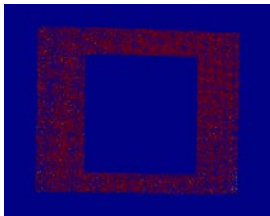
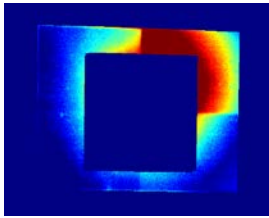


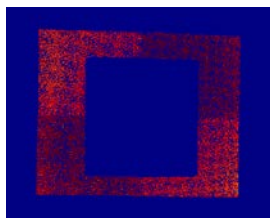
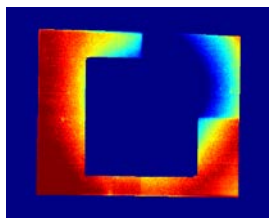


Figure 134: 12.0 in 0.5 TiO₂ LIGU 4 Colors Individual Accuracy

Table 41: LIGU 12.0 in 0.5 g TiO₂ Image with 4 Colors Endmembers

Real Image: 12.0 in 0.5 g TiO ₂		
Configurations		
Baseline	2013-3	
Blue		
 Accuracy = 0.00%	 Accuracy = 0.00%	
Yellow		
 Accuracy = 59.14%	 Accuracy = 82.25%	
Green		
 Accuracy = 0.00%	 Accuracy = 0.00%	
Red		
 Accuracy = 45.85%	 Accuracy = 89.70%	

9.3.6 CIUB 12.0 in 0.5 g TiO₂ Image with 4 Colors Endmembers

This section presents the obtained result from underwater unmixing algorithms using the 12 in with 0.5 g of TiO₂ image processed on CIUB. It is important to mention that a single configuration was used. Titanium Dioxide images were processed using Custom Bottom and Custom Unmixing Range functionalities with 4 color endmembers. Again, this configuration was selected because is the one that produced better overall accuracy in the previously presented results. Table 42 summarizes the obtained accuracies and the graph of each individual accuracy is presented on figure 134. Table 43 shows the graphical representation of these results.

Table 42: 12.0 in 0.5 TiO₂ 4 Colors Endmembers CIUB Results

Configuration	Overall Accuracy	Endmembers			
		Blue	Yellow	Green	Red
Baseline	25.00%	0.00%	100.00%	0.00%	0.00%
2013-3	27.22%	0.00%	100.00%	0.00%	8.88%

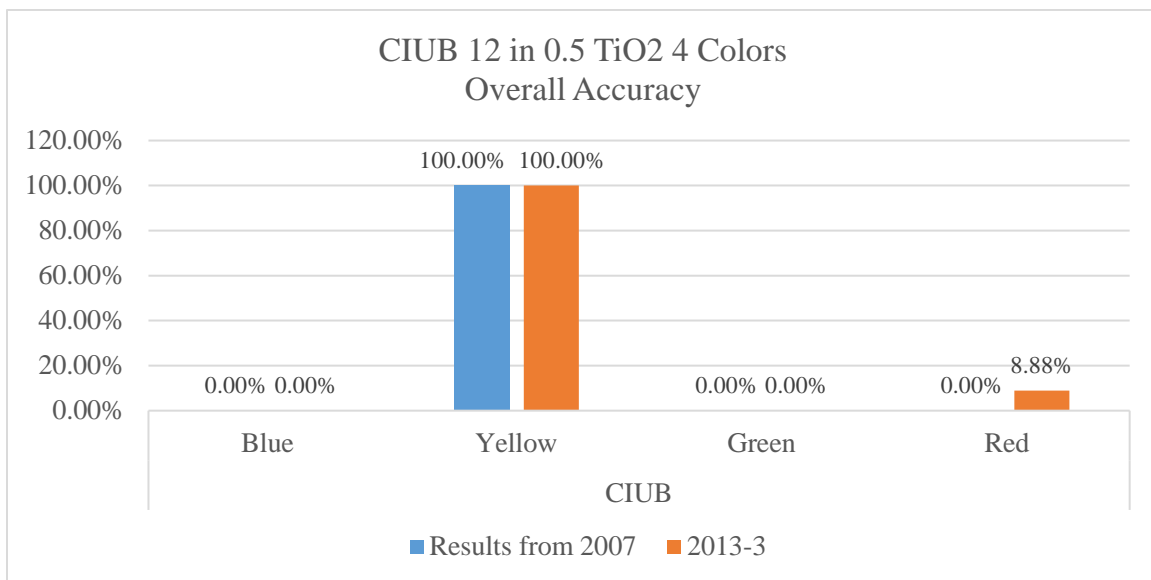


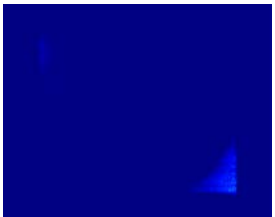
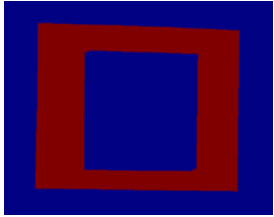
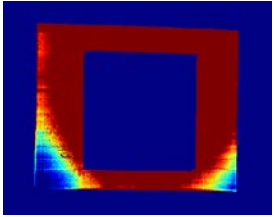



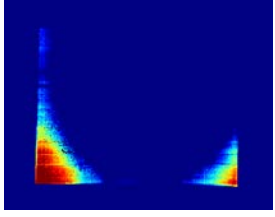


Figure 135: 12.0 in 0.5 TiO₂ CIUB 4 Colors Individual Accuracy

Table 43: CIUB 12.0 in 0.5 g TiO₂ Image with 4 Colors Endmembers

Real Image: 12.0 in TiO ₂	
Configurations	
Baseline	2013-3
Blue	
 Accuracy = 0.00%	 Accuracy = 0.00%
Yellow	
 Accuracy = 100.00%	 Accuracy = 100.00%
Green	
 Accuracy = 0.00%	 Accuracy = 0.00%
Red	
 Accuracy = 0.00%	 Accuracy = 8.88%

9.4 Extended Results – Regularization Algorithm

Results are going to be compare and analyzed based on the classification accuracy over the selected testing regions calculated in the following way:



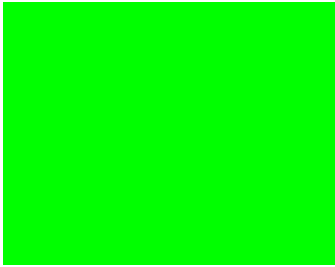
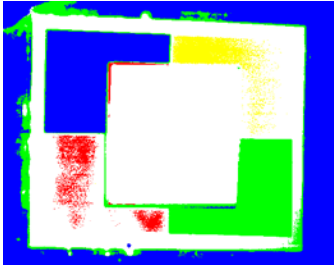

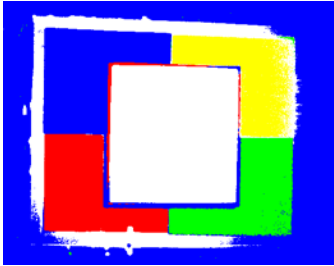
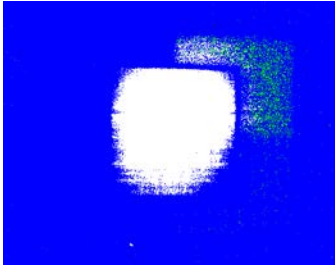
$$Accuracy = \frac{Pixel\ Correctly\ Classified}{Total\ of\ pixel\ on\ the\ image} \times 100 \quad (75)$$

Finally, for visualization, each endmember was given the color that it represents on the classification maps. For example, the red endmember is colored red on the classification maps showed as results.

9.4.1 Baseline Results

To create baseline results, images were classified with the proposed classification algorithms before being process by the Regularization algorithm. The following images were used to produce baseline results: 0", 12.0 in, 12.0 in 0.5 g TiO₂, 12.0 in 1.0g TiO₂, 12.0 in 1.5g TiO₂ and 12.0 in 2.0g TiO₂ (Refer to section 3.1.4 for image information). Since only the 12.0 in and 12.0 in 0.5 g TiO₂ were used to test the Regularization algorithms these are the result that will be presented in the following Table. For performance matrices refer to appendix sections 9.5.1 for the 12.0 in image and 9.5.2 for the 12.0 in 0.5 g TiO₂ image.

Table 44: Regularization Baseline Results Classification Maps

Real Images:		
	Classification Map	
Classification Algorithm	12.0 in	12.0 in 0.5 g TiO ₂
Minimum Euclidean Distance	<div>Euclidean Distance</div>  <div>Accuracy = 17.72%</div>	<div>Euclidean Distance</div>  <div>Accuracy = 17.61%</div>
	<div>Spectral Angle</div>  <div>Accuracy = 75.39%</div>	<div>Spectral Angle</div>  <div>Accuracy = 50.24%</div>
Maximum Unmixing Value	<div>Unmixing</div>  <div>Accuracy = 98.84%</div>	<div>Unmixing</div>  <div>Accuracy = 47.61%</div>

The following graphs summarized the obtained classification accuracy before regularization:

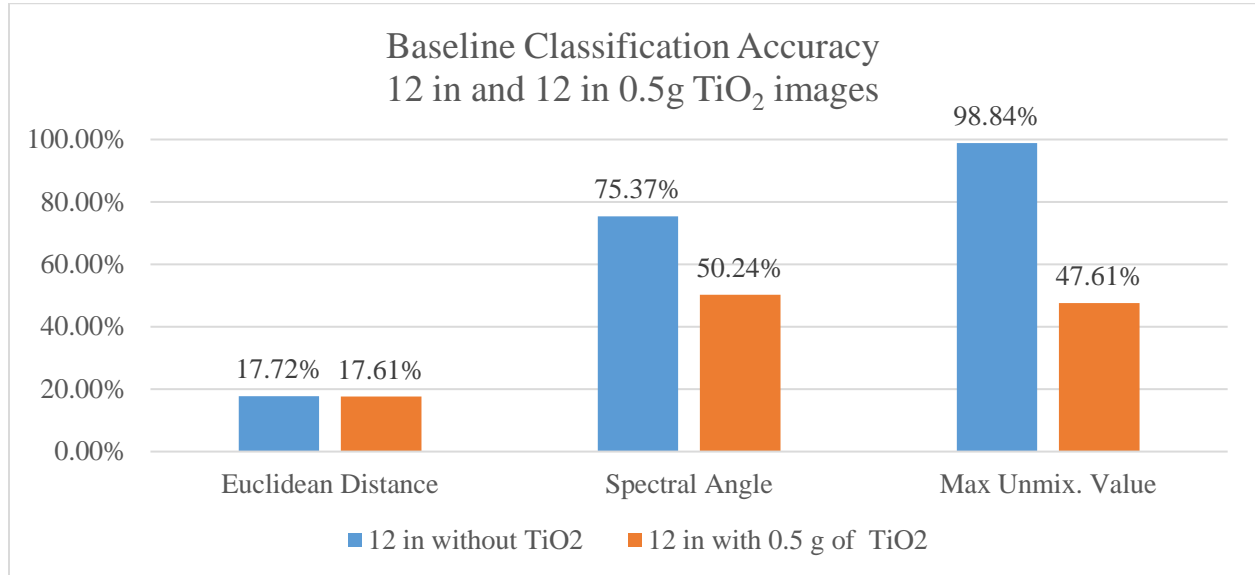


Figure 136: Baseline Result - Obtained Accuracy before Regularization

9.4.2 Numerical Approximation Classifications Results after Regularization

Numerical Approximations (NA) is one of the algorithm implemented to calculate the point of maximum curvature. It uses the method of forward difference to calculate the derivative of a concrete value vector. Refer to section 3.5 for the theoretical background. The following two sections will show the obtained result from 12.0 in and 12.0 in 0.5 g TiO₂ along with its comparative graphs with baseline results. Performance matrices are showed on appendix sections on section 9.5.3 and 9.5.4.

9.4.2.1 12.0 in Classification Results after Regularization

As mentioned before there are two methods of selecting the optimum γ : Gamma of Minimum Error and Minimum Gama their result will be compared side by side throughout this section. Results obtained using a gamma resolution of 0.1 will be showed on figures 137 and Table 45. Result for gamma resolution of 0.01 will be showed on figures 138 and on Table 46.

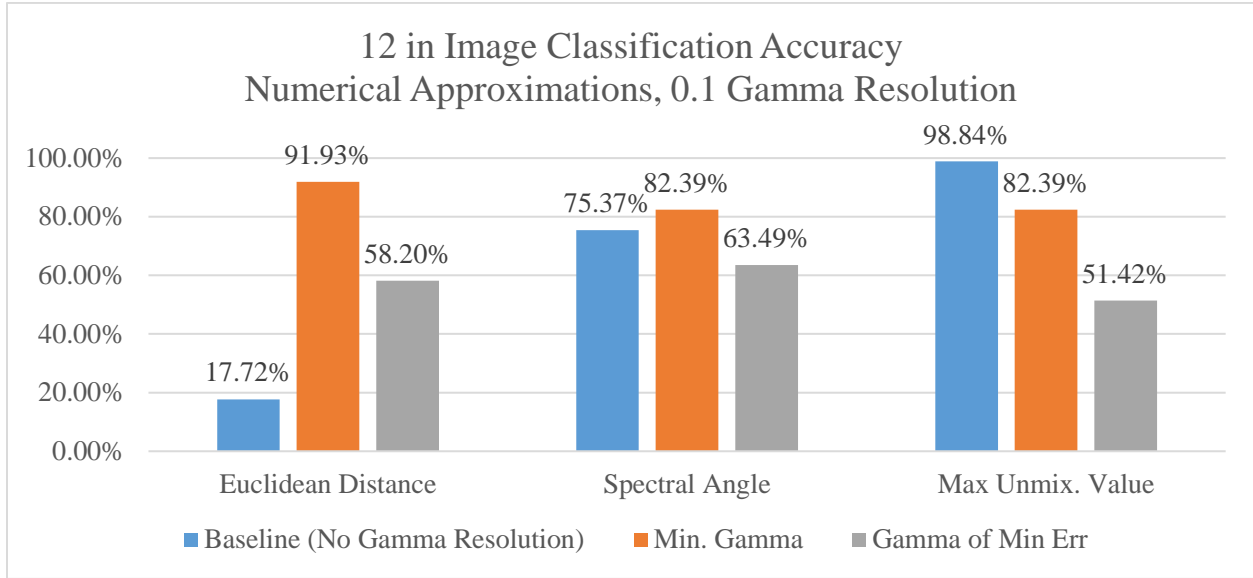


Figure 137: 12.0 in Classification Accuracy after Regularization: NA, Gamma Res: 0.1

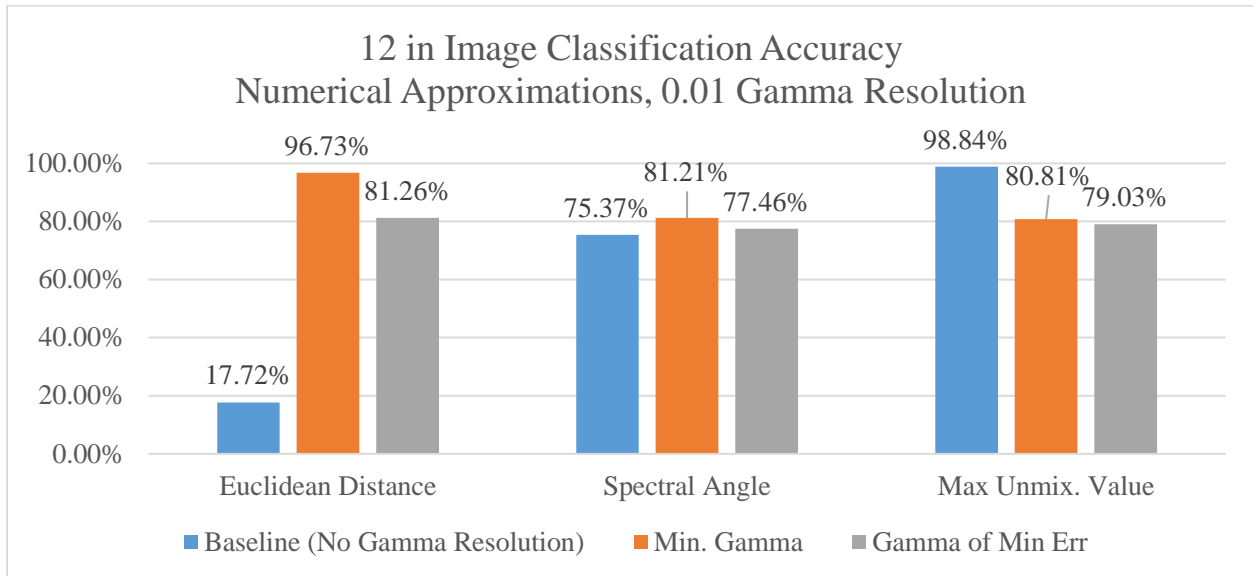


Figure 138: 12.0 in Classification Accuracy after Regularization: NA, Gamma Res: 0.01

Table 45: 12.0 in Classification Maps after Regularization: NA, Gamma Res: 0.1



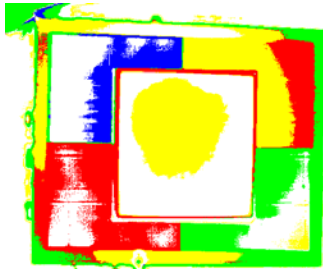
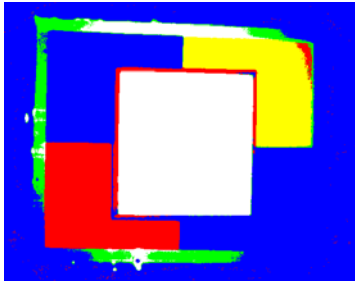
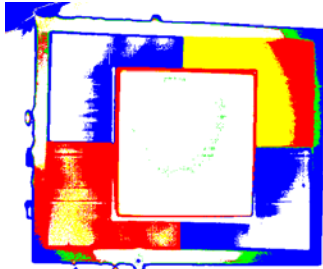
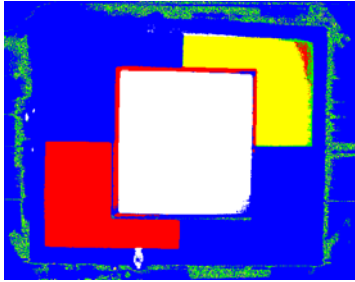
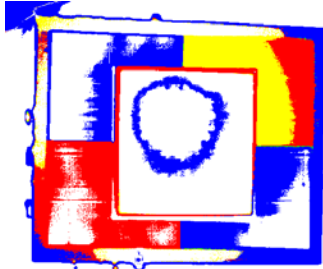

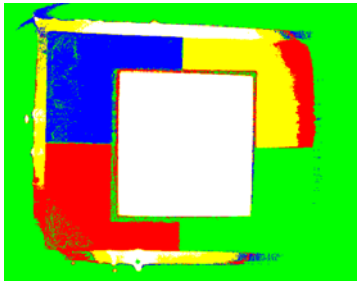
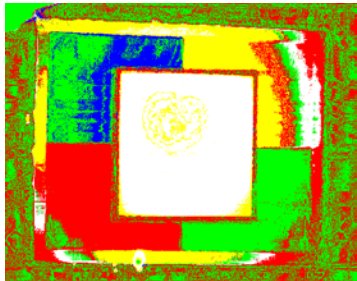
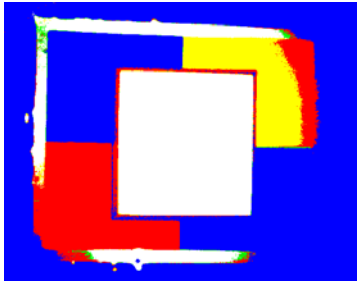
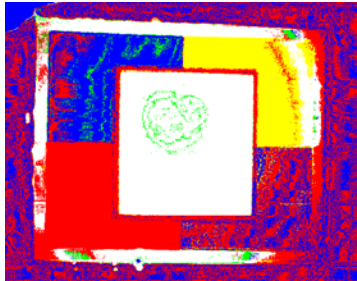
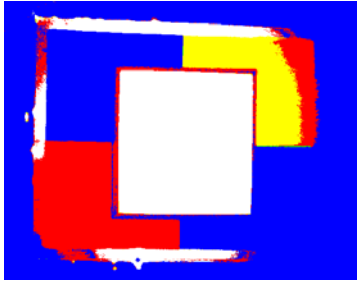
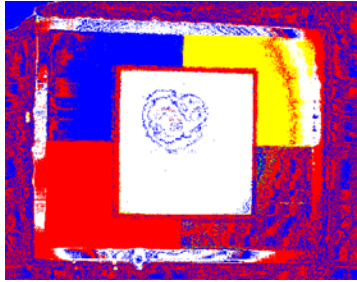
<p>Real Image: 12.0 in</p>		
<p>Classification Algorithm</p>	<p>Gamma Resolution:</p>	<p>0.1</p>
	<p>Classification Maps</p>	
	<p>Minimum Gamma</p>	<p>Gamma of Minimum Error</p>
<p>Minimum Euclidean Distance</p>	 <p>Accuracy = 91.93%</p>	 <p>Accuracy = 58.20%</p>
<p>Minimum Spectral Angle</p>	 <p>Accuracy = 82.39%</p>	 <p>Accuracy = 63.49%</p>
<p>Maximum Unmixing Value</p>	 <p>Accuracy = 82.39%</p>	 <p>Accuracy = 52.42%</p>

Table 46: 12.0 in Classification Maps after Regularization: NA, Gamma Res: 0.01

<p>Real Image: 12.0 in</p>		
<p>Classification Algorithm</p>	<p>Gamma Resolution</p>	<p>0.01</p>
	<p>Classification Maps</p>	
	<p>Minimum Gamma</p>	<p>Gamma of Minimum Error</p>
<p>Minimum Euclidean Distance</p>	 <p>Accuracy = 96.73%</p>	 <p>Accuracy = 81.26%</p>
<p>Minimum Spectral Angle</p>	 <p>Accuracy = 81.21%</p>	 <p>Accuracy = 77.46%</p>
<p>Maximum Unmixing Value</p>	 <p>Accuracy = 80.81%</p>	 <p>Accuracy = 79.03%</p>

9.4.2.2 12.0 in 0.5 g TiO₂ Classification Results after Regularization

The following graphs summarize the obtained classification accuracy after Regularization from the 12.0 in 0.5 g TiO₂ image using Numerical Approximation and Gamma Resolution of 0.1 and 0.01. Results obtained using a gamma resolution of 0.1 will be showed on figure 139 and Table 47. Result for gamma resolution of 0.01 will be showed on figure 140 and on Table 48.

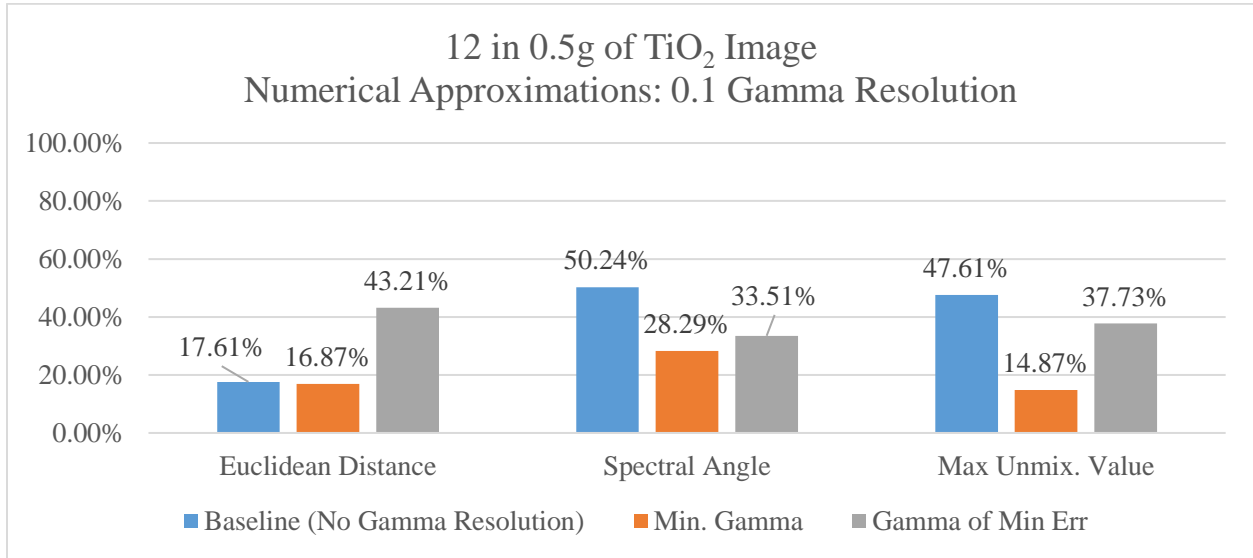


Figure 139: 12.0 in TiO₂ Classification Accuracy after Regularization: NA, Gamma Res: 0.1

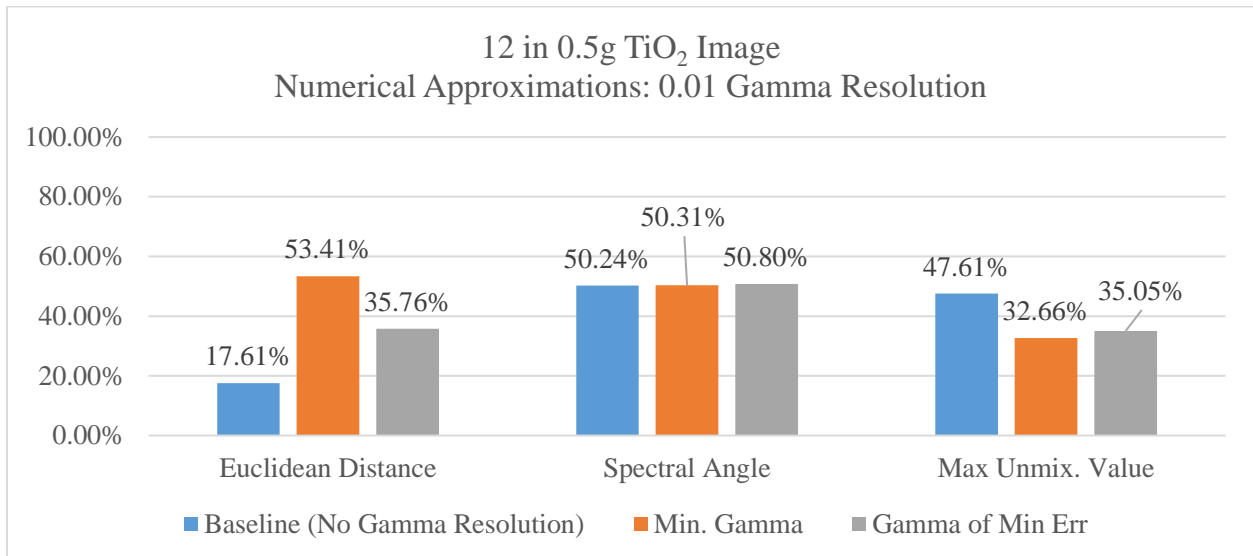


Figure 140: 12.0 in TiO₂ Classification Accuracy after Regularization: NA, Gamma Res: 0.01

Table 47: 12.0 in TiO₂ Classification Map after Regularization: NA, Gamma Res: 0.1


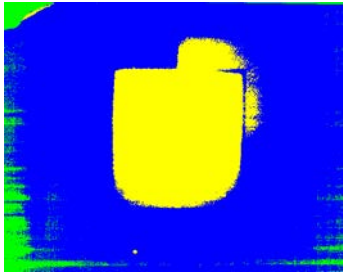
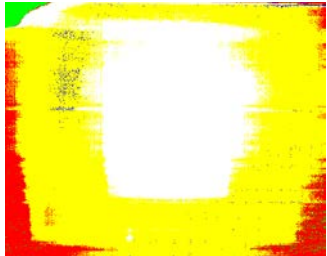
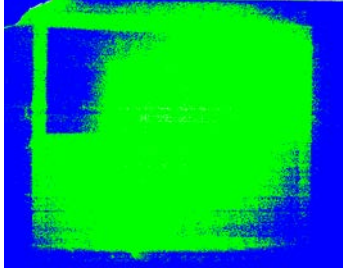
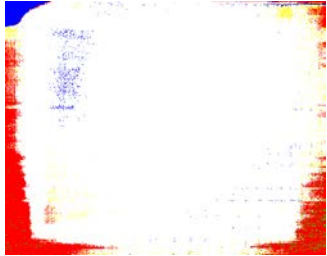



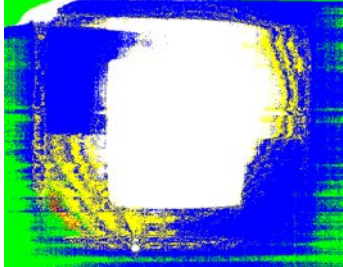
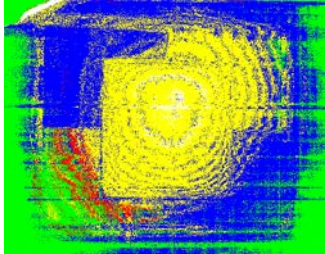
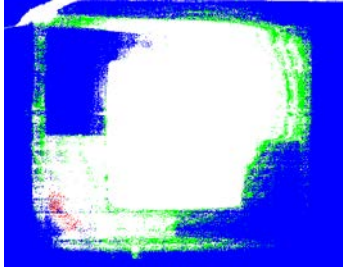
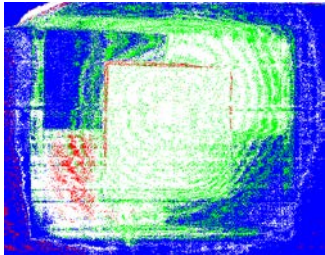
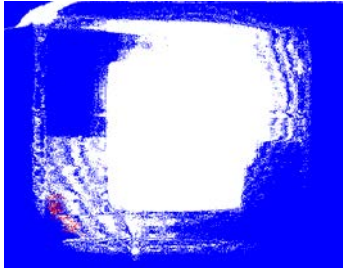
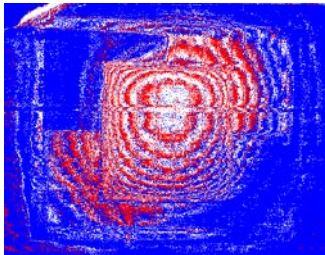
Real Image: 12.0 in TiO ₂		
Classification Algorithm	Gamma Resolution	0.1
	Classification Maps	
	Minimum Gamma	Gamma of Minimum Error
Minimum Euclidean Distance	 Accuracy = 16.87%	 Accuracy = 43.21%
Minimum Spectral Angle	 Accuracy = 28.29%	 Accuracy = 33.51%
Maximum Unmixing Value	 Accuracy = 17.87%	 Accuracy = 37.73%

Table 48: 12.0 in TiO₂ Classification Maps after Regularization: NA, Gamma Res: 0.01

Real Image: 12.0 in TiO ₂		
Classification Algorithm	Gamma Resolution:	0.01
	Classification Maps	
	Minimum Gamma	Gamma of Minimum Error
Minimum Euclidean Distance	 Accuracy = 53.41%	 Accuracy = 35.76%
Minimum Spectral Angle	 Accuracy = 50.31%	 Accuracy = 50.80%
Maximum Unmixing Value	 Accuracy = 32.66%	 Accuracy = 35.05%

9.4.3 Derived Equations Classification Results after Regularization

Derived Equations (DE) is one of the implemented algorithms to calculate the point of maximum curvature. It uses mathematically derived equations to calculate the derivative of the error curves. These equations are presented on section 3.5. The following two sections will show the obtained results from 12.0 in and 12.0 in 0.5 g TiO₂. Performance matrices are presented on Appendix section 9.5.5 for 12.0 in image and in 9.5.6 for 12.0 in 0.5 g TiO₂ image.

9.4.3.1 12.0 in Classification Results after Regularization

Results obtained using a gamma resolution of 0.1 will be showed Table 49 and in Table 50 for a gamma resolution of 0.01. Next graphs summarize the obtained classification accuracy after Regularization from the 12.0 in 0.5 g of TiO₂ image processed using Derived Equations with Gamma Resolution of 0.1 on figure 141 and of 0.01 on figure 142.

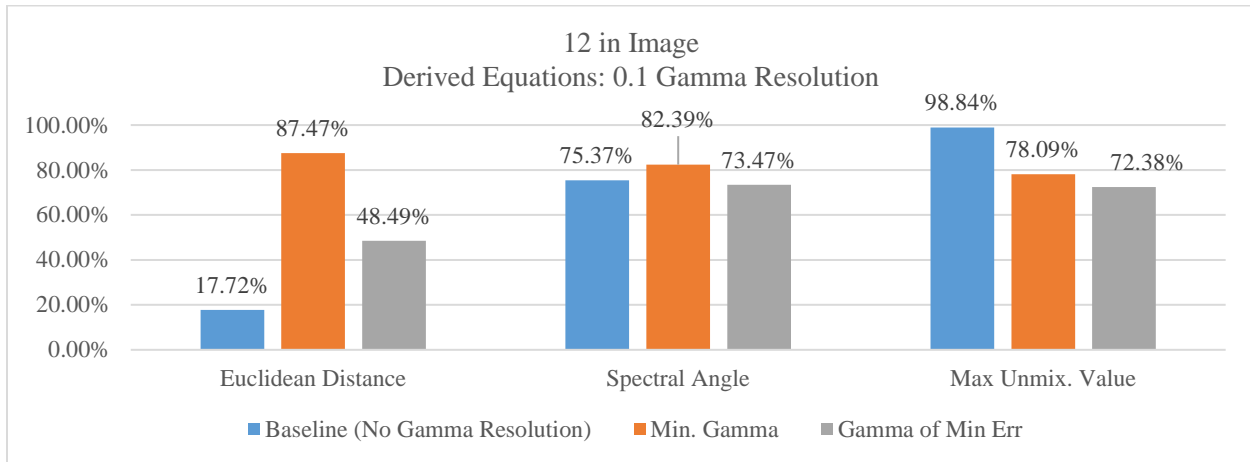


Figure 141: 12.0 in Classification Accuracy after Regularization: DE, Gamma Res: 0.1

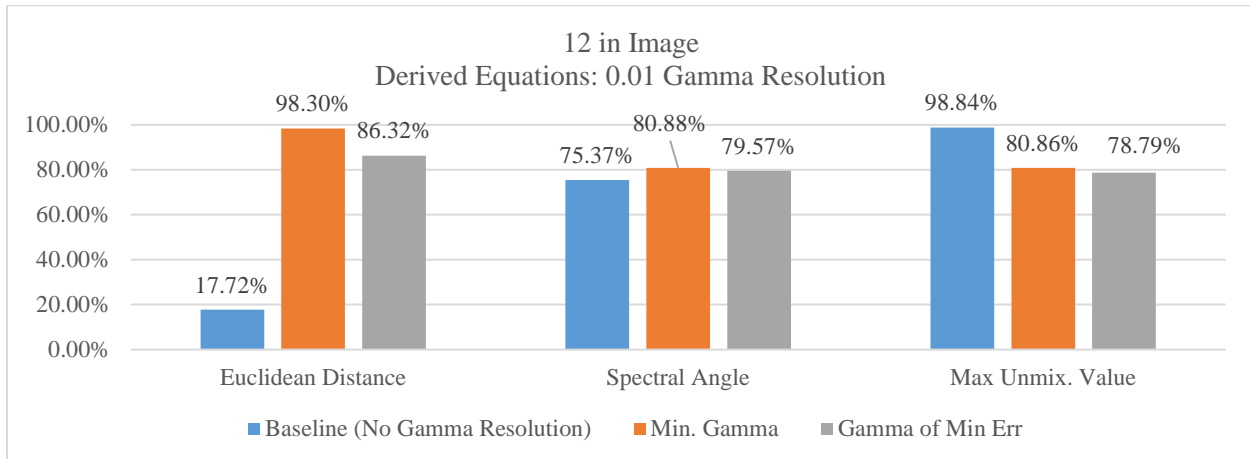


Figure 142: 12.0 in Classification Accuracy after Regularization: DE, Gamma Res: 0.01

Table 49: 12.0 in Classification Maps after Regularization: DE, Gamma Res: 0.1


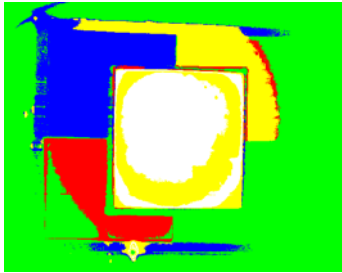
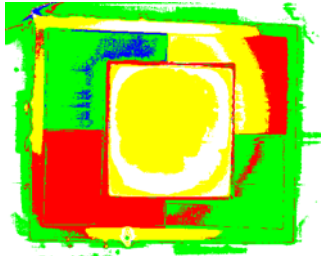
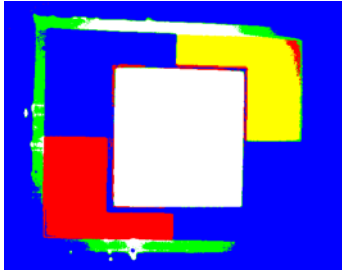
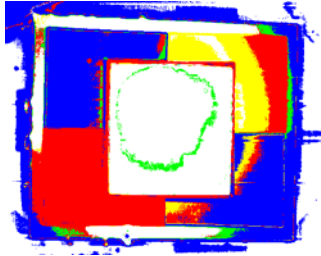
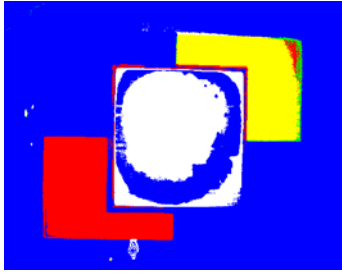
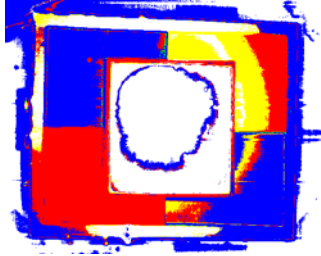

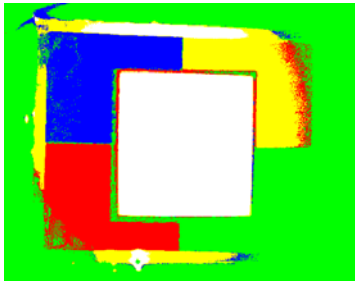
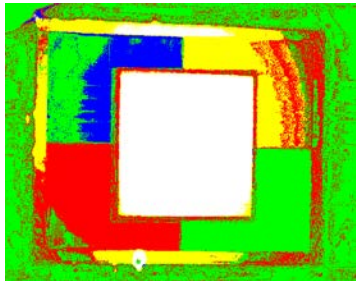
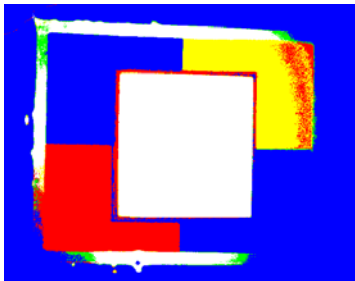
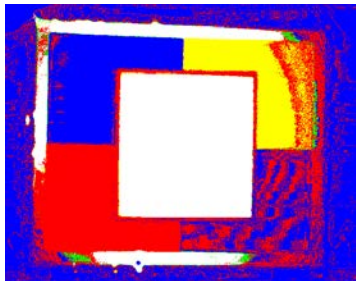
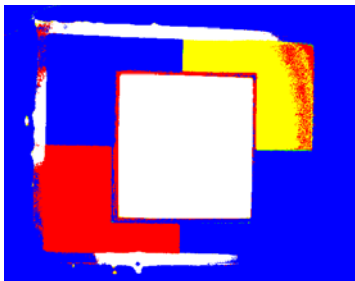
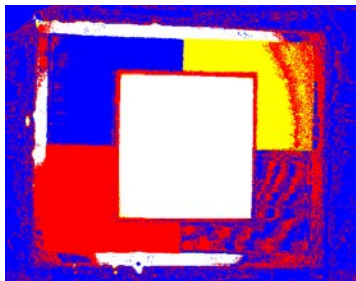
<p>Real Image: 12.0 in</p>		
<p>Classification Algorithm</p>	<p>Gamma Resolution</p>	<p>0.1</p>
	<p>Classification Maps</p>	
	<p>Minimum Gamma</p>	<p>Gamma of Minimum Error</p>
<p>Minimum Euclidean Distance</p>	 <p>Accuracy = 87.47%</p>	 <p>Accuracy = 48.49%</p>
<p>Minimum Spectral Angle</p>	 <p>Accuracy = 82.39%</p>	 <p>Accuracy = 73.47%</p>
<p>Maximum Unmixing Value</p>	 <p>Accuracy = 78.09%</p>	 <p>Accuracy = 72.38%</p>

Table 50: 12.0 in Classification Maps after Regularization: DE, Gamma Res: 0.01

Real Image		
Classification Algorithm	Gamma Resolution	0.01
	Classification Maps	
	Minimum Gamma	Gamma of Minimum Error
Minimum Euclidean Distance	 Accuracy = 98.30%	 Accuracy = 86.32%
Minimum Spectral Angle	 Accuracy = 80.88%	 Accuracy = 79.57%
Maximum Unmixing Value	 Accuracy = 80.86%	 Accuracy = 78.79%

9.4.3.2 12.0 in 0.5 g TiO₂ Classification Result after Regularization

The following graphs summarize the obtained classification accuracy after Regularization from the 12.0 in 0.5 g TiO₂ image using Derived Approximation and Gamma Resolution of 0.1 and 0.01 on figure 143 and 144 respectively. Results obtained using a gamma resolution of 0.1 will be showed on Table 51 and using a gamma resolution of 0.01 will be showed on Table 52.

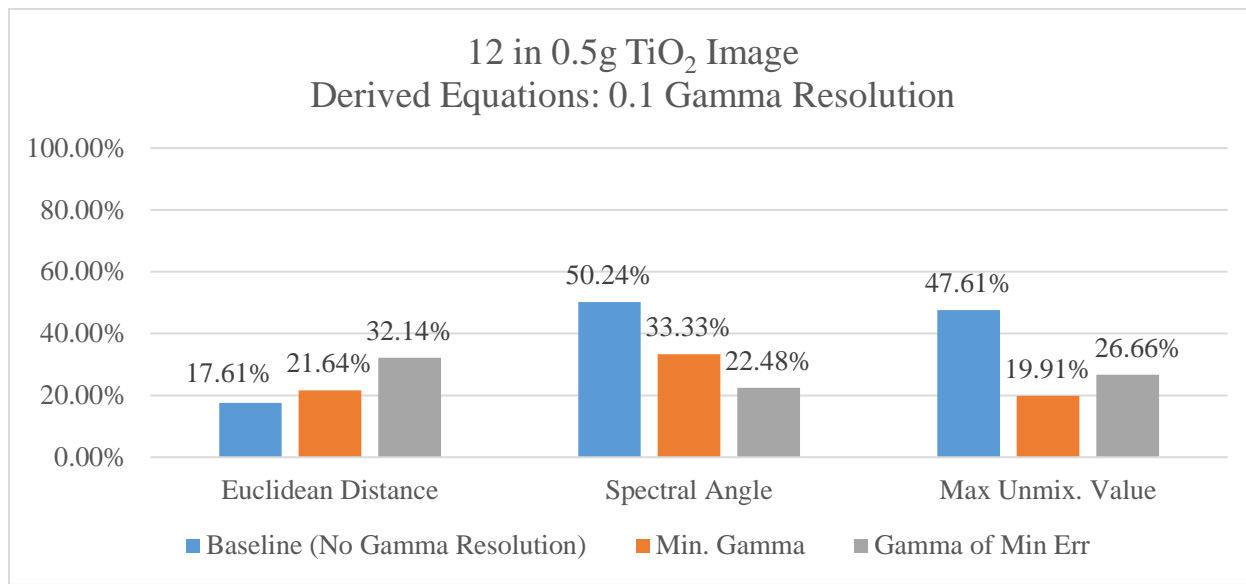


Figure 143: 12.0 in TiO₂ Classification Accuracy after Regularization: DE, Gamma Res: 0.1

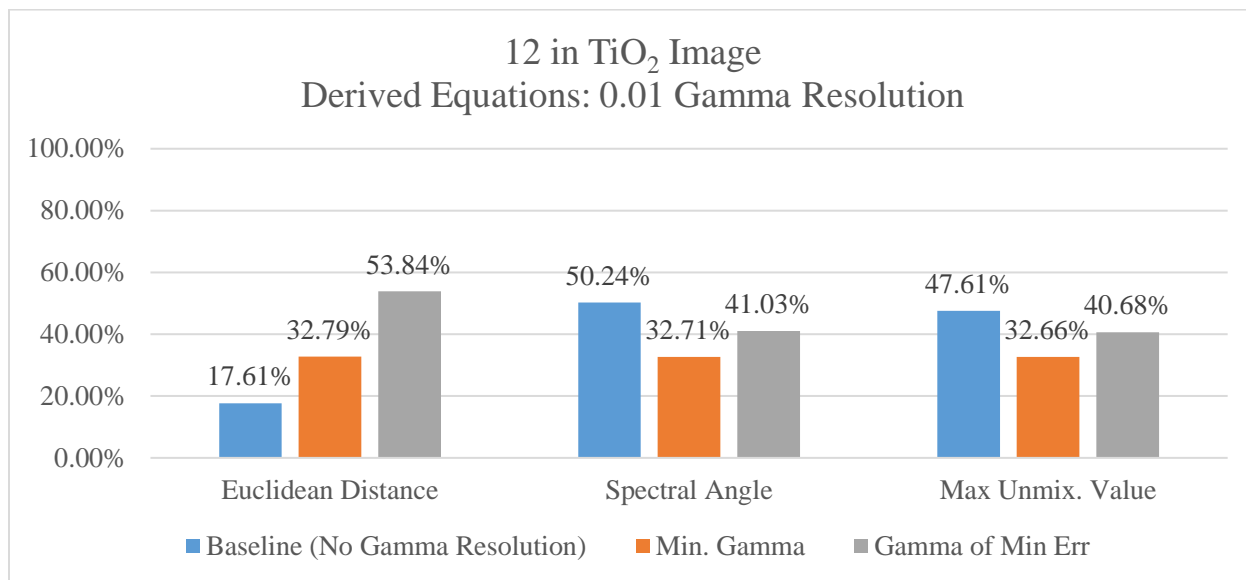


Figure 144: 12.0 in TiO₂ Classification Accuracy after Regularization: DE, Gamma Res: 0.01

Table 51: 12.0 in TiO₂ Classification Maps after Regularization: DE, Gamma Res: 0.1


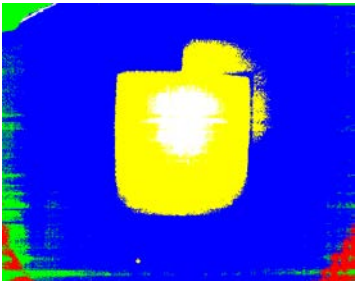
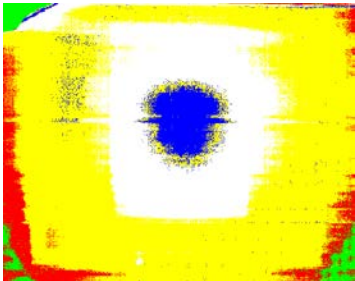
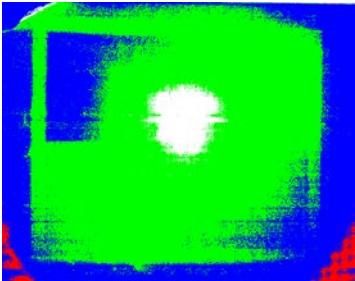

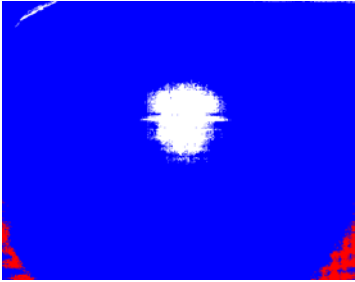
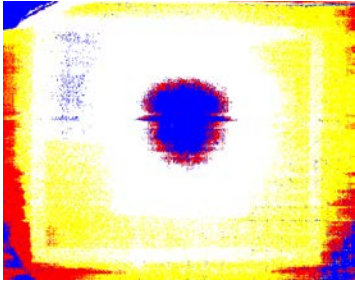

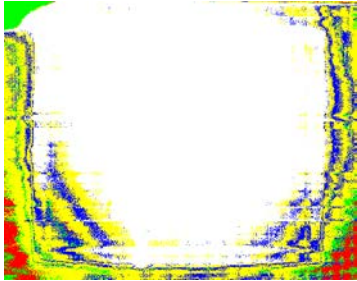
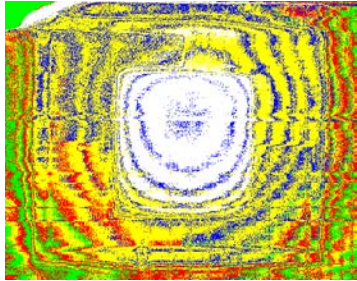
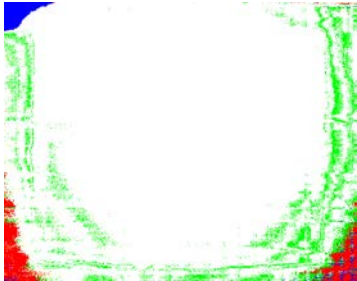
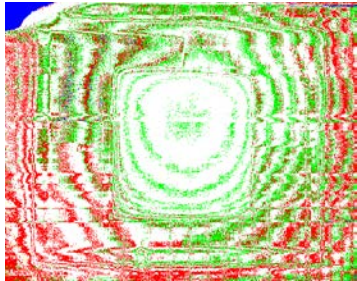
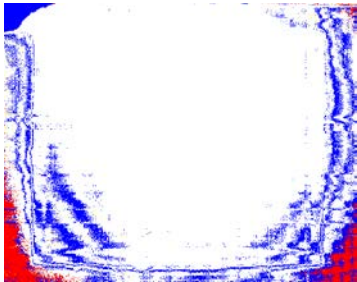
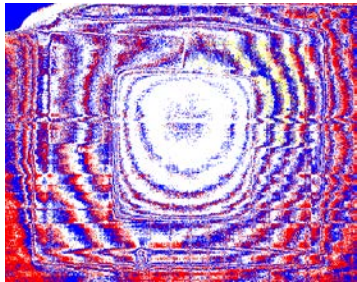
Real Image		
Classification Algorithm	Gamma Resolution	0.1
	Classification Maps	
	Minimum Gamma	Gamma of Minimum Error
Minimum Euclidean Distance	 Accuracy = 21.64%	 Accuracy = 32.14%
Minimum Spectral Angle	 Accuracy = 33.33%	 Accuracy = 22.48%
Maximum Unmixing Value	 Accuracy = 19.91%	 Accuracy = 26.66%

Table 52: 12.0 in TiO₂ Classification Maps after Regularization: DE, Gamma Res: 0.01

Real Image		
Classification Algorithm	Gamma Resolution	= 0.01
	Classification Maps	
	Minimum Gamma	Gamma of Minimum Error
Minimum Euclidean Distance	 Accuracy = 32.79%	 Accuracy = 53.84%
Minimum Spectral Angle	 Accuracy = 32.71%	 Accuracy = 41.03%
Maximum Unmixing Value	 Accuracy = 31.66%	 Accuracy = 40.68%


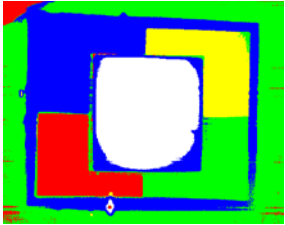
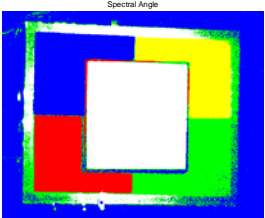
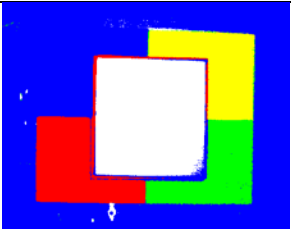
9.4.4 Example with Reduced Bands using SVD Algorithm – Derived Equations

As an example, the 12.0 in without TiO₂ and 12.0 in with 0.5 g of TiO₂ images were processed using and band reduction algorithms. The bands were reduced from 120 to 40 bands using Single Value Decomposition (SVD) feature reduction algorithm present on HIAT.

9.4.4.1 Baseline Results

Baseline result were produced by classifying the image without being process by the regularization algorithm. Table 53 present the obtained classification maps from the two images mentioned before. Next figures showed the obtained classification accuracies.

Table 53: Baseline Results from the 12.0 in without TiO₂ SVD40

Real Images:	
Classification Algorithm	Classification Map 12.0 in without TiO₂ SVD40
Minimum Euclidean Distance	 Accuracy = 100.00%
Minimum Spectral Angle	 Accuracy = 100.00%
Maximum Unmixing Value	 Accuracy = 100.00%

9.4.4.2 12.0 in without TiO₂ Classification Accuracy

The following graph compare the obtained classification accuracy from the 12.0 in without TiO₂ and table 54 show the obtained classification maps to be compared visually.

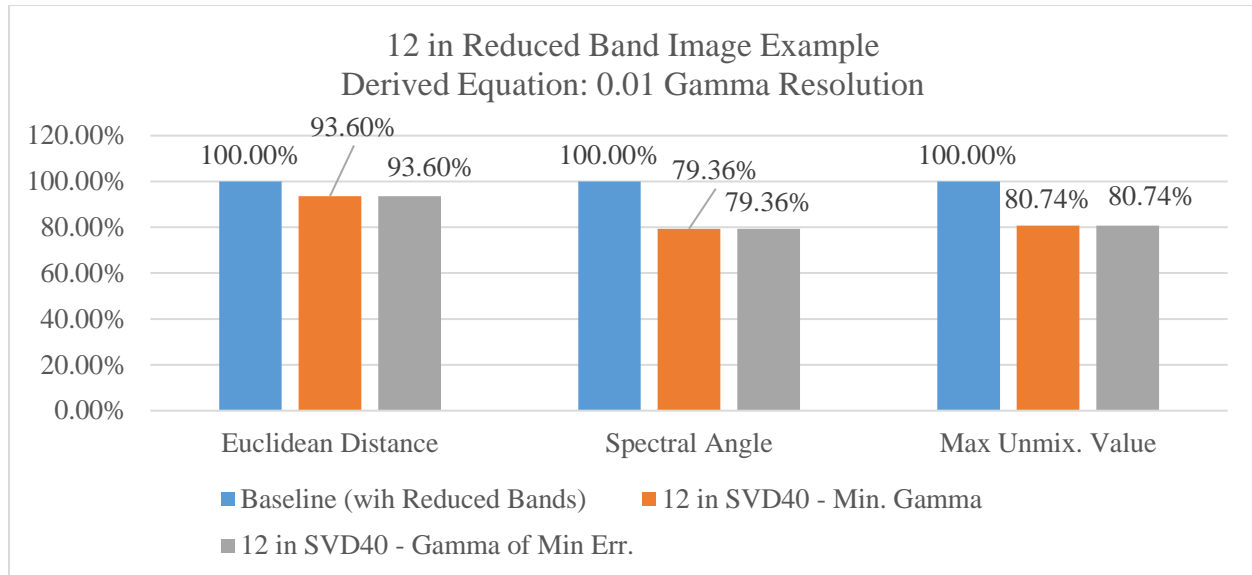
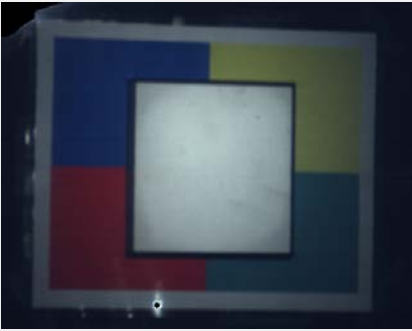

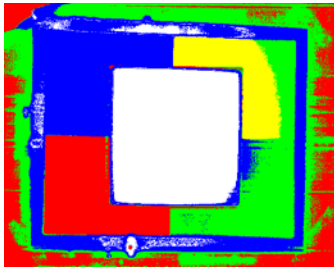
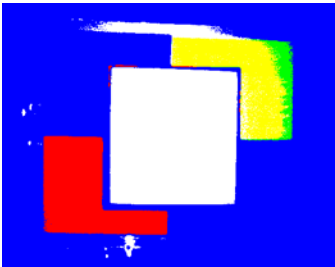
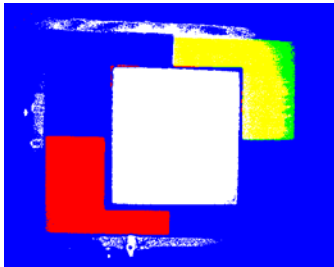
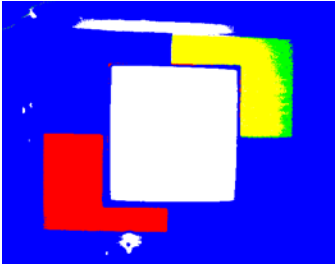
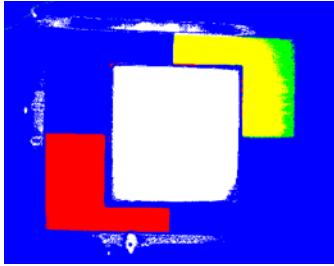


Figure 145: Example with Reduce Bands Obtained Accuracy after Regularization

Table 54: 12.0 in SVD40 Classification Maps after Regularization: DE, Gamma Res: 0.01

Real Image		
Classification Algorithm	Gamma Resolution	= 0.01
	Classification Maps	
	Minimum Gamma	Gamma of Minimum Error
Minimum Euclidean Distance	 Accuracy = 93.60%	 Accuracy = 93.60%
Minimum Spectral Angle	 Accuracy = 79.36%	 Accuracy = 79.36%
Maximum Unmixing Value	 Accuracy = 80.74%	 Accuracy = 80.74%

9.5 Performance Matrices of the Regularization Results

9.5.1 Baseline Results 12.0 in image:

- Minimum Euclidean Distance

	Euclidean Distance				
	Blue	Yellow	Green	Red	White
Blue	0	0	3402	0	0
Yellow	0	25	4460	0	0
Green	0	0	4030	0	0
Red	0	0	3498	0	0
White	0	7467	0	0	0

Correct Pixels: 4055

Total of Pixels: 22882

Accuracy: 17.72%

- Minimum Spectral Angle

	Spectral Angle				
	Blue	Yellow	Green	Red	White
Blue	3402	0	0	0	0
Yellow	0	479	0	0	4006
Green	0	0	4030	0	0
Red	0	0	0	1869	1629
White	0	0	0	0	7467

Correct Pixels: 17247

Total of Pixels: 22882

Accuracy: 75.37%

- Maximum Endmember Value:

	Unmixing				
	Blue	Yellow	Green	Red	White
Blue	3402	0	0	0	0
Yellow	0	4221	0	0	264
Green	1	0	4029	0	0
Red	0	0	0	3498	0
White	0	0	0	0	7467

Correct Pixels: 22617

Total of Pixels: 22882

Accuracy: 98.84%

9.5.2 Baseline Results 12.0 in 0.5 g TiO₂ image:

- Minimum Euclidean Distance

	Minimum Euclidean Distance				
	Blue	Yellow	Green	Red	White
Blue	0	0	3402	0	0
Yellow	0	0	4485	0	0
Green	0	0	4030	0	0
Red	0	0	3498	0	0
White	0	0	7467	0	0

Correct Pixels: 4030
Total of Pixels: 22882
Accuracy: 17.61%

- Minimum Spectral Angle

	Minimum Spectral Angle				
	Blue	Yellow	Green	Red	White
Blue	0	0	3402	0	0
Yellow	0	0	597	0	3888
Green	0	0	4030	0	0
Red	0	0	2316	0	1182
White	0	0	0	0	7467

Correct Pixels: 11497
Total of Pixels: 22882
Accuracy: 50.24%

- Maximum Endmember Value:

	Maximum Unmixing Value				
	Blue	Yellow	Green	Red	White
Blue	3402	0	0	0	0
Yellow	3092	0	1186	0	207
Green	3979	0	51	0	0
Red	3498	0	0	0	0
White	25	0	0	0	7442

Correct Pixels: 10895
Total of Pixels: 22882
Accuracy: 47.61%

9.5.3 Numerical Approximations: 12.0 in

9.5.3.1 Gamma Resolution = 0.1

- Performance matrices for Minimum Gamma:

Euclidean Distance					
	Blue	Yellow	Green	Red	White
Blue	3402	0	0	0	0
Yellow	0	2638	1619	228	0
Green	0	0	4030	0	0
Red	0	0	0	3498	0
White	0	0	0	0	7467

Correct Pixels: 21035
Total of Pixels: 22882
Accuracy: 91.93%

Spectral Angle					
	Blue	Yellow	Green	Red	White
Blue	3402	0	0	0	0
Yellow	0	4485	0	0	0
Green	4030	0	0	0	0
Red	0	0	0	3498	0
White	0	0	0	0	7467

Correct Pixels: 18852
Total of Pixels: 22882
Accuracy: 82.39%

Unmixing					
	Blue	Yellow	Green	Red	White
Blue	3402	0	0	0	0
Yellow	0	4485	0	0	0
Green	4030	0	0	0	0
Red	0	0	0	3498	0
White	0	0	0	0	7467

Correct Pixels: 18852
Total of Pixels: 22882
Accuracy: 82.39%

- Performance Matrices for Gamma of Minimum Error

Euclidean Distance					
	Blue	Yellow	Green	Red	White
Blue	1056	0	0	0	2346
Yellow	0	3283	0	1202	0
Green	0	0	3360	0	670
Red	0	0	0	2777	721
White	0	4626	0	0	2841

Correct Pixels: 13317
Total of Pixels: 22882 Accuracy: 58.20%

Spectral Angle					
	Blue	Yellow	Green	Red	White
Blue	1056	0	0	0	2346
Yellow	0	3323	0	1162	0
Green	3360	0	0	0	670
Red	0	393	0	2777	328
White	0	0	96	0	7371

Correct Pixels: 14527
Total of Pixels: 22882 Accuracy: 63.49%

Unmixing					
	Blue	Yellow	Green	Red	White
Blue	1056	0	0	0	2346
Yellow	0	3287	0	1198	0
Green	3360	0	0	0	670
Red	0	0	0	2777	721
White	2818	0	1	1	4647

Correct Pixels: 11767
Total of Pixels: 22882 Accuracy: 51.42%

9.5.3.2 Gamma Resolution = 0.01

- Performance matrices for Minimum Gamma:

Euclidean Distance					
	Blue	Yellow	Green	Red	White
Blue	3318	0	84	0	0
Yellow	0	3821	0	664	0
Green	0	0	4030	0	0
Red	0	0	0	3498	0
White	0	0	0	0	7467

Correct Pixels: 22134
Total of Pixels: 22882
Accuracy: 96.73%

Spectral Angle					
	Blue	Yellow	Green	Red	White
Blue	3402	0	0	0	0
Yellow	0	4215	0	270	0
Green	4030	0	0	0	0
Red	0	0	0	3498	0
White	0	0	0	0	7467

Correct Pixels: 18582
Total of Pixels: 22882
Accuracy: 81.21%

Unmixing					
	Blue	Yellow	Green	Red	White
Blue	3402	0	0	0	0
Yellow	0	4124	0	361	0
Green	4030	0	0	0	0
Red	0	0	0	3498	0
White	0	0	0	0	7467

Correct Pixels: 18491
Total of Pixels: 22882
Accuracy: 80.81%

- Performance Matrices for Gamma of Minimum Error

Euclidean Distance					
	Blue	Yellow	Green	Red	White
Blue	1458	0	1944	0	0
Yellow	0	2284	752	1137	312
Green	0	0	4007	23	0
Red	0	0	0	3498	0
White	0	119	0	0	7348

Correct Pixels: 18595
Total of Pixels: 22882 Accuracy: 81.26%

Spectral Angle					
	Blue	Yellow	Green	Red	White
Blue	2784	0	392	226	0
Yellow	0	4089	0	84	312
Green	1337	157	0	2536	0
Red	0	0	0	3498	0
White	0	0	113	0	7354

Correct Pixels: 17725
Total of Pixels: 22882 Accuracy: 77.46%

Unmixing					
	Blue	Yellow	Green	Red	White
Blue	3192	0	1	209	0
Yellow	0	3928	0	245	312
Green	1337	40	113	2540	0
Red	0	0	0	3498	0
White	115	0	0	0	7352

Correct Pixels: 18083
Total of Pixels: 22882 Accuracy: 79.03%

9.5.4 Numerical Approximation: 12.0 in 0.5 *g* TiO₂

9.5.4.1 Gamma Resolution = 0.1

- Performance matrices for Minimum Gamma:

Euclidean Distance					
	Blue	Yellow	Green	Red	White
Blue	3402	0	0	0	0
Yellow	4027	458	0	0	0
Green	4030	0	0	0	0
Red	3498	0	0	0	0
White	0	7467	0	0	0

Correct Pixels: 3860

Total of Pixels: 22882

Accuracy: 16.87%

Spectral Angle					
	Blue	Yellow	Green	Red	White
Blue	2773	0	629	0	0
Yellow	0	0	4485	0	0
Green	340	0	3690	0	0
Red	0	0	3498	0	0
White	0	0	7456	0	11

Correct Pixels: 6474

Total of Pixels: 22882

Accuracy: 28.29%

Unmixing					
	Blue	Yellow	Green	Red	White
Blue	3402	0	0	0	0
Yellow	4485	0	0	0	0
Green	4030	0	0	0	0
Red	3498	0	0	0	0
White	7467	0	0	0	0

Correct Pixels: 3402

Total of Pixels: 22882

Accuracy: 14.87%

- Performance Matrices for Gamma of Minimum Error

Euclidean Distance					
	Blue	Yellow	Green	Red	White
Blue	199	2514	0	0	689
Yellow	0	2222	0	0	2263
Green	7	3439	0	0	584
Red	0	3432	0	0	66
White	0	0	0	0	7467

Correct Pixels: 9888
Total of Pixels: 22882 Accuracy: 43.21%

Spectral Angle					
	Blue	Yellow	Green	Red	White
Blue	199	0	0	0	3203
Yellow	0	1	0	0	4484
Green	6	0	1	0	4023
Red	0	10	0	0	3488
White	0	0	0	0	7467

Correct Pixels: 7668
Total of Pixels: 22882 Accuracy: 33.51%

Unmixing					
	Blue	Yellow	Green	Red	White
Blue	199	12	0	0	3191
Yellow	0	967	0	0	3518
Green	7	840	0	0	3183
Red	0	1253	0	0	2245
White	0	0	0	0	7467

Correct Pixels: 8633
Total of Pixels: 22882 Accuracy: 37.73%

9.5.4.2 Gamma Resolution = 0.01

- Performance matrices for Minimum Gamma:

Euclidean Distance					
	Blue	Yellow	Green	Red	White
Blue	3317	24	0	0	61
Yellow	469	1437	0	0	2579
Green	3614	314	0	0	102
Red	852	2276	24	0	346
White	0	0	0	0	7467

Correct Pixels: 12221
Total of Pixels: 22882
Accuracy: 53.41%

Spectral Angle					
	Blue	Yellow	Green	Red	White
Blue	3313	0	4	0	85
Yellow	0	0	344	0	4141
Green	2882	0	732	0	416
Red	14	0	111	0	3373
White	0	0	0	0	7467

Correct Pixels: 11512
Total of Pixels: 22882
Accuracy: 50.31%

Unmixing					
	Blue	Yellow	Green	Red	White
Blue	3317	0	0	0	85
Yellow	551	0	0	0	3934
Green	3614	0	0	0	416
Red	891	0	0	0	2607
White	0	0	0	0	7467

Correct Pixels: 10784
Total of Pixels: 22882
Accuracy: 47.13%

- Performance Matrices for Gamma of Minimum Error

Euclidean Distance					
	Blue	Yellow	Green	Red	White
Blue	3054	311	8	29	0
Yellow	1246	3195	44	0	0
Green	3404	560	66	0	0
Red	564	990	590	1354	0
White	426	6528	0	0	513

Correct Pixels: 8182
Total of Pixels: 22882 Accuracy: 35.76%

Spectral Angle					
	Blue	Yellow	Green	Red	White
Blue	2308	0	750	0	344
Yellow	0	0	1221	0	3264
Green	1954	0	1510	0	566
Red	16	0	315	1063	2104
White	0	0	722	1	6744

Correct Pixels: 11625
Total of Pixels: 22882 Accuracy: 50.80%

Unmixing					
	Blue	Yellow	Green	Red	White
Blue	3088	0	0	119	195
Yellow	1813	0	0	1368	1304
Green	3474	0	0	143	413
Red	1219	0	0	1610	669
White	1454	0	0	2690	3323

Correct Pixels: 8021
Total of Pixels: 22882 Accuracy: 35.05%

9.5.5 Derived Equations: 12.0 in

9.5.5.1 Gamma Resolution = 0.1

- Performance matrices for Minimum Gamma:

Euclidean Distance					
	Blue	Yellow	Green	Red	White
Blue	3402	0	0	0	0
Yellow	0	2638	1619	228	0
Green	0	0	4030	0	0
Red	0	0	35	3463	0
White	0	985	0	0	6482

Correct Pixels: 20015

Total of Pixels: 22882

Accuracy: 87.47%

Spectral Angle					
	Blue	Yellow	Green	Red	White
Blue	3402	0	0	0	0
Yellow	0	4485	0	0	0
Green	4030	0	0	0	0
Red	0	0	0	3498	0
White	0	0	0	0	7467

Correct Pixels: 18852

Total of Pixels: 22882

Accuracy: 82.39%

Unmixing					
	Blue	Yellow	Green	Red	White
Blue	3402	0	0	0	0
Yellow	0	4485	0	0	0
Green	4030	0	0	0	0
Red	0	0	0	3498	0
White	983	0	0	0	6484

Correct Pixels: 17869

Total of Pixels: 22882

Accuracy: 78.09%

- Performance Matrices for Gamma of Minimum Error

Euclidean Distance					
	Blue	Yellow	Green	Red	White
Blue	535	0	2867	0	0
Yellow	0	2920	0	1202	363
Green	0	0	3283	747	0
Red	0	0	0	3498	0
White	0	6607	0	0	860

Correct Pixels: 11096 Accuracy: 48.49%
Total of Pixels: 22882

Spectral Angle					
	Blue	Yellow	Green	Red	White
Blue	3389	0	0	13	0
Yellow	0	2960	0	1162	363
Green	2469	814	0	747	0
Red	0	0	0	3498	0
White	0	0	503	0	6964

Correct Pixels: 16811 Accuracy: 73.47%
Total of Pixels: 22882

Unmixing					
	Blue	Yellow	Green	Red	White
Blue	3397	0	0	5	0
Yellow	0	2924	0	1198	363
Green	2469	814	0	747	0
Red	0	0	0	3498	0
White	646	0	0	78	6743

Correct Pixels: 16562 Accuracy: 72.38%
Total of Pixels: 22882

9.5.5.2 Gamma Resolution = 0.01

- Performance matrices for Minimum Gamma:

Euclidean Distance					
	Blue	Yellow	Green	Red	White
Blue	3366	0	36	0	0
Yellow	0	4132	4	349	0
Green	0	0	4030	0	0
Red	0	0	0	3498	0
White	0	0	0	0	7467

Correct Pixels: 22493
Total of Pixels: 22882
Accuracy: 98.30%

Spectral Angle					
	Blue	Yellow	Green	Red	White
Blue	3402	0	0	0	0
Yellow	0	4139	0	346	0
Green	4030	0	0	0	0
Red	0	0	0	3498	0
White	0	0	0	0	7467

Correct Pixels: 18506
Total of Pixels: 22882
Accuracy: 80.88%

Unmixing					
	Blue	Yellow	Green	Red	White
Blue	3402	0	0	0	0
Yellow	0	4136	0	349	0
Green	4030	0	0	0	0
Red	0	0	0	3498	0
White	0	0	0	0	7467

Correct Pixels: 18503
Total of Pixels: 22882
Accuracy: 80.86%

- Performance Matrices for Gamma of Minimum Error

Euclidean Distance					
	Blue	Yellow	Green	Red	White
Blue	1712	0	1690	0	0
Yellow	0	3044	19	1422	0
Green	0	0	4030	0	0
Red	0	0	0	3498	0
White	0	0	0	0	7467

Correct Pixels: 19751
Total of Pixels: 22882 Accuracy: 86.32%

Spectral Angle					
	Blue	Yellow	Green	Red	White
Blue	3389	0	0	13	0
Yellow	0	3853	0	632	0
Green	1817	0	0	2213	0
Red	0	0	0	3498	0
White	0	0	0	0	7467

Correct Pixels: 18207
Total of Pixels: 22882 Accuracy: 79.57%

Unmixing					
	Blue	Yellow	Green	Red	White
Blue	3393	0	0	9	0
Yellow	0	3670	0	815	0
Green	1817	0	0	2213	0
Red	0	0	0	3498	0
White	0	0	0	0	7467

Correct Pixels: 18028
Total of Pixels: 22882 Accuracy: 78.79%

9.5.6 Derived Equations: 12.0 in 0.5 *g* TiO₂

9.5.6.1 Gamma Resolution = 0.1

- Performance matrices for Minimum Gamma:

Euclidean Distance					
	Blue	Yellow	Green	Red	White
Blue	3402	0	0	0	0
Yellow	4027	458	0	0	0
Green	4030	0	0	0	0
Red	3498	0	0	0	0
White	0	6376	0	0	1091

Correct Pixels: 4951

Total of Pixels: 22882

Accuracy: 21.64%

Spectral Angle					
	Blue	Yellow	Green	Red	White
Blue	2773	0	629	0	0
Yellow	0	0	4485	0	0
Green	340	0	3690	0	0
Red	0	0	3498	0	0
White	0	0	6303	0	1164

Correct Pixels: 7627

Total of Pixels: 22882

Accuracy: 33.33%

Unmixing					
	Blue	Yellow	Green	Red	White
Blue	3402	0	0	0	0
Yellow	4485	0	0	0	0
Green	4030	0	0	0	0
Red	3498	0	0	0	0
White	6314	0	0	0	1153

Correct Pixels: 4555

Total of Pixels: 22882

Accuracy: 19.91%

- Performance Matrices for Gamma of Minimum Error

Euclidean Distance					
	Blue	Yellow	Green	Red	White
Blue	199	2514	0	0	689
Yellow	0	2222	0	0	2263
Green	7	3439	0	0	584
Red	0	3432	0	0	66
White	1382	1151	0	0	4934

Correct Pixels: 7355
Total of Pixels: 22882 Accuracy: 32.14%

Spectral Angle					
	Blue	Yellow	Green	Red	White
Blue	199	0	0	0	3203
Yellow	0	1	0	0	4484
Green	6	0	1	0	4023
Red	0	10	0	0	3488
White	2	0	1380	1143	4942

Correct Pixels: 5143
Total of Pixels: 22882 Accuracy: 22.48%

Unmixing					
	Blue	Yellow	Green	Red	White
Blue	199	12	0	0	3191
Yellow	0	967	0	0	3518
Green	7	840	0	0	3183
Red	0	1253	0	0	2245
White	1382	7	0	1143	4935

Correct Pixels: 6101
Total of Pixels: 22882 Accuracy: 26.66%

9.5.6.2 Gamma Resolution = 0.01

- Performance matrices for Minimum Gamma:

Euclidean Distance					
	Blue	Yellow	Green	Red	White
Blue	6	6	0	0	3390
Yellow	0	29	0	0	4456
Green	18	77	0	0	3935
Red	97	858	0	0	2543
White	0	0	0	0	7467

Correct Pixels: 7502
Total of Pixels: 22882
Accuracy: 32.79%

Spectral Angle					
	Blue	Yellow	Green	Red	White
Blue	0	0	6	0	3396
Yellow	0	0	0	0	4485
Green	0	0	18	0	4012
Red	0	0	38	0	3460
White	0	0	0	0	7467

Correct Pixels: 7485
Total of Pixels: 22882
Accuracy: 32.71%

Unmixing					
	Blue	Yellow	Green	Red	White
Blue	6	0	0	0	3396
Yellow	0	0	0	0	4485
Green	18	0	0	0	4012
Red	189	5	0	0	3304
White	0	0	0	0	7467

Correct Pixels: 7473
Total of Pixels: 22882
Accuracy: 32.66%

- Performance Matrices for Gamma of Minimum Error

Euclidean Distance					
	Blue	Yellow	Green	Red	White
Blue	1141	2205	11	22	23
Yellow	934	3447	0	0	104
Green	1371	2604	46	0	9
Red	279	2361	0	858	0
White	506	133	0	0	6828

Correct Pixels: 12320

Total of Pixels: 22882

Accuracy: 53.84%

Spectral Angle					
	Blue	Yellow	Green	Red	White
Blue	120	0	1005	587	1690
Yellow	0	0	1076	183	3226
Green	0	0	1424	506	2100
Red	0	0	312	902	2284
White	0	0	525	0	6942

Correct Pixels: 9388

Total of Pixels: 22882

Accuracy: 41.03%

Unmixing					
	Blue	Yellow	Green	Red	White
Blue	1152	0	0	604	1646
Yellow	1390	403	42	580	2070
Green	1467	8	0	623	1932
Red	890	26	0	902	1680
White	529	0	0	87	6851

Correct Pixels: 9308

Total of Pixels: 22882

Accuracy: 40.68%

9.5.7 Derived Equations: Reduced Bands using SVD Algorithm

Euclidean Distance					
	Blue	Yellow	Green	Red	White
Blue	3402	0	0	0	0
Yellow	0	4485	0	0	0
Green	1	0	4029	0	0
Red	0	0	0	3498	0
White	0	0	0	0	7467

Correct Pixels: 22881
Total of Pixels: 22882
Accuracy: 99.996%

Spectral Angle					
	Blue	Yellow	Green	Red	White
Blue	3402	0	0	0	0
Yellow	0	4485	0	0	0
Green	0	0	4030	0	0
Red	0	0	0	3498	0
White	0	0	0	0	7467

Correct Pixels: 22882
Total of Pixels: 22882
Accuracy: 100.00%

Unmixing					
	Blue	Yellow	Green	Red	White
Blue	3402	0	0	0	0
Yellow	0	4485	0	0	0
Green	1	0	4029	0	0
Red	0	0	0	3498	0
White	0	0	0	0	7467

Correct Pixels: 22881
Total of Pixels: 22882
Accuracy: 99.996%

9.5.7.1 Baseline Results:

Euclidean Distance					
	Blue	Yellow	Green	Red	White
Blue	3402	0	0	0	0
Yellow	0	3594	891	0	0
Green	574	0	3456	0	0
Red	0	0	0	3498	0
White	0	0	0	0	7467

Correct Pixels: 21417
Total of Pixels: 22882
Accuracy: 93.60%

Spectral Angle					
	Blue	Yellow	Green	Red	White
Blue	3402	0	0	0	0
Yellow	0	3793	204	0	488
Green	4030	0	0	0	0
Red	0	0	0	3498	0
White	0	0	0	0	7467

Correct Pixels: 18160
Total of Pixels: 22882
Accuracy: 79.36%

Unmixing					
	Blue	Yellow	Green	Red	White
Blue	3402	0	0	0	0
Yellow	1	4107	366	0	11
Green	4030	0	0	0	0
Red	0	0	0	3498	0
White	0	0	0	0	7467

Correct Pixels: 18474
Total of Pixels: 22882
Accuracy: 80.74%

9.5.7.2 Gamma Resolution = 0.01

- Performance matrices for Minimum Gamma:

Euclidean Distance					
	Blue	Yellow	Green	Red	White
Blue	3402	0	0	0	0
Yellow	0	3594	891	0	0
Green	574	0	3456	0	0
Red	0	0	0	3498	0
White	0	0	0	0	7467

Correct Pixels: 21417
Total of Pixels: 22882
Accuracy: 93.60%

Spectral Angle					
	Blue	Yellow	Green	Red	White
Blue	3402	0	0	0	0
Yellow	0	3793	204	0	488
Green	4030	0	0	0	0
Red	0	0	0	3498	0
White	0	0	0	0	7467

Correct Pixels: 18160
Total of Pixels: 22882
Accuracy: 79.36%

Unmixing					
	Blue	Yellow	Green	Red	White
Blue	3402	0	0	0	0
Yellow	1	4107	366	0	11
Green	4030	0	0	0	0
Red	0	0	0	3498	0
White	0	0	0	0	7467

Correct Pixels: 18474
Total of Pixels: 22882
Accuracy: 80.74%

- Performance Matrices for Gamma of Minimum Error

Euclidean Distance					
	Blue	Yellow	Green	Red	White
Blue	3402	0	0	0	0
Yellow	0	3594	891	0	0
Green	574	0	3456	0	0
Red	0	0	0	3498	0
White	0	0	0	0	7467

Correct Pixels: 21417

Total of Pixels: 22882

Accuracy: 93.60%

Spectral Angle					
	Blue	Yellow	Green	Red	White
Blue	3402	0	0	0	0
Yellow	0	3793	204	0	488
Green	4030	0	0	0	0
Red	0	0	0	3498	0
White	0	0	0	0	7467

Correct Pixels: 18160

Total of Pixels: 22882

Accuracy: 79.36%

Unmixing					
	Blue	Yellow	Green	Red	White
Blue	3402	0	0	0	0
Yellow	1	4107	366	0	11
Green	4030	0	0	0	0
Red	0	0	0	3498	0
White	0	0	0	0	7467

Correct Pixels: 18474

Total of Pixels: 22882

Accuracy: 80.74%

9.6 User Manual

A user manual has been prepared to act as a secondary source of information for reference and for the usage of the toolbox. To obtain a copy of this document please contact:

Name	Contact
Emmanuel Carpena	emmanuel.carpena@upr.edu ecarpena3@gmail.com